ISSUES OF PARTICULATE MATTER EMISSION FROM DIESEL ENGINE AND ITS CONTROL

A thesis submitted for the degree of Doctor of Philosophy

By

Nehemiah Sabinus Iheadindueme ALOZIE

College of Engineering, Design and Physical Sciences
Brunel University London
United Kingdom
January 2016

ABSTRACT

Particulate matter (PM) emitted from diesel engines encompasses soluble (volatile) and insoluble (non-volatile) matter. The concept of volatility or solubility depends on the method of separation. The volatile matter includes sulphates and nitrates which are bound to water vapour; and myriads of hydrocarbon species. The solid matter is comprised of black carbon and ash. Its mitigation combines the use of internal engine design and operating factors like fuel injection and spray, air and fuel mixing, chamber designs and fuel improvements. Control technologies that act on the exhaust gases are called ‘after-treatments' which include the use of oxidation catalysts, filter trap and reductant of nitrogen oxides along the exhaust system. The central issues of this thesis are measurement schemes that involve stripping the PM of volatile matter in order to determine the actual values of nano-size solid carbon particles that pose significant health risk and their mitigations.

In the experimental measurements, exhaust gases were generated at low engine load which are rich in unburnt hydrocarbons that nucleate into particles at low temperatures. Similarly, exhaust gases generated at medium load contain volatile and soot components; these were used to study dilution effects on PM emission. The interplay of mixing and cooling was used to explain the behaviour of saturation characteristics of the volatile fractions in the dilution process which influenced nucleation of volatile species. The parameters of particle number concentration reduction factor (PCRF) and volatile removal efficiency (VRE) were used to give extended interpretation to dilution of PM during conditioning, than mere dilution ratios. On this basis, comparison was made on the effect of carrier gases on dilution process and it was found that air is superior when there is need for volatile reduction while nitrogen is better when it is necessary to freeze further reaction, especially at low dilution ratios. In addition, a two-stage hot dilution technique was used to mimic the Particle Measurement Programme (PMP) prescription, and it gave better PCRF and VRE values. The study of PM mitigation by filter traps focused on burning-off the accumulated matter to allow free flow of exhaust gases, and the energy it takes to initiate and maintain PM combustion. Therefore a fundamental study of soot oxidation relevant to regeneration of diesel particulate filter (DPF) was made. This

was extended to investigate if blending of petrodiesel with biodiesel affects PM oxidation. It is deducible that oxidation of PM generated from fuel with biodiesel blends is slightly faster compared to that from pure petrodiesel. A feasible use of microwave power to regenerate catalysed and non-catalysed silicon carbide (SiC) diesel particulate filters (DPFs) using an available multimode microwave cavity was also carried out. Results show that with catalysed DPFs, catalyst light-off temperature reduced by 100^{o}C under the influence of microwave irradiation, while for non-catalysed DPF, regeneration was achieved within 550-600^{o}C at a time estimated to be lower compared to electrical resistance heating approach.

ACKNOWLEDEGEMENTS

I wish to thank the government of the Federal Republic of Nigeria and Management of University of Lagos Nigeria, for financial support through the Tertiary Education Fund (TETFUND) Academic Staff Development Project.

I am most grateful to my principal supervisor Dr Lionel Ganippa for every effort to guide and assist me through the study. I am also grateful to my second supervisor, Professor Alasdair Cairns, the Head of our Centre for Advanced Powertrain and Fuels Research Professor Hua Zhao, other academics in our research group – Professor Thanos Megaritis and Dr Apostolos Pesiridis for every co-operation. The support from the technical staff are also appreciated; the Head Dr. Benjamin McCalla, the Chief Technician Mr Christopher Allan, the technicians of the Engines and Thermodynamics Laboratory, Andrew Selway, Kenneth Anstiss, Costas Xanthos, Clive Barrett; the gentlemen in the store – Les Botwright, Minal Shah and Lee Charge. I thank Dr George Fern for collaboration and access to Thermal and Microscopy Laboratories and those that ran my tests: Abdul Ghani, Dr Ashley Howkins and Nita Verma. Similarly, I am grateful to Professor Wamadeva Balachandran for the opportunity given to me to join his project team for a part of my study and also his research team: Dr Nadarajah Manivannan with whom I worked more in the project and gave valuable assistance, Dr. Maysom Abbod and David Brennan all at the Centre for Electronic Systems Research. Dr Radu Beleca was also friendly and helpful before he left the research group.

I enjoyed friendship with many senior colleagues in the research group and interestingly all have earned their PhDs in the order we came: Dr Barbara Menkiel, Dr Barnaby Coates, Dr Stephen Hemmings, Dr Mohammadreza Attar, Dr. Gholamreza Abbaszadeh Mosaiiebi, Dr Mohammed Moore Ojapah, Dr Martin Lawrence, Dr Fanos Christodoulou, Dr Pin Lu, Dr Ben Moxey and Dr Jun Ma. Dr Yan Zhang is an unassuming gentleman whose presence as a Post-Doctoral Fellow was of immense benefit to many of us. I worked closest and concurrently with David Peirce using the same engine and our relationship deserve a special mention. Dave, I am quite grateful for every comfort enjoyed from you. Same goes other colleagues Quan, Kenwoo, Ian, Maclene, Thompson, Vinicius, Ward and others who came after

me in the research group. I also remember with appreciation the benefits of visiting the Indian Institute of Science Bangalore India, in company of David Peirce to the laboratory of Professor Ravikrishna on exchange programme where I met good friends: Dr Madan Avulapti, then a research student and later joined our group here in Brunel for post-Doctoral Research, Prasad, Krishna, Saurabh and his wife Kajal Shah. Dr Hayder Dhahad of University of Technology Baghdad spent some time with us as Bench student in the test cell and we also shared ideas. Beyond the engines research group are also many colleagues who graduated from other research groups; Dr Austin Briggs, Dr Evans Ashigwuike, Dr Giovanna Cossali, Dr Emily Pike-Wilson, and office colleagues Mrs Bridget Kogo, Milad Beheshti and Mohammad Khan. My special thanks also go to Dr Peter Eastwood and Dr Phil Price both of Ford Dunton Technical Centre UK, Mr Jeremy Gidney of Johnson Matthey at Royston Hertfordshire UK and Abiodun Adeyemi for every assistance. I thank many seniors and colleagues at University of Lagos who helped me in many ways, especially Professors A Salau, O Fakinlede, P Nwilo, F N Okafor, D Esezobor and J Ajiboye - all of the Faculty of Engineering; Professors C Igwilo and T Ogundipe who administered TETFUND in University of Lagos successively, and equally to Professor and Dr Mrs Olabaniyi.

On the home front, I cannot thank my wife **Blessing**, enough for keeping faith with me all these years and maintaining the home while on this study. I consider that my children **Chibuzor** and **Godspower** made the biggest sacrifice for my PhD by enduring my absence from home. I pray that through this work, God will open the door of wisdom, wealth and power for you people to live above ordinary lives in JESUS NAME. Not to forget that **Leona** has been in the house for me and my wife during this time. My senior brother **Alphonsus** is a phenomenon! You have a special place in my life. You and my other brothers Bethran, Goddy, Zeph and our mother **Benedicta,** have all been of great support. Thanks also to my uncles **Albert and Dr Collins** who were instrumental to earlier parts of my education. I thank **Sir Albert Odu**, my Secondary School Principal whom I have a duty to honour. I also thank Pastor Femi Oladipo of the Mountain of Fire and Miracles Ministries Headquarter in London.

CONTENTS

TABLE OF FIGURES

LIST OF TABLES

NOMENCLATURE

General Abbreviations

AMP	Accumulation mode particles
ASI	After start of injection
ASTM	American Society for Testing and Materials
BDC	Bottom dead centre
BMEP	Brake Mean Effective Pressure
BS	British Standard
CAA	Clean Air Act
CAD	Computer Aided Design
CARB	California Air Resources Board
CFR	Co-operative Fuel Research
CI	Cetane Index
CIE	Compression ignition engine
CLD	Chemiluminscene detector
CN	Cetane Number
CPC	Condensation Particle Counters
CPMC	Cumulative particle mass concentrations
CPNC	Cumulative particle number concentrations
CS	Catalytic stripping
CVS	Constant volume sampler
DMA	Differential mobility analyser
DOC	Diesel oxidation catalysts
DPF	Diesel particulate filter
DR	Dilution ratio
DSC	Differential scanning calorimeter
EAA	Electrical aerosol analyser
EC or BC	Elemental carbon, soot, or black carbon
ECU	Electronic control unit
EGR	Exhaust gas recirculation

EMS	Electrical mobility spectrometer
EPA	Environmental protection agency
ET	Evaporation tube
EU	European Union
EVC	Exhaust valve close
EVO	Exhaust valve close
F/A	Fuel Air ratio
FCE	Faraday cup electrometer
FCU	Flow control unit
FEFD	Full exhaust flow dilution tunnel
FEM	Finite Element Method
FID	Flame ionisation detector
FIE	Fuel injection equipment
FOEE	Fish oil ethyl ester
FOT	Final oxidation temperature
FSN	Filter smoke number
FTP-75	Federal Test Procedure
HACA	Hydrogen abstraction, carbon addition
HC	Hydrocarbon
HMN	Hepta-methyl nonane
HRR	Heat release rate
HRTEM	High resolution transmission electron microscope
HSDI	High speed direct injection
ISO	International Standards Organisation
IVC	Intake valve close
IVO	Intake valve open
LEV	Low emission vehicle
MAF	Mass Air Flow
MEP	Mean effective pressure
MLRT	Maximum mass loss rate temperature

NAAQS	National air quality standards
NDIR	Non-dispersive infrared
NMHC	Non-methane hydrocarbon
NMP	Nucleation mode Particles
NOx	Nitrogen oxides
NTPR	Non thermal plasma reactor
PAH	Polycyclic aromatic hydrocarbons
PCRF	Particle number concentration reduction factor
PLN	Pump line nozzle
PM	Particulate matter
PMP	Particle measurement programme
PNC	Particle number concentrations
PND_1	Primary hot diluter
PND_2	Secondary cold diluter
PTD	Porous Tube Diluter
RME	Rapeseed methyl ester
SME	Sun Flower Methyl ester
SOF	Soluble organic fractions
SOT	Starting oxidation temperature
SPNMS	Solid particle number measurement system
TD	Thermo-desorption
TDC	Top dead centre
TGA	Thermogravimetric analyser
THC	Total hydrocarbon
TOT	Triggering oxidation temperature
UCOME	Used cooking oil methyl ester
UHC	Unburnt hydrocarbon
UNECE	United Nations Economic Commission for Europe
VOC	Volatile components

VOF	Volatile organic compounds
VPR	Volatile particles remover
VRE	Volatile removal efficiency

Symbols

A/F	Air Fuel ratio
Bsfc	Brake specific fuel consumption
isfc	Indicated specific fuel consumption
r_c	Compression ratio
sfc	Specific fuel consumption (g/kW.h)
V_c	Clearance Volume
V_d	Swept Volume
η_v	Volumetric efficiency
Λ	Relative air/fuel ratio
Φ	Fuel/air equivalence ratio

Chemical Symbols

$CaSO_4$	Calcium sulphate
CO	Carbon monoxide
CO_2	Carbon dioxide
H_2SO_4	Sulphuric acid
HNO_3	Nitric acid
NH_4HNO_3	Ammonium nitrate
NO	Nitrogen Oxide
NO_2	Nitrogen dioxide
NO_3^-	Nitrate ions
OH^-	Hydroxyl ion
SO_4^{2-}	Sulphate ions

CHAPTER 1

INTRODUCTIONS

The discovery of fire transcends all known human civilisations and if mythical perspective be referenced, Biblical narratives show that even the creator gave charge concerning fire outbreak and the need to protect the environment (Exodus 22:6 and Numbers 35:33-34).

"If fire break out, and catch in thorns, so that the stacks of corn, or the standing corn, or the field, be consumed therewith; ***he that kindled the fire shall surely make restitution. You shall not pollute the land in which you live….You shall not defile the land in which you live…****"*

Of utmost significance in man's ability to harness the benefits of fire is the development of internal combustion engines which, the diesel engine has become a choice power plant for almost a century. It operates on the principle of compression ignition to convert the chemical energy of diesel fuel into mechanical power. In the process, air is admitted into the cylinder, compressed to a sufficiently high temperature to ignite and burn finely-atomised fuel sprays in the combustion chamber. The force generated by rapidly expanding combustion reaction acts on the piston-top surface and pushes it into the cylinder. This force is harnessed through designed movement of the connecting rod, which acts on the crankshaft to produce useful work. This principle has to its credit, a higher efficiency, better fuel economy and ease of burning without detonation or knocking, greater expansion ratio leading to more power output, over its rival; - the spark ignition engine! (Stone R. , 1999; Heywood, 1988). However despite these benefits, the exhaust emissions arising from diesel engines are not friendly to the environment. The emissions '*pollutes and defiles'* the atmospheric environment and therefore requires '*restitution*' from the hands of men that have produced the engine. The regulated emissions include carbon monoxide (CO), unburnt hydrocarbons (UHC), nitrogen Oxides (NO_x) and particulate matter (PM). They pose serious implications for human health and of concern in this study is PM which has been classified as carcinogen to humans (EPA, 2002; HEI, 2010). As efforts to mitigate these emissions through design improvements approach their limits due to very stringent regulations, focus has

shifted to after-treatment technologies to ensure attainment of the high emission standards as a way of making Biblically prescribed '*restitutions'*.

1.1 Research Motivation

In Africa and with reference to my home country Nigeria, issues of emissions from all manner of combustion devices are still at the lowest ebb. We import large numbers of second-hand automotive products, majority of our diesel engines in the haulage sector belong to the generations of diesel engines almost phased out in Europe and North America. In addition, there is no concerted effort to monitor the emissions deposited to the atmospheric environment as a criterion to certify vehicles plying the roads. The high volume of vehicular traffic in big cities could sometimes be a nightmare as in Figure 1.1. Like many developing nations, our society still grapples with the challenge of managing visible solid wastes and pollution of water resources; with attendant massive cost of health care delivery due to prevalent infections related to dirty environment and poor sanitary habits. The challenges posed by automotive engine exhaust emissions to the atmosphere which involve complex issues that are not yet properly understood in scientific context or the managerial requirements, are not yet of high priority.

A

B

C

Figure 1.1 Vehicle traffic in Lagos City Nigeria [A: Heterogeneous mix of commuter and haulage vehicles on a major road, B: Scene of typical nodal point and market place, C: Fuel haulage vehicles powered by diesel engines near Apapa Wharf]

Many unaccounted deaths associated with stroke, cardiac arrest, respiratory diseases, tumors and cancers are better ascribed to the anger of unseen gods. But these are health problems associated with pollution of the atmospheric environment if only toxicological and epidemiological records are reliably kept and proper statistics deducted from them; with due regards to peoples lifestyles, dwelling locations and working environments (Cantrell, B. K., and Watts, W. F., 1977; Birch, M. E. and Cary, R. A. , 1996; Pronk, A., Coble, J., and Stewart, P. A., 2009, 19). One can imagine the health effects of automotive exhaust emissions to a market woman who sits by a bus-stop every day to do her petty trade, or a motor park tout and a hawker who live by sales made at traffic hold-ups as in Figure 1.1B. The concern about

these situations gave inspirations for fundamental study on engine-out emissions with special interest in particulate matter. This is in order to develop scientific expertise for policy prescriptions that will help towards protection of our atmospheric environment. In this regard, the current efforts of the Federal Environmental Protection Agency could be enhanced by incorporating regulations that restrict and manage exhaust emissions from diverse combustion devices in line with developed economies. In effect governments and institutions in the sub-Saharan Africa can have platform to develop political-will in adopting strategic goals for better mix in energy consumption, thereby become partners to the new world order towards environmental protection. In the US, the state of California has the highest regulatory standards for engine emissions regulated through the Air Resources Board (CARB). However, the Federal Environmental Protection Agency (EPA) enacted the 'Clean Air Act' which is used to regulate emissions within the federal states (Dieselnet, 2014). In Europe, the particle measurement programme (PMP) developed as a complement to the United Nation Economic Commission for Europe (UNECE) was fully implemented through 2009-2014 in all EU states and was later joined by Japan and South Korea (Andersson et al 2007). The zeal to become relevant and competitive in international community has forced China to upgrade national standards based on the European regulations with major cities like Beijing, Shanghai and Guangzhou championing the implementation while the regulations are still watered down at local levels (DieselNet, 2015). India is also copying Europe with about 13 cities currently implementing Euro 4 and proposing this level nationwide by 2017 (DiselNet, 2015). In most African states, some form of regulations may exist statutorily, as copied from colonial relationship of major European countries that shadow automotive businesses; but it is doubtful if it is ever understood, let alone implemented. Although South Africa and Nigeria are showing interest, but the regulation of PM is not yet on the map (Rayne, 2015). Therefore a starting point for African involvement is a sincere humility to understand the issues that are involved through a careful study of scientific principles, measurement devices, and ability to discern and design appropriate control techniques relevant to one's endowment. It is in this context that the research questions could be asked. The first research question to answer is: What is diesel PM? Then, how is it formed during engine combustion? How is it measured? To what regulatory standard can measurement be subjected? How can it be controlled? What are the possible control techniques? Myriads of

questions call for experimental investigation but for the purpose of this report, the study has been designed around some objectives that have helped me to develop a core knowledge base, develop expertise in the design of measurement techniques and the use of measurement devices, and to use the same to carry out investigations on PM regeneration as a way of mitigation. These are as itemised in the next section.

1.2 Aims and Objectives

The aims of this study were to investigate the issues involved in PM measurement and control. Exhaust gas emissions used in the study were generated from the high speed direct injection (HSDI) diesel engine. Central to accurate measurement is the quantitative influence of dilution during sample conditioning; and central to control is the oxidation of trapped PM which is the key to efficient design and regeneration of the DPF. The objectives were therefore structured to include but not limited to the following:

(i) To fundamentally study the nature of diesel engine generated PM and factors that lead to their emissions

(ii) To study the PM measurement techniques and to carry out a series of experimental tests in line with current regulatory protocols and standards

(iii) To study the influence of dilution in PM measurement at various temperatures and ratios or proportions

(iv) To carry out PM oxidation studies relevant to real time soot burn-out during DPF regeneration used in mitigating PM tail pipe emissions from automotive diesel engines

(v) To investigate the effect of blending petro-diesel with biodiesel during soot oxidation

(vi) To study the feasibility of regenerating DPF using available microwave cavity in Electronics and Computer Engineering Laboratory.

These objectives are viewed to cover issues fundamental to PM formation, transport, measurement and control based on what is known of modern diesel engine technology.

1.3 Overview of the Thesis

In considering the above objectives, this thesis reports issues of diesel PM emissions in the following chapters:

Chapter 2

In this chapter, reviews on diesel emissions have been presented as a consequence of engine combustion. The nature of diesel fuel with respect to its physical and chemical properties, diesel engine design, the nature of in-cylinder combustion and the associated exhaust emissions have been reviewed. The in-cylinder combustion process and how it leads to emission of different species has been reported based on the spray combustion model.

Chapter 3

In this chapter, many issues about PM emissions from diesel engines are presented. Although the interest is more in the realm of engine-out processes, the in-cylinder emission processes have been reviewed, along with its nature and composition, as well as transport. This effort highlighted PM as comprising of condensed volatile matter and soot. In this regard, in-cylinder PM has been presented as the ultimate state of composite matter arising from diesel fuel in advanced combustion state at blowdown where lowering of temperature freezes further oxidation reaction. Therefore soot is posited as diesel fuel in intermediate state still possessing energy value in the combustion process, which is erroneously regarded as one of the products of the combustion process like CO_2, H_2O and NOx; and also opened up the implications of its mitigation. As the soot is ejected from the exhaust port (at blowdown), chemical processes cease and complex physio-transport processes and surface adsorption begin. It is this process that shapes the nature of PM emission into the atmospheric environment and its complexity makes measurement effort cumbersome. This led to review of PM transport processes in the exhaust system, in the atmosphere, and in the laboratory. The health effects, issues pertaining to PM measurements especially sample conditioning, the equipment used and their techniques, regulations and the particle measurement programme are all reviewed.

Chapter 4

This chapter reports the experimental facilities available in our engine test cell used in emissions measurements. Concurrent descriptions of the techniques in their use are explained. Essentially, the test engine coupled with eddy-current dynamometer and data acquisition systems are described, the equipment for measuring and analysing different species of exhaust gas are described. These include the AVL smoke meter, the Horiba gas analyser, and the Electrical mobility spectrometer for particulate measurements. Experimental set ups and the methodologies, sampling conditioning, and modifications to the exhaust line as related to particular tests are incorporated to the relevant chapters where the study is reported. The description of tests and methodologies of post-sample processing that involved the use of facilities in other research laboratories are also given in the relevant chapters (7 and 8).

Chapter 5

This chapter reports the initial tests done to characterise the engine performance and the associated exhaust emissions within the range of operating conditions. These include the effect of engine load and speed on emission characteristics, effects of injection parameters on emission characteristics. These have been used to establish baseline characteristics of PM generated for different studies.

Chapter 6

In this chapter, the reports of PM measurements using pre-determined two engine-load operating conditions are presented. One is low load condition that produced PM laden with volatile matter and another is medium load condition that produced PM containing more soot. These were used to study the influence of dilution conditions on PM number concentrations and size distributions. Extended studies were made to investigate the effect of dilution gases on particle number concentrations. The criteria of particle number concentration reduction factor and volatile removal efficiency were used to re-assess dilution ratio as a parameter for dilution measurement. Then the electrical mobility spectrometer (EMS) was adapted to pursue the particle measurement programme’s criteria of two-stage dilution and the set up was also used to compare PM emissions from petro and biodiesels.

Chapter 7

This chapter reports on investigation into the oxidation of PM generated when fuelling on petro-diesel compared to PM generated when 20% and 40% blends of three different biodiesels were used. The samples were collected using a pall quartz tissue filter and the experiment was designed to bear relevance to soot oxidation during DPF regeneration. Assessment was first made on the oxidative reactivity of PM from petro-diesel using three isothermal temperatures. The result compares favourably to other studies reported in literature. Then comparative assessments of soot oxidation as derived from different blends were made using non-isothermal sweeps. These were carried out using a combined thermogravimetric analyser/differential scanning calorimeter (TGA/DSC). Image of the microstructures of the PM samples were taken with high resolution transmission electron microscope (HRTEM).

Chapter 8

In this chapter, report of the efforts to establish the feasible use of microwave power to regenerate diesel particulate filter (DPF) is presented. Trapping of engine generated soot using a DPF has become an established after-treatment technique in modern diesel engine technology. However, the technical problem of occasional burn-out of accumulated soot in the DPF currently constitutes a penalty to the overall engine power economics. The use of microwave power is perceived as a viable option for DPF regeneration due to favourable dielectric properties of silicon carbide material used in making it and the soot proper, to lower energy demands. It was possible to overcome the challenge of using an existing multi-mode microwave cavity and regeneration was achieved. Observations highlight that this approach to DPF regeneration will consume less power compared to electrical resistant heating method. The benefit of using catalysed DPF to lower regeneration temperature was also demonstrated.

Chapter 9

This chapter concludes the thesis and highlights suggestions for further work.

1.4 Contribution to knowledge

The contributions to knowledge from this study are viewed in the way investigations were carried out using systematic and simplified experiments to address issues outlined in the objectives. Original contributions made are in key results presented in chapters 6 to 8 and could be itemised as follows:

i. Investigations on the effect of dilution of PM made use of unique small mixing tube diluter unlike complex and expensive outlays normally used to dilute aerosol. Effort was made to relate particle number measurement to mass estimation by exploring the underlying physics involved in dilution, and this was well correlated. The implication of using mixing and cooling of aerosol to explain the evaluation and behaviour of saturation characteristics of the volatile fractions in the dilution process, unlike mere reference to dilution ratio, has been demonstrated as a key outcome.

ii. Comparison has been made on the influence of air, nitrogen and filtered exhaust as dilution gases on the PM measurement. It shows that air has superior volatile removal efficiency (VRE) at low dilution ratios. This has implications for equipment design in terms of aerosol residence time in the carrier gas before measurement. Similarly the use of VRE and particle number concentration reduction factor (PCRF) as dilution parameters, give extended and better interpretations of aerosol dilution than ordinary dilution ratios.

iii. In addition, a novel set-up was used to pursue two-stage dilution which successfully mimicked the PMP protocol with good and consistent results.

iv. The study demonstrates that use of biodiesel fuel or the blend can reduce soot content of the PM emission and also enhance its oxidation as in many studies. However this study revealed that characteristic oxidation temperatures are similar, only the oxidation time is shorter. This is perceived to be due to the natural faster reactivity of biodiesel due to fuel oxygen and less ordered microstructure of the soot.

v. This study has also demonstrated the potential of using microwave energy to reduce energy requirement for the regeneration of diesel particulate

filter (DPF). This is based on selective absorption of microwave energy by susceptible materials of which the DPF silicon carbide substrate and soot itself are good examples. The novelty here was more on the ability to harness an existing multi-mode microwave cavity designed for another purpose by modifying and adapting it to achieve DPF regeneration. Similarly, it was possible to establish that microwave energy enhances the catalytic activity during regeneration.

CHAPTER 2

DIESEL ENGINE COMBUSTION AND EMISSIONS

2.0 Historical Background

The concept of initiating combustion solely by injecting liquid fuel spray into an enclosed, high pressure-compression-heated air is recognised to have been formally outlined by the German engineer, Dr. Rudolf Diesel (1858-1913). He took a British patent in 1892 where this was described. His early engines were experimented with pulverised coal, before describing the final prototype that worked on ideal Carnot cycle which could burn variety of fuels, whether in solid, liquid and gaseous states. However it was difficult to produce a reliable engine until 1897 when he adopted air injection to atomize liquid fuel and initiated combustion by utilizing high temperature compressed air. Coincidentally, a contemporary English engineer Herbert Akroyd-Stuart took out several patents between 1885 and 1890 where he described improvements in oil engines. He described a version of 'airless' injection of liquid fuel that was heated externally in a separate chamber to burn in air charge with lower compression ratio (compared to that of Diesel) towards the end of compression stroke. Although Akroyd-Stuart engine was completed ahead of Diesel's prototype, Rudolf Diesel was given the credit for describing the fundamental concepts of high pressure compression ignition engines. Modern CI engine could be said to have evolved from combination of both concepts described by Diesel and Akroyd-Stuart (Owen, K., and Coley, T., 1995). Over the years, the diesel engine technology has undergone lots of optimised improvements to become an indispensable power unit employed in the automotive, aviation, and marine propulsions; and for host of industrial appliances.

2.1 Basic operating principles of CI engine

The CI engine has undergone lots of improvements compared to that patented by Rudolf Diesel, but the principle remains essentially same. The geometry used to describe the compression ignition engine is shown in Figure 2.1. It involves intake of air charge into the engine cylinder, air compression by the piston, injection of finely-atomised fuel into the compressed air, ignition and burning of fuel-air mixture, rapid expansion of the reacting gases and expulsion of the burnt gaseous products. These

processes are completed in four piston-strokes in each cylinder. (Heywood, 1988; Stone, 1999; Pundir, 2002). The four strokes are accomplished in two crankshaft revolutions described as follows:

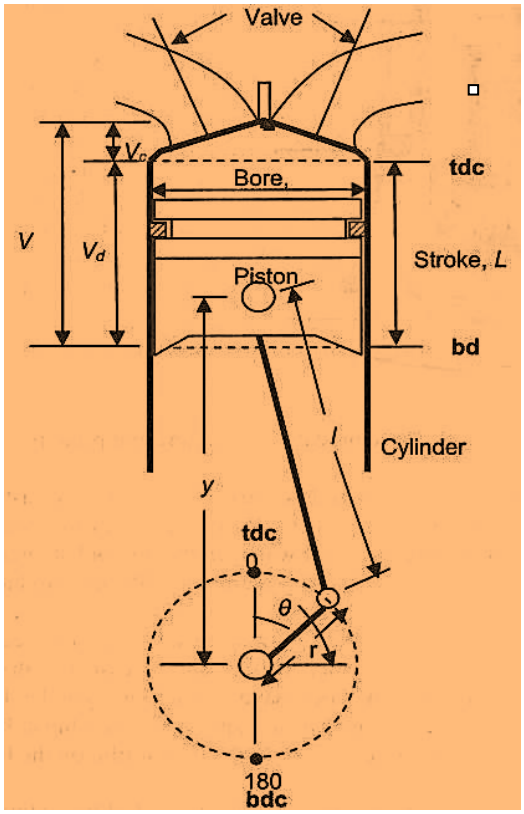

Figure 2.1 Basic Geometry of a compression ignition engine (Pundir, 2002)

(i) ***Intake stroke*:** This starts with the piston moving down from the top dead centre (*tdc*) to the bottom dead centre (*bdc*) while the intake valve is open and the exhaust valve is closed. Technically, the intake valve opens shortly before the tdc and closes after the bdc thereby drawing fresh mass of filtered air into the cylinder with higher density compared to burnt gases thereby displacing it from below and enhance scavenging of the cylinder of exhaust gases from previous cycle.

(ii) ***Compression stroke*:** With the intake and exhaust valves closed and the piston moving up from bdc to tdc, the air inside the cylinder is compressed to a small fraction of the total cylinder volume. As the piston approaches the *tdc*, diesel fuel is injected into the hot compressed air at a

temperature sufficiently high to ignite the fuel. The fuel burns and releases high heat and high pressure energy about the tdc.

(iii) ***The Power or Expansion stroke*:** The expansion of high temperature and pressure burning gases pushes the piston down from the *tdc* to *bdc* giving the useful power stroke. This is also called the work stroke because the high pressure of the expanding gases act on top of the piston surface, and impacts the force that rotates the engine crankshaft, producing work. During this process, both valves are theoretically closed between the centres, but practically the exhaust valve is timed to open some degrees before bdc to initiate pressure drop inside the cylinder which allows burnt gases to escape.

(iv) ***Exhaust stroke*:** The upward movement of the piston again from *bdc* to *tdc* pushes out the burnt gases through the fully open exhaust valve. As the piston approaches the *tdc* the intake valve also opens. This allows admission of fresh air whose density is greater than that of burnt gases into the cylinder, displace them and fill up the cylinder again. The pressure drop created by early opening of the exhaust valve also reduces the work done by the piston in pushing out the burnt gases. The cycle then continues.

2.2 Engine design considerations relevant to emissions reduction

The CI engine is a core heat engine designed to give maximum power output at minimal fuel consumption. Although great improvements have been made leading to engine downsizing, pollutant emissions still pose challenge as design improvement that reduces one pollutant tends to aggravates another. This has led to the development of technologies that control emissions to comply with regulations. Key design parameters normally considered for improvements towards reduction of emissions include:

Air Induction:

The air induction system consists of air filter, ducts, intake manifold, intake port and intake valve designs. The air charge induced into the cylinder is related to power output, quality of combustion and exhaust emission during a cycle. Cylinder displacement is fixed based on engine geometry; therefore naturally aspirated capacity is constrained. Design improvement to increase induction capacity is by compressing air to higher density prior to introduction into the cylinder. This is referred to as *boosting* or *supercharging*. Typical method of supercharging diesel engines is by allowing a portion of the escaping exhaust gases at high thermal and kinetic energy levels to flow and expand through turbine blades. The power imparted on the shaft is used to drive a centrifugal compressor which is axially connected on the same turbine shaft to compress more air into the cylinder. This is known as *turbocharging* and the increased air charge boosts the power output from the fixed cylinder volume. Optimal design of turbochargers has increased power-to-weight ratio, improved engine efficiency, lowered exhaust emission and general engine downsizing (Heywood, 1988; Majewski, W. A. and Khair, M. K., 2006; Pesiridis, 2014; Stone R. , 1999).

Fuel injection Equipment:

Fuel injection equipment systems supply finely atomised fuel sprays into the combustion chamber at precisely controlled time. Types of injection systems include *pump-line-nozzle* (P_L_N), *unit pump, unit injector* and *common rail injection* systems, all support high power output, high fuel economy and reduced emissions. Modern engine fuel injection systems are controlled by dedicated electronics giving rise to precise fuel spray at high pressures. Adoption of direct injection concept in four-stroke diesel engines with fuel spray profiles that match engine combustion aerodynamics have greatly improved the exhaust emissions. Many manufacturers especially for heavy duty diesel engines have developed proprietary electronic fuel injection systems relevant to their total engine management system. The variety of fuel injection systems classified according to their actuation systems are summarised in Figure 2.2.

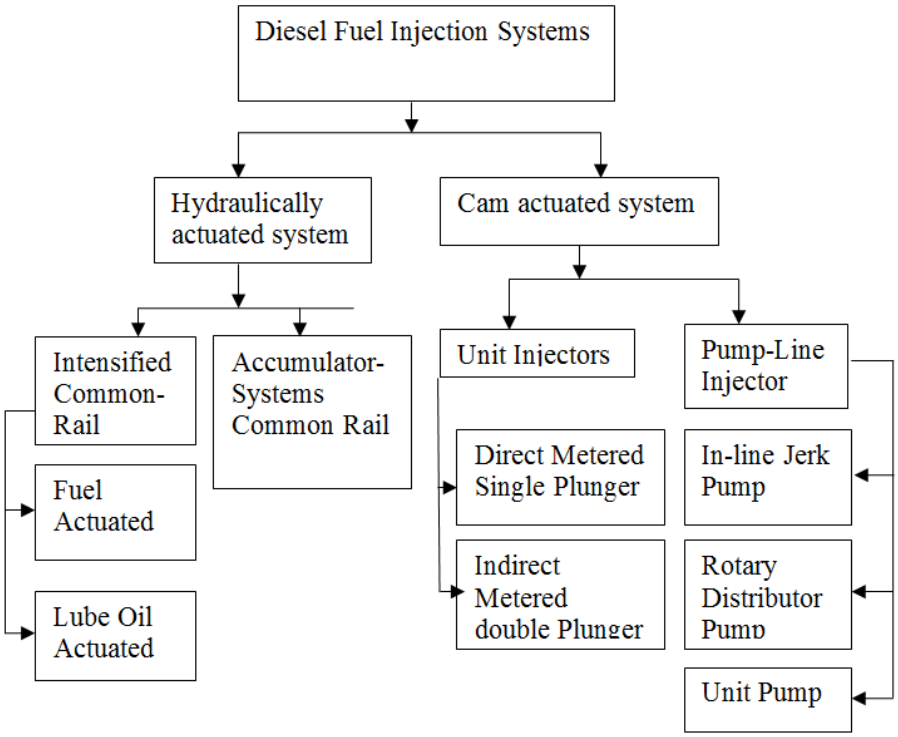

Figure 2.2 Classification of diesel engine fuel injection systems (Pundir, 2002)

Gas exchange Mechanism:

The changes that occur in in-cylinder pressure, volume and mixture composition are used to evaluate events describing the operation of the engine based on the four stroke principle. It is highly influenced by the gas exchange mechanism governed by valve actuations. Shown in Figure 2.3 are valve actuation events in a typical pressure-volume diagram of a four stroke naturally aspirated diesel engine. The sequence of valve actuations are numbered 1 to 4 in tandem with the basic geometry outlined in Figure 2.1.

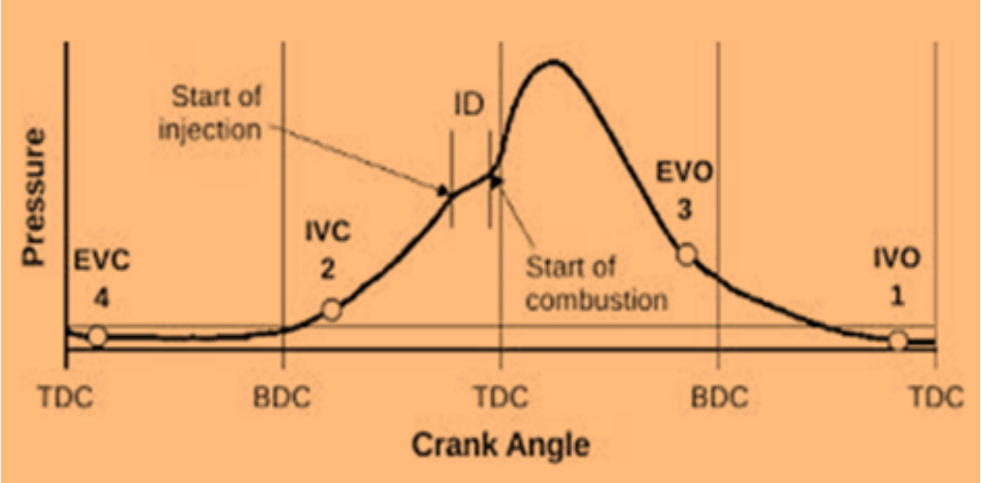

Figure 2.3 In-cylinder pressure-crank angle diagram showing history and sequence of valve actuations and processes in four stroke CI engine. [IVO: Intake valve open, IVC: Intake valve closure; EVO: Exhaust valve open; EVC: Exhaust valve closure; TDC: Top dead centre; BDC: Bottom dead centre] (Majewski, W. A. and Khair, M. K., 2006)

Point 1 indicates intake valve opening, 2 is intake valve closure, 3 is exhaust opening and 4 gives exhaust valve closure. A momentary period of valve overlap occurs between points 1 and 4 when both valves are open expressed in degrees of crank angle. This period is significant to the engine performance and emission characteristics because the volumetric efficiency, particularly in the absence of boosting depends on the in-cylinder filling during this period. As valve openings and closures are not instantaneous, the timing is designed to ensure that both are fully open when the benefit of maximum pressure difference will cause the working fluid to flow across them. In current designs the poppet valves are located in overhead position in the cylinder head. The geometric profile of intake manifold, intake port and the poppet valves are designed to enhance air breathing capacity of the engine and also to impact motion like swirl and/or squish to the bulk flow into the cylinder. The optimisation of this parameter is very significant to the level of exhaust emissions.

Combustion Chamber/In-cylinder flow Design:

The air utilisation during combustion process is dependent on how well it is pre-mixed with fuel sprays prior to combustion or accessible during diffusion burning. Engine combustion chamber is designed to complement the effect of fuel spray profile while the air motion enhances mixing/burning process. These determine the

level of combustion reaction and ultimate exhaust emission. In modern *high speed direct injection* (HSDI) engines, the induction system is designed to provide initial air swirl, complemented by the chamber design which also provides squish area to enhance intensity of air motion and the desired level of turbulence.

Heat Transfer:

The heat transfer considerations in the engine environment are complicated as all modes are involved at the combustion chamber. Preservation of the structural integrity and geometric profiles of the mating surfaces necessitates removal of heat generated during combustion, particularly from the hottest regions. Engine heat transfer involves use of cooling water jackets around the regions with highest heat fluxes; the hot water is then pumped to the radiator where heat is lost to ambient environment by forced convection. Some low duty designs adopt the use of air cooling as it flows past an increased surface area created by fins around the cylinder head and/or wall linings. The engine efficiency, performance and emissions are greatly affected by heat transfer as such; it is optimised in order to retain heat required to maintain normal engine working temperature and the excess transferred to the cooling medium. This explains the inefficiency usually encountered during cold starting when the work transfer to the piston is reduced as high heat transfer occurs to the chamber walls and other working parts for warming up period. Similarly, during this transient period, heat transfer affects the process of formation gaseous and particulate matter emissions both within the cylinder and exhaust line where post combustion reactions occur (Majewski, W. A. and Khair, M. K., 2006; Heywood, 1988).

Engine Application:

Diesel engines are installed on motor vehicles, agricultural machines, construction equipment, industrial applications as in compressor/pump drives and in stationary power generating sets. In all these applications light, medium and heavy duty versions are produced. The design of individual components, units and the system integration to build ‘the engine’ is a matter of compromise to achieve relative engineering issues involving the nature of fuel, the power-to-weight ratio, noise and

engine-out emissions. In most cases, legislations and market forces dictate compromises made.

2.3 Definitions of Performance parameters

Besides engine efficiency, its reliability, durability, operating cost as determinants of return on investment are also criteria for assessment. The emissions should be eco-friendly and within legislation. Technical performance assessments are usually described with geometric and thermodynamic parameters. The chemical energy in the fuel based on the calorific value, the thermal and kinetic energy level of the air mass induced, give baseline value of energy input to the system, while the mechanical work output and dissipated thermal energy give the output from the system. The useful work output obtained after the inevitable losses is the measure of the efficiency of the work conversion process. The parameters used in describing the performance of an engine are defined as follows:

2.3.1 Geometric parameters

With reference to figure 2.1, the geometric parameters used in describing the engine are the stroke, L; the bore, B; the connecting rod length, l and the crank radius, r. As piston reciprocates inside the cylinder, it changes the displacement volume. When the piston is at top most position, the crank position is called *top dead centre (tdc)* and when at the bottom position, it is referred to as *bottom dead centre (bdc).* The cylinder volume is maximal at *bdc*, while it is minimal at *tdc*. The minimal volume is termed *clearance volume* V_c, the difference between the minimum and maximum volume is the *swept volume* V_d. The ratio between the swept volume and the clearance volume is the *compression ratio* r_c.

2.3.2 Input parameters: Air and Fuel

The major constituents of matter entering the engine system are fuel and air. Their controlled reaction in the enclosed cylinder forms the basis of the thermodynamic analysis. Terms used to describe their consumption rates are:

Air-Fuel ratio (A/F) and Fuel-Air ratio (F/A):

These terms are used to define the ratio of mass of air to fuel or fuel to air respectively during typical engine combustion cycle.

$$\frac{A}{F} = \frac{\dot{m}_a}{\dot{m}_f} = \frac{m_a}{m_f} \tag{2.1}$$

$$\frac{F}{A} = \frac{\dot{m}_f}{\dot{m}_a} = \frac{m_f}{m_a} = \frac{1}{A/F} \tag{2.2}$$

The *stoichiometric* air-fuel ratio $(A/F)_s$ is the chemically correct air-fuel proportion that will completely burn to yield only water, carbon dioxide and nitrogen. Details of these ratios are further explained in section 2.5.3

Specific Fuel Consumption (sfc):

This is the mass of fuel consumed per unit power output as determined during engine testing. In engine research, it is usual to measure the rate of fuel consumption in mass flow rate $\dot{m}_f$ (mass flow per unit time) but, the *sfc* gives a measure of how efficiently the engine uses fuel to produce work. When evaluated in terms of indicted power, the term is qualified as *indicated specific fuel consumption (isfc)* but when evaluated as fuel consumed for the engine output to overcome a unit load using dynamometer (brake) testing, it is qualified as *brake specific fuel consumption (bsfc).*

$$isfc = \frac{Fuel\ consumption\ per\ unit\ time}{Indicated\ power\ output} \tag{2.3}$$

$$bsfc = \frac{Fuel\ consumption\ per\ unit\ time}{Brake\ power\ output} \tag{2.4}$$

This is with units:

$$sfc\ (mg/J) = \frac{\dot{m}_f(g/s)}{P(kW)}$$

Volumetric Efficiency (η_v):

Volumetric efficiency measures the effectiveness of the induction process during engine operation. It is the ratio of the inducted mass of air into the engine cylinder to the theoretical mass of air in the displacement volume of the cylinder at inlet air conditions.

2.3.3 Output parameters

Power output:

The power output from an engine sometimes called rated power is evaluated using the maximum torque at any given speed. As the fundamental purpose of engine is to produce work, and power is defined as rate of doing work, engine testing technique has been devised through the use of a 'brake' or 'resistance' to engine power called dynamometer, which measures engine power in terms of torque output at a given speed. Therefore power delivered to or absorbed by the dynamometer is referred to as *'Brake'* power and defined as product of torque and angular speed.

$$P = 2\pi NT \qquad (2.5)$$

Where N is the crankshaft rotational speed, T is torque and π is a constant.

Indicated work per cycle:

This is evaluated from direct impact of gas pressure on the cylinder head surface over an operating cycle. It is theoretically obtained by integration of the cylinder pressure curve over a given area in a typical pressure-volume plot during a combustion cycle. The net indicated work per cycle is determined by taking the difference between the positive work output and the pumping work, as well as the frictional losses, over the four-stroke cycle.

Mechanical efficiency:

This term is used to express the ratio of useful power output from the engine after deduction of the inevitable power losses due to pumping work and frictional effects. From the earlier definitions, the mathematical expression is:

$$Mech.efficiency\ (\eta_{mech}) = Brake\ Power\ (P_b)\ /Indicated\ Power\ (P_i) \qquad 2.6$$

Mean Effective Pressure (mep):

This expresses the relative performance of engine in terms of work output irrespective of the size. The work output is calculated by the cylinder pressure and the displacement volume, therefore engine power and torque are dependent on size. However as the gas pressure exerted on the piston varies from cycle to cycle, the mean effective pressure is adopted as relative measure of work output independent of the engine dimensions. The terms *'brake' or 'indicated'* are used to modify the pressure as *brake or indicated mean effective pressure (bmep, imep)* depending on how power is being calculated.

2.4 The Diesel Fuel

Diesel fuels are complex mixtures of hydrocarbons distilled from crude petroleum at the temperature range of 150 to 380^{o}C. Their nature and combustion characteristics have been fundamental to the design and improvement of diesel engine. Key properties used to express the quality of diesel fuel are based on testing methods of 'Standards' authorities like the British Standards (BS), American Society for Testing and Material (ASTM) and International Organisation for Standards (ISO).

2.4.1 The nature and properties of diesel fuel

Crude petroleum from various parts of the globe differs in hydrocarbon constituents, therefore optimal techniques are used to maximise refinery yields. Current diesel fuels are composed of fractions obtained from straight runs as well as cracking. In effect, paraffins, olefins, naphthenes, iso-paraffins and aromatic fractions are present in a typical diesel fuel in varying proportions. The structure of each constituent hydrocarbon is determined by carbon and hydrogen atoms that make up its molecule and the type of bond. Fuel molecular structure and size determine their physical properties and combustion characteristics (Owen, K. and Coley, T., 1995; Majewski, W. A. and Khair, M. K., 2006; BS, 2013; Pundir, 2002). Some of the properties relevant to combustion and emissions from engines include:

Cetane number (CN):

The cetane number characterizes diesel fuel ignition quality. The ignition qualities of two reference diesel fuels are used to evaluate tendency to ignite when sprayed into hot compressed air. These are: *hepta-methyl nonane* (HMN) with a low ignition quality assigned with a reference number of 15 and *cetane (n-hexadecane, n-$C_{16}H_{34}$)* which has a very high ignition quality with assigned reference number of 100. The CN is evaluated by comparing the ignition quality of any fuel with that of a reference fuel on a test engine. Test with variable compression ratio Cooperative Fuel Research (CFR) engine using the ASTM D613 is well recognised method. The CN is evaluated as (Majewski, W. A. and Khair, M. K., 2006):

$$CN = \%(n-cetane) + 0.15\ (\%\ HMN) \qquad (2.7)$$

Fuels with high proportion of aromatic components derived majorly from cracking are low in CN values, while those with higher paraffinic content normally obtained from straight runs are high in CN values. Diesel engines operate well with CN values between of 40 to 55, but modern HSDI diesel engines use fuels with CN values over 50 for optimum performance.

Cetane Index (CI):

Cetane Index is a correlated quality value of diesel fuel evaluated from its density and volatility properties in effort to estimate the CN. It is specified as a check-value for the quality of base fuels in order to determine the volume of additives that could be used to improve fuel quality.

Density:

Diesel Fuel density is simply its mass measured per unit volume. It is strongly interrelated with other physical properties like viscosity and volatility. Density inherently affects the metering and injection characteristics of the fuel supply system thereby influencing the engine power output and emissions especially PM and NO_x. It is important to have low fluctuation in fuel density and it is specified within narrow limits in modern HSDI engines. Current specification within the EU at 15^{o}C varies from 820.0 to 845.0 kg/m^3.

Volatility:

This is a property of diesel fuel that expresses the tendency of component fractions to boil at various temperatures. It is of significance in fuel distillation characteristics as it depends on the fractional chemical composition. Therefore other properties like density, viscosity and cetane number are also influenced by it. Good blend of diesel fuel possess optimal proportions of fractions that boil at low temperatures to enhance easy cold starting and quick warm up; as well as fractions that boil later to produce useful power at peak combustion. Too low or too high volatility of fuel will make it difficult to control combustion, and increases exhaust emission.

Viscosity:

This property of fuel relates to its tendency to resist flow. It is affected by engine operating temperature, being low at high temperature and high at low temperature and could therefore affect the operation of fuel delivery and injection system. Diesel fuel viscosity is usually specified around $40^{o}C$; fuels of viscosity values higher than 5.5 centistokes at this temperature will operate better for low speed engines.

Lubricity:

Lubricity is the property of diesel fuel that describes its lubricating quality. Modern trends in diesel fuel processing aimed at reducing the sulphur content reduce the lubricating quality, and this is usually compensated for by use of fuel additives. It is necessary to uphold the lubricity of fuels in order to protect injection pumps and injectors from wear and untimely failure in operation.

Flash point:

This is the temperature fuel will be heated to give enough vapour whose combination with the ambient air will support combustion if ignition source is available. Flash point of pure diesel fuels has less significance on its auto ignition and combustion characteristics compared to gasoline that has low flash point. However it provides criterion to assess fuel safety for storage and during shipping operations as small fraction of gasoline in diesel can greatly lower its flash point and cause fire hazard.

Sulphur content:

Sulphur occurs naturally in crude petroleum in various amounts depending on its origin. Therefore diesel fuel contains sulphur, which is good for fuel lubricity but impacts negatively on exhaust emissions. Modern refinery technology aim at eliminating sulphur in diesel fuel as it causes deposits in combustion chamber, wear of engine moving parts, corrosion of exhaust pipe; sulphur dioxide and sulphate particulate emissions. Currently, additives are used to compensate for fuel lubricity as this property is destroyed in process of removing sulphur.

Relationship between fuel properties and diesel engine emissions

According to the British Standard BS EN 590:2013, the general requirements a for automotive diesel fuel are shown in Table 1 (BS, 2013)

Table 2.1 Diesel fuel Specifications in UK and EU

Property	Unit	Limits	
		Minimum	Maximum
Cetane number		51.0	-
Cetane index		46.0	-
Density at 15^{o}C	kg/m^{3}	820.0	845.0
Distillation			
%(V/V) recovered at 250^{o}C	*%(V/V)*		< 65
%(V/V) recovered at 350^{o}C	*%(V/V)*	85	
95 % (V/V) recovered at	^{o}C		360
Viscosity at 40 ^{o}C	mm^{2}/s	2.00	4.50
Lubricity, corrected to wear scar diameter(wsd 1.4) at 60^{o}	μm	-	460
Flash point	^{o}C	Above 55.0	-
Sulphur content	mg/kg	-	10.0

The properties of diesel fuel highlighted above have fundamental influences on engine combustion and ultimate emissions. However it is difficult to isolate specific properties as they are interrelated. Typical example is the relationship between

density of fuel, cetane number and aromatic fraction content. Diesel blends that are low in cetane number have high density and usually contain high aromatic fractions. To decouple each of these properties and study their emission characteristics is quite cumbersome. The design of engine for low or high duty application has influence on the kind of emissions arising from it. Similarly, the type of technology used in fuel metering and control, influences combustion and exhaust emission. In emission testing for certification, test cycles differ and the techniques to be adopted are prescribed by the regulatory body. Considerations are generally made with respect to influence of fuel properties on emission characteristics. Sulphur content appears to be one exception as its influence on particulate matter emission is well known and mitigated by use of additives. Key exhaust emissions, the HC, CO, NO_x and PM are all affected by diesel fuel properties.

2.4.2 Diesel combustion phases in the engine

Combustion of diesel fuel is a mere oxidation process during which the chemical energy stored in the fuel is released. Oxygen, a freely occurring element in the air is central to this process thereby making air combination with fuel the central influence on the combustion phenomenon. Characteristically, fuel is injected into the combustion chamber in liquid form; therefore the approach to mixture preparation dictates the combustion phases in the engine. With reference to Figure 2.4 heat release diagram obtained from diesel engine is used to describe the combustion process as follows.

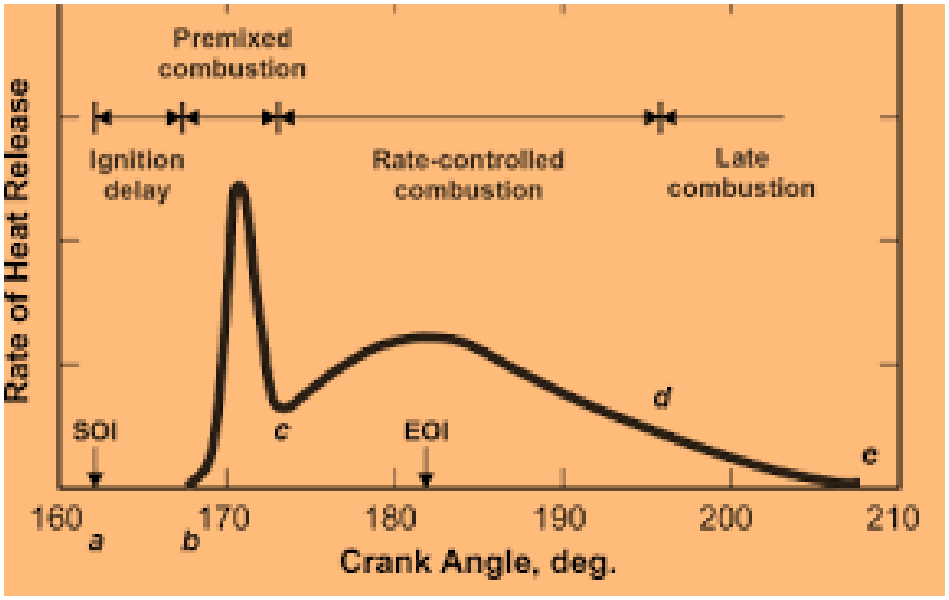

Figure 2.4 Typical DI engine Rate of Heat Release Diagram (Heywood, 1988)

(i) ***The ignition delay period (ab):***

This refers to the time fuel injection starts till when noticeable pressure rise appear on cylinder pressure trace. Essentially, it is a period of mixture preparation because the fuel undergoes both physical and chemical processes. Physical processes include fuel evaporation and air entrainment, and also mixing to form a combustible charge. Concurrent auto-accelerating chemical reactions occur and reach explosive level regarded as start of combustion *(b)* which gives the noticeable pressure rise. The reaction rate is influenced by the fuel composition or quality, the mixing pressure and temperature. The period of ignition delay has effect on the entire combustion process and ultimate level of exhaust emissions.

(ii) ***Kinetic or Premixed Combustion (bc):***

Portions of the fuel spray into compressed hot air are able to vaporise during the ignition delay period and form the initial *premixed fraction.* Combustion of this premixed fraction leads to high heat release rate and consequently leads to initial-sudden, cylinder pressure-rise. The rate of reaction is controlled by chemical kinetics and the consequent steep peak rise in the heat release profile is characteristic of this phase due to burning of previously evaporated fuel mixed with air.

(iii) ***Diffusion Burning or mixture controlled combustion phase (cd):***

The rapid combustion in the kinetic phase leads to fast burn out of premixed charge during which time; in-cylinder temperature is high. The rate of chemical kinetics is faster than the physical processes could keep pace; therefore combustion rate is controlled by the rate at which fuel species diffuse and mix with air. Since time is limited for the physical processes to take place, high temperature fuel pyrolysis leads to formation of soot. However soot burnt-out occurs in the presence of oxygen at the high temperature regime. Inevitably, not all the soot will be oxidised during this phase and the remaining are carried over as emissions.

(iv) ***Late combustion phase (de):***

In this phase, heat release rate is low as small fraction of fuel remains for burning and temperature falls due to further expansion of the piston into the cylinder. However, fuel-rich combustion products burns out with more mixing and as the charge become less homogeneous in space. The rapid fall in temperature slows down reaction to extinction and the unburnt fuel and soot are carried out as emissions.

2.5 Factors influencing diesel engine combustion and emissions

Many factors affect engine combustion efficiency, and of great interest in diesel engine emission is the tendency to produce soot. These factors include fuel injection pressure, injection timing, ignition delay, fuel atomisation, spray-configuration, technique of supplying air, swirl and level of turbulence (Khan, 1969). They are related to the way fuel is introduced, mixed and ignited in the chamber to achieve good air utilisation in the combustion process; and also inherently depend on the very nature and properties of diesel fuel. It is therefore convenient to group them as factors due to the fuel injection and spray; and factors due to in-cylinder flows. In addition there is challenge of heat transfer, which has proved to be a complex phenomenon in the engine system. Therefore engine designs and optimisations have centred on these issues as each factor poses strong influence in the overall engine

performance and emission. Modern controls of practical engine operations are integrated as engine management system in effort to optimise performance.

2.5.1Factors of Fuel Injection and Spray

All injection systems are integrated to meter and timely deliver fuel towards achievement of good spray penetration and atomisation in the hot swirling air. The extent to which these functions are met, determine the combustion efficiency, power output and exhaust emissions quality. Different types of diesel injection systems can be categorised as: Pump-line-nozzles, Unit injectors and Common-rail injection systems. Their complexities in designs and operations are not part this write-up but, each system has unique benefits that provide criteria for describing the engine performance in their respective applications. In order to meet the engine operating demands, the relevance of injection factors towards engine emissions are as follows:

Injection Pressure

All diesel fuel injection equipment (FIE) systems are high pressure units. Fuel lifted from the tank by the lift pump to the high pressure pump, is pressurised and delivered to the injector nozzles. High injection pressures have been used to reduce sooting tendency due to increased density of carbon atoms at elevated pressure (Henein, 1976). It has been explained that pressure increases the rate of formation of polycyclic aromatic hydrocarbons (PAHs) and soot (Mansurov, 2005); which at high temperatures, are oxidised to carbon monoxide CO and carbon dioxide CO2, meaning better combustion due to faster soot burn-out (Pickett, L. M. and Siebers, D. L., 2004). This is attributed to improved contact of the fuel species during mixing as droplets sprayed at high pressure are finer and offer deeper penetration (Pierpont, D. A. and Reitz, R. D., 1995; Wakisaka, Y. and Azetsu, A., 2002; Boggavarapu, P. and Singh, S., 2011). The deeper penetration implies increased velocity of fuel jet and fuel lift-off length which enhances better air entrainment. Therefore more stoichiometric proportions are achieved faster during mixing-controlled regime, which prevents soot-forming reactions along the plume stem (Tree, D. R. and Svensson, K. I., 2007).

Injection Scheduling

Injection scheduling implies injecting a given fuel quantity at required time. This design factor could be in single or multiple schemes to match engine duty. Timing and quantity supply could alter the constituents of exhaust emission. Advancing the injection timing prolongs ignition delay which favours premixed phase of combustion as air-fuel mixing is enhanced (Nwafor, O.M. I., Rice, G., and Ogbonna, A. I., 2000). This condition reduces particulate emission while promoting nitrogen oxides (NOx). However, piston bowel geometry could alter the impingement of liquid fuel on the wall (Pickett, L. M. and Lopez, J. J., 2005). For a given bowel shape, retarding the injection will lead to increased production of particulates and less NOx due to inadequate mixing and this leads to the well-known trade-off for particulates and NOx in diesel engine combustion and emissions for calibration purposes (Mansurov, 2005; Tree, D. R. and Svensson K. I., 2007; Eastwood P. , 2008). Reduction in soot has been achieved through post-injection technique, where the FIE is timed to give a short fuel injection and afterwards, a longer main injection. It has been attributed to enhanced fuel-air mixing and increase in temperature (Bobba, M., Musculus, M.,and Neel, W., 2010; O'Connor, J. and Musculus M, 2013), injection duration and dwell effects (Dantes et al 2007; O'Connor, J. and Musculus M, 2013); as interaction between the post-injection and soot from main injection is the driver of soot reduction mechanism (O'Connor, J. and Musculus, M., 2014).

Injection Spray

The fuel spray profile in the combustion chamber is determined by the cumulative effects of injection pressure; the geometry, number and orientation of the nozzle holes; the geometry of the piston bowl and the in-cylinder flows (Majewski, W. A. and Khair, M. K., 2006). The degree of its atomisation is determined by the injection pressure that impacted the transport energy; penetration is related to the pressure as well as the nozzle-hole geometry which shapes the profile while angular orientation dictates the direction. The degree of air utilisation is strongly dependent on the spray profile because it determines fuel accessibility to air. The small differential pressure towards the end of injection leaves large particles called '*spray tail'* during the last part of the spray. Similarly, most injection systems produce secondary injection at high loads. These fuel parcels are significant contributors to exhaust emissions as

there is hardly enough time for normal burning process to take place; therefore they contribute to emission of particulate matter or could best be oxidised to CO.

2.5.2Factors of In-cylinder flows

The way air is channelled to flow inside the cylinder of diesel engine is important for adequate fuel-air mixing and to sustain combustion processes. It flows down the cylinder in axial swirl. In most heavy duty engines, power output is increased through boosting or supercharging.

Swirl and Chamber Design

Swirl is the ordered flow pattern about the cylinder axis created by introduction of properly oriented intake charge with angular momentum through the ducts. The main types of duct orientations in common use include; the helical, tangential and filling ports. The helical port design enhances better mixing process due to its geometry that restricts major part of the flow to rotate around the valve stem. Therefore the bulk mass of gas is forced into the combustion chamber according to desired swirl direction but with some pressure loss Figure 2.5. Tangential port gives better breathing but less mixing quality due to tangential orientation to the combustion chamber, it generates high swirl but at moderate flow. Filling port design is utilised in very low flow resistance intake ports guided on upright position in operation.

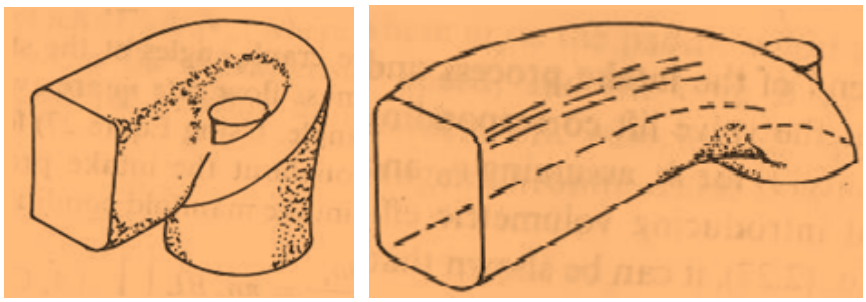

(A) (B)

(B) Figure 2.5 Types of Swirl generating inlet ports (A) helical (B) Tangential (Heywood, 1988)

The swirl impacted during charge intake usually persists through the compression, combustion and expansion periods but is reduced in combustion chambers with bowl-in-piston design. Matching of swirl motion with other engine operating

parameters is desirable for improved engine performance and emissions. Over swirl or under swirl will produce more soot either way, therefore careful optimisation is required to suit design specifics (Eastwood P. , 2008; Mehta, P. S., and Tamma, B., 1998; Kook et al 2006; Zhu, Y., Zhao, H., and Ladommatos, N., 2003).

Supercharging or Boosting

The fixed geometries of the engine induction system comprising of air filter, inlet ducts, manifold, port and valves; as well as their frictional resistances pose limitations to the quantity of air that could be naturally inducted into the engine cylinder. This has implication for power output and quality of exhaust emissions. '*Supercharging or boosting'* is a technique that compresses more air charge into the cylinder to increase power output, improve combustion and emission quality. Boosted air charge raises the density before introduction to the engine. The devices used for compression are grouped into three *superchargers, turbochargers* and *wave superchargers*.

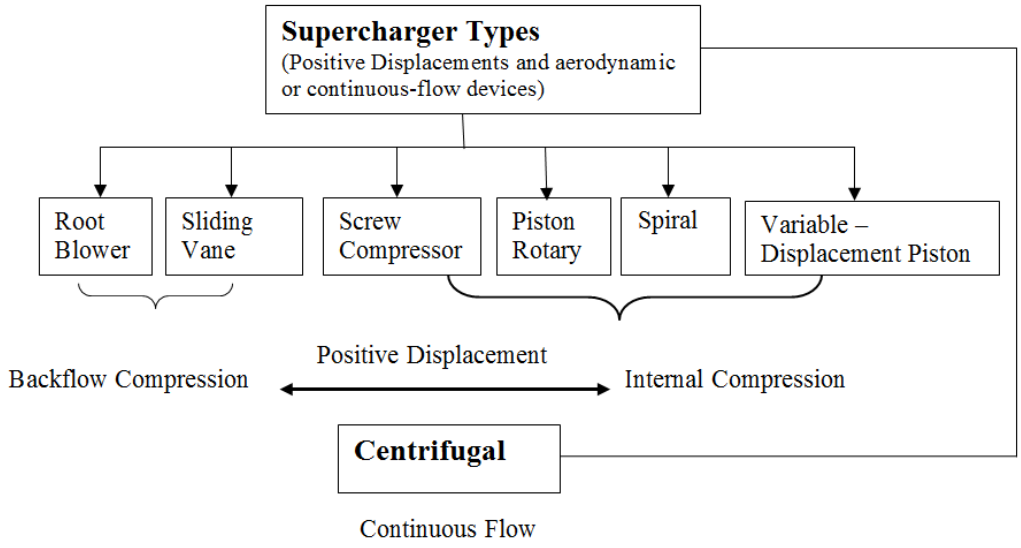

Figure 2.6 Types of superchargers (Majewski, W. A. and Khair, M. K., 2006)

Superchargers:

These are external air compressors primed by part of the engine generated power to charge the air pressure and raise its density before channelling it into the cylinder.

Common types of superchargers are positive displacement devices that deliver a given amount of air per revolution. Their designs perspectives differ as shown in Figure 2.6.

Turbochargers:

These make use of energy recovered from the exhaust flow to drive a turbine that primes the compressor. Turbochargers are commonly used in diesel engines employed in automotive and medium duty industrial applications as well as stationary engines. The axial-flow turbine is located on the flow path of hot exhaust gases with recoverable heat energy at high pressure. The energy impacted on the turbine blades by the expanding gases, turns the shaft onto which a radial-flow compressor is coupled at the other end. The compressor draws in ambient air, raises the pressure and temperature which reduces its density. In heavy duty applications, an inter-cooler is used to cool the compressed air and re-compressed it in another stage(s) before channelling it to the engine cylinder; thereby increase the density and pressure of air further.

Wave supercharger:

This combines the technology of supercharger and turbocharger. The principle of operation is based on the use of pressure wave from the pulse of exhaust gas flowing at higher energy level to act on stream of filtered air in a channel met within a given volume. The energy of the exhaust flow impacts potential energy that accelerates the flow of the filtered air to the inlet port. The time of impact is only a fraction of a second otherwise, mixing will occur which will dilute the freshness of the intake air.

Implications of engine boosting

The turbocharger has become synonymous with supercharging in automotive applications. Modern turbochargers can exceed the speed of 150,000rpm which is not dependent on engine speed but on the net power produced by the exhaust driven turbine utilised to drive the compressor. Matching of turbocharger with the engine requires careful optimisation to balance its performance with engine duty. In diesel engines turbocharging has become essential for performance improvement through better engine combustion and fuel economy. By implication, it has led to reduction in emission of the carbonaceous particulate matter (Karabektas, 2009; Hofeldt, D. and

Chen, G.,, 1996; Kolmanovsky, 1999; Khair, 1998; Majewski, W. A. and Khair, M. K., 2006)

2.5.3 Factors of Fuel-air thermo-chemistry

The combustion of fuel-air mixture is central to generation of power and emissions from the engine. In the diesel engine, it is a complicated event due to partly premixed, and majorly, unsteady-turbulent diffusion process encountered in vaporization of liquid fuel and mixing of the fuel and air in a very short time. As highlighted in section 2.4.1, diesel fuels contain different fractions of alkyl and aromatic components and fuel combustion mechanisms depend on the molecular structures of different species. These structures are based on the intra-molecular carbon bonds that may be single, double or triple bonds; and straight, branched or ringed chains. They determine the combustion characteristics associated with diesel fuels (Owen, K., and Coley, T., 1995).

Fuel Chemistry:

The chemistry relevant to automotive diesel fuel is majorly that of hydrocarbons. The structural differences of some component groups are show in Figure 2.7 Paraffinic components occur as straight chain, single-bonded and saturated in their molecular structure (C_nH_{2n+2}). They also exhibit saturated single-bonds with branch chains that are named with reference to the branch location on the carbon-to-carbon main chain. Typical of these are iso-octanes. Similarly, there are single-bond unsaturated ringed-carbon hydrocarbons which on further hydrogenation can be saturated; these are called Cycloparaffins or naphthenes. They are named according to the number of carbon atoms like cyclopropane, cyclobutane and cyclopentane.

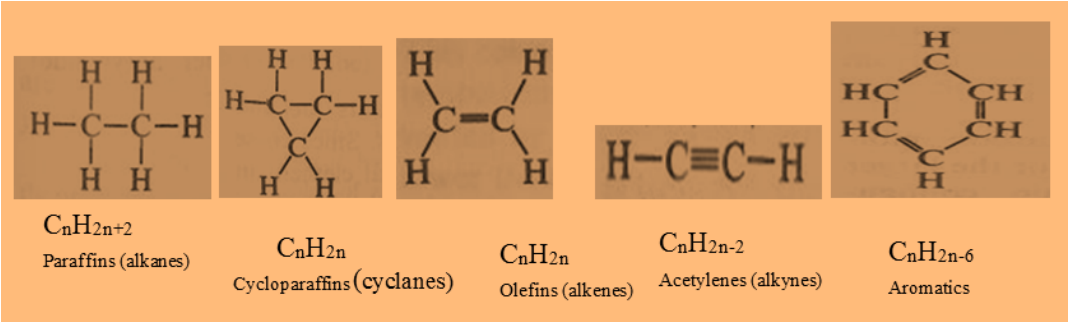

Figure 2.7 Functional structures of some fuel molecules (Heywood, 1988)

The alkenes or olefins have carbon-to-carbon double bonds and therefore unsaturated (C_nH_{2n}). The first three molecules in the homologous series have straight chain structure but as from the fourth (butane) molecule, isomeric structures are possible and are named with reference to the position of the double bond in the main carbon-to-carbon chain. Similarly, the acetylenes or alkynes have an unsaturated triple bond in the carbon-to-carbon chain (C_nH_{2n-2}). Higher members of the homologous series occur in similar structure like alkenes. The aromatics have ringed structure of six carbon atoms linked by three single bonds and three double bonds (C_nH_{2n-6}). Benzene (C_6H_6) is the simplest in this series and is the basic building block of aromatic hydrocarbons that are characterised by their stability. Several structures are possible and the more complex molecules could accommodate mono and poly alkyl side chains (Heywood, 1988).

Recent developments in fuels technology have seen rapid utilisation of biodiesels or their blends with petro-diesel. Biodiesels are trans-esterified vegetable oil or animal fat base (triglyceride) with alcohol; of which methanol and ethanol are commonly used. Biodiesels produced with methanol are methyl esters, while those produced with ethanol are ethyl esters. Potassium or Sodium hydroxides are the common base catalysts. Popular biodiesel – the Rape Methyl Esther (RME) is a product of trans-esterification of rapeseed oil with methanol.

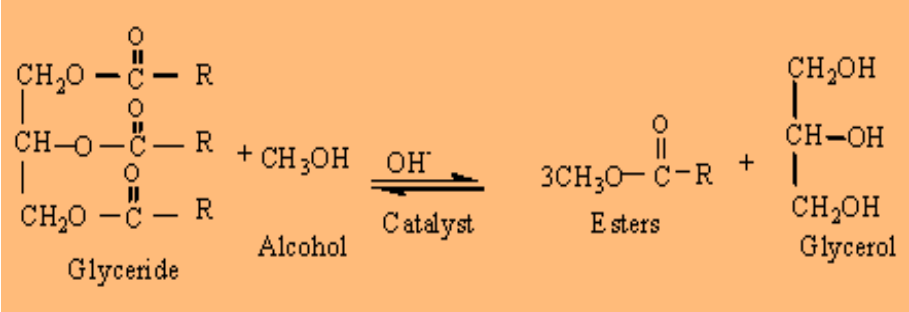

Figure 2.8 Functional structure of biodiesel

Combustion Stoichiometry

The *stoichiometric* air-fuel ratio $(A/F)_s$ or its reciprocal as defined in equations 2.1 and 2.2 is the chemically correct air-fuel proportion that will completely burn to yield only water, carbon dioxide and nitrogen. It is dependent on the chemical composition of the fuel. Engine combustion makes use of atmospheric air which contains nitrogen; therefore a general expression for complete combustion of a molecule of hydrocarbon fuel C_aH_b with air is given as:

$$C_aH_b + \left(a + \frac{b}{4}\right)(O_2 + 3.773N_2) = aCO_2 + \frac{b}{2}H_2O + 3.773\left(a + \frac{b}{4}\right)N_2 \quad (2.8)$$

Equation (2.8) defines the stoichiometric ratio of fuel and air reaction that could be utilised for gravimetric analysis of complete fuel combustion in air. It depends on the fuel molecular structure. In engine combustion analysis, it is usual to also express $(A/F)_s$ as a reciprocal, meaning fuel-air ratio $(F/A)_s^{-1}$. Either way is useful in expressing engine operating condition because during engine testing, both air and fuel flow rates are measured to determine if the mixture is rich or lean. The degree to which fuel is rich or lean, is central to engine performance analysis especially with regards to emission considerations. The products of combustion emitted in either of the mixture situation differ significantly due to fuel chemical composition and structure. In this regard, a parameter: *fuel/air equivalence ratio* (ϕ) that expresses the actual fuel/air ratio to the stoichiometric value is normally adopted for expressing the composition of mixture.

$$\phi = \frac{\left(\frac{F}{A}\right)_{actual}}{\left(\frac{F}{A}\right)_s} \quad (2.9)$$

In alternative the inverse of ϕ could be used as *relative air/fuel ratio,* λ (Lambda) is similarly defined as:

$$\lambda = \phi^{-1} = \frac{(\frac{A}{F})_{actual}}{(A/F)_s} \qquad (2.10)$$

Comparatively, mixture strengths are expressed as follows:
Fuel rich mixture: $\phi > 1,\ \lambda < 1$
Fuel lean mixture: $\phi < 1,\ \lambda > 1$
Stoichiometric mixture: $\phi = \lambda = 1$

Combustion thermodynamics

It is difficult to capture details of energy flow path in the engine due to complications in engine flow factors, combustion chamber profile, fuel structure, injection spray and mixing with air. In addition, heat transfer being a complex phenomenon in the engine environment, complicates such exercise more. The application of the first law of thermodynamics enables energy balances in terms of heat and work transfers to be evaluated by relating end states of reacting mixtures without recourse to the rigours of the processes. Such simplifications, although dubious; offers insight if reference internal energy and enthalpy states are reasonably considered. By resolving the flow parameters and employing modular knowledge of the thermo-physical properties of fuels, it is possible to analyse adiabatic combustion processes relevant to the engine system. Similarly, in conjunction with the second law, work transfers and overall engine efficiency could therefore be theoretically postulated and estimated by the current power of computer simulations. Although volumes of literature exist on studies of engine combustion analysis, of concern to this study is the exhaust emissions associated with the relative degrees of combustion efficiency; especially the particulates, which is desired to be eliminated from engine through combustion. From equation (1.8), exhaust emissions associated with engines combustion on stoichiometric condition are carbon dioxide (CO_2), water (H_2O) and nitrogen (N_2). However this is not possible in practical engine combustion as other emissions like carbon monoxide (CO), unburnt hydrocarbons (UHC), nitrogen oxides (NOx), oxides of sulphur and soot are inevitably present. These emissions arise due to

unsteady combustion, post combustion and engine cycle-to-cycle fluctuations. During combustion and some degrees past the *tdc* at start of expansion stroke, the composition of combustion products corresponds to local equilibrium with respect to pressure, temperature and equivalence ratio. But as expansion stroke advances, recombination reactions of active species occur, and their compositions are changed. Due to fast changing cylinder condition during this period, recombination reaction is not able to maintain the species in chemical equilibrium. At blow-down, exhaust process forces specie compositions to be frozen as they are expelled from the cylinder. By implication, even if the fuel-air mixture was lean, not all fuel will have opportunity to be fully oxidised. Also, it is not possible to equally match all the in-cylinder flow conditions in a multi-cylinder engine; therefore it is difficult to have the same exhaust composition from all cylinders. During testing, engines are calibrated to meet transient and stable operations of which fuel-air mixtures vary from rich to lean conditions, thereby giving various emission levels. Therefore evaluation of engine-out emissions is cumbersome and is best approached through experimental measurements (Heywood, 1988).

2.6 Diesel Engine Combustion and Emissions

The challenges posed to diesel engine designers at the current level of stringent emission requirements with simultaneous demand to improve engine efficiency are enormous. Hence it becomes imperative to have good understanding of combustion and emissions formation processes in the diesel engine. Combustion in diesel engine involves complex three dimensional multi-phase reactive flows occurring at high temperatures and pressures. Prior to development of optical accessible engines with laser diagnostics, direct measurement of combustion events inside the engine cylinder was difficult; high speed movies were used to record the spread of fuel jets and flame propagations. It has been possible to calculate fuel injection rates from measurements of fuel injection parameters; and the associated heat release rates from engine pressure data in order to gain insights about the combustion process but, much detail could not be extrapolated about the true in-cylinder reactions. Early description of in-cylinder diesel combustion process used adaptations of spray combustion in controlled flames of reacting jets with over-laying diffusion flame

front and auto-ignition occurring at portions of air-fuel mixture near stoichiometry (Robert Bosch , 1993). The development of laser diagnostics enabled in-situ measurements to be made as in-cylinder diesel-spray combustion reactions occur. The planar images recoded with good temporal and spatial resolutions, generated data that offered better interpretations.

2.6.1 Diesel Spray Combustion

The fuel injection spray trajectory, combustion and extinction is the conceptual basis for describing combustion in diesel engine and as present there are quantitative and qualitative insights into the complexity of fuel spray, air-fuel mixture formation, combustion and resultant emission formation through modelling (Reitz, R. D,. and Patterson, M. A., 1998; Naber, J. and Reitz, R.,, 1988) and experiments (Siebers D. L., 1998; Pickett, L. M. and Siebers, D. L., 2004; Kosaka, H., Aizawa, T., and Kamimoto, T., 2005). The conceptual model presented by Dec in 1997 based on laser sheet imaging (Dec J. E., 1997) is the hallmark of several efforts made with his co-workers at Sandia National Laboratories and other authors towards contributing to the current understanding (Loye, Z., Siebers, A. O., and Dec, J. E., 1990; Dec, J. E., zur Loye, A. O., and Siebers, D. L., 1991; Espey, C. and Dec, J. E., 1993; Dec, J.E. and Coy, E. B., 1996) . Host of other pioneering efforts were reviewed and previous misconceptions held about spray combustion corrected. Previous views centred on two concepts: one comprised zones of varying fuel-air mixture from liquid core centre to the spray edge with flame sheet over pockets of reacting droplets. Another is the concept of ‘sheath’ combustion or ‘droplet’ combustion depending on a parameter “G” - the ratio of the heat exchange between the liquid and vapour phases to the heat of vaporisation. Consensus views adopted then were on modelling spray combustion as containing a liquid-phase core jetting out of the nozzle with fuel droplets ‘near’ or ‘within’ the combustion zone depending on view point of ‘sheath’ or ‘droplet’ combustion; that combustion was diffusional within the peripheral envelop of the jet and that soot occurred in a shell-like region around the jet periphery.

The laser sheet imaging diagnostics revealed the true nature of in-cylinder processes like: entrainment of air as liquid fuel ejects from nozzle and mixes with hot swirling

air to form combustible mixture, images of poly-aromatic hydrocarbons, the auto-ignition event, soot formation which starts well from the upstream and central regions of the jet toward the head vortex, (contrary to former views); to the relative particle size distributions of soot emission, and soot concentrations (Dec J. E., 1992; Dec, J. E. and Espey, C., 1995; Epsey et al 1994). Separate investigations made for fuel-air mixing, combustion and post-combustion reactions were used to establish the conceptual model (Figure 2.9) as a framework for describing spray combustion (Dec J. E., 1997). Subsequent studies that gave information on fuel jet ignition (Higgins, B., Siebers, D. and Aradi, A., 2000), penetration (Siebers D. L., 1998; Musculus, M. P. B., Miles, P. C., and Pickett, L. M., 2013), lift-off length (Pickett, L. M. and Siebers, D. L., 2004; Siebers, D. L.and Higgins, B. S., 2001) and others (Majewski, W. A. and Khair, M. K., 2006; Tree, D. R. and Svensson K. I., 2007; O'Connor, J. and Musculus M, 2013), have dwelt on this model to elucidated the combustion phenomenon. The original work of Dec used large bore diesel engine with near-quiescent flow-field, and represented 'quasi-steady' free jet combustion without collision or wall impingement. The temporal sequence of the conceptual model with modifications to include some recent contributions (Musculus, M. P. B., Miles, P. C., and Pickett, L. M., 2013) is described and adapted here with Figure 2.10. The crank angle degree after the start of injection (ASI) is indicated on the left side of each image where 1^{o} = 139 micro-second (μs).

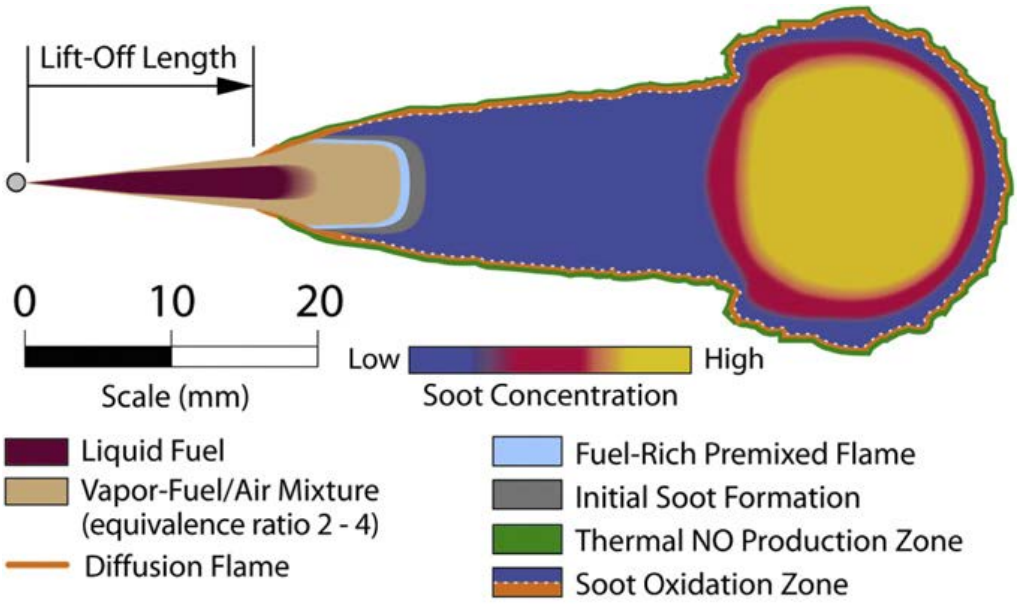

Figure 2.9 Dec's conceptual model of quasi-steady spray combustion in conventional diesel engine [Dec 97]

Fuel Jet and air entrainment (0.0^o – 4.5^o ASI):

The fuel sprays from the injector nozzle holes penetrate the combustion chamber and expand to near conical shapes. Based on the investigations in (Espey, C. and Dec, J. E., 1995), the images were captured at intervals of 0.5^o of crank angle degrees. From onset at 1.0^o, liquid jet core (dark brown) moves a maximum of 23mm downstream corresponding to 3.0^o ASI, where entrained air vaporises the fuel and limits liquid core penetration. The gas-phase jet penetrates downstream and develops vortex-head due to further entrainment. Correlations for entrainment in (Naber, J. D. and Siebers, D. L., 1996) and direct fuel vapour measurement in (Pickett et al 2011) show that as entrainment increased downstream there is inverse variation of equivalence ratio along the jet axis. Here the description of equivalence ratio is given as the ratio of local fuel-ambient charge mass ratio to the stoichiometric fuel-ambient mass ratio (Musculus, M. P. B., Miles, P. C., and Pickett, L. M., 2013). The liquid fuel is heated and vaporised by the thermal energy of the entrained in-cylinder air, therefore at some distance downstream referred as *liquid length*, all liquid fuel vaporize. The entrainment correlations have been used to determine this distance and also establish that it could be shortened if the ambient charge density is increased, as in the case of

boosted aspiration. Mixing was shown to be central influence for vaporisation of in-cylinder high pressure injected fuel (Siebers D. , 1999).

Auto-Ignition (3.0^o – 5.0^o ASI)

The beginning of flame initiation is not definite; however Chemiluminscene imaging offers opportunity to examine auto-ignition in diesel combustion. The arrows under the vortex head in jets 3.0^o – 5.0^o ASI Figure 2.10, indicate the Chemiluminscene region of the jet which may even appear earlier. At onset around 3.0^o -3.5^o ASI, the vapour fuel-air mixture is thin and around 4.5^o ASI, most of the Chemiluminscene emerge from the leading edge portion of the vapour-fuel/air mixture and indicates fuel breakdown and formation of PAH in the region 4.5^o – 5.0^o ASI.

Pre-mixed Combustion (4.0^o- 6.5^o ASI)

From the accompanying curve of heat release rate (light green) on top of Figure 2.10, the rate starts to rise after 3.0^o and the sharply from 4.0^o – 5.0^o ASI. During the same time emergence of Chemiluminscene is followed by rapid fuel breakdown and formation of PAHs increasingly in the leading edge of the jet where an equivalence ratio is about 2 – 4.

Figure 2.10 Evolution of Spray jet prior to quasi-period in heavy-duty diesel engine used in describing Conceptual model for combustion (Dec J. E., 1997; Musculus, M. P. B., Miles, P. C., and Pickett, L. M., 2013).

The initial burning of this premixed rich mixture is indicated by sharp rise in the heat release rate followed by rapid PAH and soot formation between 5.0^{o} – 6.0^{o} ASI downstream of the jet (Dec, J. E. and Espey, C., 1995) . Upstream, there is more fuel break-down due to increase in temperature, as typified by jet at 6.0^{o} ASI.

Early Diffusion Flame (5.5^{o} – 6.5^{o} ASI)

Concurrently towards the peak of apparent heat release during pre-mixed burn period, and on the periphery around the border region of the vapour-fuel/air mixture, thin diffusion flame appears. This usually results because products of fuel rich pre-mixed combustion now burns comfortably in the presence of air, (signified by thin yellowish-green colour) visible in the jet at 6.0^{o} ASI. Quickly as shown at 6.5^{o} ASI, the whole periphery of the jet downstream is covered by this thin diffusion flame burning at high temperature with consequent formation of nitrogen oxides. The flame sheet is limited upstream to a point referred as *'Lift-off Length'* from the nozzle tip which corresponds to the border region of the vapour-fuel/air mixture (Siebers, D. L.and Higgins, B. S., 2001). Here the flame is lifted and due to increased local heating, the rate of fuel break-up increases evidenced by decrease in the liquid-fuel length by about 2-3mm.

Last part of Pre-mixed combustion (7.0^{o} – 9.0^{o} ASI)

As fuel-air mixing rate increases, PAH and soot formation are enhanced towards the end of pre-mixed combustion, and this extends length of the jet downstream. At about 8.0^{o} ASI, the soot concentration is high and almost fills the jet cross-section bulging more towards the leading edge to form a head vortex. At the periphery of the jet, the thin sheet of turbulent diffusion flame produces larger soot particle that moves inwards to mix with the inner smaller soot particles in the bulk volume of the jet, but this is more active at the leading edge where concentration is more. As the last portion of the pre-mixed charge burns, small sized soot particles fills up the entire jet volume extending up to 27mmfrom the tip of the injector but soot is entirely lifted-off the nozzle tip for the reference low sooting fuel.

Mixing-controlled combustion (9.0^o ASI to end of injection)

At about 9.0^o ASI, the combustion has entirely become mixing-controlled and the appearance of the jet as used to hypothesise the conceptual model fully established at about 10.0^o ASI. At this point, the sizes of soot particles remain small from upstream edge where the last portions of the pre-mixed burns, but the concentration increases downstream as shown in the colour codes of the codes of Figure 2.9. The concentration is more at the centre of vortex head which becomes very prominent and filled with large soot particles signified by red and yellow colours. This last image was ordinarily taken as representing the final stage of jet development as it is typical of the observations made of the remaining mixing controlled burn ups until injection ends.

The Conceptual Model

The sketch in Figure 2.9 represents a typical conceptual model used to explain full spray combustion during mixing-controlled phase towards the end of fuel injection. The model is an intuitive modification of the last stage in jet development captured about 10.0^o ASI and to highlight the peripheral turbulent combustion. The sketch is magnified especially at the vortex end to amplify the observations made in the whole processes involved especially the dynamics of soot evolution using colour codes. At full jet development, the entrainment of turbulent air vaporise all liquid fuel about 19.0 mm from the nozzle tip; similarly, uniform fuel-air non reacting mixture is achieved within the 20.0 to 27.0 mm length. This is made up of fuel rich mixture and PAHs which afterwards, burn to generate small soot particles that fills and extends the jet length. The soot concentration and sizes increase downstream in a length referred to as ‘plume stem’ towards the leading edge and larger particles recirculate within the vortex. In the course of vortex recirculation, some soot particles reach peripheral flame front where they are further oxidised by OH radicals. Descriptively, the conceptual model could therefore be visualised as having four main zones viz. The lift-off length, the premixed zone, the plume stem and the vortex head as in Figure 2.11 (Eastwood P. , 2008). The emissions and other contributions associated with combustion processes have been the subject of many further investigations.

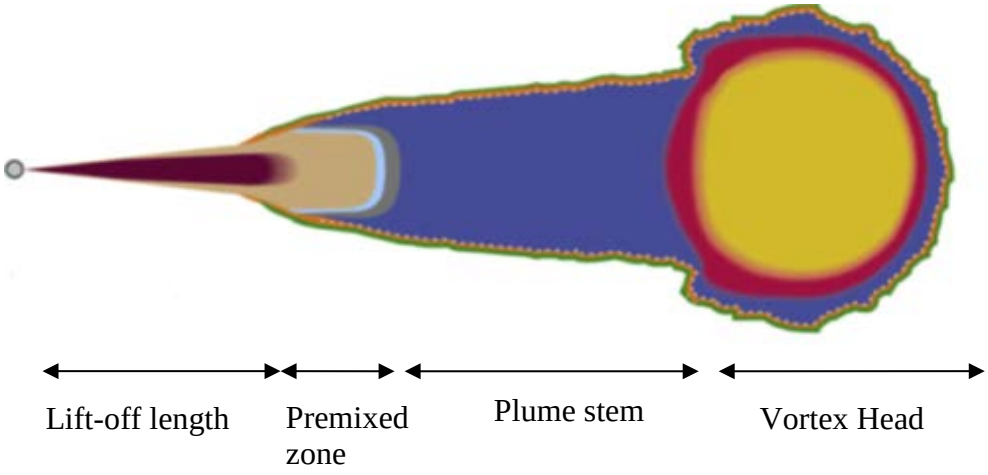

Figure 2.11 Zones of Dec's Conceptual Model

2.6.2 The Diesel engine Exhaust Emissions

Regulated exhaust emissions from the diesel engine include HC, CO Nox and PM. The conditions under which each of these is generated are interrelated in a complex web of factors; and many studies have focused on measures to improve the combustion process in order to counter their generation. These 'internal measures' target the earlier highlighted emission factors of higher injection pressures, injection rate shaping, improvements to combustion chamber designs, turbocharging and intercooling, transient control and swirl (Eastwood P. , 2008). Measures targeting the actual emission in the exhaust system are considered as after-treatments which deal with elimination of harmful products arising from the combustion process prior to release into the atmosphere. Combustion emissions generated during combustion are presented as follows:

The Hydrocarbon (HC)

It is conventional in the domain of engine emission to refer the unburnt hydrocarbons (UHC) simply as 'hydrocarbons' (HC). The concentrations could range from 20-300 ppm; and for control purpose, distinction is often made of total hydrocarbons (THC) and non-methane hydrocarbons (NMHCs) by excluding methane gas from the total hydrocarbons. HC emissions contain several compounds, the variety and concentrations differ as the engine operating influencers also vary. Small fraction of total unburnt hydrocarbon emerge as the originally sprayed fuel

that survived oxidation during combustion, while higher proportion emerge as different intermediates due to pyrolysis and partial oxidation of fuel and lubricants. The diversity includes alkanes, alkene, alkynes and aromatic, meaning that HC emissions occur as single, double and triple bonds or in combinations; straight and branched chains or ringed chain structure as in aromatics (Majewski, W. A. and Khair, M. K., 2006). Aromatics with benzene basic ring structure are the building blocks for higher cyclic-structures known as polycyclic-aromatic hydrocarbons PAH which can occur from fuel breakdowns and also from of incomplete combustion of fuel. The emission of hydrocarbons in diesel engines is significantly influenced by engine operating conditions of which light load to idling modes are most culprits (O'Connor, J. and Musculus, M., 2014). The prevalent reasons include over-mixing of fuel with air which leads to over-leaning and therefore difficult to support combustion particularly at low temperatures; under-mixing which causes over-rich mixture and so difficult to ignite; flame quenching at the chamber walls at low temperatures causes partial burning and misfire. Figure 2.12 is schematic representation of hydrocarbon formation mechanisms in diesel engine which show the underlying factors for hydrocarbon emission during two periods of fuel injection.

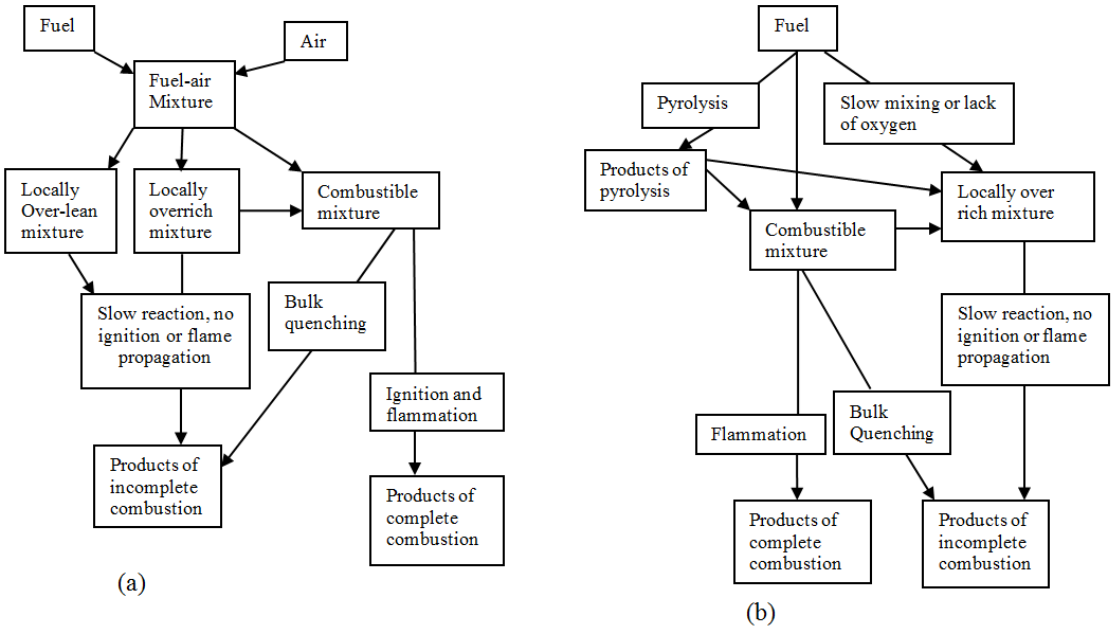

Figure 2.12 Diesel hydrocarbon formation mechanisms (a) Fuel injected during delay period; (b) Fuel injected while combustion is occurring (Heywood, 1988)

During ignition delay the equivalence ratios attained by fuel-air mixture varies within a wide range. Some portions of the mixture are favourable to auto-ignition; some are locally too rich to burn while others are too lean to support combustion. For fuel injected when combustion has commenced, high temperature favours rapid oxidation of fuel-air charge to complete combustion. However, there is also overrich portion of the mixture due to slow mixing of fuel and high quantity of intermediate products of pyrolysis due to high temperature and local starvation of air, as well as wall quenching. These lead to products of incomplete combustion and fuel in the exhaust. Many forms of intermediate products of incomplete combustion involve 'oxygenates' which are not pure hydrocarbons. Along with hydrocarbons, they constitute volatile components (VOCs) which condense as particulate matter as temperature drops on the exhaust line.

Carbon Monoxide (CO)

During oxygen deficient combustion process, fuel will not be fully oxidised and CO, an intermediate product on the fuel reaction path is produced along with HC as products of incomplete combustion. However combustion in most diesel engines is practically lean beyond stoichiometric, therefore CO emission is normally low except during transient operation.

Nitrogen Oxides (NOx)

The oxides of nitrogen relevant to diesel engine emission are nitrogen oxide (NO) and nitrogen dioxide (NO_2). Nitrous oxide (N_2O) is not a regulated emission and occurs only in heavy engines at very low quantity. They are collectively referred to as Nitrogen Oxides (NOx) of which, NO is the more dominant in emission during combustion and NO_2 is formed as a consequence of further oxidation. In the presence of ultra-violet light, NO_2 forms a photochemical smog with non-methane hydrocarbon. The mechanisms of NOx formation has been summarised in (Peirce et al 2013) based on the deductions in (Heywood, 1988; Turns, 2012; Bowman, 1992; Miller, J. A. and Bowman, C. T., 1989) as follows:

> The extended Zeldovich or thermal mechanism in which O, OH, and N_2 species are in equilibrium and atoms of N are in steady state. Generally, this route involves a direct chemistry of fuel combustion with oxygen forming O and OH species. The concentration of the O and OH radicals and temperature

are instrumental to the direction of the reaction. If fuel combustion completes without significant NO formation, the processes could be decoupled and assuming sufficient timescale, the N_2, O_2, O, and OH concentrations will remain at their equilibrium values.

$N_2 + O \leftrightarrow NO + N$
$N + O_2 \leftrightarrow NO + O$
$N + OH \leftrightarrow NO + H$

Mechanisms where formation of NO is more rapid than predicted by the thermal mechanism, grouped as:

- Fenimore mechanism that is intimately linked to hydrocarbon combustion chemistry CN and HCN pathways. In the scheme, hydrocarbon radicals form amines and cyano-compounds in primary reaction with nitrogen molecule.

  $CH + N_2 \leftrightarrow HCN + N$
  $C + N_2 \leftrightarrow CN + N$

  The amines and cyano-compounds then converts to intermediate compounds and ultimately to NO.

  $HCN + O \leftrightarrow NCO + H$
  $NCO + H \leftrightarrow NH + CO$
  $NH + H \leftrightarrow N + H_2$
  $N + OH \leftrightarrow NO + H$

- There also exists a scenario of super-equilibrium concentrations of O and OH radicals in conjunction with the extended Zeldovich mechanism that favours the formation of NO.

- N_2O-intermediate mechanism: This route is associated with fuel-lean, low temperature combustion. Reaction steps are:

$O + N_2 + M \leftrightarrow N_2O + M,$

$H + N_2O \leftrightarrow NO + NH$

$O + N_2O \leftrightarrow NO + NO$

- The NNH mechanism is predominant pathway for combustion of hydrogen and hydrocarbons with high carbon-to-hydrogen ratios. Reaction steps involve:

  $N2 + H \rightarrow NNH$

  $NNH + O \rightarrow NO + NH$

The fuel-nitrogen mechanism:

In this scheme, nitrogen is bound to the fuel and it is first converted to hydrogen cyanide or ammonia and then to NO.

During combustion of pure hydrocarbon fuel that does not contain nitrogen, oxidation of atmospheric nitrogen by the thermal mechanism is the major source of NO emissions formed when the fuel-air equivalence ratio is near unity in the flame front and in post flame gases. Typical ratios of NO_2 to NO are usually low at normal engine temperatures which for diesel combustion may be up to 10%. The mechanism for formation of NO_2 is the rapid oxidation of NO in the reaction zone as in:

$NO + HO_2 \rightarrow NO_2 + OH$

At temperatures encountered during optimum loads, equilibrium considerations will lead to conversion of NO_2 to NO as:

$NO_2 + O \rightarrow NO + O_2$

If the flame front bearing the NO_2 encounters lower temperatures through fluid mixing or lower temperature chamber walls, the NO_2 will be quenched and emitted. Similarly at low temperature region of the flame, HO_2 is relatively stable and can react with NO that diffuses from high temperature region to form NO_2 (Bowman, 1992). This explains the relatively higher proportion of NO_2 emission during low load operation of diesel engines.

Many techniques have been in use for the reduction of NOx, but majorly as a consequence of its dominance through thermal oxidation mechanism, combustion modifications are pursued to reduce NO formation rate through management of oxygen concentration and combustion temperature.

Particulate Matter (PM)

The term particulate matter (PM) is used to describe any matter that could be trapped on a sample filter paper when the exhaust gases are cooled to 52^{o} C or less. In effect, it includes all condensates formerly in vapour state from various substances like sulphates, nitrates, organics, as well as solid black carbon particles (soot) and ash.

The sources and reasons for the emission of PM are so immense when the considering the variety of species contained. However due to the associated health effects the most regulated aspects that have tasked researchers are the condensates that arise from unburnt hydrocarbons and the solid carbonaceous particles. The core subject of this study is on issues of PM emissions from diesel engine and is reviewed in chapter 3.

Summary

In this chapter the general issues that relate to diesel engine combustion and emissions have been presented. This gives an overview of implications in utilising petrodiesel fuel for power production and consequent emissions at the tail pipe. The emission factors are seen to be interwoven between the nature of fuel, the engine operating factors involved in fuel-air mixing, the flow factors and the thermo-chemistry of combustion. It is in this realm that the regulated exhaust emissions CO, HC, NOx and PM were introduced. By positing PM as one the regulated diesel emissions, its occurrence and mitigation will be better appreciated within the overall framework of diesel emission and control.

CHAPTER 3

DIESEL PARTICULATE MATTER

3.0 The Nature of Diesel Particulate matter

The diesel particulate matter (DPM or simply PM) as typically collected on sample filter paper when cooled, is a complex substance. The physical state is quite different compared to that formed in the engine due to the diversity of chemical species formed during combustion process and released at blow down at the prevailing temperature. There are myriads of volatile organic and inorganic substances in the exhaust stream that condense to liquid particles as temperature falls, as well as small particles of solid carbon (or soot) and ash. The multi-phase and complex nature of particulates provide for the different ways it could be accounted for. PM is characterised by chemical composition and physical characteristics. Physically, the sizes at which PM occur bears greatest attribute to the way it is characterised. Three distinct sizes have become customary in the description of particulates viz: *the nucleation mode, accumulation mode and coarse mode particles* as depicted in Figure 3.1. The nucleation mode particles are the smallest particles that occur through nucleation of species in vapour state. The size varies from the small nuclei that forms, to identifiable film drops but are usually attach to aggregates of solid particle if present. They are characterised by high number concentrations which is affected by heat, during which they could drastically reduce due to vaporisation. Characteristically, they occur within the sub 40 nano meter. It is possible however that some small solid particles occur at this size range. The accumulation mode particles are usually aggregates of primary particles that form as solid carbonaceous core upon which condensates of volatile particles adhere. Coarse mode particles are larger, perceived as accumulation mode particles that were deposited at the walls and latter carried back to the aerosol bulk stream (Eastwood P. , 2008).

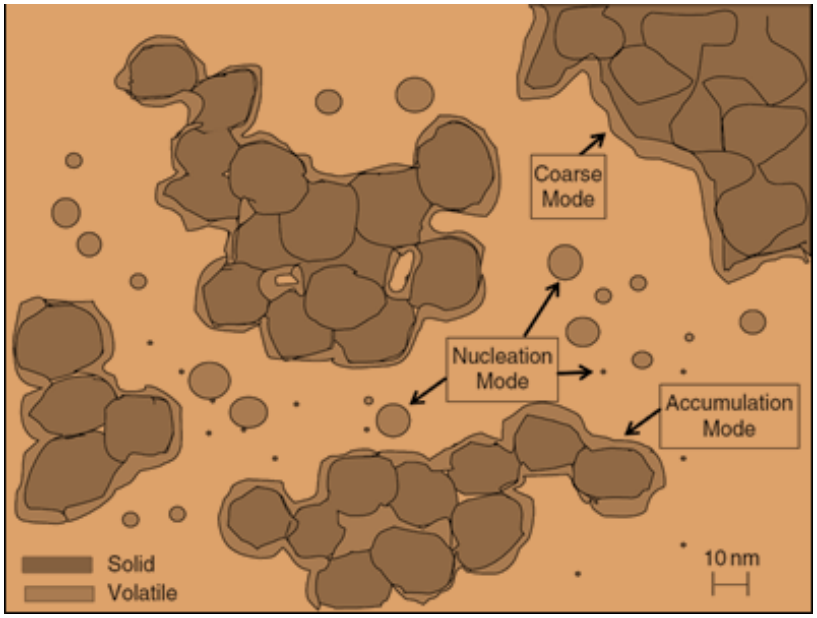

Figure 3.1 Typical particle likely to be emitted from a diesel engine showing nucleation, accumulation and coarse mode particles. (Eastwood P. , 2008)

3.1 Composition of PM

As stated, the PM is composed of volatile or soluble (depending on mode of separation) and the non-volatile or insoluble components. These are further classified according to their chemical speciation in assay. Various regulatory authorities prescribe the acceptable test protocols and procedures. Figure 3.2 is a conceptual model of the five different fractions that typifies the composition of diesel PM which includes: sulphates, nitrates, organics carbonaceous and ash (Eastwood P. , 2001; Heywood, 1988; Kittelson D. B., 1998.)

3.1.1 The Volatile (Soluble) Fractions

The major components the volatiles or solubles as collected on the filter paper except condensed water (which is not counted as a regulated substance) are:

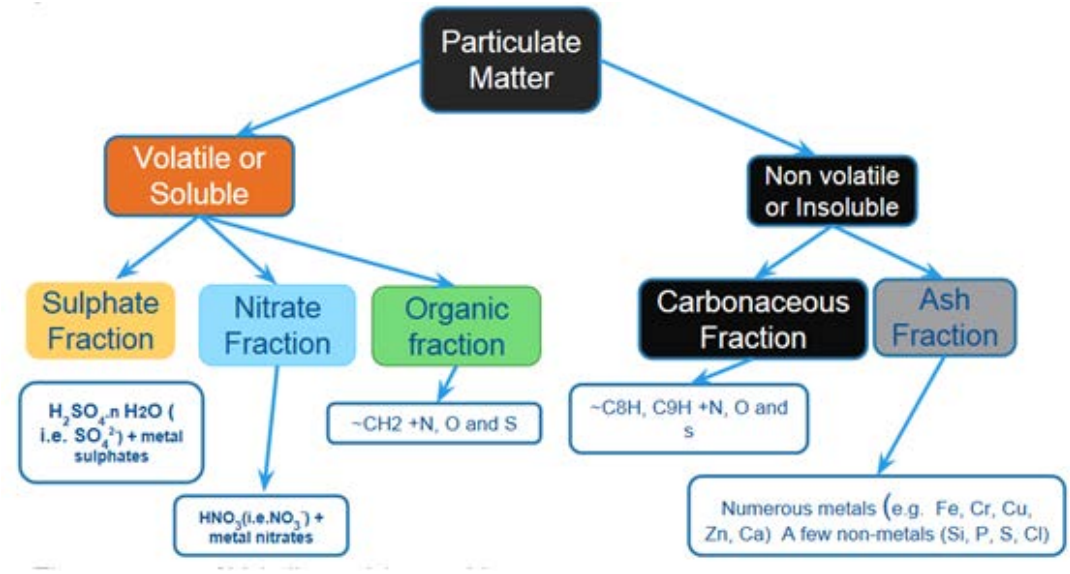

Figure 3.2 Conceptualisation of the composite fraction of Particulate Matter

The Sulphates

Sulphate ions SO_4^{2-} as commonly emitted from diesel engine is water soluble and in effect, is bound to water molecules and is majorly sulphuric acid. Therefore, this is assayed through solubility of the 'chemical' sulphuric acid not the physically condensed water. This necessitates pre-conditioning of the particulate-bearing filter for a given time in a steady and pre-defined environment in order to correctly account for the acid and achieve a reliable result. Other possible sulphate particulates include metallic salt like calcium sulphate $CaSO_4$. The metal ion may originate from lubricant additives which actively react with sulphuric acid. They are less hydrophilic compared to sulphuric acid. Sulphate particulates has been drastically reduced in modern automotive engines as result of improvements in fuels technology leading to achievement of ultra-low sulphur diesels blended with synthetic lubricity additives. However fuel for heavy-duty marine engines still has higher sulphur content which preserves the needed lubricity properties of sulphur in fuel (Eastwood P. , 2008).

The Nitrates

The nitrates are similarly water soluble and this also dictates the assaying technique. The major component formed by NO_3^- ions is nitric acid (HNO_3) in the reaction perceived to be due to NO_2 and water.

$2NO_2 + H_2O \rightarrow HNO_2 + HNO_3$

$3HNO_2 \rightarrow HNO_3 + 2NO + 2H_2O$

Although the formation mechanism has not been well reported, the presence of HNO_3 in diesel exhaust is not in doubt. It has been reported to be released by aerosol nitrate on quartz-fibre filter, both by NH_4HNO_3 dissociation (if NH_4NO3 is present) and by reaction with H_2SO_4 present in diesel exhaust (Okamoto, W. K.,Gorse, R. A. and Pierson, W. R., 1983). HNO_3 and all nitrates were extracted by dissolution and it showed that particulate nitrate emission rate is about ~ 0.15mg/km and the HNO_3 emission rate was1.3mg/km. Nitrate particulates are more researched in atmospheric science where acid – ammonia reaction dominate. The formation HNO_3 and NO_3^- rates show significant dependence on ambient temperature and relative humidity in a moist atmosphere. Similarly, HNO_2 concentration was found to be lower during the summer, while HNO_3 and NH_3 concentrations were higher, particulate NO3was reported to have significant seasonal variation with lower levels observed in autumn and summer (Lin, Y. C., and Cheng, M. T., 2007; Lin et al 2006).

Organic Fractions

If organic components are assayed by heating or vacuum evaporation, it is referred to as volatile organic fraction (VOF); if by dissolution in organic solvent, it is called soluble organic fraction (SOF). Either way, the masses obtained are reasonable approximates if proper adjustments are made for the non-organic matter in the case of heating. During heating process, evaporated fraction may include water-bound species, and are therefore the term volatile components (VOC) is used to imply organic and non-organic particles. The VOF is by far the most complex of the diesel PM because many organic compounds are present. Typical diesel emitted VOF are from unburnt or partially combusted hydrocarbons arising from fuel and lubricant as described in section 1.3.2.1 '*The Hydrocarbon'*. Studies have shown that VOF is chiefly emitted during low engine loads when the exhaust temperatures are low (Heejung, J., Kittelson, D. B. and Zachariah, M. R., 2003 .; Roy, 2006; Majewski, W. A. and Khair, M. K., 2006; Maricq M. M., 2007)

3.1.2 The Non-volatile (solid) Fractions

The non-volatile fractions are basically the carbonaceous fractions and ashes of burnt metals.

Carbonaceous Fraction

The carbonaceous fraction is also referred in many ways as elemental carbon (EC), soot, black carbon (BC) and graphite carbon. In this study, the term “Soot” will be simply adopted for reference. Soot particles are generated during premixed and diffusion regimes of the heterogeneous diesel fuel combustion in engines. Diesel soot is basically generated as primary particles occurring in sizes as small as 20-50nm which accretes to form identifiable aggregate structures, whose size depends on material availability and exhaust line temperature (Kittelson D. B., 1998.; Maricq, 2007; Eastwood P. , 2008).

Ash Fraction

Ash fraction denotes the burnt or incombustible ashes that arise from metals. Substances such as oxides, sulphates and phosphates of metals used in lubricants additives are likely to be found as well as burnt material of the worn engine components.

3.2 Particulate Matter Emission Processes

Formation of PM in the engine is complex and follows the combustion processes outlined in section 2.6.1. PM originates from fuel, lubricant, dust from the air, and worn out materials from the engine. Improvements in air filtration and use of ultra-low sulphur fuel have narrowed PM emissions and after-treatment efforts to focus more on the carbonaceous and organic fractions. The classic presentation of spray combustion process did not emphasise PM formation; however it is actually the process for soot formation. If the soot formation pathway is not followed, partially oxidised fuel exists as complex intermediates that constitute the volatile organic fractions in the exhaust stream that condense as particles of organic matter. The soot process in engine involves conversion of liquid fuel to vapour phase and then to solid

particles which are oxidised back to gaseous products. The un-oxidised particles are emitted as the visible black soot.

3.2.1 Soot Formation Process in the Engine

The identifiable steps in soot process could be outlined as pyrolysis, nucleation, coalescence, surface growth, agglomeration and oxidation. The first five steps are outlined as in Figure 3.3 but, any of these activities in the formation process could be terminated through oxidation.

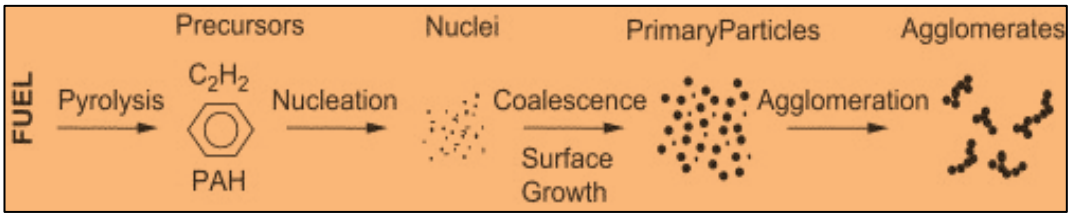

Figure 3.3 Steps in sooty formation process (Tree, D. R. and Svensson, K. I., 2007).

The soot oxidation process does not necessarily follow in the sequence but recognised as the final step in the combustion process which could occur anytime and convert hydrocarbons to CO, CO_2 and H_2O. This means that the precursor feedstock, the nuclei, the primary and agglomerated particles could be consumed in the oxidation process into gaseous products at any stage. In effect, this highlights soot emission as an intermediate product due to incomplete combustion in the engine. Therefore reduction of soot emission through engine combustion process will involve prevention of its formation, promotion of its complete oxidation or both.

Pyrolysis of fuel

Fuel pyrolysis is the altering of its molecular structure at high temperature without actually being oxidised even in the presence of oxygen. Pyrolytic reactions have been shown to involve breakdown of the original fuel molecular structures and formation of new aromatic hydrocarbons from the decomposed small units. These new units are precursors for soot formation and predominantly occur as acetylene (C_2H_2) and polycyclic aromatic hydrocarbons (PAH) with benzene (C_6H_6) as core building block. It is temperature dependent, different in pre-mixed and diffusion flames, and this dictates the level of competition between the soot precursor

formation and precursor oxidation by the hydroxyl radical, OH (Tree, D. R. and Svensson, K. I., 2007). Diesel fuel is multi-component and the implications for detailed chemistry are complex compared to mono-component fuels. Therefore pathways involved in laboratory studies using simple gases like methane, ethylene or acetylene (Simmie, 2003) do not give good picture of soot formation chemistry equivalent to liquid hydrocarbon fuels that contain alky carbon-carbon bonds, allylic bonds, alkyl rings, and benzenoid rings. Studies of soot formation chemistry relevant to liquid hydrocarbon fuels have highlighted some significant chemical concepts that explain fuel decomposition and the pathways to formation of aromatics compounds. (McEnally et al 2006; Richter, H. and Howard, J.B., 2000; Miller et al 2005; McEnally, C. S. and Pfefferle, L.D., 2005; McEnally, C. S. and Pfefferle, L. D., 2004a; McEnally, C. S. and Pfefferle L. D., 2004b). These are itemised as follows:

Strengths of the chemical bonds

These are basic molecular properties that highlight the reaction rates and have direct bearing on the heats of formation.

Resonantly-stabilized radicals

The concept of 'resonantly stabilised radicals' refer to the species that possess multiple electronic structures corresponding to the same nuclear structures (McEnally et al 2006). Shown in Figure 3.4 are two examples: Allyl and Propargyl radicals with specie structures having same carbon and hydrogen atom configuration but differently located radical sites and high-order C-C bonds. For the aromatics, they possess multiple resonating structures built around a basic benzene ring-structure. These radicals are thermodynamically more stable than non-resonating radicals and this stability is the basis for the rate of decomposition. Resonantly-stabilized radicals decompose preferentially to non-resonantly-stabilized radicals leading to higher aromatic formation rates. They also dissociate more slowly, and react slower with O_2 than non-resonantly stabilized radicals. The net effect becomes that concentrations of resonantly stabilized radicals are more and favour formation of aromatic species.

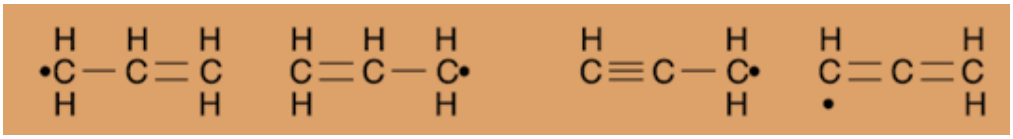

Allyl radical Propargyl radical

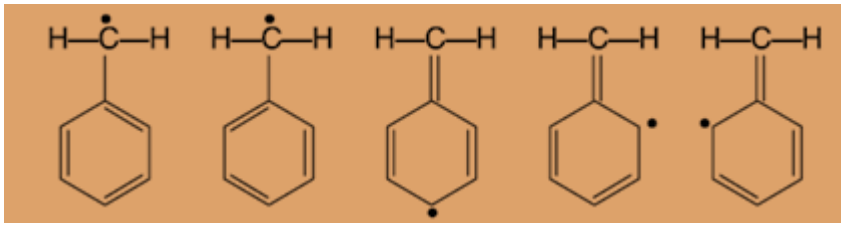

Benzyl radical

Figure 3.4 Resonantly-stabilised radical with multiple electronic configurations corresponding to common nuclear structure (McEnally et al 2006).

Stable hydrocarbon decomposition

There are three pathways that stable hydrocarbons decompose in flames:

H-atom abstraction: In this pathway, a chain-carrying radical removes an H-atom as follows:

$$CH_2=CH-CH_2-CH_2-CH_3 + X \rightarrow CH_2=CH-CH\cdot-CH_2-CH_3 + HX \quad \text{(R.1)}$$

$$CH_2=CH-CH_2-CH_2-CH_3 + X \rightarrow CH_2=CH-CH_2-CH\cdot-CH_3 + HX, \quad \text{(R.2)}$$

Simple fission: In simple fission pathway, two radical emerge from a broken bond.

$$CH_2=CH-CH_2-CH_2-CH_3 \rightarrow CH_2=CH-CH_2 + \cdot CH_2-CH_3 \quad \text{(R.3)}$$

$$CH_2=CH-CH_2-CH_2-CH_3 \rightarrow CH_2=CH-CH\cdot-CH_2-CH_3 + H, \quad \text{(R.4)}$$

Complex fission: In this pathway, multiple bond are broken and two stable hydrocarbon molecues are formed.

$$CH_2=CH-CH_2-CH_2-CH_3 \rightarrow CH_3-CH=CH_2 + CH_2=CH_2\cdot \quad \text{(R.5)}$$

Decomposition pathways are strongly dependent on the fuel molecular structure and temperature. Uni-molecular pathways of simple and complex fission reactions have higher activation energies than hydrogen atom abstraction (bimolecular pathway), therefore they occur preferentially at high temperatures; on the other hand, bimolecular pathways are favoured in large chain-carrying radical concentrations. Therefore uni-molecular decomposition pathways are more likely with large hydrocarbons because they contain weaker bonds and more atoms to change from four atoms to six atoms transition states. Similarly, H-atom abstraction pathways have been used to explain small hydrocarbons in flames or large hydrocarbons in low temperature reactors.

Formation of Aromatics

There exist wide ranges of reactants that form aromatics, some basic examples of benzene and naphthalene pathways based on extensive reviews in (Miller et al 2005; McEnally et al 2006) are presented in Figures 3.5 (a-d) as follows:

(i) The formation of phenyl radical and benzene by addition of acetylene to the C_4 radicals (*n*-C_4H_3 and *n*-C_4H_5) as in figure 3.5a. Since there is high concentration of acetylene in flames of fuel-rich hydrocarbons and the transfer of H-atoms from C-atoms is not necessary, reactions (a) and (b) are favourable pathways for aromatic formation. However the C_4 radicals are not stable isomers and their proportion is low in flames.

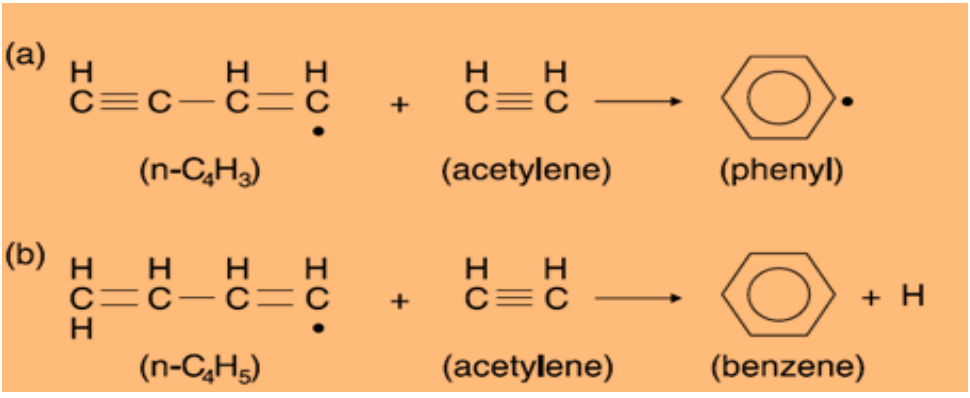

Figure 3.5 (a) Formation of single-ring aromatic hydrocarbon from Aliphatic hydrocarbons

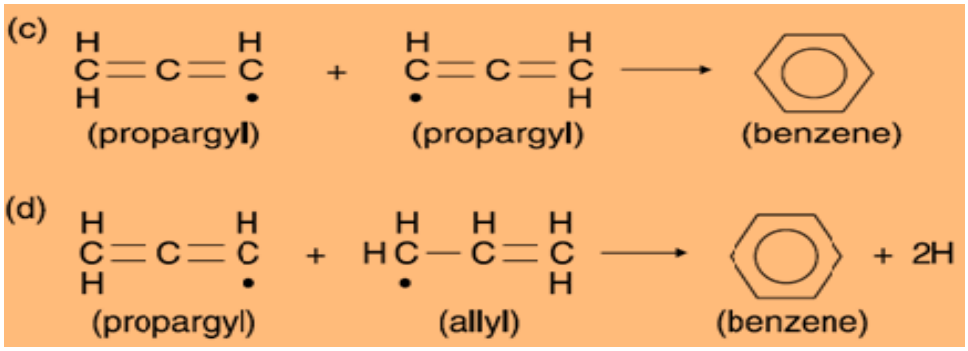

Figure 3.5 (b) Formation of single-ring aromatic hydrocarbons from Aliphatic hydrocarbons

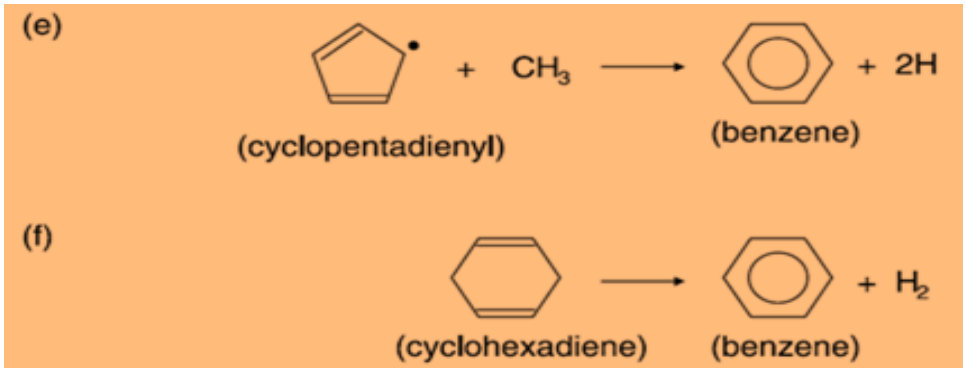

Figure 3.5 (c) Formation of single-ring aromatic hydrocarbons from Aliphatic hydrocarbons

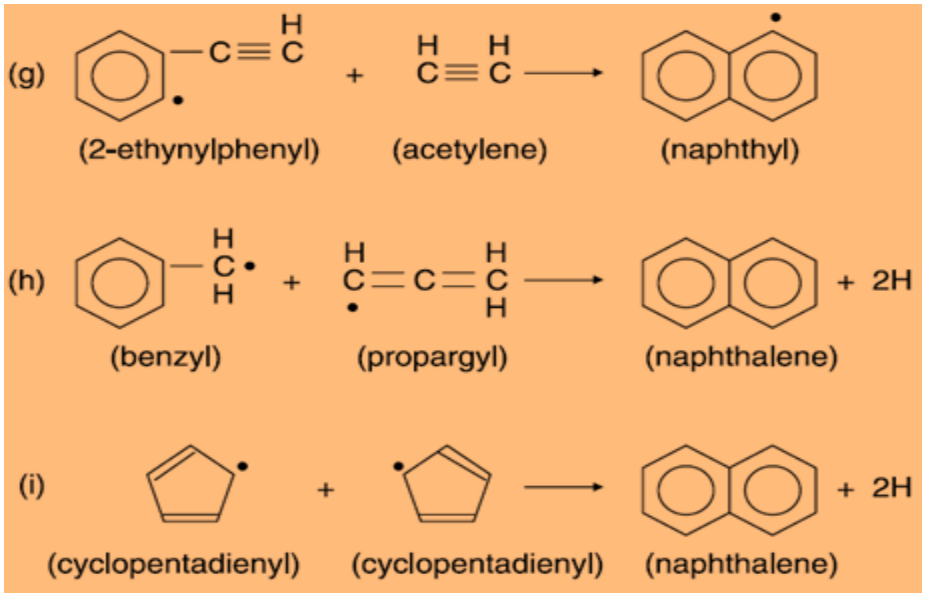

Figure 3.5 (d) Formation of two-ring aromatic hydrocarbons from single-ring Aromatic and aliphatic hydrocarbons

Figure 3.5 Aromatic formation pathways (McEnally et al 2006)

(ii) Reactions (c) and (d) show formation of benzene from two radicals of Propargyl or a propargyl with an allyl radical. The concentrations of radical-radical reactants are usually low and their reactions are most times insignificant. However as the reactants in (c) and (d) are resonantly stabilized radicals, they can reasonably accumulate to a high concentration. Reaction (c) is an elementary reaction while (d) is a global process but both require H-atom isomerization.

(iii) In reaction (e), benzene is formed by enlargement of the cyclopentadienyl radical, which is also a global process.

(iv) Reaction (f) forms benzene by uni-molecular elimination of H_2 from cyclo-hexadiene. The overall pathway can occur in two-step radical mechanism: H-atom abstraction producing resonantly stabilized cyclo-hexadienyl radical and unimolecular dissociation.

(v) In reaction pathway (g), acetylene addition to 2-ethynylphenyl radical produces a naphthyl radical. The formation of 2-ethylnylphenyl could be through abstraction of H-atom from phenyl acetylene and both reactions constitute example of H-abstraction-C_2H_2-addition mechanism (Hydrogen abstraction, carbon addition - HACA).

(vi) Reaction (h) is a global process where addition of propargyl radical to benzyl radical produces naphthalene. As radical-radical reactants, they are resonantly stabilized.

(vii) Reaction (i) gives formation of naphthalene from combination of two cyclopentadienyl radicals which is also a global process.

The above review brief show the variety of precursors through which benzene and naphthalene could be formed. The pathways for benzene could be through all possible combination of carbon sizes ($C_1 + C_5$, $C_2 + C_4$, $C_3 + C_3$). Therefore fuel structure is of great influence on the formation mechanisms of benzene and naphthalene in flames particularly for large molecular-hydrocarbons that could easily decompose to smaller products. Typical diesel engine combustion has initial premixed regime and more diffusion burn; therefore aromatic formation studies will involve radical measurements in both regimes. However large scale uncertainties are usually encountered and reliable data can only be achieved through well-articulated strategies. Studies involving premixed flames are relatively easier because

stoichiometry of fuel-air mixture remains fairly constant and therefore gives stable flame. However for non-premixed flames the fuel and oxidiser are at opposite sides of the flame front quite unlike the pre-mixed regime where they are mixed; therefore products of decomposition process recombine with themselves and form larger molecules most commonly viewed as successive chain of H-abstraction and C-addition until polycyclic aromatics hydrocarbons (PAH) are formed. In this sense, a sequence is set up whereby H-abstraction 'activates' aromatic molecules and C-addition 'propagates' the molecular growth and cyclisation. In the following example, A**ï** is a phenyl radical where higher-order ring A_{i+1} is constructed from a lower order unit A*i*, of which subscript *i* contains the number of joined rings and the PAH continues to grow (Eastwood P. , 2008).

A*i* + H → A**ï** + H_2,

A**ï** + C_2H_2 → A**ï**C_2H_2,

A**ï**C_2H_2 + H → A**ï**C_2H + H2,

A**ï**C_2H + C_2H_2 → A_{i+1}

Nucleation

The nucleation is regarded as the inception of particles formation from gas phase species in soot process. Most studies acknowledge acetylene to be a contributor for the emergence of PAH as a soot precursor but there is serious experimental difficulty as well as huge computational cost in modelling soot inception via this root (Glassman, 1988; Simmie, 2003 ; Tao, F., Golovitchev, V. I.and Chomiak, J., 2004; Miller et al 2005; Richter, H. and Howard, J.B., 2000; McEnally et al 2006). One study which accounted for diesel engine peculiarity used acetylene chemistry coupled to *n-heptane* ignition mechanism (Hong et al 2005). The acetylene was considered as a primary soot nucleation contributor whose monomers composed of two carbon atoms as in the reaction:

$C_2H_2 \rightarrow 2C_{soot} + H_2$

The initiation of soot primary particle was through consolidation of 16 soot monomers that forms instantaneously. This was after investigation of the effect of primary particle size on the overall soot model which was assumed to contain 32 carbon atoms. By using soot density of $\rho_{soot} = 1.8 g/m^3$ for a spherical particle, it enabled the calculation of soot diameter using the model –

$$\frac{\pi d_m^3}{6} = \frac{mC_{soot}}{\rho_{soot}} \quad (3.1)$$

This model determined smallest identifiable primary particle of about 1 nm similar to that of (Tao, F., Golovitchev, V. I.and Chomiak, J., 2004). These are comparable to the earlier works reported in (Bartok, W. and Sarofim, A. F., 1991) where smallest solid particles in luminous flames were to be around 1.5 – 2.0 nm.

Surface growth

The increase in soot size regarded or surface growth results from addition of mass to incipient soot nuclei due to continuous chemical reaction that producing acetylene (and PAH) in the HACA mechanism. Several reactions paths are listed in (Hong et al 2005) which include the mechanism of possible acetylene elimination from soot radical (reaction G3) and show the acetylene addition as components of a reversible radical formation (reactions G4f and G4b) and cyclization reaction (reaction G5) in Table 3.1. There is no marked end of nucleation and commencement of the growth process as the processes overlap. However, the growth process continues as the particles drift further from the primary reaction zone and generates primary particles called spherules whose sizes are limited to few tens of nano meters (Tree, D. R. and Svensson K. I., 2007)

Table 3.1 Soot surface growth and oxidation mechanism (Kitamura, 2002) adjusted by (Hong et al 2005)

Table 3.1 Surface growth and oxidation mechanisms

	Reaction	$k = A\exp(-E/RT)$	
		A (cm^3/mol s)	E (kcal/mol)
G1f	C_{soot}-H + H → C_{soot}• + H_2	2.5×10^{14}	12.0
G1b	C_{soot}• + H_2 → C_{soot}-H + H	4.0×10^{11}	7.0
G2f	C_{soot}• + H → C_{soot}-H	2.2×10^{14}	–
G2b	C_{soot}-H → C_{soot}• + H	2.0×10^{17}	109.0
G3[a]	C_{soot}• → C_2H_2 + products	3.0×10^{12}	62.0
G4f	C_{soot}• + C_2H_2 → C_{soot}CHCH•	2.0×10^{12}	4.0
G4b	C_{soot}CHCH• → C_{soot}• + C_2H_2	5.0×10^{13}	38.0
G5	C_{soot}CHCH• → C_{soot}-H + H	5.0×10^{10}	–
G6	C_{soot}• + O_2 → products	2.2×10^{12}	7.5
G7	C_{soot}CHCH• + O_2 → products	2.2×10^{10}	7.5
G8	C_{soot}-H + OH → products	Reaction probability = 0.13	

Coagulation or Coalescence

Coagulation which is also known as coalescence is a process where two particles collide and coalesce fusing into one particle. In effect this process decreases the number of particles while maintaining the mass. Soot particle growth by collision and coagulation is usually modelled using modified Smoluchowski's coagulation rate equation (Hinds, 2011).

$$\frac{dN}{dt} = -KN^2 \qquad (3.2)$$

Where N is the number concentration, t is time and k is the coagulation (or agglomeration) coefficient.

Modification accounts for the considerations made, whether for simple monodisperse or polydisperse coagulation and also if the collision process is caused by Brownian motion (hence *thermal coagulation*) or by external forces (*kinematic coagulation*). Soot emission from diesel automotive engines is usually in the transition region between the free molecular and continuum regimes (Hinds, 1999). Therefore coagulation rate in the transition could be determined by the use of interpolation formula employing continuum mean approximation (Hong et al 2005).

Agglomeration

The spherules that collide and stick together form close bonds and grow bigger in size. Successive collisions of the spherules form large particles and results in

morphologies that characterise soot particles in aggregate forms that they are known. This process is referred to as agglomeration. The process differs from surface growth in that it is a physical instead of chemical reaction and represents mature status of soot particle in the aging process. During coalescence, the original identity of the spherule is lost in the newly formed soot although the nuclei are not lost. Many models of the process follow the Smoluchowski's general aerosol equation with modification for the agglomeration constant as in equation 3.2. The rate of particle decline could be evaluated from it as:

$$\frac{N}{N_o} = \frac{1}{1+(kN_o)t} \tag{3.3}$$

Where N in the number concentration, N_o is the initial number of particles and k is the agglomeration constant. This gives inverse relationship between rate of agglomeration and time (Hinds W. C., 1999; Lighty, J. S., Veranth, J. M., and Sarofirm, A. F., 2000). The application of agglomeration mode to engine soot emission is subject to many simplifications as engine generated particles are not rigorously monodisperse spheres. The single shapes of coagulated particles can be correctly approximated as spherical while the agglomeration of these primary particles forms chain-like clusters which by implication, reduces the number of primary particles without affecting the accumulated mass. The final size and morphology characteristic of diesel generated soot depends on many engine operating variables like load, speed, injection conditions, air/fuel ratio and EGR (Lapuerta, M.,Martos, F. J., and Herreros, J. M., 2007; Neer, A., and Koylu, U. O., 2006; Tree, D. R. and Svensson K. I., 2007).

3.2.2 Particulate Matter Transport Processes

Many *PM* processes are studied in the realm of its transport which could be viewed from the moment of soot maturity in the engine, (most likely coincident with blowdown) and then in the phases of flow through the exhaust system. The fundamental knowledge gained during this process forms the basis for development of after-treatment technologies. Essentially, mature soot agglomerate that survives oxidation in the engine starts another growth process outside the engine through

adsorption of more particles that condensed from volatile intermediate matter carried in the exhaust stream. Therefore physio-chemical reactions involving homogeneous gas-phase reactions as well as gas-to particle reactions go on during this period. Temperature is the predominant factor influencing phase reaction as thermal loss increases along the exhaust pipe. Similarly, *PM* transport studies could be extended to tailpipe emissions when the plume is ejected into the atmosphere. Further physical reaction in the atmosphere involves dilution of the exhaust species through extensive mixing and rapid cooling with air; and this dictates the extent of pollution to which engine tailpipe emissions are viewed. Much of what is known about engine generated *PM* emissions are through experimental measurements and most devices cannot handle the concentration of raw exhaust. This necessitates dilution of raw exhaust to mimic the atmospheric dilution process. Therefore aerosol transport processes normally considered in *PM* measurements include the undiluted flow through the exhaust system, the fast mixing and cooling process in atmospheric flow and the flow through the laboratory dilution/deposition schemes.

PM transport within the exhaust system

Exhaust gases that leave the engine exhibits two peaks of particulate mass emission as a function of crank angle movement when measured on filters. These have been recognised as during blowdown when high in-cylinder gas pressure caused expulsion of exhaust gases and during piston displacement by exhaust stroke. These periods impact different energies to the flowing *PM* and consequently different quantities of matter are involved. The mass of *PM* emission during blowdown was said to be twice more than during piston displacement (Kittelson, D., Ambs, J., and Hadjkacem, H.,, 1990). Soot thermophoretic deposition on the wall and subsequent re-entrainment was postulated to have protected it from oxidation. The engine speed determines the residence time available for soot particle growth, while the sizes, number and morphologies change during transport phases along the exhaust line. The vapour-phase condensed particles adsorb on agglomerated soot particles which grow bigger into chain-like structures, while small soot particles reduce in number (Lee et al 2001; Lee, K. O. and Zhu, J., 2005; Lee et al 2002). Flow of *PM* along the exhaust system is principally associated with two particle deposition processes: *thermophoresis* which is due to thermal gradient in relation to engine operating characteristics (as major) and *inertial impaction* dictated by gas flow which is related

to engine speed (as minor). By these mechanisms the *PM* temporarily deposits on the wall of the exhaust system especially at flow restriction areas of EGR coolers, catalytic converters, filters and mufflers. Deposition is most likely to be high at low engine speed which encourages low temperature and mass flow rate. On the other hand, high engine speed leads to increased flow rate and the fluid shear force scraps the particles deposited on the wall back to the bulk stream of exhaust flow in a process is called *re-entrainment*. These mechanisms provide avenue for design of exhaust after-treatment devices (Eastwood P. , 2008).

PM Transport in the atmosphere

The exhaust gas that flows out from the tailpipe to the atmospheric environment encounters very rapid mixing of the volatile-phase matter as well as suspended solid particle species with air in addition to cooling. The phenomenon of mixing and cooling of the volatile matter leads to gas-to-particle conversion which affects the morphology, number and size of the original particles in the exhaust stream ejected from the tailpipe. This phenomenon is termed dilution; which implies species mass transport as well as heat transfer and differentiates the *PM* transport in the exhaust system from its dynamics in the atmosphere. Similarly, while *PM* transport in the exhaust system is influenced by the engine operating conditions and exhaust system design, its atmospheric transport is in addition influenced by local wind speed, temperature and humidity. Therefore the extent of dilution in the atmosphere is not constant but varies to infinite levels as the plume moves from the tailpipe. In effect, exposure level is relative to distance from the tailpipe with genuine considerations for the atmospheric variables. Efforts to study exposure levels are carried out through 'chase experiments' during which potable aerosol measurement devices are carried along to 'pursue or chase' the vehicles whose emissions are being measured. This has been achieved for different speeds, distances and angles with respect to the tail pipe for different vehicles and at different locations (Kittelson et al 2000; Pirjola et al 2004; Ntziachristos et al 2004). Exposure levels can be quantitatively evaluated if the 'dilution ratio' is properly determined. This involves the complex resolution of vehicle speed relative to the local wind speed and the associated fluid dynamic pathway in the complicated mixing process. A major concern in understanding the real values of PM emissions is the nucleation of vapour-phase matter which easily adsorbs to the existing particles and affects the values depending on the metric

considered. Regulations have recently shifted emphasis from mass to number metric. By this metric, it becomes cumbersome to account for the ubiquitous nanoparticles that agglomerates during dilution, upon which volatile particles adsorb and the value of which remains highly sensitive to variations in the atmospheric dilution process. Therefore experimental efforts have involved highly intuitive approaches and subjective probabilities spelling out the relevant physics considered. The reports in these regards are compilations of such schemes to give reasonable insights to the emission levels from various types and categories of vehicles. Closer examinations that have eliminated atmospheric complexities and allowed better control of the mixing variables are achieved in the realm of laboratory dilutions.

PM Transport in the Laboratory

Laboratory tunnels are traditionally used to study the dilution process, especially the full *exhaust flow dilution tunnel* (FEFD-tunnel) or *constant volume sampler* (CVS) allows for complete exhaust flow to be diluted in the tunnel. CVS tunnels operate at reasonable dilution ratio up to 1:10 therefore has to be large; implying erection of expensive structures. The system is not normally heated due to the sheer size hence; temperature control is difficult thereby allowing nucleation and condensation to occur. The implication is that independent studies of the effect of cooling and mixing are not feasible with the CVS system. However it enables direct determination of total mass emitted as the mass of material collected on a filter times the ratio of flow rate in the tunnel to sample flow rate (Burtscher, 2005). Similarly number concentrations emitted during sampling time could be determined. To overcome the limitations of the CVS system, scaled tunnels are used whereby small portion of raw exhaust is channelled to a dilution chamber through a transfer line. Flow through a transfer line is a diversion to an unnatural flow-path and could result in particle deposition onto the wall of the transfer line and this distorts the size distributions in measurements. In order to achieve constant volumetric flowrate in the tunnel, a positive displacement pump is normally used to draw ambient air past a filter bank up stream of the tunnel. In some designs depending on tunnel capacity, a critical flow venture and heat exchanger are used in conjunction to accelerate and cool aerosol respectively as in Figure 3.6.

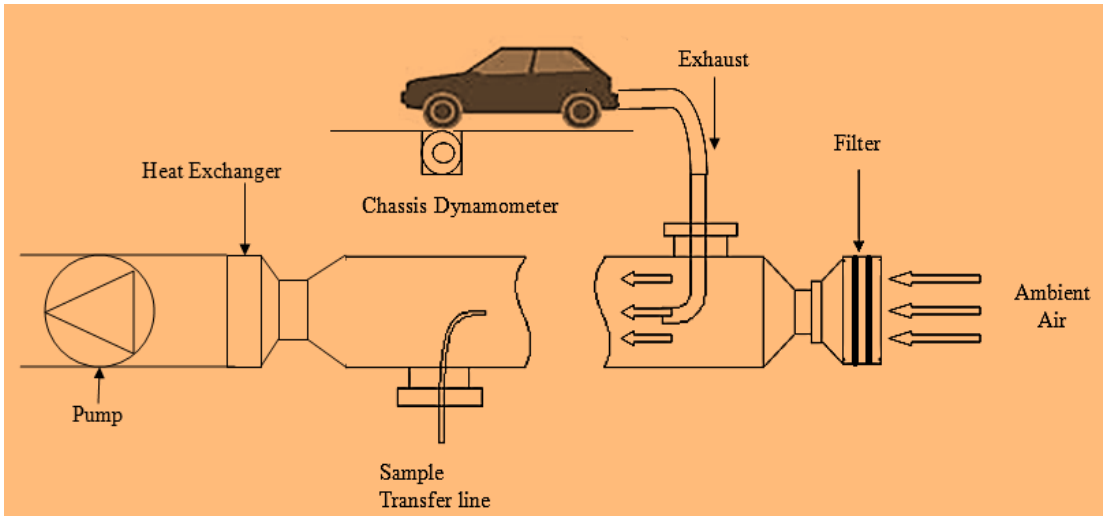

Figure 3.6 Schematic of CVS dilution tunnel (Burtscher H. , 2005)

The small diameter transfer line with high surface area-to-volume ratio encourages thermophoretic deposition of particles, intensifies exhaust gas cooling and deepens radial thermal gradient (Eastwood P. , 2008; Ushakov, 2012). In effect false and misleading measurements could result, which in most cases are not reproducible. The transfer of raw exhaust into the dilution tunnel exposes the particles to another flow encounter with filtered ambient air. The flow path depends on tunnel design which varies according to the purpose of dilution but generally the interplay of cooling and mixing works out. Laboratory diluted aerosols are commonly analysed in mass metric through filter deposition and in number metric, through various mobility analysers. The mechanism of deposition that enables particle analysis in any case depends on the particle size. Nucleation mode particles are purely subject to diffusional deposition; accumulation mode particles are partly diffusional and partly depositional while the coarse mode particles are predominantly depositional. These are reviewed more in the measurement section.

3.3 Environmental and Health Effects of Particulate Matter

The implication of particles deteriorating the visibility and atmospheric environment as well as being hazardous to health has now been established. *PM* from the diesel exhaust engine is one source among the host of other contributors like coal, biomass and other waste materials (Lighty, J. S., Veranth, J. M., and Sarofirm, A. F., 2000; Friedrich, R. and Reis, S, 2004). The *PM* from diesel engine is known to be complex,

consisting of organic and inorganic particles that nucleated and condensed from gas-phase onto the solid particles. These condensates are toxic substances such as cancer-causing aldehydes (like formaldehyde and PAH) and their composition varies extensively depending on engine class, operating conditions, lubrication and after-treatment. Figure 3.7 gives a pictorial model of a typical diesel-emitted particle (DCEN, 2014), which could assume any size in the sub-micron regime. Although current improvements in diesel engine technology have brought huge reduction in emissions through improved designs, fuel

Sawyer, R. F. and Johnson, J. J., 1995) concern for exposure risk especially for sub 100 nm sized particles remains, as studies have established the possibility of their passage through the lung tissues. The perspective for the relative sizes that could penetrate the body tissues is shown in Figure 3.8 (Fernandez, 2012).

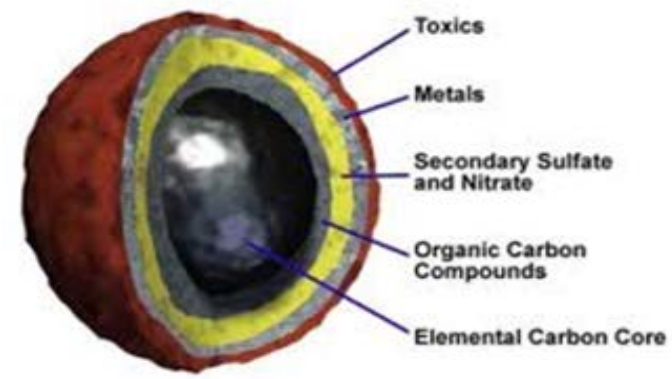

Figure 3.7 Pictorial model of Particulate Matter (DCEN, 2014)

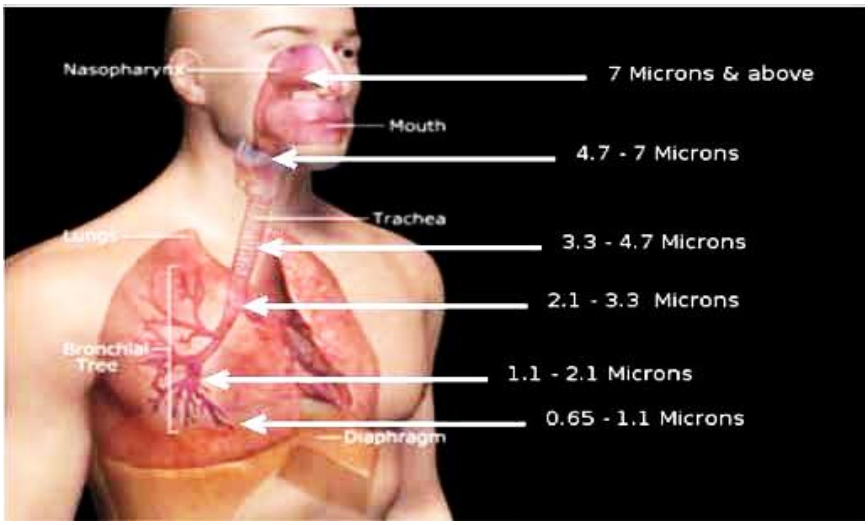

Figure 3.8 Perspectives of Particle sizes and their penetrations into the body tissues (Fernandez, 2012)

In 1988, the IARC classified diesel as 'probably carcinogenic' to humans (Class 2A) as no rigorous study then had established a correlation between diesel fumes and cancer. In 1989 the body upgraded it to 'possibly carcinogenic' (Class 2B). But later studies in combustion generated *PM* especially occupational health and safety in the mining industry show that diesel emissions are more hazardous than previously thought and linked diesel exhaust fumes to lung cancer. Array of epidemiology and toxicology studies reviewed in (Lighty, J. S., Veranth, J. M., and Sarofirm, A. F., 2000) and traffic studies in particular, have suggested increased rates of respiratory disease, cardiovascular disease, risk of premature death and Oxidative Stress in Humans near busy urban streets or highways (Pope et al 2002; Nauss, 1995; Dockery et al 2005; Hawley et al 2014; Huang et al 2009). The IARC press release in June 2012 declared: "***The scientific evidence was compelling and the Working Group's conclusion was unanimous: diesel engine exhaust causes lung cancer in humans"*** thereby awarded diesel exhaust emission a 'Class 1' status. The Working Group also stated that diesel exhaust has a positive association (*limited evidence*) with an increased risk bladder cancer (IARC, 2012). Since then, there appear to be no limit in the interest and studies of associated health effects from *PM* emission.

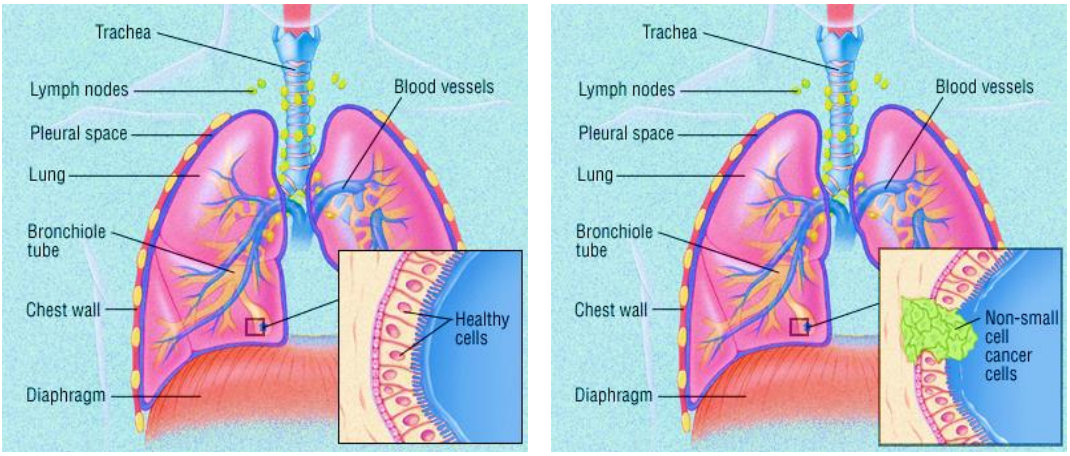

Figure 3.9 Cancer cells in the lungs (Harvard, 2012)

3.4 PM Regulations and Standards

In response to many of the perceived health and environmental effects, the diesel engine exhaust emissions have been subjected to legislation for a long time, both

road or off-road, light or heavy duty application. The emission of PM is of special concern due to the effects on human health. The characteristic nature and sources of the *PM* in the atmosphere are diverse but *PM* originating from diesel combustion devices is known to consist of solid and liquid particles. Some particles are large or dark enough (soot) to be seen as smoke while majority are so small to be detected except with special devices based on several techniques. The legislations concerning PM are as contained in the different regional and international frameworks involving determination of regulatory standards for the exhaust emissions as a whole. The frontline regions championing emissions legislations are the United States, the European Union and Japan (UNECE, 2013).

Brief overview of Emissions Legislations

On a historical perspective, the emission standards in California the United States are prescribed as 'low emission vehicle (LEV) standards' while the Federal Environmental Protection Agency (EPA) enacted the 'Clean Air Act (CAA)'; the two run in parallel but with the former more stringent in the California region. Based on the Federal Test Procedure (FTP-75) expressed in gram/mile or gram/kilowatt, separate standards are provided for different categories of vehicles with more allowances for heavy-duty vehicles. The current national low emission level vehicle programmes (NLEV) came into effect as a voluntary harmonisation of legislations through agreement with the north-eastern states and auto-manufacturers. In effect, emission legislations in the US from the Federal perspective have undergone three basic tiers of standards from 1990 to date with some flexible supplementary amendments during transitional periods (Dieselnet, 2014). Tier-1 standards, published in 1991 were phased-in between 1994 and 1997; Tier-2 standards were phased-in from 2004 to 2009; while Tier-3 standards will be phased-in from 2017 – 2025. The evolution of California LEV standards is similar: LEV- I extended through the year 2003, LEV- II were phased in through years 2004 – 2010 and LEV-III are to be phased in through years 2015 – 2025. In these phases, permissible levels of all the regulated emissions are prescribed. The levels for *PM* emission and exposure have been issue of all round rolling reviews by EPA through avalanche of toxicology and epidemiology studies to ascertain health effects. Through reviews of air quality criteria and national air quality standards (NAAQS) for PM, revisions were made to stipulate suitable levels to provide requisite protection for the public health (EPA F.

R., 2013; Esworthy, 2013). Reference is taken with particles sizes less than or equal to 2.5micrometers ($PM_{2.5}$) in diameter. In Canada, regulation follows the US standard where $PM_{2.5}$ reference level from diesel powered engines employed in off-road fleet have decreased emission to about 75% between 1985 and 2010 compared to Europe. In the Europe, apart from individual national guidelines there has been EU Directive (NEC Directive) on National Emission Ceilings for some regulated pollutants since 2001 but, it was in 2002 that the Sixth Environment Action Plan (6EAP) set out long term objectives for air quality achievements. In 2008, the Air Quality Directive merged most of the loosely operated pieces of legislations to target control of ambient concentration of pollutants; and the $PM_{2.5}$ reference (fine particles) was introduced as a variable for air quality (EC E. C., 2001; EC E. , 2008). On a more global scale, the initiative to harmonise regional efforts also started since 1999. The USA aligned with Canada; the EU Member States together with the Central and Eastern European States started to negotiate a "multi-pollutant" protocol in Gothenburg under the auspices of United Nations Economic Commission for Europe (UNECE) Convention on Long-Range Trans-boundary Air Pollution (CLRTAP) (UNECE G.-6. , 2013). The parties involved in CLRTAP were only able to reach consensus on a revised Protocol in 2012. It sets new ceilings for emission of NO_X, SO_2, NH_3 NMVOCs and $PM_{2.5}$ for year 2020 and beyond.

Prior to emission reduction being a major regulatory issue, the UNECE world forum had a working party for harmonisation of vehicle regulations (WP.29). In 1997, a group was established under this working party to develop a harmonised world-wide test cycle for heavy duty engines. The work of this group led to the establishment of a subsidiary group on pollution and energy (GRPE) in 2006 to harmonise the UN global technical regulations (UN GTR No. 4) on certification procedure for heavy-duty engines. The outcome of their work provided a common reference for measuring the performance of existing and future engines' exhaust emissions for both transient test cycle and steady state test cycle (UNECE G.-6. , 2013; UNECE, 2007). Similar regulation for development of light duty vehicle test procedures (WLTP) was started in 2007. The regulations governing permissible levels of exhaust emissions from all types of light diesel engines are contained in the various frameworks coordinated by UNECE (EMEP/EEA, 2012; ECE, 2012). Current directives have prescribed increasingly stringent limits for new vehicles sold within the member states. The regulated emissions from diesel engine include CO, NOx,

HC +NOx and PM; which for passenger and light duty commercial vehicles are currently prescribed as Euro 5/6 (Regulation 715/2007), finalized in 2007 and implemented through 2009 - 2014. It contains revisions of various standards in previous versions with regard to fuel quality and emission testing procedures. Highlights of the diesel engine emission limits provided by the standards over the years are summarized in Tables 3.1. With reference to particulates, current metric for measuring emission is now in number concentrations. This has been developed by the Particle Measurement Programme (PMP) of the UN-ECE joined by Japan and South Korea. It offers the advantage of knowing the size distributions of the component particles as they occur from engine.

Table 3.2 EU Emission standards for Diesel Engine: Passenger Cars (Category M_1 *) (AVL, 2012).

Stage	Date	CO	HC + NOx	NOx	PM	PN
			g/km			#/km
Euro 1†	1992 .07	2.72 (3.16)	0.97 (1.13)	-	0.14 (0.18)	
Euro 2 IDI	1996 .01[a]	1.0	0.7	-	0.08	
Euro 2 DI	1996 .01	1.0	0.9	-	0.10	
Euro 3	2000 .01	0.64	0.56	0.50	0.05	
Euro 4	2005 .01	0.50	0.30	0.25	0.025	
Euro 5a	2009 .09[b]	0.50	0.23	0.18	0.005[f]	
Euro 5b	2011 .09[c]	0.50	0.23	0.18	0.005[f]	6.0×10^{11}
Euro 6	2014 .09	0.50	0.17	0.18	0.005[f]	6.0×10^{11}

*At Euro 1...4 stages, passenger vehicles > 2,500 kg were type approved as category N_1 vehicles.

† Values in brackets are conformity of product (COP) limits

a. until 1999.09.30 (after that date DI engines must meet the IDI limits)
b. 2011.01 for all models
c. 2013.01 for all models
d. And NMHC = 0.068 g/km
e. Applicable only to vehicles using DI engines
f. 0.0045 g/km using the PMP measurement procedure
g. 6.0×10^{12} 1/km within first three years from Euro 6

3.5 Issues in PM Measurement

The major challenge in PM measurement is to give a characteristic representation of it in the atmospheric environment where humans are exposed to. Laboratory

measurements are easily affected by conversion of semi-volatile matter into particles and in addition, issues of cleanliness and instrument calibration can result in artefact error. Similarly, measured values vary greatly with operating conditions of the engine from cold and transient periods to hot and steady operations. These factors contribute to difficulty in inter-Laboratory comparisons. There are also differences in measurement techniques; these in effect, are related to the kind of instrument used, which are contrived to exploit aerosol properties. Therefore, host of issues are considered to PM measurements but majorly based on particle conversion due to volatile matter. This makes dilution a central issue in aerosol sampling, handling and measurement. Avalanche of reports abound in effort to explain the effect of dilution on PM measurement depending on the objective of the study and has attracted establishment of regulatory protocol, the PMP.

3.5.1 Sampling and Transport Deposition and Losses.

Some mechanisms associated with particle transport were highlighted in section 3.2.2. Legislation stipulates that PM to be measured by drawing sample from dilution tunnel with constant flow sampler. In most techniques this is only the primary dilution section, from where sample is drawn into the secondary dilution sub-systems; or to a measurement system of interest. Measurement of particulate mass accumulated on a filter has been a customary metric but in addition, particle number has recently been introduced in current legislation. Either or both ways it is important to draw diluted sample in a manner that it will not lose matter from emission location to the entrance of the measurement device. Particle penetration into sampling probe in ideal situation is '*isokinetic*' and '*isoaxial*' meaning that the probe is aligned parallel to gas streamlines and that gas velocity enters sampling probe with the same free stream velocity as it approached the inlet along the same flow axis. Otherwise, it is '*anisokinetic*', and if not the same axis, it is '*anisoaxial*'. Therefore particle losses, biased or unrepresentative population sizes could occur if extraction is either anisokinetic or anisoaxial. Particle number or mass could be affected by transformations that occur due to internal process during transport like coagulation/agglomeration, fragmentation and gas-to-particle conversion. Similarly, external processes like convective diffusion and thermophoresis; and processes that

occur in stationary aerosols could affect measurement results (Giechaskiel et al 2012; Hinds W. C., 1999; Brockmann, J. E., 2011).

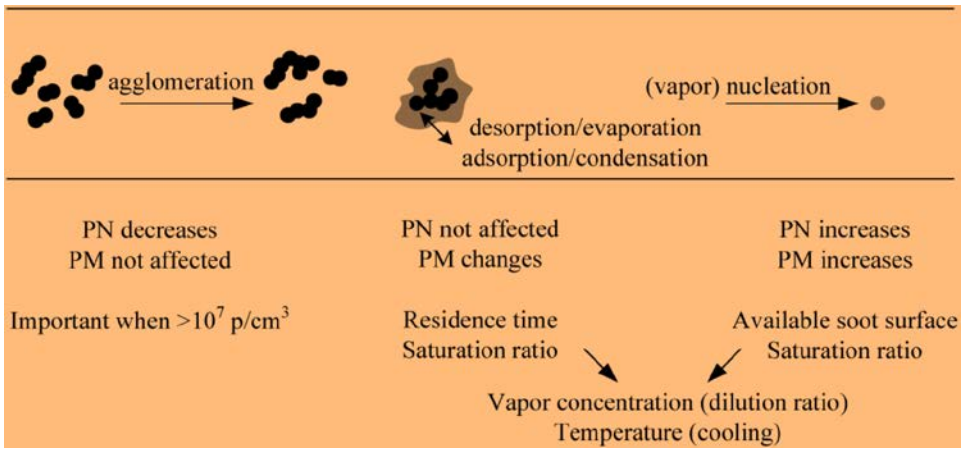

A: Internal processes affecting particle dynamics.

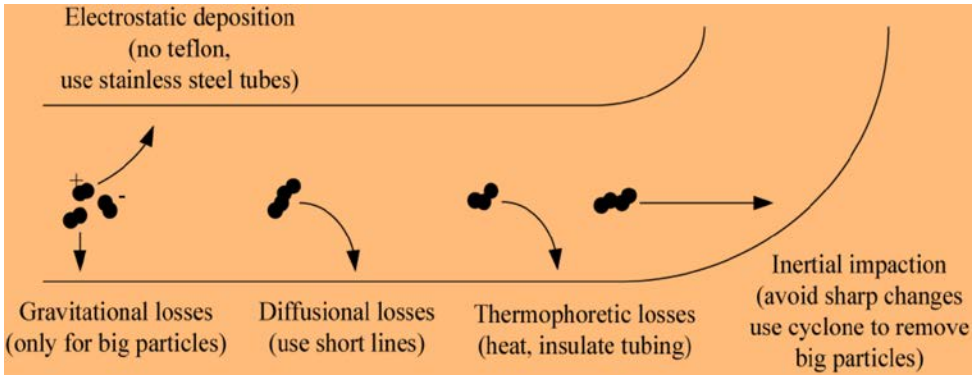

B: External processes that could influence particle loss

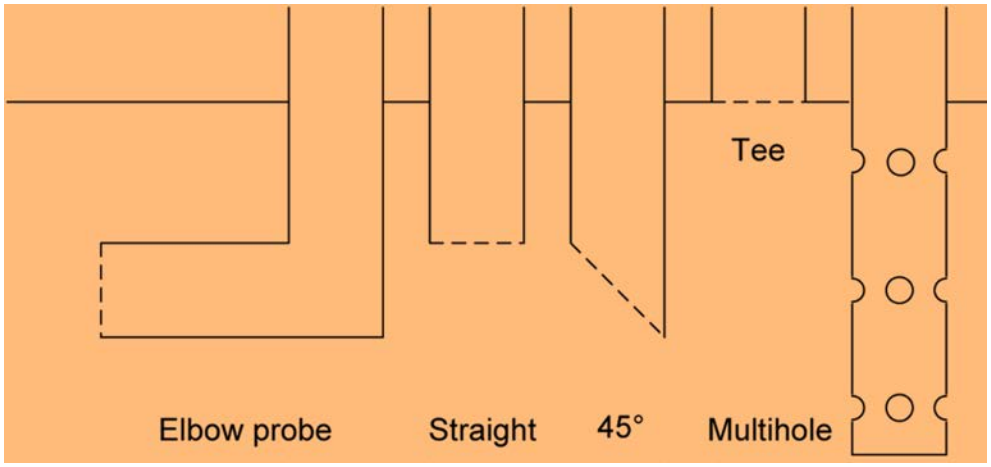

C: Different types of sampling probes

Figure 3.10 Internal and external factors that could affect particle losses during sampling and the types of sampling probes (Giechaskiel et al 2012A)

The theoretical considerations for these losses in the different sampling techniques, with application examples; consideration for tubing materials and different types of sampling probes are excellently presented in (Giechaskiel et al 2012A). Of great significance is the reality and implications of 'anisokineticity' and 'anisoaxiality' of flows during sampling with different types of probes. These present obvious challenges of inevitable errors during measurements particularly in low scale laboratory efforts. Therefore inter-laboratory repeatability of measurement is difficult and makes acceptability of result dependent on the level of relevant physics considered. These errors are due to particle deposition or losses and are grouped according to the following mechanisms (Marjamäki, M. and Keskinen, J., 2005; Kittelson, D. B., Arnold, M. and Watts,W. F. (Jr)., 1999; Brockmann, 2011; Hinds W. C., 1999):

Thermophoresis

This is a deposition mechanism associated with force interactions on the particles due to temperature gradient. Particles spatially on higher temperature side possess greater mobility and move towards cooler surface. The deposition of soot on the inner walls of exhaust and sampling system is attributed to this mechanism. Ordinarily, bulk particle mobility is far greater than this force so, the influence is not much especially for large diameter pipes.

Inertial Impaction

The inertia possessed by a particle which is the product of its mass and velocity could be appreciably high that it strikes the wall of exhaust or sampling system, instead of following the gas streamlines. This is more prevalent when particles experience bends or contractions in the exhaust or sampling system. Obviously, it depends on S*tokes number* defined for the characteristic dimension of the specific flow-path however; this is also not of much influence on nano particles. For particles possessing Stokes numbers of ~ o.6 in filter monoliths for example, half will strike the surface and half will follow the streamlines. Impaction falls off rapidly with Stokes number, with no deposition below a critical value of 0.25 (Eastwood P. , 2008).

Diffusion

The movement of particles through a boundary layer to the walls of the exhaust or sampling system could create losses due to diffusion. Diffusion coefficient of a particle is inversely proportional to particle size and on this account, particle of smaller sizes diffuse quicker than larger sized-particles. It is quite significant for sub 50 nm diameter particles which is representative of diesel exhaust aerosols. Diffusional losses are much less in laminar flows compared to turbulent flows where in fact, very small particles have a high diffusion rate.

Electrostatic Deposition

The combustion process naturally impacts charges into the diesel exhaust particles; therefore electrostatic deposition could occur during aerosol flow if the transfer or sampling line is made of materials that can be electrically charged. If this occurs, preferential charged particles will be drawn to deposit on the walls of the transfer line. This is the core reason for the use of metallic materials and avoidance of Polytetrafluoroethylene (PTFE) materials to minimise electrostatic build up on sample lines.

Sedimentation

This deposition mechanism is purely associated with influence of gravitation on particles which could only be relevant if the size exceed 40 μm. Its impact is minimal in the loss of diesel PM however; if there is re-entrainment of wall deposited particles into the sample flow stream, some measure of variability will be introduced in measurement. This is preventable by designing the sampling line to be as short as possible particularly for samples where large particles may settle.

3.5.2 Dilution of Particulate Matter

Laboratory dilution of diesel aerosol attempts to mimic real-world dilution; however unlike atmospheric dilution that progress to infinity, laboratory dilution is according to fixed dilution ratio. As atmospheric dilution is influenced by elements of whether, chase experiments have been used to study relative sample extracts to get clues about dilution rates, dilution ratios, temperature and humidity as well as residence time as exhaust plumes dilute and expands. One obvious observation is the inevitable change

in the nature of PM as it is dilutes; which compounds the study of *PM* relative to its composition as generated by the engine. Apart from the need to simulate atmospheric scheme, it is essential to reduce the concentration of typical diesel aerosol to the level most measurement devices can handle. Dilution has therefore become a sensitive conditioning issue in *PM* measurement and characterisation studies. This is due to difficulty in obtaining repeatable measurements after dilution caused by gas-to-particle conversion as aerosol encounters low temperature in the dilution process. Although the design criteria may vary, there are two principal aspects of dilution tunnelling – the *full flow* tunnels where the whole exhaust gas is diluted and - the *partial flow* tunnels where only a fraction of the exhaust gas is extracted and proportionally mixed with dilution gas. Either way, laboratory dilution schemes are conducted within finite boundaries and dilution ratios; and also subject to the interplay of the other variables as encountered in the atmosphere. Implicitly, the end state of diluted aerosol sample prior to measurements depends on the initial conditions of the dilution gas with regards to its temperature and humidity, the dilution ratio (DR), and residence time in the tunnel. Dilution implies mixing and cooling; it has been extensively reported as aerosol conditioning parameter (Burtscher H. , 2005; Kasper, 2004; Abdul-Khalek, I., Kittelson, D. B., and Bear, F.,, 1999; Kawai, T., Goto, Y., and Odaka, M., 2004; Mathis et al 2004; Giechaskiel et al 2012). The two physical processes of mixing and cooling act in different ways on aerosol depending on the thermal state of dilution gas (Alozie et al 2014A). By assuming that mixing of aerosol with dilution gas is adiabatic, interpolation of dilution air and aerosol temperatures gives the final temperature of diluted sample as:

$$T_{mix} = T_{exh}\left(\frac{1}{D}\right) + T_{air}\left(1 - \frac{1}{D}\right) \qquad (3.4)$$

Where *D* is the dilution ratio, T_{exh} and T_{air} are exhaust and dilution air temperatures respectively. The temperatures are in absolute scale and equation satisfies two extreme situations of *no dilution* (where D = 1, $T_{mix} = T_{exh}$) and *huge dilution* (where $D \rightarrow \infty$, $T_{mix} \rightarrow T_{air}$) (Amann et al 1980) cited in (Eastwood P. , 2008). Similarly, the way dilution ratio is defined may vary but it naturally will depend on the mass flow rates of aerosol and dilution gas which in turn depend on their densities,

temperatures and volumetric flow rates. DR has been defined as (Wei, Q., Kittelson, D. B., and Watts, W.F, 2001) :

$$DR = \frac{m_{mix}}{m_{exh}} = \frac{(m_{air}+m_{exh})}{m_{exh}} \quad (3.5)$$

If the above physical variables are assumed constant, the concentrations of gaseous components or particle numbers could serve as alternative criteria for defining DR; for example, with N as particle number concentration:

$$DR = \frac{[N_{exh}-N_{air}]}{[N_{mix}-N_{air}]} \quad (3.6)$$

Many measurement devices have been designed to suite different approaches to dilution. The exact nature of exhaust emission as it leaves the engine (particularly the solid elemental carbon) is of interest in characterisation studies, therefore most dilution efforts aim at freezing a proportional sample from further reaction due to changes in temperature and humidity. This entails understanding the dilution process as it affects saturation of the volatile matter contained in exhaust gas during dilution to final mixing temperature. This is related to *saturation ratio* defined here as the ratio of partial pressure of volatile species to the saturation pressure of the same species. Usually interest is on the volatile organic species, which are emitted as unburnt diesel fuel and complex combustion generated hydrocarbon intermediates. Therefore the saturation ratios (S) that will determine the gas-to-particle conversion of the complex vapour-phase organic species in the exhaust gas are not easily defined at a particular temperature. Ordinarily equilibrium plays a vital role on the direction of phase conversion as condensation will occur when the $S > 1$ (Hinds, 1999); which for homogeneous species will result in homogeneous nucleation, but for multi-component matter, it becomes possible that nucleation could occur even for $S < 1$. Therefore complex nucleation and condensation processes are involved. Changes in saturation condition have long been identified to influence the formation of nuclei mode particles from diesel engine volatile matter during dilution whether in the laboratory or atmosphere, which could follow homogeneous or heterogeneous path. This is also viewed to affect adsorption because as the process begins, (although the

model description held temperature constant during adsorption process) vapour molecules form single molecular layer by physically binding to surface sites available for attachment. Subsequent adsorption occurs on top of the initial layer in a manner that follows condensation process (David Kittelson, D. B., Watts, F. W ., and Arnold, M., 1998). Mixing exhaust gas with dilution gas at high temperature will decrease the partial pressures of volatile species and prevent phase conversion when cooled to low temperatures. Contrarily, if hot exhaust is mixed with dilution gas at low temperature, the cooling effect will initially decrease the saturation vapour pressure of the volatile fractions and enhance gas-to-particle conversion. If mixing is sustained, the effect will dominate the physical reaction and cause the partial pressures of volatile species to decrease and ensure particle-to- gas conversion. Therefore the way exhaust sample is mixed and cooled is very relevant to particle formation in dilution process; and the pathways are central to the different dilution techniques available for sample conditioning.

3.5.3 Laboratory Systems for Particulate Matter Dilution

The CVS system highlighted under PM transport (section 3.22) is a traditional dilution system not easily affordable for most laboratory studies. Most dilution systems fall under partial flow dilution tunnel where proportional extract of exhaust sample is diluted by different dilution systems. Many dilution system designs follow volume or mass flow rates proportions in the mixing schemes and these include:

Ejector Diluter

A unit manufactured by '*Dekati*' functions by critical pressure difference (*dP*) across an annular nozzle created by flow of dilution gas which also draws the sample to flow through the nozzle Figure 3.11. The dilution air flow is controlled by a critical orifice at the inlet side where the inlet pressure is set. Since the exhaust flow pressure is constant, the pressure difference is determined by the dilution gas pressure controlled by the critical orifice. By this principle, increase in the flow of dilution gas increases the flow of sample in the same proportion thereby maintaining a given dilution ratio. In most applications particularly when used in sampling hot exhaust, it is normally employed in two stages. In this way vapour pressures of the volatile species and temperature can be reduced in the two stages according to the dilution

objective. Each diluter is independently calibrated and inlet pressures checked at 800-1050 milibar for each dilution ratio (HEI D. L.).

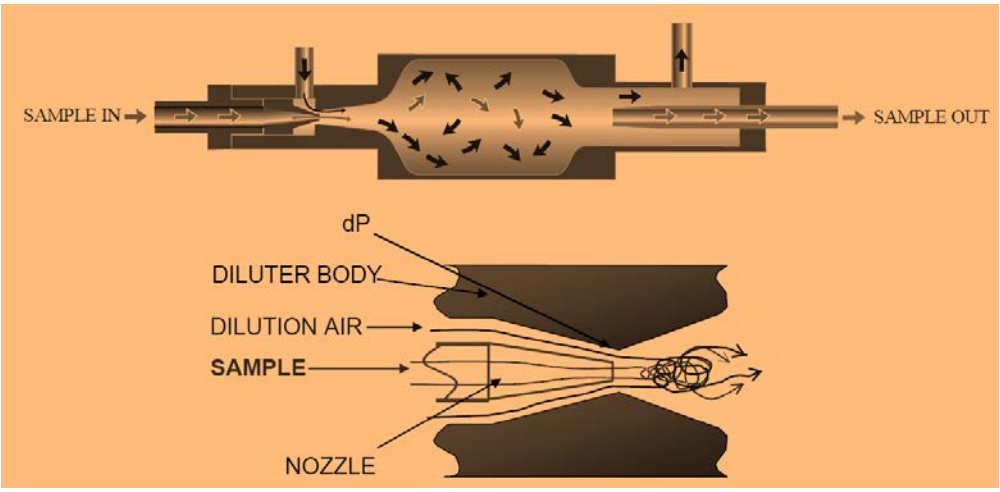

Figure 3.11 Operating principles of the Dekati ejector diluter (HEI D. L.)

Rotating Disk Thermo-diluter

A unit produced by '*TSI Instrument*' which uses a unique rotating disk method to dilute aerosol sample. To enable the selection of dilution ratios, two disks with cavities are used in one unit as shown in Figure 3.12. In operation, exhaust is trapped in each cavity of the rotating disk and channelled to mix with filtered dilution air. The dilution ratio is a linear function of the disk calibration factor (volume of cavity and number of cavities per disk), the rotation frequency and the flow rate of the dilution air (TSI). This is given as:

$$DR = \frac{Disk\ Calibration\ factor\ X\ Disk\ Rotation\ Frequency}{Dilution\ Air\ flow\ Rate}$$

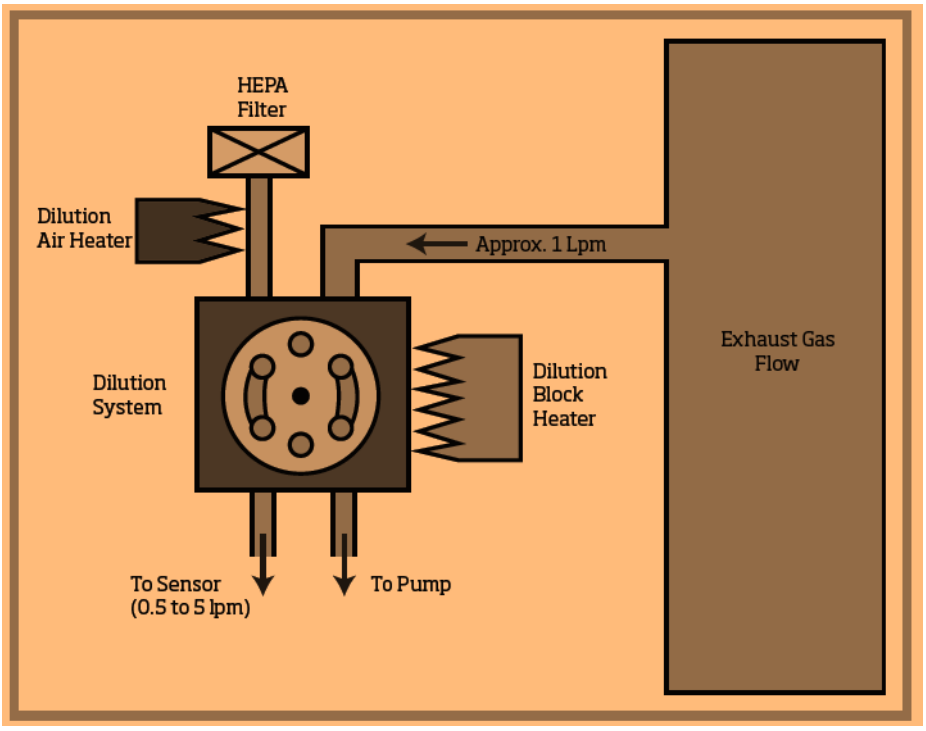

Figure 3.12 Diluter head block diagram (TSI)

Porous Tube Diluter

The porous tube diluter consists of an inner perforated tube concentrically placed inside an outer tube whereby dilution gas is forced through very fine perforations to mix with raw exhaust sample. It is efficient in diluting exhaust sample without significant nucleation compared with other dilution systems (lyyränen et al 2004). In '*Dekarti FPS 4000*' unit, it is incorporated as a primary diluter in a two-stage dilution system. The dilution factor of the primary dilution stage can be adjusted by changing the dilution airflow into the primary diluter as in Figure 3.13 (Dekati., 2015).

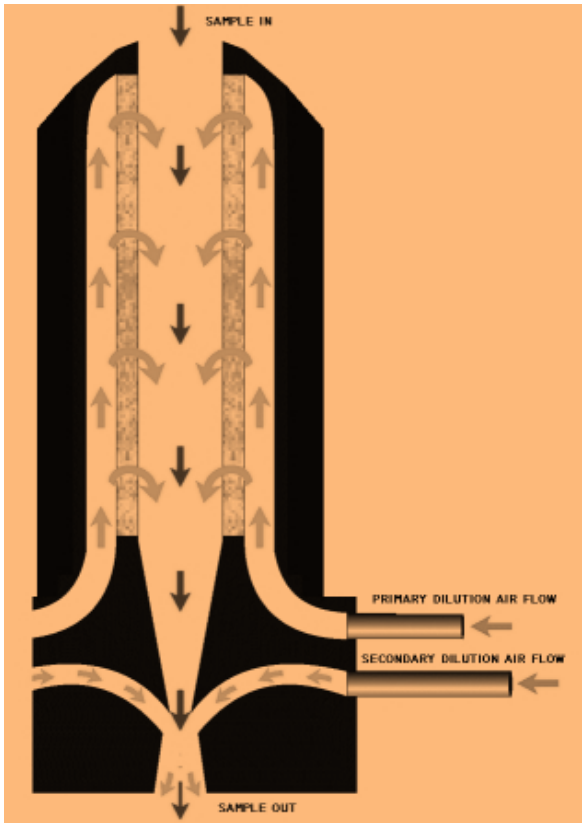

Figure 3.13 Porous Tube Diluter (Dekati., 2015)

3.5.4 Particulate Matter Sample Conditioning Techniques

Conditioning of the exhaust sample prior to measurement aims at ensuring that nucleation of new particles from volatile species does not occur to give erroneous value of particle number concentration. While dilution can prevent formation of new particles by subverting nucleation, some other techniques like thermo-desorption (TD) and catalytic stripping (CS), are used to physically remove volatiles or particles that condense from exhaust sample during the conditioning process, and thereby minimise measurement errors. These techniques are reviewed as follows:

Cold and Hot Dilution; Thermo-dilution and post dilution thermo-conditioning

The pathways for gas-to-particle conversions and vice versa have been explained with phase diagrams (Kasper, 2004; Burtscher, 2005). Exhaust gas emitted at state ‘X’ and diluted to state ‘G’ in a CVS will contain particles that condensed from volatile species since the nucleation line was crossed during cooling as in Figure 3.14 (A). To remove the condensed particles, the sample will have to be diluted further to state ‘N’ at the same temperature. Process ‘XG’ caused gas-to-particle conversion

because cooling initially had major influence while 'GN' is a particle-to-gas-conversion due to influence of mixing. On the other hand, process 'XH' indicates mixing at the same exhaust temperature that reduced the partial pressures of volatile species to the same concentration as 'N' and when cooled to the same state, saturation could not be reached and therefore prevent nucleation.

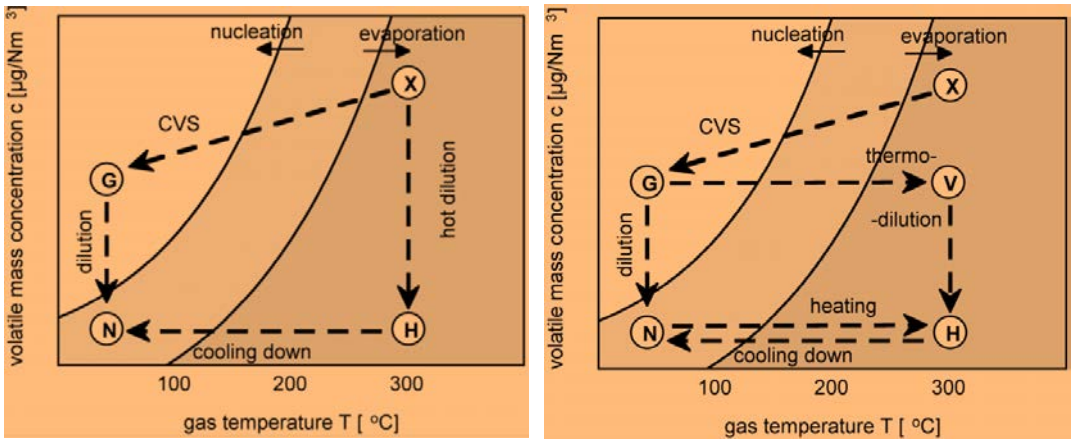

(A) (B)

Figure 3.14 A- Phase conversion pathways due to mixing and cooling. B- Thermo-dilution (G-V-H-N) and post-dilution thermo-conditioning (G-N-H-N) (Kasper, 2004)

The interplay of mixing and cooling during dilution is fundamental to the conception of the thermo-dilution system. In the scheme, a heating section is incorporated to vaporise the volatiles and then diluted at high temperature to reduce the vapour pressure before cooling to avoid nucleation. The phase pathway is 'G-V-H-N in Figure 3.14B; however if volatile concentrations are high or if there be any cold spot along the line, nucleation could still occur. To arrest such situation, the path 'H-N' will involve heating instead of cooling; this has been described as post-dilution thermo-conditioning (Kasper, 2004) where the diluter and heater sections were interchanged as in Figure 3.15.

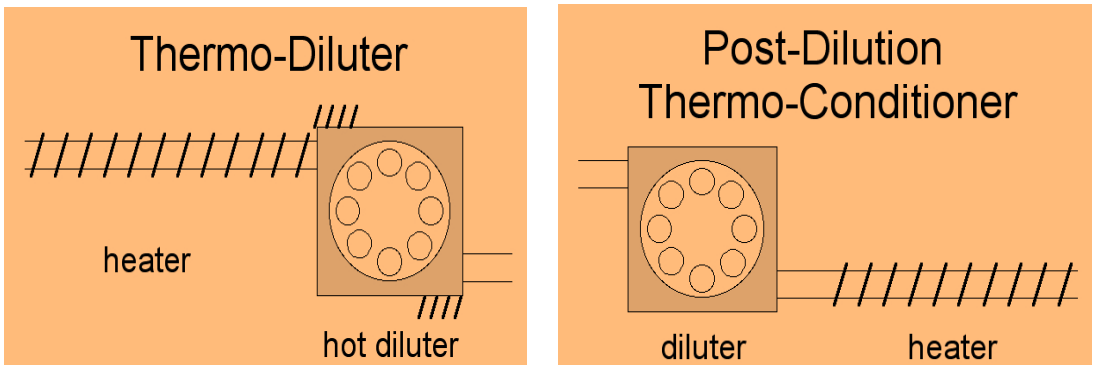

(A) (B)

Figure 3.15 Thermo-dilution and Post thermo-conditioning

Thermodesorption (TD)

This technique involves physical removal of volatile species contained in the exhaust by the use of activated charcoal (Burtscher et al 2001; Swanson, J., and Kittelson, D.,, 2010). The implication is that the species must be in vapour state and through molecular diffusion, adsorb on the charcoal surfaces as it cools. Therefore if sample has been diluted to state 'G' as before in a CVS, 'heating' process is depicted as process 'GV' and desorption occurs in process 'VN' as in Figure 3.14 (A). The efficiency of thermo-desorption is size dependent as nucleation could still occur if volatile concentration is high or if cooling rate is rapid. Other shot-comings of TD are requirements for regular maintenance especially replacement of activated carbon and loss of particles through sedimentation, diffusion and thermophoresis (Swanson, J., and Kittelson, D., 2010; Fierz, M., and Burtscher, H., 2003; Kasper, 2004). A design developed by 'Dekarti' could allow a high flow rate of 10-20 l/min, and operates with charcoal paper as absorber to overcome most of these draw backs. The thermodesorber is also known as thermo denuder and have been well utilised in the study of atmospheric aerosols.

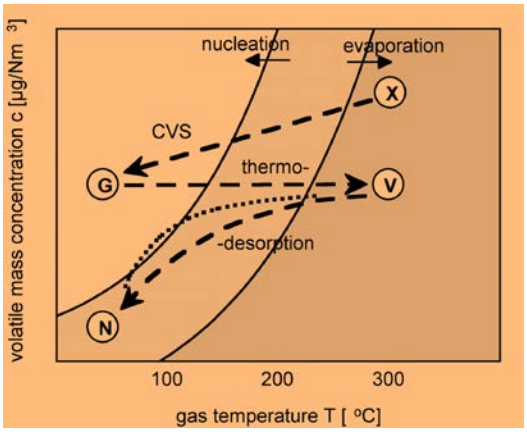

(A) (B)

Figure 3.16, A: Phase Path for Thermodesorber, B-thermodesorber by 'Dekarti': Curved red part is heater and the steel tube contains charcoal paper. (Kasper, 2004; Fierz, M., and Burtscher, H., 2003)

Catalytic Stripping (CS)

Catalytic stripping involves passing diluted hot exhaust through a chamber of catalytic converter that is maintained constant at about 300 ^{o}C and the sample is stripped of the volatile components without significant removal of the solid soot particles as reported in the initial work by (Abdul-Khalek, I. S., and Kittelson, D., 1995). The stream of exhaust sample was passed alternately through the stripper (a heated oxidation catalyst) and bypassed around it. This enabled comparison to be made of the particle concentrations in the bypassed and stripped flows for volatile, solid soot and total number concentrations. The stripper was characterised with laboratory aerosols and thereafter was used in conjunction with electrical aerosol analyser (EAA) for further characterisation of particles emitted from diesel and spark ignition engines. It gave complete removal of volatile sulphate and hydrocarbon particles but lead to 15-25% loss of solid particles. This technique was further developed to overcome the loss of solid particles (by thermophoretic deposition) due to cooling by dilution instead of using a cooling coil (Khalek I. A., 2007). This improved version is the concept used to develop a complete stand-alone solid particle number measurement system (SPNMS) (Khalek, I.A., and Bougher, T., 2011). Exhaust sample is maintained at 300^{o}C through a heated line and passed via the first stage of the three stage dilution system to the CS, which is simply a micro diesel oxidation catalyst (m-DOC) as in Figure 3.17.

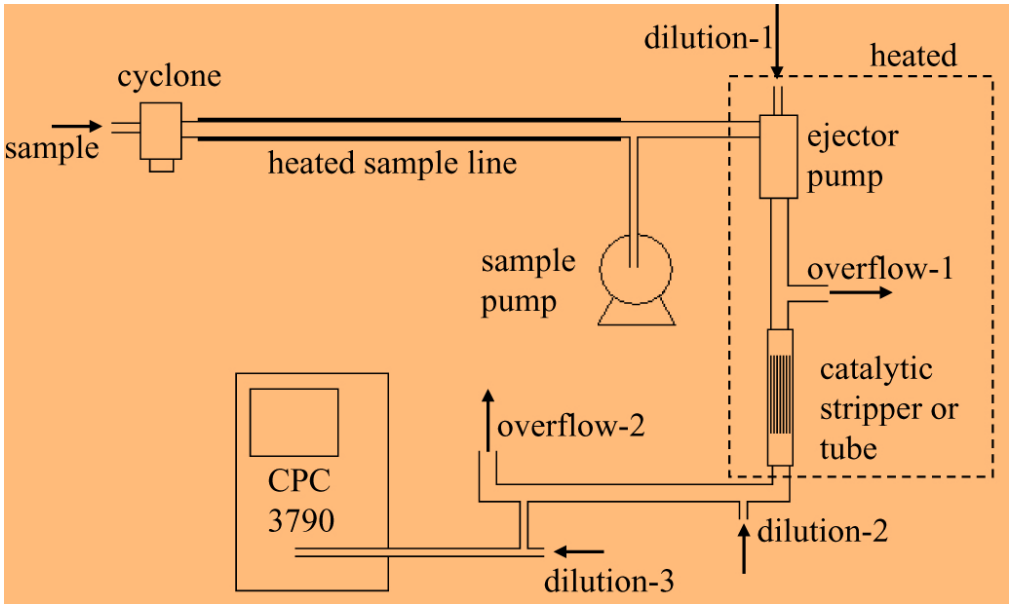

Figure 3.17 Flow Diagrams of the SPNMS (Khalek, I.A., and Bougher, T., 2011)

3.5.5 PM Measurement Techniques

The different ways to dilute and condition aerosol sample prior to measurement have given rise to variety of aerosol measurement devices. Classic groupings of the different approaches to measurement of aerosols are detailed in (Kittelson, D. B.,Watts, W. F., and Arnold, M., 1998; Brokckmann, 2011). Aerosol properties are harnessed to develop the principles and techniques on which these devices function, either on real time or for remote analysis of extracted samples. Particle parameters such as mass, number, size, surface area and volume are influenced by the chemical and physical transport processes from engine generation to point of sample collection and conditioning as already highlighted. Accordingly, different instruments are used to analyse and measure PM based on properties that relate to mass, number, surface area and volume distributions. These instruments offer different criteria for assessment of aerosol distribution inherent in their calibration and method of manipulation or control in order to get results. Some techniques for classifying, analysing and detection of particles used in aerosol characterisation studies are summarised as follows.

Inertial, Gravitational, Centrifugal and Thermal Techniques

Some devices that operate on inertial techniques are inertial classifiers which include conventional impactors, virtual impactors, and cyclones. Particle classification by inertial impaction is through capturing of those particles that deviate from the streamlines as they flow by virtue of the inertia they possess while the smaller ones remain in the flow. The '*Stokes Number*' is the important dimensionless parameter that influences particle's impaction on a body and is defined as the ratio of particle's stopping distance to the physical dimension of the body's collector:

$$Stk = \frac{\rho_p U C_c d_p^2}{18\eta d_b} \qquad (3.7)$$

Where ρ_p is the particle density, U is the flow velocity, Cc is the slip correction factor, d_p is the particle diameter, η is the air (or gas) viscosity and d_b is the body diameter. Array of impactors have been described and grouped according to applications and host of manufacturers in (Marple, V. A., and Olson, B. A., 2011) where for conventional impactors, the *Stokes Number* is defined as the ratio of stopping distance to the radius of a circular nozzle or half the width of a rectangular nozzle. In diesel aerosol industry, the prominent instrument that utilises this technique is the *Electrostatic Low-Pressure Impactor (ELPI)* which classifies particles sizes according to their aerodynamic diameters. New versions from *DEKATI* can enable measurements from 6nm to 10μm on real time basis and also for gravimetric measurements. Particles are usually charged prior to entry into impaction stage and the stages are individually connected to electrometers to detect the impact of each particle. It is such detection that enables size distribution measurements to be made over the wide range of sizes and therefore makes it suitable for diesel aerosols to be measured whether for transient or steady engine operations. Similarly, it is utilised in pharmaceutical aerosol development, air quality monitoring and general aerosol research. Instruments based on based on gravitational, centrifugal and thermal techniques are rarely used in diesel aerosol measurements. Settling chambers centrifuges and thermal precipitators are typical devices. The settling chamber measures settling velocity directly and therefore naturally suited for measuring aerodynamic velocity since by implication, a particle's aerodynamic diameter is the equivalent diameter of a unit density sphere having the same gravitational settling

velocity. Settling chambers are not suitable for sub-micron particles which are of interest in diesel aerosol due to low settling speeds; for instance, particle of 1μm has a settling speed of about 0.0035cm/sec while a particle of 10μm has a settling speed of 0.305cm/sec. The interference of Brownian motion on settling speed of small particles is said to a lower limit of about 0.6μm (Marple, V. A., and Olson, B. A., 2011).

Centrifuge technology is almost phased out but it offers advantage of measuring aerodynamic diameters of irregular shaped particles once calibrated. In operation, the particles and carrier gas are rotated at a high speed and the centrifugal force separates the particles and deposits them across the chamber according to their sizes. By implication, the larger sizes are deposited nearer to the center due to their resistance as they spin while the smaller particles fall further towards the edge.

The class of instrument that operates due to thermophoretic forces is thermal precipitators. The temperature gradient in the gas provides the thrust for the particles to move from warmer side to cold surface. They have been used in the United Kingdom for sampling particles size that could be inhaled from the mines.

Electrical Mobility Techniques

Measurement systems based on electrical mobility techniques are best utilised in the laboratory studies of diesel aerosols. This is inherent in the sub-micron sizes of particles generated from engines which are naturally charged in the combustion process. Technically, classification is achieved by the application of known electrostatic force over the charged particles. This technique has been developed as electrical mobility analyser in which charged particles are passed through variable electric field. Under the influence of the field, the charged particles are impacted with different drift velocities according to the balance between the electrostatic force and the aerodynamic drag acting on them. Therefore the electrical mobility depends on their sizes in terms of aerodynamic diameter d_p and electrical charge i, and these offer avenue to separate or classify the particles according to their mobilities (Flagnan, 2011; Reischl G. P., 1991 A; Kittelson, D. B., Arnold, M. and Watts,W. F. (Jr)., 1999). Most designs of electrical mobility analysers incorporate chargers on the line and can enable the classification of very low particle sizes as small as 7nm. Laboratory units that operate on this technique come in different names like: *Electrical Aerosol Analyser, Differential Mobility Particle Sizer, Scanning Mobility*

Particle Sizer etc. A Vienna-type electrical mobility spectrometer is available in our laboratory for PM measurement and is described in chapter four. Its differential mobility analyser (DMA) classifies charged particles based on their drift velocities in the cylindrical field in between inner and outer electrodes using a sheath flow that is free from particles. It incorporates a faraday cup electrometer (FCE) for particle detection and counting.

3.5.6 Detection and Counting Instruments

Particle detection instruments are usually incorporated to the electrical mobility analysers. Principal instruments used in measurement devices are condensation particle counters and electrometers.

Condensation Particle Counters (CPC)

Condensation particle counters detect and count submicron particles by condensation technique. The processes are based on super saturation of the working fluid, growth of particles condensed, then their detection and counting. The processes commonly applied to induce super saturation in commercial instruments include adiabatic expansion, thermal diffusion, and mixing of hot and cold airstreams (Yung-Sung, 2011).

Expansion-Type CPCs

The expansion type CPC uses water as the working fluid in which aerosol is initially passed through a humidifying chamber to reach the water vapour saturation at ambient temperature and subsequently passed through an expansion chamber where it is suddenly cooled either by volume expansion or decrease in pressure. The expansion ratio associated with the change in volume or pressure is related to the geometry of the expansion column expressed with respect to initial and final conditions:

$$Pressure\ expansion\ ratio = \frac{Pressur_{\ initial}}{Pressure_{\ final}}$$

$$Volume\ expansion\ ratio = \frac{Volume_{\ final}}{Volume_{\ initial}}$$

It is usual to adopt values of ideal gas adiabatic expansion for air and water vapour due to the negligible time for heat transfer in the short expansion process to determine supersaturation ratio of vapour used in CPCs. Hence it has been easy to determine the saturation ratio in terms of the volume or pressure expansion ratios and the saturated vapour pressures. In operation, aerosol and vapour in this type of CPC flows in a cycle, first filling the chamber and followed by the expansion process; then the particles emerge and their concentrations are determined.

Conductive Cooling CPCs

Steady flow measurement devices like diffusion battery and electrical mobility spectrometer require CPCs that also operate as steady-flow systems unlike the cyclic expansion type. Conductive cooling CPCs satisfy this criterion through a system of saturator, condenser, and particle detector. Many commercial units by 'TSI' use butanol as working fluid Table 3. 3. Typical schemes have a reservoir of alcohol where aerosol is passed to get saturated according to set temperature and residence time; then passed through the condenser for supersaturation via conductive cooling by the walls. The choice of Ethanol or Butanol is because their molecules are relatively larger than those of water and this accounts for their vapour concentration remaining high during cooling since the diffusional transport to the condenser walls is low. Therefore particle growth due to condensation is activated along the path of supersaturation and the concentration of which is amenable to numerical evaluation of heat and mass transfers in the design process.

Differential Diffusion CPCs

Differential diffusion CPCs are also steady flow systems but use water instead of alcohol with the advantage of eliminating alcohol fumes and possible spills in the immediate environment. As mass diffusivity of water is greater than thermal diffusivity of air, it implies that water vapour will diffuse to the condenser walls quicker than the bulk flow is cooled thereby lowering supersaturation compared to mixing streams of saturated hot and cool air (Hering, S. V., Stolzenburg, M. R.,, 2005).

Table 3.3 Commercial Particle Counters (Yung-Sung, 2011)

Company	Model	Type	Working Fluid	Detection Limit (nm)
KAN	3885	Mixing	Propylene glycol	10
GRI	5.401	Conductive Cooling	Butanol	4.5
TSI	3007	Conductive Cooling	Butanol	10
TSI	3772	Conductive Cooling	Butanol	10
TSI	3775	Conductive Cooling	Butanol	4
TSI	3776(UCPC)	Conductive Cooling	Butanol	2.5
TSI	3785	Differential diffusion	Water	5
TSI	3786(UCPC)	Differential diffusion	Water	2.5

Electrical detection instruments – Electrometers

These instruments normally referred to as electrometers, operate by detecting electrically charged particles and are well suited for diesel particles detection and counting. They are normally used in conjunction with DMAs which classify the particles. The detection scheme is enhanced by ensuring that particles are properly charged. In most designs this is achieved with a corona charger prior to classification and then particles are flown past the electrometer for detection and counting. In essence charging has become a conventional compliment to detection of the particles in most instruments. The particles receive charges proportional to their diameters of which, the average also depends on the density of the ions (N_i) and the residence time (t) in the charger, called the $N_i t$ product. This is related in a power law as$(q \sim d_p^x)$ where the exponent x depends on the $N_i t$ product and d, the size of the particle size range (Dhaniyala, S., Fierz, M., Keskinnen, J., and Marjamaki, M., 2011). Other parameters like temperature, gas pressure, particle morphology, dielectric constant and ion properties affect the level of particle charging but to a lesser extent. Early expressions for particle charging was based on Fuchs theory which dealt purely on diffusion charging, but this has been extended to include the presence of strong electrical field in addition to diffusion charging for particle diameters ranging from 30 to 100nm, of which the electric field strength is limited to 10kV/cm (Marquard, 2007). A typical detection device is the Faraday cage electrometer which is very sensitive in picking very low current. In operation, the aerosol containing charged and classified particles according to size of interest is shielded by a metal as it is passed into a housing containing a filter. The filter is

surrounded by a conducting enclosure which acts as a faraday cage. As the particles pass through the faraday cage, the electric inside field is isolated by the cage which produces induced charge equal to that carried by the particles as they enter the cage. The electrometer that is connected to the cage measures the resultant current (I) which is related to the total number of particle concentration (N) according to equation 3.8.

$$q = I/(N.Q) \qquad (3.8)$$

where I is the current carried by the charged particles, N is the particle number concentration at the inlet (cm^{-3}), and Q is aerosol flow rate (cm^3/s) (Dhaniyala et al 2011). The low current associated with aerosol detection demands that electrometers be treated with care to avoid interferences that could emanate from variations in the immediate environment like light intensity, radio frequency, humidity and mechanical vibrations. For this reason, electrometers are designed with large feedback resistances that regulate their signal-to-noise ratio. A faraday cup electrometer (FCE) is coupled to the DMA of our measurement device – the electrical mobility spectrometer presented in chapter 4.

3.6 The Particulate Measurement Programme (PMP)

The PMP was originally a collaborative effort of the governments of France, Germany Netherlands, Sweden and United Kingdom that teamed up to develop analytical systems by which a regulatory framework to measure ultrafine particles could be developed. It gained UN-ECE mandate and was later joined by Switzerland, and during the validation stage South Korea and Japan participated. The three-phased project was chaired by the Department of Transport of the United Kingdom. The mandate given to the working group was to develop new particle measurement techniques to complement or replace the then existing (only) particle mass measurement with special consideration for measuring particle emissions at very low levels. The procedures for measuring non-volatile particle number emissions for both light duty (LD) and heavy duty (HD) vehicles were drafted by the group and adopted by the United Nations Economic Commission for Europe UN-ECE GRPE

(Andersson et al 2007; Andersson et al 2010). Emphasis was on development of standard technique that accurately determined non-volatile particle emissions using number metric, in order to regulate the emission of exhaust particles at very low levels. For LD vehicles, round robin tests were pursued using a prescribed reference measurement system (RS) to assess good repeatability and reproducibility of results (Giechaskiel, B., Dilara, P., and Anderson, J., 2008B; Giechaskiel et al 2008; Giechaskiel et al 2011; Giechaskiel et al 2012B). The scheme adopted the technique of thermo-dilution in pre-conditioning the exhaust sample. It specified the use of a volatile particles remover (VPR) and a particle number counter (PNC). The (VPR) consists of a primary hot diluter (PND_1), an evaporation tube (ET) and a secondary cold diluter (PND_2) in series. Initial aerosol dilution is prescribed at a temperature more than 150^{o}C and at dilution ratio (DR) of at least 10:1. Further heating in the ET is at a temperature of 300-400^{o}C to vaporise condensed volatile fractions before diluting again at the PND_2. The two stage dilutions reduce the partial pressures of the volatile species to a level that cannot support their condensation and therefore suppresses nucleation of new particles as aerosol cools. The particle number as at the exit of PND_2 remains the same without further addition from volatile matter condensation. The technique ensured that only solid carbon particles devoid of the confounding volatile matter were counted. This was described as golden particle measurement system (GPMS) and used Peugeot 407 HDi 2.0 litre car as the golden vehicle for light duty circulated to all collaborating laboratories. The golden vehicle did not necessarily represent the best car technology but was supplied to the joint research centre as a vehicle that met specifications for the study. It was powered by a common rail direct injection diesel engine with exhaust after-treatment system that comprised of diesel oxidation catalyst (DOC), an uncoated silicon carbide wall flow diesel particulate filter (DPF), operated on fuel doped with cerium catalyst, used post-injection and EGR shut-off to generate an exotherm for periodic regeneration of DPF. It therefore met Euro 4 emissions regulation standard. Other vehicles used in the tests are as presented in Table 3.4; they predominantly met Euro 4 limits although two were calibrated locally in Japan (Andersson et al 2007).

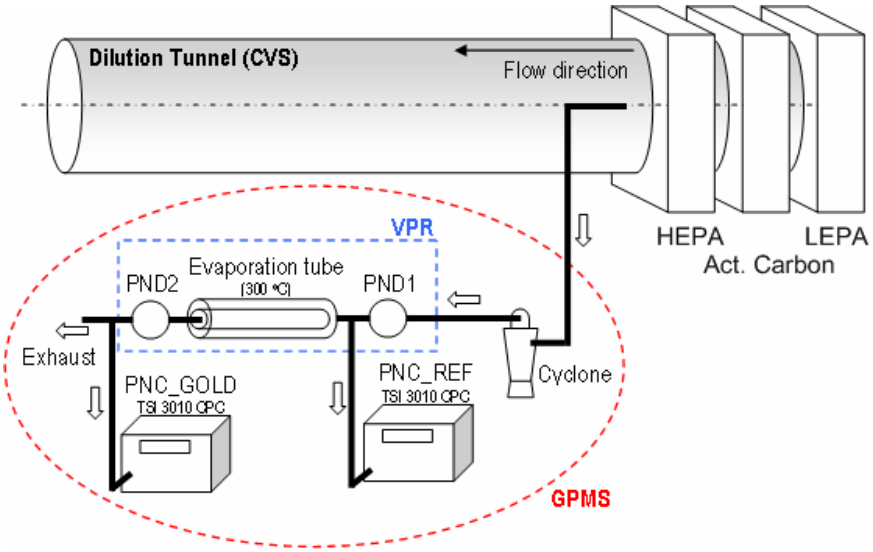

Figure 3.18 The Golden Particle Measurement System (GPMS) for Light duty engine (Andersson et al 2007)

Table 3.4 List of Vehicles used in Inter –laboratory Correlation Exercise (Andersson et al 2007)

Vehicle	Type	Lab	Code
Peugeot 407 HDi FAP 2000cc	DPF Diesel (Oxicat, uncoated DPF, FBC)	All	Golden Vehicle
BMW 525d catalysed DPF equipped, 2500cc	DPF diesel (Oxicat, catalysed DPF)	RICARDO	DPF#1
Mazda Bongo catalysed DPF, 2000cc	DPF Diesel (Oxicat, catalysed DPF)	NTSEL	DPF#2
Toyota Avensis D-CAT 3000cc	DPF Diesel (Oxicat, deNOx, catalysed DPF)	SHELL	DPF#3
Mercedes Vito Van DPF 3000cc	DPF Diesel (Oxicat, catalysed DPF)	SHELL	DPF#4
Peugeot 206 HDi FAP	DPF Diesel (Oxicat, uncoated DPF, FBC)	UTAC	DPF#5
FIAT, Idea, MI, EURO-4,TWC, 1400cc	Port-injected gasoline	JRC	MPI Vehicle
Mitsubishi, Carisma, GDI, TWC/deNOx 1800cc	Direct-injection Gasoline (lean)	RWTUV	GDI Vehicle #1
VW, GOLF FSI, TWC/deNOx 1600cc	Direct-injection Gasoline (lean)	JRC	GDI Vehicle #2
Toyota Crown G-DI, 3000cc	Direct-injection Gasoline (lean)	NTSEL	GDI Vehicle #3
BMW 120d PMFC 2000cc	Conventional Diesel	SHELL	Non-DPF #1
Audi A2, TDi, EURO-4, Oxicat, 1500cc	Conventional Diesel	RICARDO	Non-DPF #2
VW, GOLF TDi, non-DPF, Oxicat, 1900cc	Conventional Diesel	RWTUEV	Non DPF #3
Honda Accord i-CTDi, EURO-4, Oxicat/deNOx, 2200cc	Conventional Diesel	LAT	Non DPF #4
Kia Pride, non-DPF, 1500cc	Conventional Diesel	NIER	Non DPF #5
Vauxhall Astra, CDTi,1700cc	Conventional Diesel	SHELL	Non DPF #6

The group's final report for light and heavy duty engines were used to revise existing regulatory framework for particulate measurements, conventionally known as DR83 and DR49 for light and heavy duty engines respectively. It also formed the basis for laboratories to have a comparative platform to standardise their test in particulate sampling and testing both in number and mass metrics.

3.7 Reduction of Particulate Matter Emission

The task of reducing PM from the diesel engine is in understanding its nature and the complex variables that either promote or obstruct its formation in the engine, and its ejection into the atmosphere. This has necessitated telling the whole particulate story so far in the reviews. Implicitly, PM reduction is tied to the combustion phenomenon at the formation stage, and if not controlled by the combustion process then, after-treatment process that involves further reaction is the recipe to avoid its emission to the atmosphere. Therefore PM reduction or removal strategies based on combustion factors will imply improvement in the combustion quality of diesel fuel itself, improvements in the combustion chamber design, and optimal calibrations of the fuel injection equipment and engine operating parameters. The after-treatment methodologies have been in enhancing further chemical reaction of the unburnt hydrocarbons and soot. For soot, it involves physical trapping and positive ignition to periodically burn it out.

3.7.1 Fuels quality and combustion improvement

Exhaust emissions generally is a reflection of the nature of fuel burnt and/or how well it was burnt in the engine. Studies of fuel effects on emissions have been at the forefront of mitigation efforts and have led to great improvements in modern automotive diesel. The improvement in fuel quality is more in the domain of refiners who have commercial interest to fulfil and much depend on the origin of the crude oil. The core interest of the engine designer is on greater power output which is done around fuel properties. Raw properties of diesel have good performance indices however, engine emissions created early distaste in acid rain which was due to fuel sulphur content. Fuel improvement by desulphurisation led to compromise in diesel

fuel lubricity and oxidative stability, two critical conditions that made the powertrain liable to seizure and early failure thereby necessitating compensation with additives. The influence of physio-chemical properties of fuel on spray and combustion characteristics have been explained in chapter 2 and the related soot emissions in section 3.2.1. These are inherent to the fuel molecular structure that defined the oxidation pathways. In addition, diesel fuel has somehow been improved by blending with biodiesel which is known to chemically contain fuel oxygen that improves combustion and thereby reduces sooting (Giakoumis, 2014). Effect of biodiesel blending on PM emission is examined in this study.

3.7.2 Engine design and operating strategies

Apart from fuel improvements and in a way arising from it, engine designs factors have been complimentary to reduction in PM. Predominant in this regard are improvements in fuel injection systems, engine aspiration and chamber designs. In every design targeted to actualise market or regulated emissions level, early developmental studies are around specific fuel quality. Rigorous calibrations are normally conducted to optimise engine parameters like limits for fuel scheduling and the consequent combustion phasing, matching of turbocharger according to duty if aspiration is boosted, as well as matching the EGR according to target duty and emissions level. The description of the test engine used in this study is presented in chapter 4 and the operating conditions adopted in specific tests are presented in subsequent chapters.

3.7.3 Engine after-treatment strategies

The PM emitted from diesel engine is made up of solid soot particles and condensed volatiles of which, the organics are predominantly unburnt hydrocarbons. The after treatment technologies being developed and implemented to mitigate them are the diesel oxidation catalysts (DOCs) which further oxidise the hydrocarbons and the diesel particulate filter (DPF) which trap the soot particles or all PM in the absence of the DOC. The trapped PM (or soot) is subsequently ignited by a positive heat source and burnt (Eastwood P. , 2001).

***Diesel oxidation catalysts* (DOCs)**

These are catalytic converters that accelerate the oxidation of CO and HCs fully into CO_2 and H_2O. The engine generated volatile organic compounds (VOCs) or the PAHs which are part of the PM are included as HCs and therefore are prevented from being emitted to the atmospheric environment.

***Diesel Particulate filter* (DPF)**

This has become established approach to capture PM and substantially reduce its escape to the atmospheric environment. However, the volatile fractions are not captured effectively by this approach. The PM trapped by the DPF builds up as deposit at the upstream surface and causes back pressure. The deposit is a major technical challenge in the utilisation of DPF as the obstruction to free flow of exhaust gases affects normal engine operation and reduces power output. It therefore requires regular oxidation or burn-out in a process called *regeneration*. Filter regeneration requires optimum combustion temperature and adequate supply of oxidant which in most cases is supplied by the exhaust gas itself in the presence of a catalyst. The catalyst lowers the oxidation temperature and makes it possible for combustion to be initiated at pre-determined levels of PM deposits in a continuous cycle of build-up (*passive regeneration*). Through dedicated electronic controls it is also possible to initiate regeneration through in-built electric heaters at the filter surface that bears the accumulated PM at pre-determined levels (*active regeneration*). This study is purely about diesel PM emissions; trapping PM with DPF and subsequent regeneration constitutes a chapter in this study.

Summary

The control of diesel PM has tasked the effort of researchers over the years as the regulatory limits tighten. In this chapter, the story of PM emission from diesel engine with due regard to its origin from fuel combustion has been presented. Some factors affecting its emission are internal to the engine, which are the design and operating factors while the flow factors from the moment it is expelled from the engine cylinder, all through the exhaust line are regarded as external factors and can only be controlled thereafter by after-treatment considerations. A single source library that gives annual reviews in developments of PM emissions and their controls is from the stable of **Corning Incorporated** (Engine Emissions Reviews). The incorporation of PM after-treatments has led to attainment of new level in diesel engine technology through development of advanced components and complete system integration. In the scheme, the complete picture is an engine with efficient combustion system based on advanced fuel injection systems, advanced engine breathing systems that enable better air utilisation, and excellent controls that optimise all aspects of engine operations. Similarly the quality of diesel fuel has improved with combustion improvers even as the sulphur content has been drastically reduced. Additionally, blending of petro-diesel with bio-fuels is in practice in many regions of the world according to some political and economic pursuits. The PM emission that arises after combustion management is handled through after-treatment technologies. These technologies have developed along the line of target species that are emitted. After-treatments of diesel PM have become major interest in the integrated engine exhaust control and management since combustion related strategies have proved insufficient to meet up with the stringent emission levels set for a modern engine. This in line with the near global regulatory frameworks that auto manufacturers are made to follow in order to keep market share particularly in the advanced regions of the world where emission regulations are highly implemented.

In this study, issues of PM from diesel are of interest. From the narratives in chapter two and this chapter, experimental studies of PM emissions reduction will be carried out along the line of engine performance characteristics, fuel blending and influence of after-treatment.

Chapter 4

EXPERIMENTAL FACILITIES AND TESTS SET UPS

4.0 Introduction

The experimental test facilities in our laboratory used in my studies include a Ford diesel engine coupled to a Schenk eddy-current dynamometer, exhaust monitoring and measurements are through AVL-415 Smoke meter used to measure filter smoke number (FSN), a Horiba Mexa-7170 for monitoring all the exhaust gases and Electrical Mobility Spectrometer for measuring particulate matter (PM) emissions. Fuel supply is through a central sully tank and an over-head blend tank through which bio-fuels or blends were metered.

4.1 Experimental Diesel Engine

The engine is a 2.0-litres, 4-cylinder; high speed direct injection (HSDI) engine equipped with common rail fuel injection system. It is a pre-production prototype Duratorq engine with twin over-head camshafts and twin intake and exhaust valves per cylinder. Two specifications are different in this prototype unit compared to the production engines: first, the air intake manifold has incorporated designs that promote swirl like variable swirl port in production engines; whereas this prototype has straight cylinder feeds. Similarly, this prototype engine has a slightly lower compression ratio of 18.2 compared to 19.1 in the production model of 2.0liter engines. This is due to modification in the bowl design that features slightly larger bowl volume in production engines. The fuel injection is with high pressure Delphi common rail injection system and spray is through injector nozzles that have six holes per injector with nominal diameter of 0.154mm and 154 degree spray-hole-angle and the injection pressure could reach 1600 bar at maximum speed. The engine specifications are as in Table 4.1, the engine and its lay-out in the test cell are shown in Figure 4.1 (A&B)

Table 1.1 laboratory Test Diesel Engine specifications

Design	In-line
Number of Cylinders	4
Displacement [cm^3]	1998.23
Cylinder Bore [mm]	86
Stroke, [mm]	86
Compression ratio	18.2:1
Connecting Rod length	155
Injection system	CommonRail
Aspiration	Turbocharged (But used on Natural Aspiration mode)
EGR	Installed (But not used)
Cooling	Water cooled
Fuel	Ultra-low sulphur diesel [ULSD]

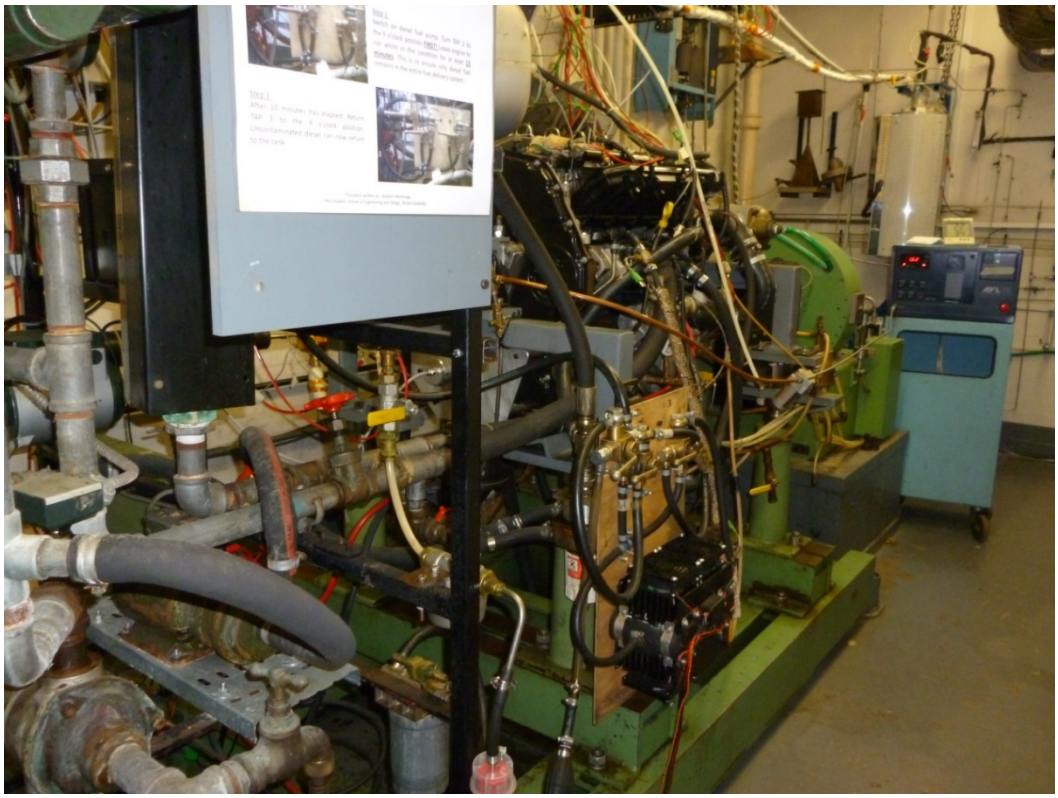

A: Ford Duratorq diesel test engine

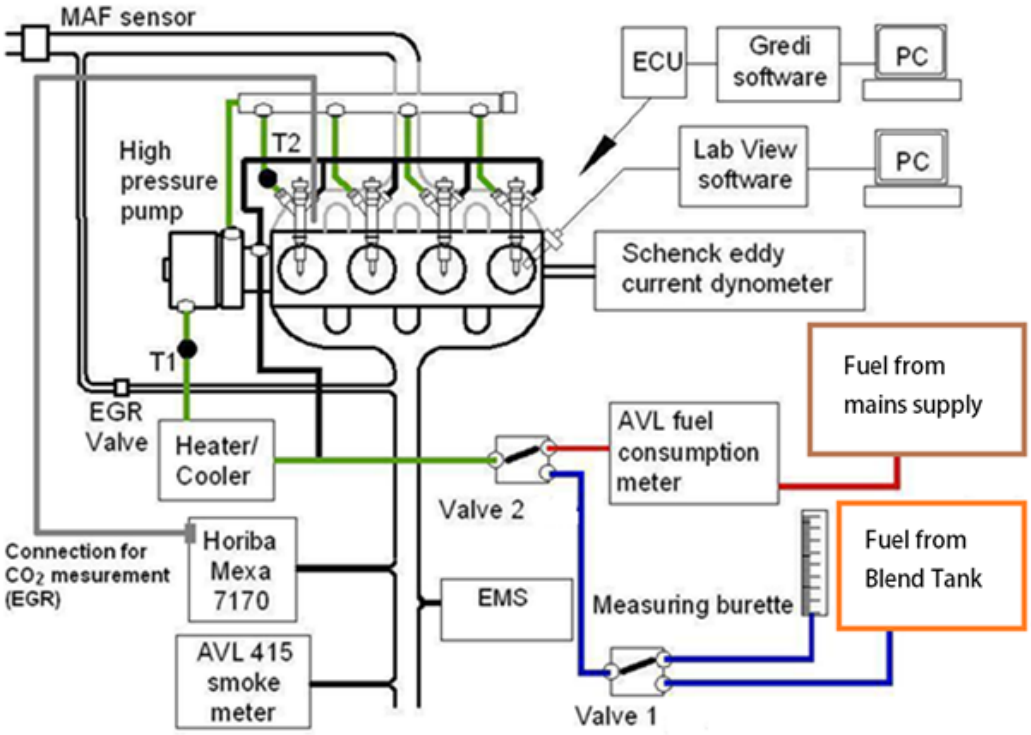

B: Lay-out of the engine test cell

Figure 4.1 Ford Duratorq diesel test engine and lay-out of the engine laboratory facilities

4.1.1 Engine Aspiration

The engine is equipped with a turbocharger and exhaust gas recirculation (EGR) units, however these were not used in the limit of operating conditions chosen. Prior to admittance into the engine, air is primarily filtered at the rotary air flow meter incorporated on the intake system to measure the velocity of the air at room temperature. The frequency of the meter rotation is digitally displayed on the engine monitoring dashboard and could be used to calculate the Mass Air Flow (MAF). The air is further filtered with micron-pore filter paper to remove any air borne particle from entering the engine system.

4.1.2 Engine Fuel Supply System

Diesel fuel used by the engine is centrally supplied from a reservoir through a lift pump for conventional petro-diesel operations. Although the fuel used in the course of my studies were supplied at different times, it is taken to be of constant properties as supplied by shell and stored in central reservoir. The reservoir integrity is constantly monitored as part of the University's overall health and safety

programme. In addition, a blend tank is installed in the test cell for the use of alternative fuel (Biodiesel) or blends. An AVL mass flow meter is incorporated along the main fuel line to measure the fuel mass flow rate to the engine, while a burette is installed to measure fuel volumetric flow rate on the alternative fuel line. This volume flow rate is converted to mass flow rate by multiplying with measured fuel and/or blend density. In operation, fuel is delivered and maintained at high pressure by the common-rail injection system which is capable of giving multiple injections per engine operating cycle. The fuel injection pressure is controlled by the electronic control unit (ECU) via the injection control unit (ICU) sub-system, which controls the volume and matches the schedules from engine operating parameters.

4.1.3 Engine cooling

Engine cooling is achieved through two separate coolant circuits. One circuit cools the cylinder head and block and another cool the lubricant. Heat picked by the coolant in these circuits is in turn removed at the Bowman heat exchanger by cold water supplied from a laboratory header tank. The coolant inlet and outlet temperatures are controlled by a thermostat which ensure normal engine operating temperatures which varies from 75 to 85 °C for our typical medium load operation. In addition, safety cut-off are installed to shut down the engine should the coolant be approaching the boiling point.

4.1.4 Engine lubrication

The lubricant grade normally used for the engine is 10W/40 which is periodically changed according to engine utilisation. The oil pressure sensor is integral of the instrumentation system of the test bench and is maintained within 2.5 to 3 bar of gauge pressure during typical operation. The engine oil temperature cooling is also integral to the overall engine cooling system which ensures normal working well below 100^{o}C.

4.1.5 The Dynamometer

The engine-power output shaft is coupled to a W130 Schenck eddy-current dynamometer via a rubber coupling by which it is insulated from engine vibrations.

The dynamometer is used to control engine operation either in a constant torque-variable speed mode, or constant speed-variable torque mode as the fuel feed rate is increased. A typical cut-away section of the dynamometer is shown in Figure 4.2. In operation, magnetic field is generated by the coils parallel to the machine axis and as the dynamometer rotor spins by the rotation of the engine in the gap, it causes constant change of the magnetic flux distribution in the loss plates. The resultant eddy current and the power developed is dissipated away as electrical resistive losses to the circulating water via the loss plates as well as to the surrounding air in the gap between the plates and rotor (Martyr, A. J., and Plint, M. A., 2007). The load cell connected to the dynamometer casing and speed sensor were together used measure the engine load (torque) and speed respectively.

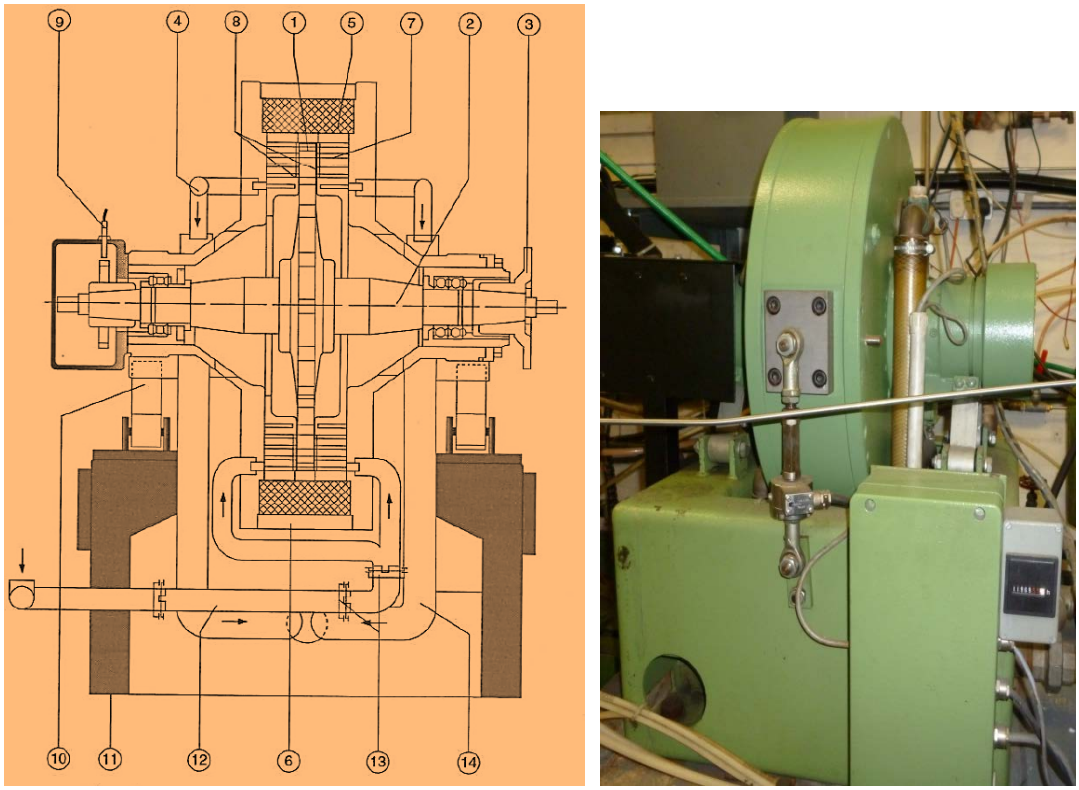

Figure 4. 2 The Schenck disc type eddy-current dynamometer
A: Typical sketch, B: Picture of a Schenck disc type eddy-current dynamometer: 1, rotor; 2, rotor shaft; 3, coupling flange; 4, water outlet thermostat; 5, excitation coil; 6, dynamometer housing; 7, cooling chamber; 8, air gap; 9, speed pick-up; 10, flexure support; 11, base; 12 water inlet; 13, joint; 14, water outlet (Martyr, A. J., and Plint, M. A., 2007).

4.1.6 Engine operations monitoring and controls

The electronic control unit (ECU) is managed through 'GREDI' software which enables operating parameters to be monitored on real time basis. It displays parameters like injection pressure, injection timing, injection strategy (single or dual mode), level of exhaust gas recirculation (EGR), and boosting as they are being monitored or controlled. The software offers flexibility to modify engine maps to suit operator's criteria. Although separate gauge measurements are available depending on experimental interest, the flow rates readings (fuel, air), voltages (battery), temperatures (oil, coolant) and pressures are captured during operation. These are used to monitor safe engine operations and to verify desirable measured data taken during experiments.

4.1.7 Engine data acquisition system

A thermally resistant Kistler Piezo Quartz 6125A transducer is fitted into an adapter and properly sealed into the modified glow plug hole of the first cylinder. A diaphragm on the quartz crystal element is used to sense the in-cylinder gas pressure p (bar); which is transformed into electrostatic charge Q (pc = Pico Coulomb). The sensitivity of the transducer is 16.8 pC/bar and these charge signals are amplified by a Kistler 5001 charge amplifier. The amplified signals are then captured with a computer using LabVIEW software during operation. The set-up is presented in Figure 4.3, (1) shows section of the cylinder head with the fitted pressure transducer in an adapter. The transformed pressure data signals are measured at a synchronised position of the piston. To achieve this, a high sensitive heavy-duty encoder (model ET758 from Encoder Technology with sensitivity of 0.017^{o}) was utilised during calibration (2) in the figure, in conjunction with the TDC sensor (3) to dynamically detect when the piston was at the top dead centre (tdc) position. The resolution was set to 1440 pressure data points for one crankshaft revolution, resulting to four data points per crank angle degree. The maximum in-cylinder pressure was determined when the engine was on motored mode during calibration. This calibration was conducted with other colleagues that used the same engine for their tests (David Peirce, Fanos Christodoulou and two exchange research colleagues from IISC Bangalore India - Prasad and Madan).

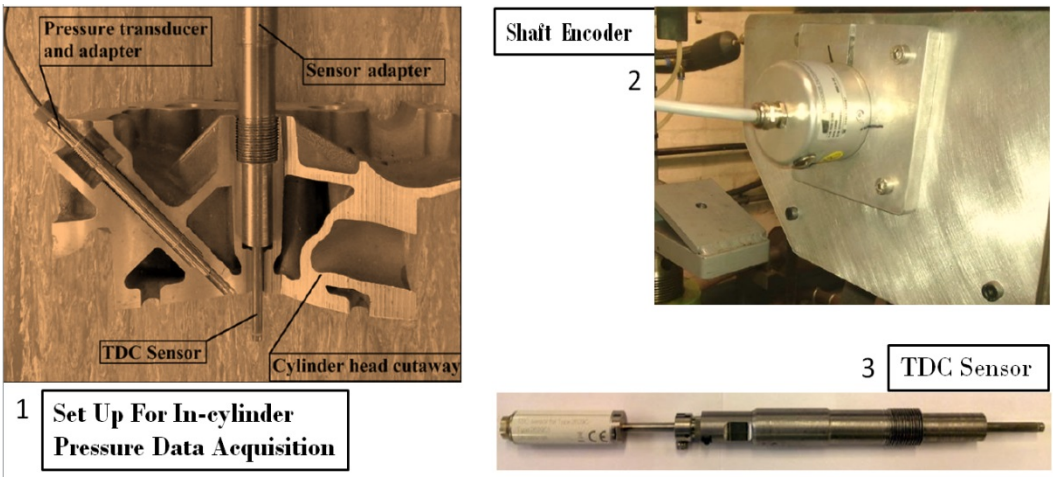

Figure 4.3 Data Acquisition System (1) Cross-sections of a Cylinder Head with pressure transducer, Shaft Encoder and TDC sensor (2) Shaft Encoder (3) TDC Sensor

4.2 Measurement of engine exhausts emissions

The key interest of the study is on exhaust emissions. The available measurement facilities include the smoke meter for measuring filter smoke number, the Horiba gas analyser and the Electrostatic mobility spectrometer (EMS) for particulate analysis. These were used to measure exhaust emissions from different perspectives as outlined hereafter.

4.2.1 Sampling Ports

The exhaust system of the engine incorporates a pipe, downward from the exit of the turbocharger. It has a number of holes to which pipes leading to the Horiba, smoke meter and EMS respectively are plugged-in, as shown in Figure 4.4.

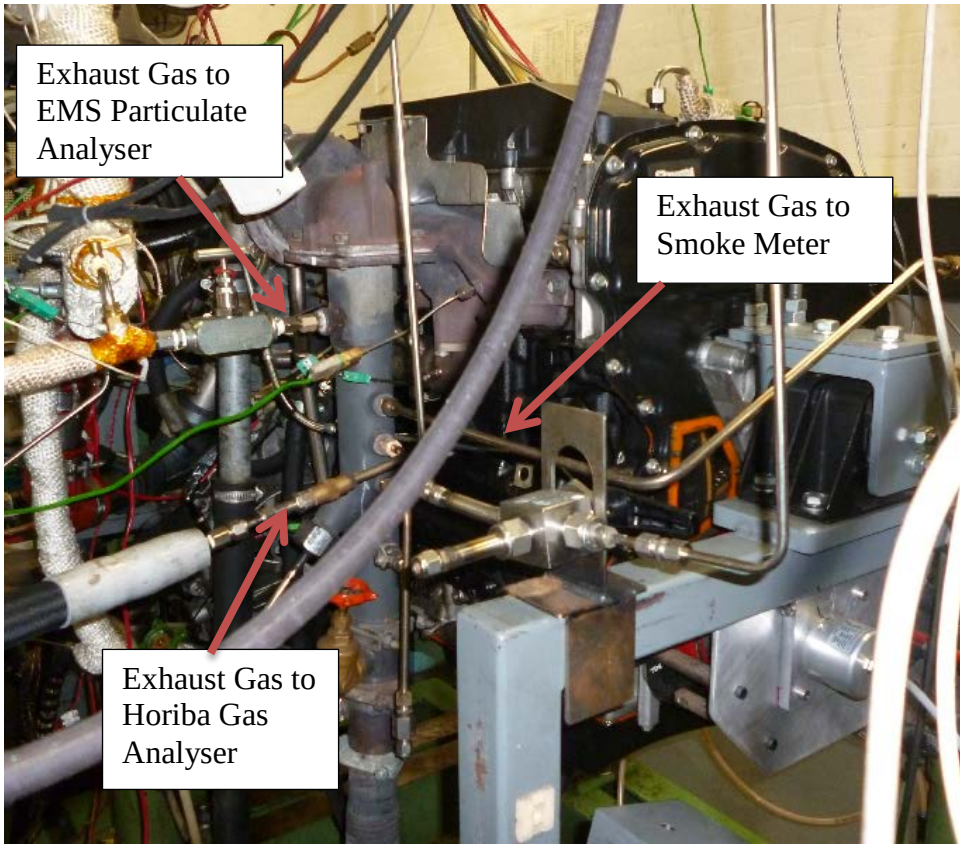

Figure 4.4 Exhaust Sampling Points

Ideally, exhaust gas sampling is supposed to follow isokinetic pathway. Isokinetic sampling in a strict sense involves aligning the inlet axis of the probe parallel to the exhaust gas streams such that it has the same gas free-stream velocity profile on entering the probe inlet as in Figure 4.5. By implication, this will involve a laminar flow because true isokinetic sampling is not possible with turbulent flows (Giechaskiel et al 2011). The sampling probe used for particulate line is shown in Figure 4.6 and like others, was inserted to extract sample from the centre of the exhaust pipe at 90^{o} to the exhaust gas flow. In essence and for sake of probity, the gas flow will simply be taken as mean velocity of the exhaust gas stream entering a multi-hole probe.

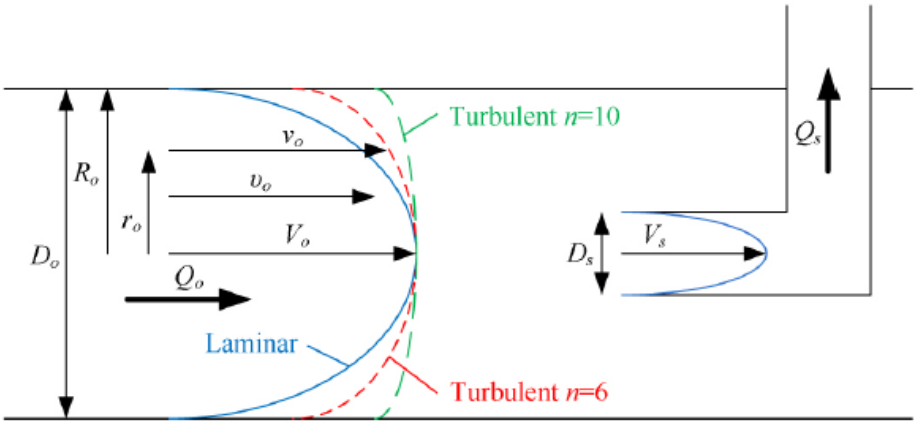

Figure 4.5 Velocity profiles in the exhaust pipe (subscripts o) and in the sampling probe (subscript s) (Giechaskiel et al 2012A)

Figure 4.6 Multi-hole probe

4.2.2 Smoke Number Measurement - AVL Smoke Meter

The smoke meter used to measure the 'Filter Smoke Number' (FSN), is the AVL - 415 which incorporates an electronically operated diaphragm pump (Figure 4.7). It is an established method of determining soot emission from diesel engines. 'Soot' as expressed by this technique is the 'intensity light-absorbing black particulate matter consisting mainly of graphitic carbon'. It uses a special case of the diffuse reflection ("remission") technique, (Christian et al 1993). In operation, undiluted exhaust gas drawn from the exhaust pipe (Figure 4.6) using a probe, is sucked through a filter paper. The principle is demonstrated in Figure 4.8 where the blackening of the filter paper caused by the filtered soot is measured with a reflectometer which indicates the soot content in the exhaust gas compared to no soot condition of unblackened filter paper.

(A) AVL-415

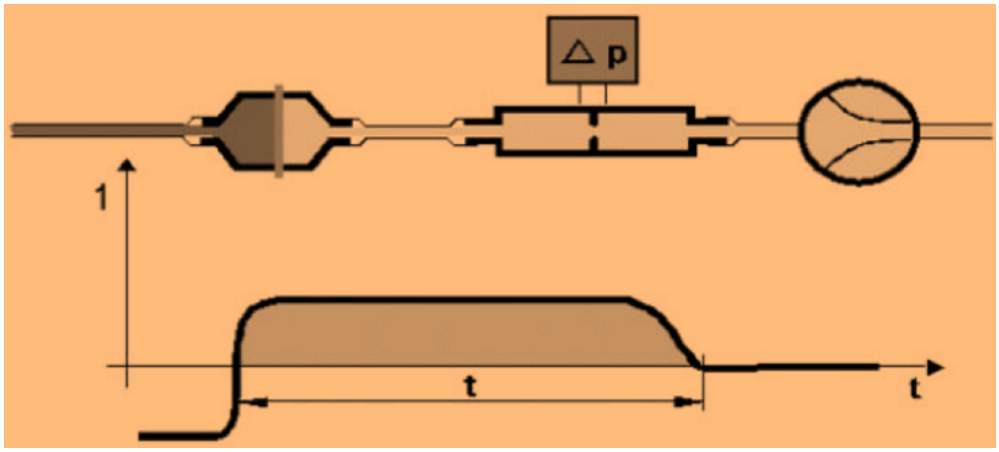

(B) Diaphragm Sampling principle

Figure 4.7, A: AVL -415 Smoke Meter; B: Sampling principle by using diaphragm pump (AVL, 2005)

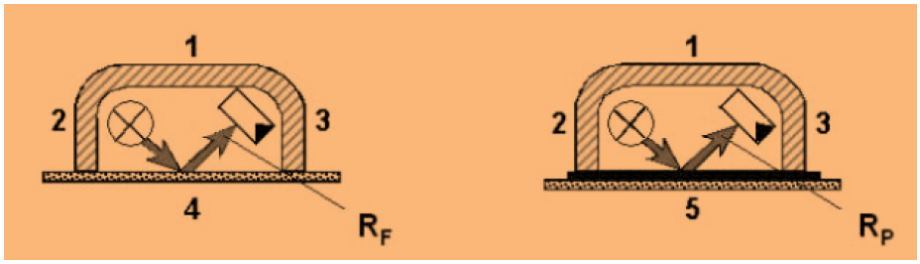

(A) Components of the reflectometer and measuring principle: 1.Reflectometer, 2. Light source, 3. Detector, 4. Clean filter, 5 Blackened filter

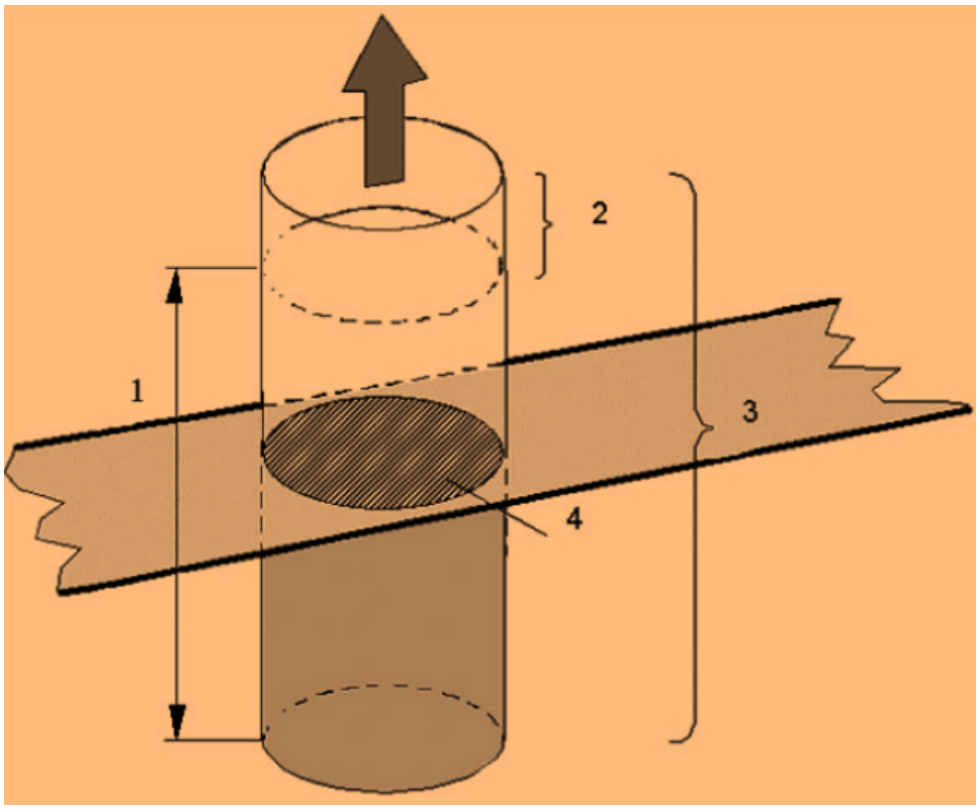

(B) Relationship between sample volume, effective length and filter area:

1. Effective sampling length, 2. Dead volume, 3. Sampled volume. 4. Filter area

Figure 4.8 AVL-415 Smoke meter Sampling Technique (AVL, Smoke Value Measurement with the Filter Paper Method (ATE1007E), 2005) .

The ‘concentration of soot’ deposited on the filter paper and the ‘effective sampling length’ are determinants of the blackening intensity. The blackening value of the filter paper is proportional to the change in reflected light intensity; it has assigned value of 0, for a plain filter paper; a value of 1 for 10% change and 10 for 100% reference value for absolute blackness when fully loaded with soot (Adachi, 2014; AVL, Smoke Value Measurement with the Filter Paper Method (ATE1007E), 2005). The effective sampling length has been defined by ISO DP 10054 as:

$$Effective\ Sampling\ length = \frac{Sampled\ volume - dead\ volume - leakage\ volume}{Filter\ Area}$$

Test using the ISO DP 10054 standard prescriptions of 1bar, 298 k in smoke meter with Bosch hand pump and a sampled volume of 330 cm^3 loaded on filter with surface area of 8.15cm^2 (Ø 32) gave the effective length as 405 mm. The FSN measured at this standard is also referred to as Bosch Number. In this respect, paper blackening intensity is calibrated from 0 to 10 (AVL, Smoke Value Measurement with the Filter Paper Method (ATE1007E), 2005) and expressed as:

$$PB = \frac{100 - R_R}{10} \quad \text{...} \ (4.1)$$

Where:

$R_R = \frac{R_P}{R_F}.100\%$

R_p …. Reflectometer value

R_f …. Reflectometer value of plain paper

R_R …. Relative brightness of the sample (relative radiance factor)

4.2.3 Horiba Exhaust Gas Analyser

The regulated exhaust gases CO, HC and NOx were measured using Horiba 7170 DEGR gas analyser which in addition, measures O_2 and CO_2. It also incorporates a secondary feed port for CO_2 which enables EGR levels to be determined through simultaneous measurement of CO_2 concentration from the inlet manifold gas stream. The measurement of the various emission gases were modularised according to the principle used gas detection. These modules are non-dispersive infrared (NDIR) absorption detector for CO and CO_2, flame ionisation detector (FID) for THC, and Chemiluminscene detector (CLD) for NOx (NO + NO_2).

Measurement of CO and CO_2: By non-dispersive infrared (NDIR) detection

The detection technique by NDIR absorption was used to measure the concentrations of CO and CO_2. The infrared absorption technique follows the principle that many chemical compounds, whether solid, liquid or gas, absorb infrared energy; and the absorbed wavelengths depend on the chemical structure of the compound. In this module, infrared absorption of other gases like HC, NO and H_2O were suppressed in other not to interfere with the measurement of CO and CO_2. Typical infrared absorption spectra for CO, CO_2 and H_2O are shown in Figure 4.9 where inverse of the wavelength has been plotted as the wave number against the absorbance (Adachi, 2014):

$$A(\sigma) = -log\frac{I(\sigma)}{I_0(\sigma)} \quad \text{..... (4.2)}$$

Where

A(σ): Absorbance at wave number σ

σ: Wave number [cm^{-1}]

I(σ): Light intensity transmitting the sample (at wave number σ)

I_0(σ): Light intensity radiated to the sample (at wave number σ)

The absorbance is ideally proportional to sample concentration, a property expressed as:

$$A(\sigma) = \varepsilon(\sigma) * c * L \quad \text{..... (4.3)}$$

Where

$\varepsilon(\sigma)$: Absorption coefficient at wave number σ

c: Sample concentration

L: Light path length in the sample

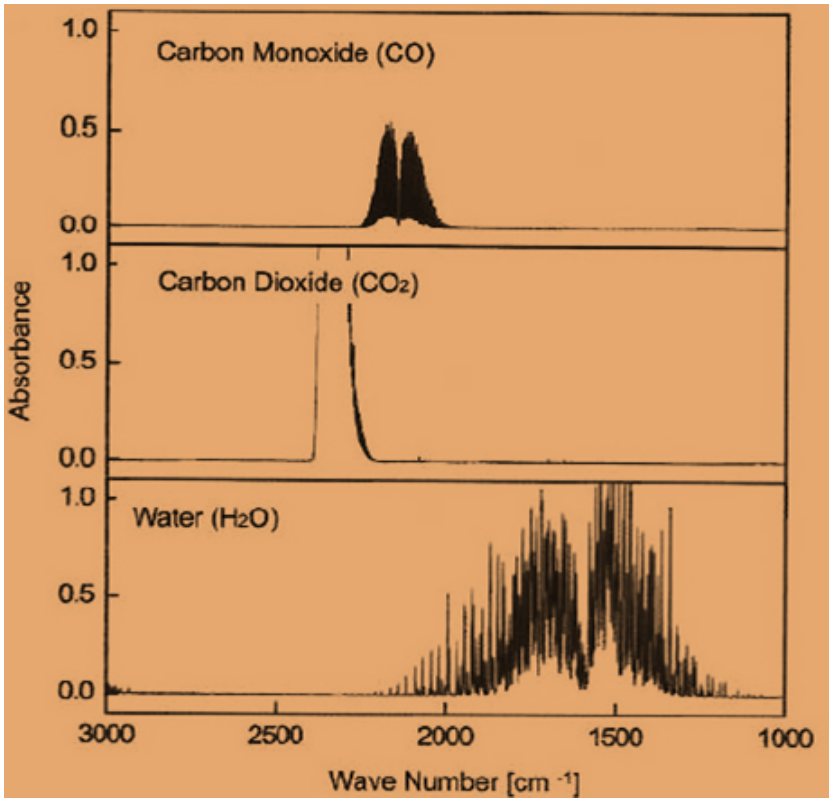

Figure 4.9 Infrared absorption spectra of CO, CO2, and H20 (Adachi, 2014)

The Horiba NDIR module has two cells, one serve as reference and another for measurement, illustrated in Figure 4.10. As the principle relies on the characteristic absorption spectra of the different molecules which strongly depend on their concentrations, the spectra of the CO and CO_2 gases are transmitted on the sampling cell and an optical filter to the detector where it is measured according to set pre-amplification that is related to the specie concentrations.

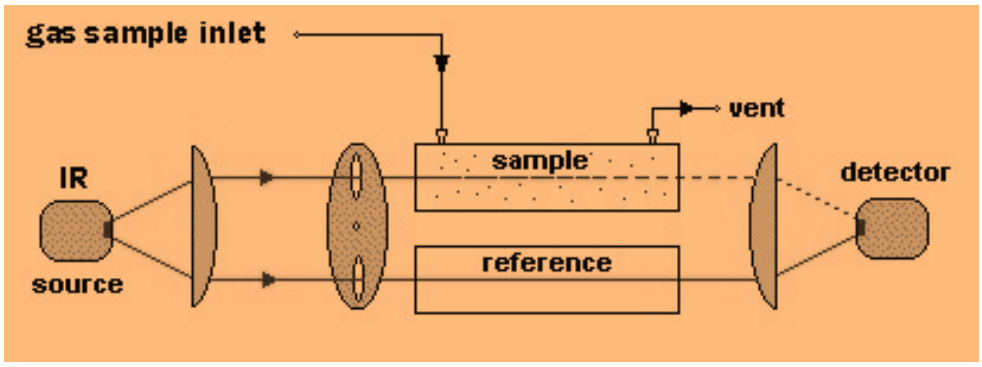

Figure 4.10 Principle of NDIR (Schutz, 2015)

Measurement of THC: By flame ionisation detection (FID)

The Horiba 7170 DEGR gas analyser has FIA-720 module that measures the THC concentration. It uses hydrogen gas mixed helium, oxidised with air to analyse concentration of hydrocarbon based molecules of the exhaust gas. The hydrocarbon of the exhaust gas is ionised on a hydrogen-based flame which is surrounded by an electrode that collects the ions. Electric potential applied across the nozzle and the collector electrode generates current that is linearly proportional to the concentration (in ppm) of the hydrocarbon concentrations (Adachi, 2014). A sketch is shown in Figure 4.11.

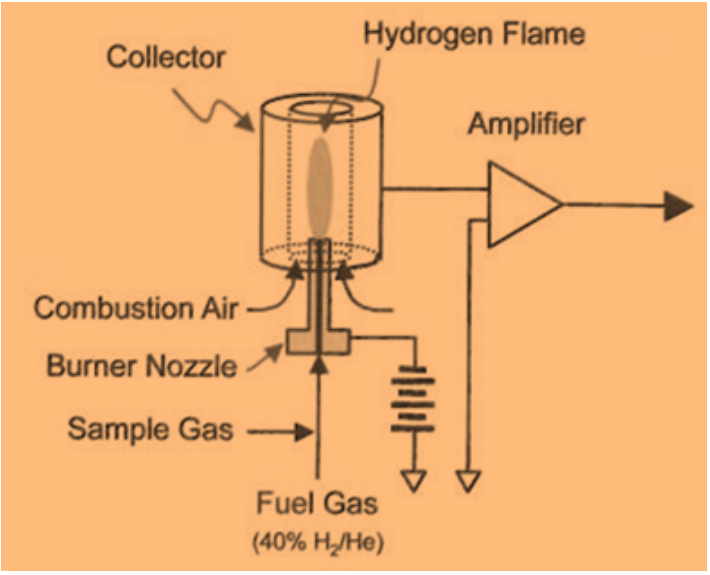

Figure 4.11 Configuration of FID detectors (Adachi, 2014)

Measurement of NO_x: By Chemiluminscene

The CLA-720 module of the Horiba measures the NO_x using the CLD technique. It is based on the principle of NO oxidation with ozone. Exhaust gas and ozone are introduced into a reactor where the NO reacts with ozone to produces NO_2. About 10% of the NO_2 produced in the reactor exists in excited state as NO_2^*. In the course of NO_2^* decaying to its ground state, excitation energy is emitted as photons as in equation 4.4.

$$NO + O_3 \rightarrow NO_2^* + O_2$$

$$NO_2^* \rightarrow NO_2 + hv \qquad \text{..... (4.4)}$$

The intensity of its luminescence is proportional to the amount of NO reaction with O_3.Therefore detection of the luminescence intensity with a photoelectric element provides avenue to measure NO concentration in the exhaust gas. The scheme used in measurement and typical Chemiluminscene spectrum (Adachi, 2014) is shown in Figure 4.12 (A&B).

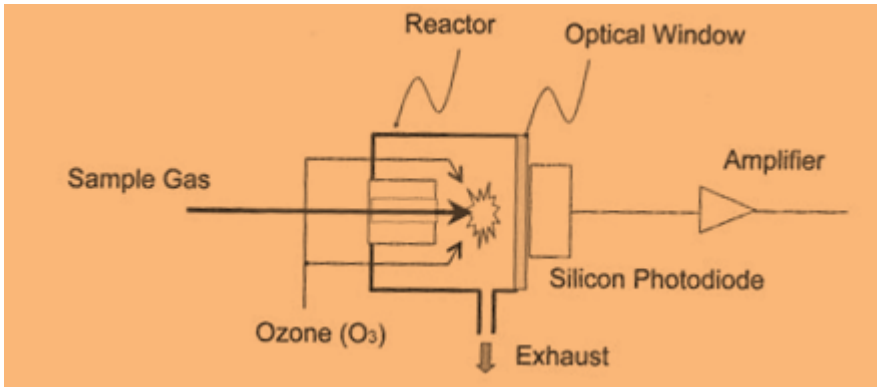

A

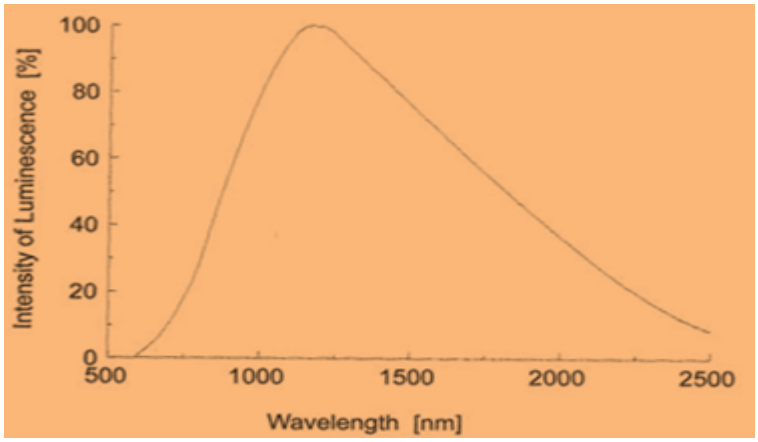

B

Figure 4.12 Structure of NO detector utilising CLD and Chemiluminscene Spectrum of NO_2^* (Adachi, 2014)

The CO_2 and H_2O ontained in the engine exhaust can interfere with CLD measurement of NOx however, the module has a dehudifier that treats the sample gas. In effect, CLD can be calibrated to measure NO as well as total NOx. For only NO measurement, a NOx converter (carbon filter) is used to convert NO_2 to NO before detection.

Measurement of Oxygen concentration

The Horiba has another module, MPA-720, which measures Oxygen (O_2) by Paramagnetic detection (PMD). It is a techniqure that uses the different levels of magnetic influence on gases to operate. Oxygen by nature has a high magnetic susceptibility compared to other gases found in diesel engine exhaust thereby making it amenable to fast detection by this technique. On a comparative scale among the exhaust gases, O_2 has a magnetic susceptibility of +100, followed by NO that has +45, NO_2 has +2.89 and all other gases have negative values (Adachi, 2014). As the NO concentration in diesel exhaust is much lower compared to O_2, its magnetic interference is usually negligible. Figure 4.13 shows the configurations of the PMD method for O_2 measurement.

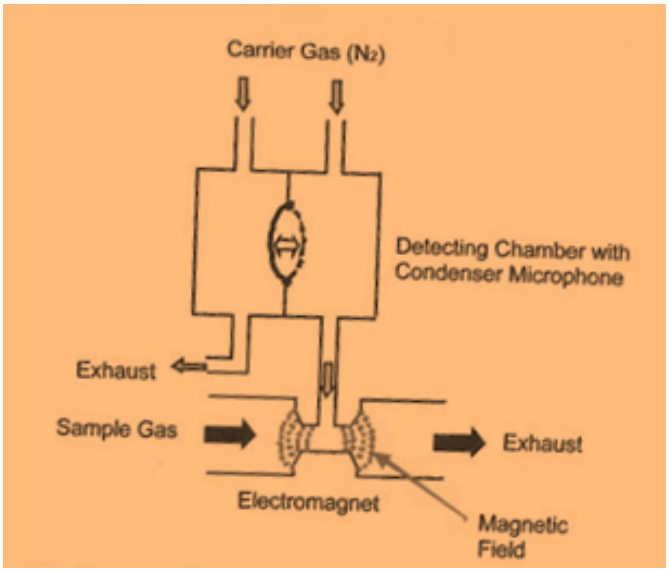

Figure 4.13 Configuration of PMD methods for O2 detection (Adachi, 2014)

Alternating magnetic field is created between the poles of an electromagnet as current flows through it and as exhaust gas is fed into the magnetic field, O2 with high susceptibility is preferentially drawn towards the magnetic poles and creates local pressure rise according to its concentration. The magnitude of the pressure is given as

$$\Delta p = \frac{1}{2} H^2 * \chi * \mathcal{C} \qquad \text{.....(4.5)}$$

Where Δp is the pressure rise, H is intensity of the magnetic field, χ is the magnetic susceptibility of the magnetic gas (O_2), and $\mathcal{C}$ is the concentration of the magnetic gas (O_2).

4.2.4 The PM Measurement Device – Electrical mobility spectrometer (EMS)

Measurements of PM number concentrations and size distributions were carried out using the Electrical Mobility Spectrometer EMS (Model VIE-11) which incorporates a Differential Mobility Analyser (DMA). The EMS is a computer controlled measurement system which operates the DMA under optimal conditions. All the components have been developed and optimised to ensure ease of operation, the scope of which can be found in (Winklmayr, 1991). The layout of the device when coupled to its dilution subsystem and the hardware systems, are the built in two units: the flow control unit (FCU) and the EMS process control unit (EPC) housed together in a purpose built frame and the DMA with the FCE in another frame. Flows between them are through interconnection with hoses as shown in Figure 4.14. The DMA is used to classify and analyse fine and ultrafine particle sizes covering the range from 4 to 600 nm. Particle size separation in the DMA is based on the principle of electrical mobility which determines their drift velocities under the influence of an electrical field. A charger is used to establish a well-defined distribution of charge before it enters into DMA where the particles are classified in relation to their electrical mobility, the sheath gas flow velocity, geometry of the DMA and the strength of the electric field.

A B

Figure 4.14, A: FCU with connections to DMA; B: DMA with connections from the FCU.

The strength of the electric field is varied by changing the voltage between the electrodes of the DMA. The flow through the DMA and Faraday-Cup Electrometer (FCE) are controlled by the Flow Control Unit (FCU). After classification, the particle number concentration in the sample flow is determined by the FCE. The control of the high voltage and the counting of particles in FCE are achieved through dedicated electronic controls, the data are reduced, displayed and stored with a computer. The DMA as well as the FCE are not sensitive to sure changes, and can be operated at low and high static pressures.

The Differential Mobility Analyser (DMA)

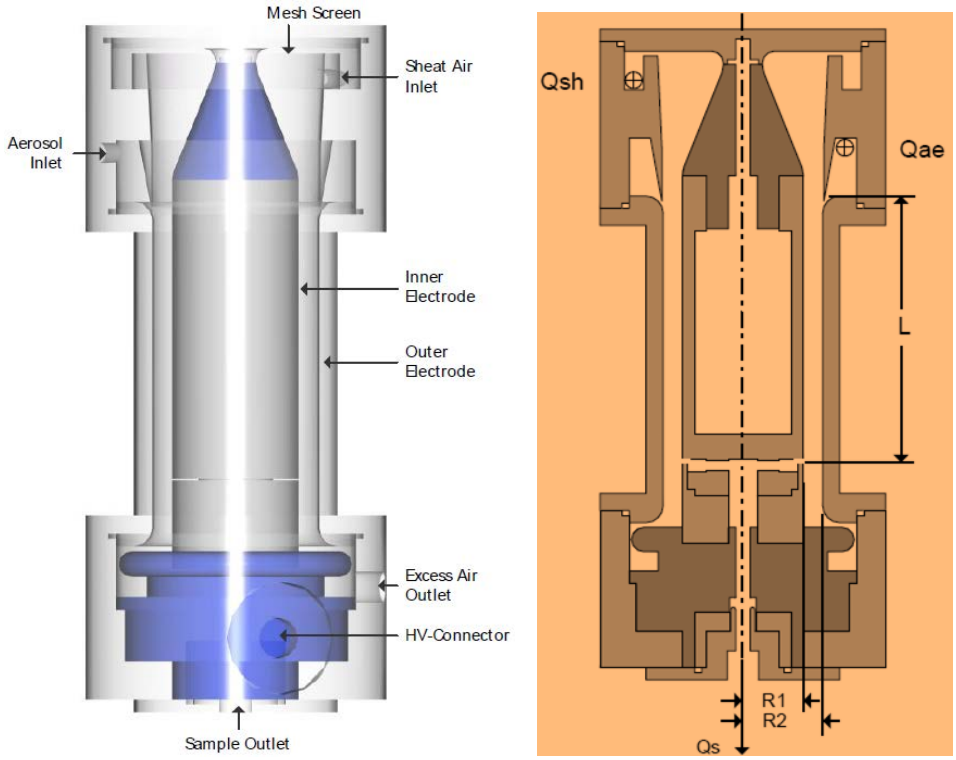

A: DMA schematic insight B: Location of the critical dimensions in DMA

Figure 4.15 The Differential Mobility Analyser (DMA). A: Schematic insight; B: Critical dimension and their locations (Analysessysteme, 2008)

The DMA is manufactured to precision with aluminium and is bolted to a rigid frame that supports its weight via insulating pads to help damp out vibrations. The classification of charged particles with it is based on the drift velocities of the particles in between inner and outer electrodes using filtered sheath flow. Figure 4.15 show the cross sections of the DMA with the sheath air and aerosol inlet side in upright position. However, in operation, this is on the down side while the axial sample outlet side is in upright position to bear the FCE (Figure 4.14B). This mode of operation results in less mechanical stress to the electrometer and offers the benefit of stable signal since gravitational effects on classified particle is of no relevance. The connecting hoses are colour coded for sheath air and aerosol flows; numbered for proper referencing and connectivity. The effective performance of a DMA is based on stable and accurate gas flows. This is achieved by an integrated flow control unit (FCU) which is optimised with DMA to balance the size resolution and sensitivity when sheath flow into the DMA and excess air out of it are equal; and

similarly the aerosol flow into the DMA and the sample flow out are equal as explained further under FCU.

Neutraliser

The EMS incorporates a neutraliser that electrically charges the aerosol by bipolar ion diffusion. Figure 4.16 shows the cross section of EM-10 mini charger. Its activity is from a single source version of 60MBq ±30%. The radioactive source is Am-241 as oxide rolled in a silver foil activity and covered with 2µg gold/palladium. The source installed into the neutralizer housing by QSA Global Braunschweig Germany.

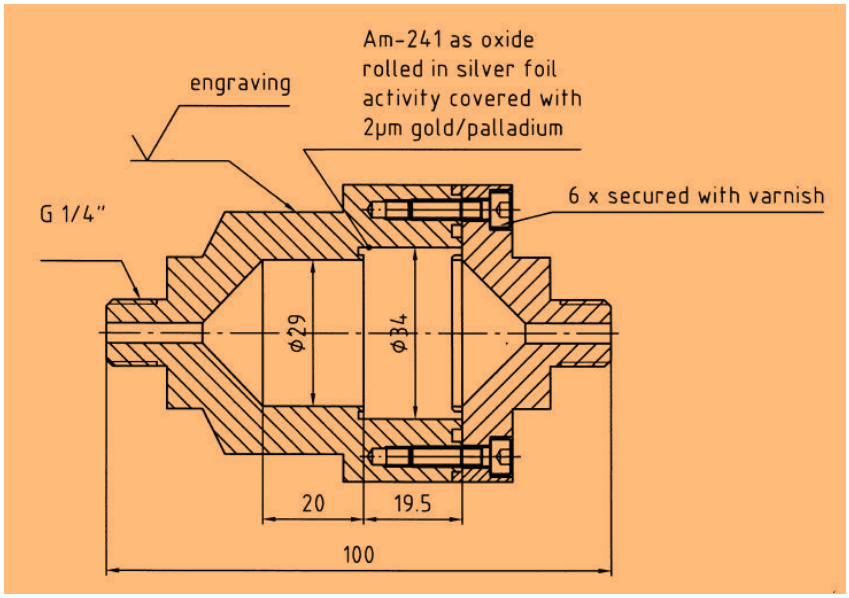

Figure 4.16 EMS-10 Mini charger cross section – single source version (Analysessysteme, 2008)

The Flow control unit FCU – 11

The EMS has an integrated flow system that generates the necessary vacuum and conditioning of aerosol as well as the pressurised air supply required for DMA operation.

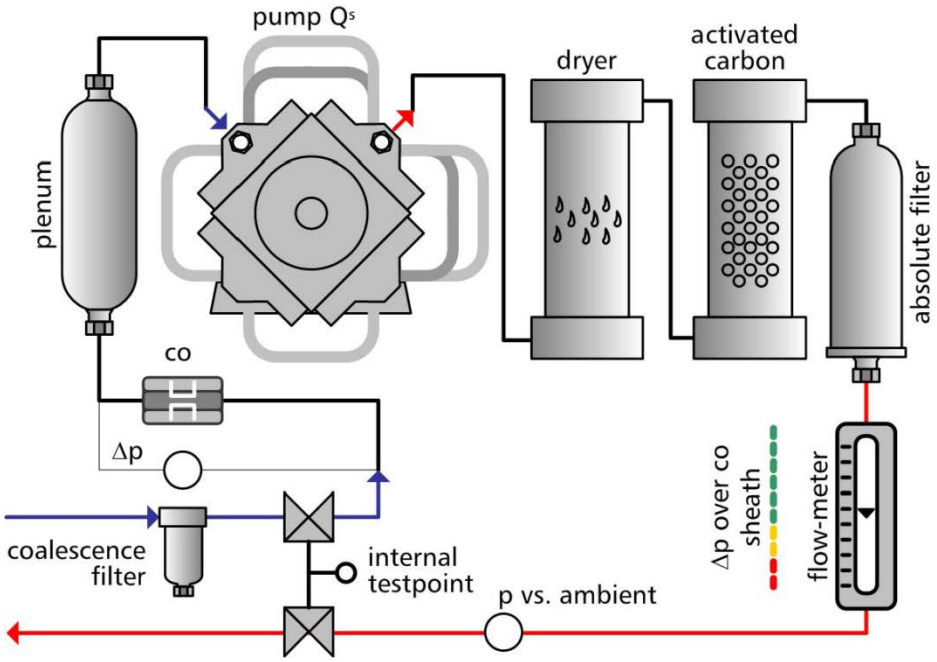

Figure 4.17A Closed loop sheath air flow system (Analysessysteme, 2008)

The flow and the sheath air conditioning are shown in Figure 4.17A. The components are housed inside and only the front panel offers avenue for operation of the main switches as seen in Figure 4.14A and diagrammatically reproduced in Figure 4.17B. The operation of the valves and pumps are controlled by the EMS-software. In operation, the coalescence filter removes any particle from the air compressed for use as the sheath flow in order to protect the diaphragm pump and the critical orifices. The critical orifice limits the flow rate according to requirement and a plenum is used to compensate for variation in pump-frequency pressure. The sheath air passes through three banks of filtration: silica gel to remove humidity and activated charcoal to remove hydrocarbons, both of which are capped with filter pads and are externally assessable and are occasionally replaced. The last filtration occurs at the absolute filter (a Pall HEPA capsule) located inside the FCU housing. A flow meter with a feedback to the ambient air control valve checks the sheath air flow rate.

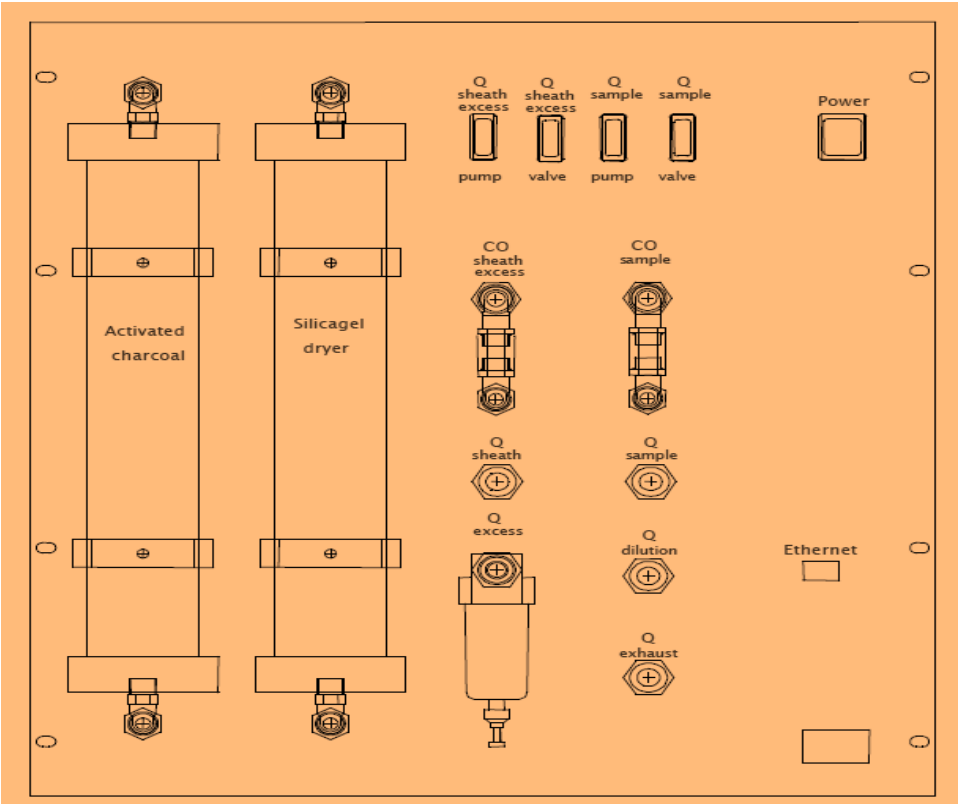

Figure 4.17B Closed loop sheath air flow system (Analysessysteme, 2008)

A similar control by critical orifice pressure drop is used to in aerosol metering according to dilution ratio selection as in Figure 4.14C. A plenum is also used to compensate for the pump-frequency pressure variation as shown in Figure 4.17C

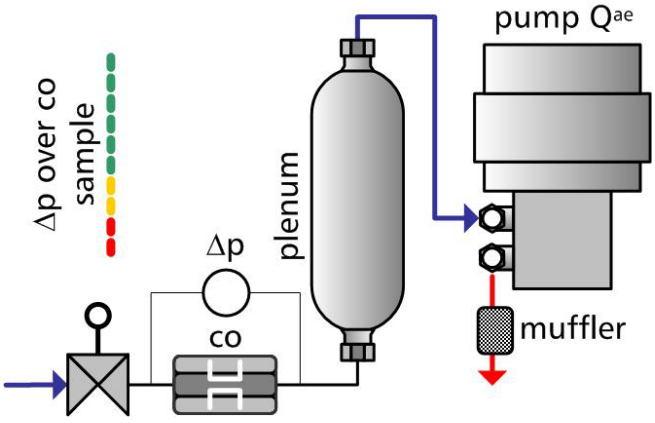

Figure 4.17C Aerosol flow system (Analysessysteme, 2008)

Aerosol Dilution

Magnified section of the dilution probe, Figure 4.18, shows the mixing tube where raw exhaust mixes with dilution gas. It is a major component of the dilution sub-system, covered with a heating jacket to enable dilution at various temperatures to alter the sampled aerosol temperature. This feature can therefore be used to mix aerosol at different temperatures.

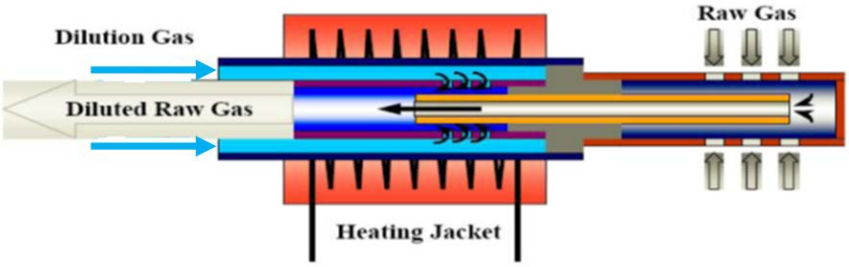

Figure 4.18 EMS Dilution Probe showing the Mixing Tube Diluter (Analysessysteme, 2008)

Faraday Cup Electrometer

The Faraday Cup Electrometer which operates on the principle of faraday cage is a bespoke design for the EMS VIE. It is controlled by the system's sophisticated software for high sensitivity in particle detection and counting as configured at the time of manufacture. A cross-section of the unit in the EMS is sketched in Figure 4.19. A pre-amplification unit is cased in the electrometer housing and a sensor module which conditions the signal and converts it to 12C interface bus is also built into the housing. Similarly, a Mykrolis filter cartridge is installed from the base of the housing; it is an absolute filter that has removal rating to a very minute specification of 0.003 micron.

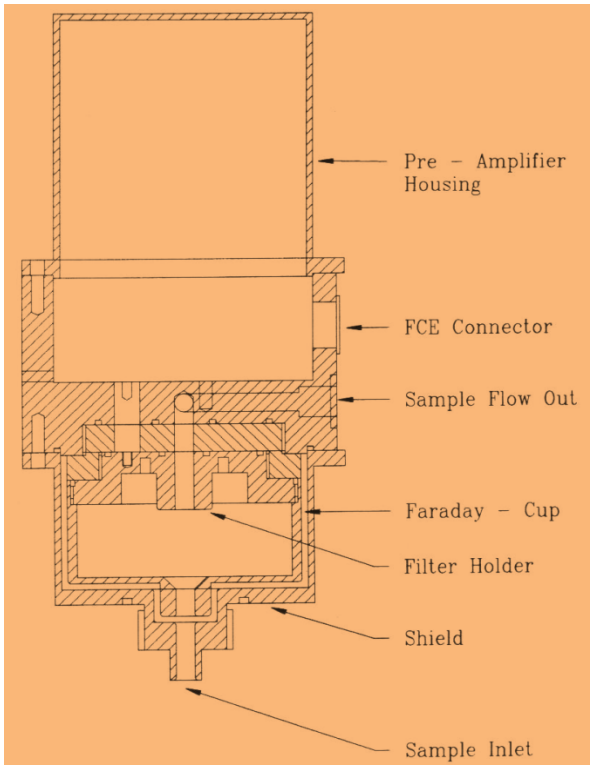

Figure 4.19 Schematic cross section of Faraday-Cup Electrometer Sensor FCE (Analysessysteme, 2008)

In operation, aerosol sample from the DMA outlet is deposited on the absolute filter and the electrical charges carried by the particles into the cage are compensated by current to the outside of the Faraday Cup. This measured by the computer system configuration in its absoluteness. From the known flowrates, the transfer function of the DMA and the charged fraction of the aerosol, this current is related to the aerosol concentration by the system control program. The compensated current is amplified, filtered and converted to a voltage signal according to pre-amplification settings. After further amplification, the final signal is converted to binary information by an analog to digital converter and sent to the EPC on the 12C interface bus. (Analysessysteme, 2008).

High Voltage Supplies (HVS)

The EMS has a high voltage supply module powered by a 12V supply line. It is built as a cassette and mounted on the housing in additional safety container. It has an output of 10,000 volts and controlled by the EPC firmware programme and the EMS-CC software.

EMS Process Control (EPC-11)

The EPC is the system's internal computer which interfaces with the 12C interface bus. It contains programmes that enable measurements to be taken and the interface firmware that enable operation of the EMS. Experimental controls like starting and stopping are initiated by the Client Software EMS-CC that runs on a PC connected to EPC via a LAN interface. Once started through the client's programme, the EPC carries out predefined measurement programme and device operations and sends the data to the EMS Client software. External devices like particle sensors and HVS are connected directly to the EPC (Analysessysteme, 2008).

4.3 Engine Exhaust line modifications for PM Sampling

In the course of the experiments, the exhaust line was modified to suit the experimental purpose. These include PM dilution rig, PM trap on pall tissue filter and PM trap on the DPF. Full description of each is presented in the various chapters where the experiments involved were reported.

CHAPTER 5

DIESEL EMISSIONS AND ENGINE OPERATING CONDITIONS

5.0 Introductions

The exhaust emissions that arise from diesel engines lack homogeneity, but rather influenced by the operating conditions of the engine. The oxides of nitrogen (NOx) and particulate matter (PM) are major candidates; and with emphasis on PM, its measurement by filter smoke number, analysed to obtain gravimetric quantity according to pre-defined reference scales, have been an established technique in engine testing and calibration (Christian et al 1993). Current PM Measurements for certification of engines are based on particle number metric; however deductions made from both metrics remain the same only that quantity of matter involved differs. Engine operating parameters that significantly affect exhaust emissions include load, speed, fuel injection parameters, and type of aspiration including exhaust gas recirculation (Heywood, 1988; Majewski, W. A. and Khair, M. K., 2006; Pundir, 2002; Khan, 1969; Pesiridis, 2014). The test engine has been presented in chapter four, the objective of this chapter is to conduct its emissions panorama with special interest in particulates measured by filter smoke number as engine operating parameters are varied and establish base line conditions for further tests.

5.1 Effects of load and speed on engine emission characteristics

In naturally aspirated diesel engine, the speed and load are twin influencers of air-fuel ratios for localised portions of the in-cylinder charge. Exhaust emissions are inherently related to these parameters. Engine power determined by dynamometer testing is a product of torque and angular speed. It is increased at fixed speed according to the amount of fuel injected, and calculated from indicated work per cycle which is related to the indicated pressure (Heywood, 1988). The experimental study started with preliminary sweeps of engine loads and speeds to view its performance characteristics and the consequent emissions in order to establish baseline conditions. The limit of operating condition is meant to correspond to light duty engines for city drive at low load.

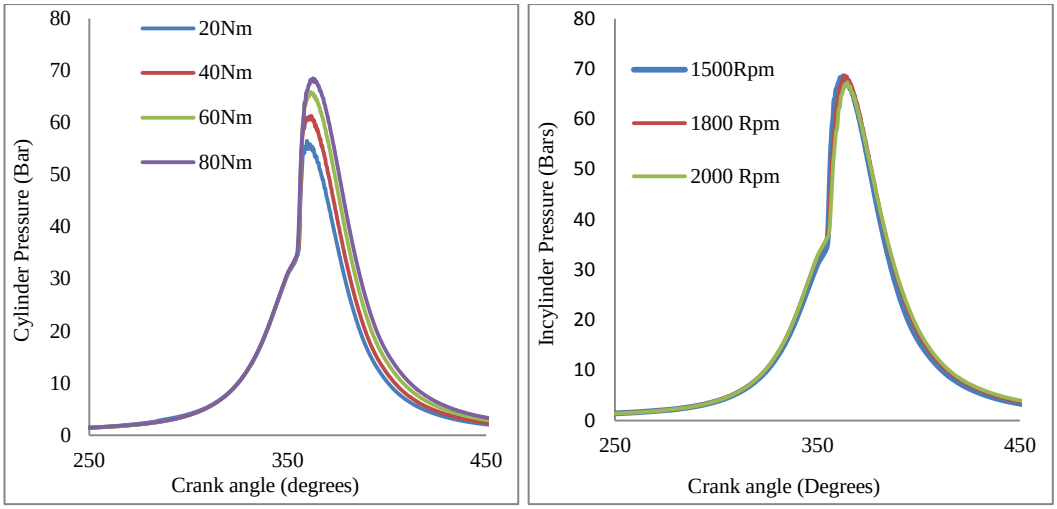

A B

Figure 5.1 A: Cylinder pressure for various loads at 1500Rpm. B: Cylinder pressure for various speeds at 80Nm

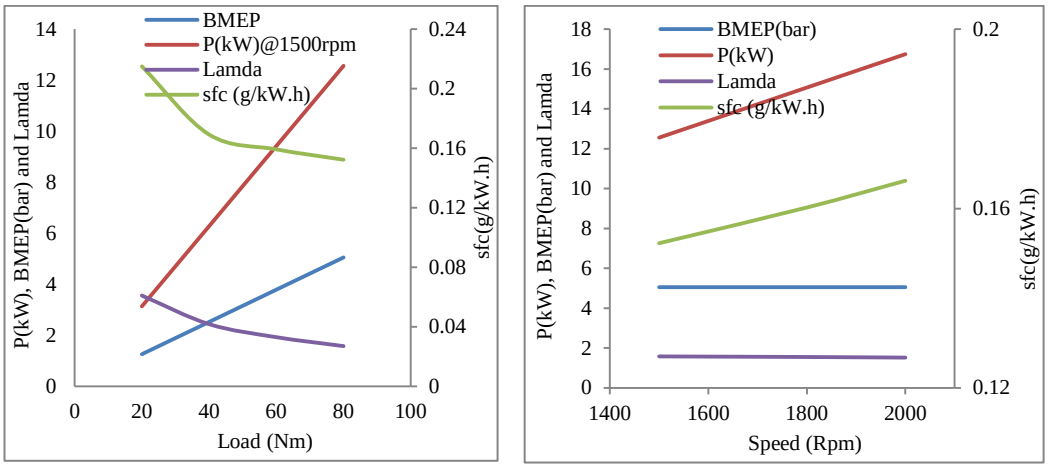

A B

Figure 5.2 A: Engine power outputs and fuel consumption at various loads and constant speed of 1500Rpm. B: Engine power output and fuel consumption at various speeds at constant load of 80Nm

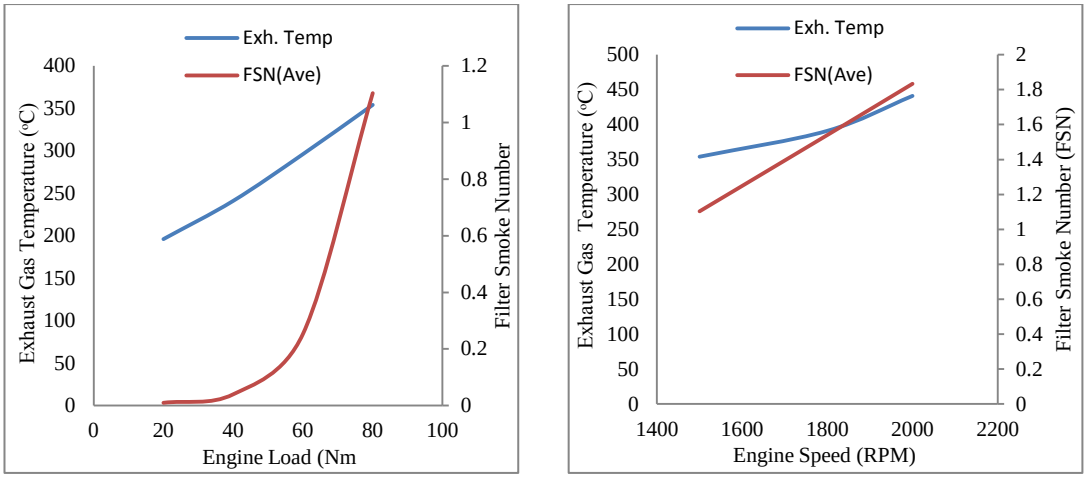

A B

Figure 5.3 A: Effect of engine loads on exhausts temperature and filter smoke number at 1500Rpm. B: Effect of engine speed on exhaust gas temperature and filter smoke number at 80Nm

Figures 5.1 A and B show the in-cylinder pressure at different loads and speeds which for typical diesel engine are in the low range, and also adopted for safe operations in the test cell. This was at injection pressure of 800 *Bars* and timing of 9^{o} *BTDC*. It shows that the cylinder pressure increases with load at a chosen speed of 1500Rpm. When the load was kept constant at 80Nm, in order to check effect of speed at1500, 1800 and 2000 Rpm respectively, there was no much effect on the in-cylinder pressure at this load. The plots of Power developed and fuel consumed under these conditions are presented in Figures 5.2A and B. It shows high specific fuel consumption at low loads which decreases as load increased. This is attributed to the relatively low temperature of the engine at low loads when more energy was dissipated as heat to attain operating temperature. The power developed by the engine increased as more fuel was injected (corresponding to the load standardised in terms BMEP). The accompanying exhausts temperatures and filter smoke numbers are given in Figure 5.3A and B. Similarly the increase in fuel injection (load) led to reduction in the air-fuel ratio, typified by lambda values as shown in Figure 5.4A. It has a profound influence on exhaust temperature and filter smoke number as well as NOx which increased.

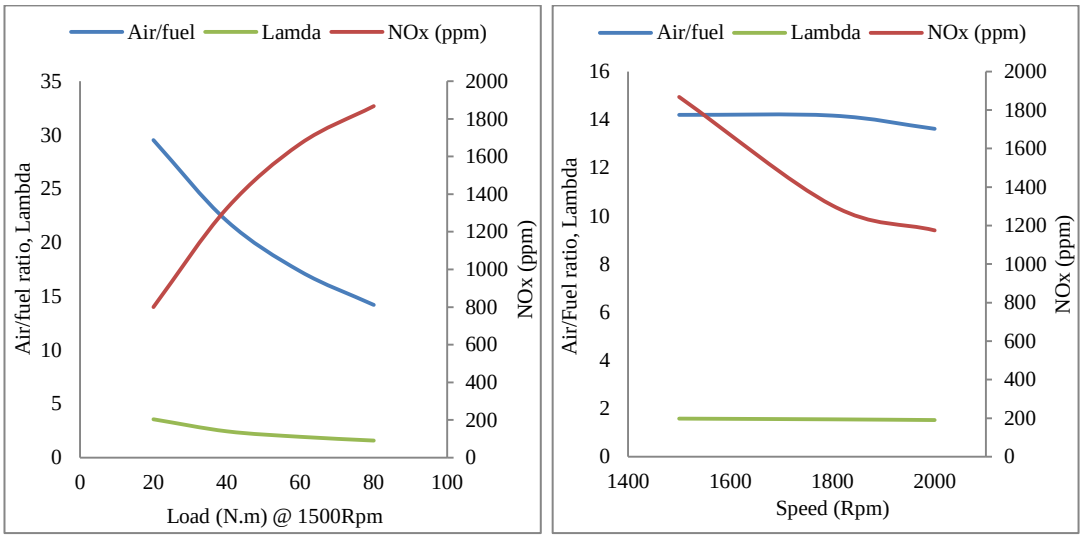

A B

Figure 5.4 Effect of (A) Engine load, (B) Engine speed, on Air/Fuel ratio and NOx;

The reviews in sections 2.6.2 and 3.2.1, show that unburnt hydrocarbons are produced in the exhaust when combustible mixture is too lean or too rich (to support or) during combustion as typified by transient and idling periods. During idling and low load conditions, small amounts of fuel are injected, combustion occurs within the periphery of the injector spray and the rate of reaction is quite low due to low rate of local rise in temperature and leads to significant quantity of unburnt hydrocarbon being in the exhaust. This condition however changes with increase in fuel injection from low load to full load. As the load is increased, the air fuel ratio decreases but there is sufficient air to support combustion so the temperature is increased and correspondingly leads to increase in NOx emission. However, some fuel parcels ultimately hit the combustion chamber walls, and with the low rate of combustible mixture formation during the diffusion burning regime, there is incomplete combustion especially as temperature begins to fall with expansion stroke. Therefore soot particles reaction freezes along with other intermediate species formed within this period. These are contained in the exhaust stream expelled at the tailpipe. This explains the reason for sharp rise in filter smoke number (Figure 5.3A) which is an index of blackness of the exhaust stream occassioned by the presence of dry soot particles. As the aim of the engine sweeps was to determine appreciable loads with different levels of sooting tendency, the three loads: 40Nm, 60Nm and 80 Nm were

classified as low, intermediate and high loads respectively for the purpose of this study. At the highest load chosen, the effect of engine speed was thereafter investigated for at three magnitudes: 1500Rpm, 1800Rpm and 2000rpm. The effect of increase in speed also gave a linear increase in exhaust temperature and filter smoke number but with less gradient compared to increase in load. Similarly, there was a marginal increase in fuel consumption but with a substantial decrease in NOx and slight decrease in Air/Fuel ration. Therefore the baseline adopted for relative sooting tendency is as follows: The engine was optimised for stable low load operation at 42.7Nm, 1500Rpm to generate PM with substantial amount of unburnt hydrocarbon which constitutes volatile organic fractions. To generate PM with both unburnt hydrocarbon and good quantity of soot, 80Nm load at 1500Rpm was used; and for high sooting condition, a baseline of 80NM and 2000Rpm was used.

5.2 Effects of Injection Parameters on emission characteristics

Injection parameters have influence on fuel spray and atomisation and invariably the emission characteristics. Two parameters of interests in fuel scheduling are the injection pressure and injection timing.

5.2.1 Investigation on the influence of Injection Pressure on Combustion and Emissions characteristics

The pressure at which fuel is injected into the engine combustion chamber, influences the combustion and by extension, the quality of exhaust emissions. Five injection pressures from 800 to 1200 Bars were investigated at 80Nm, 2000 Rpm and at 9^{o} BTDC. The plots of these characteristics are shown in Figures 5.5 and 5.6. The plot of in-cylinder pressures for the various injection pressures are presented in Figure 5.5A. It shows an increasing character due to more atomisation of fuel injected. It led to faster fuel evaporation which enhanced combustion rate (Majewski, W. A. and Khair, M. K., 2006). More fuel was therefore burnt at higher injection pressure during premixed burn period and resulted in increased cylinder pressure as well as the peak of heat release rate (HRR).

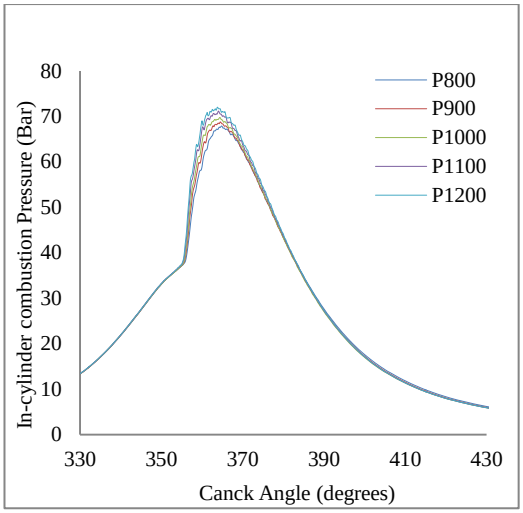

A: In-cylinder Pressures

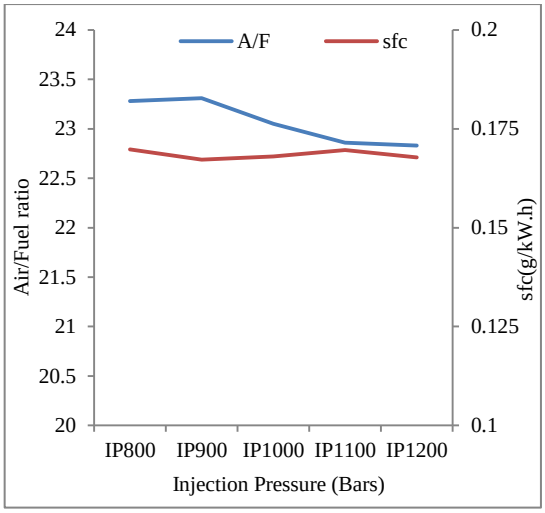

B: Air Fuel ratio and Fuel consumption rate

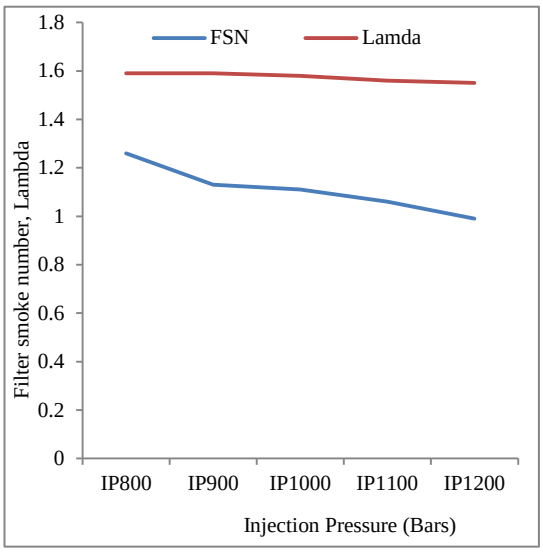

C: Filter smoke Number and Lambda

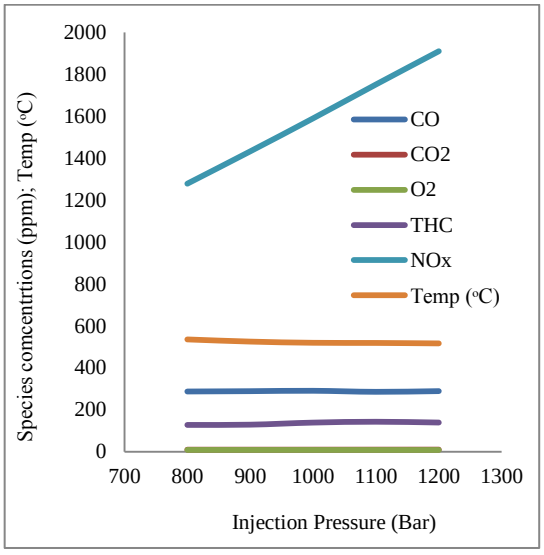

D: Exhaust gas emissions and Exhaust Temperature

Figure 5.5 Combustion and Exhaust Emission characteristics at different Injection Pressures

This is corroborated with the heat release diagrams in Figure 5.6 where the portion of diffusion burning quantified by the area under the (HRR) curve right of the red line is largest at 800Bars and smallest at 1200 Bars and conversely the peak of the HRR occasioned by kinetic burning is smallest at 800 Bars and highest at 1200 Bars. There is improvement in the combustion efficiency due to better air utilisation occasioned by fine atomisation.

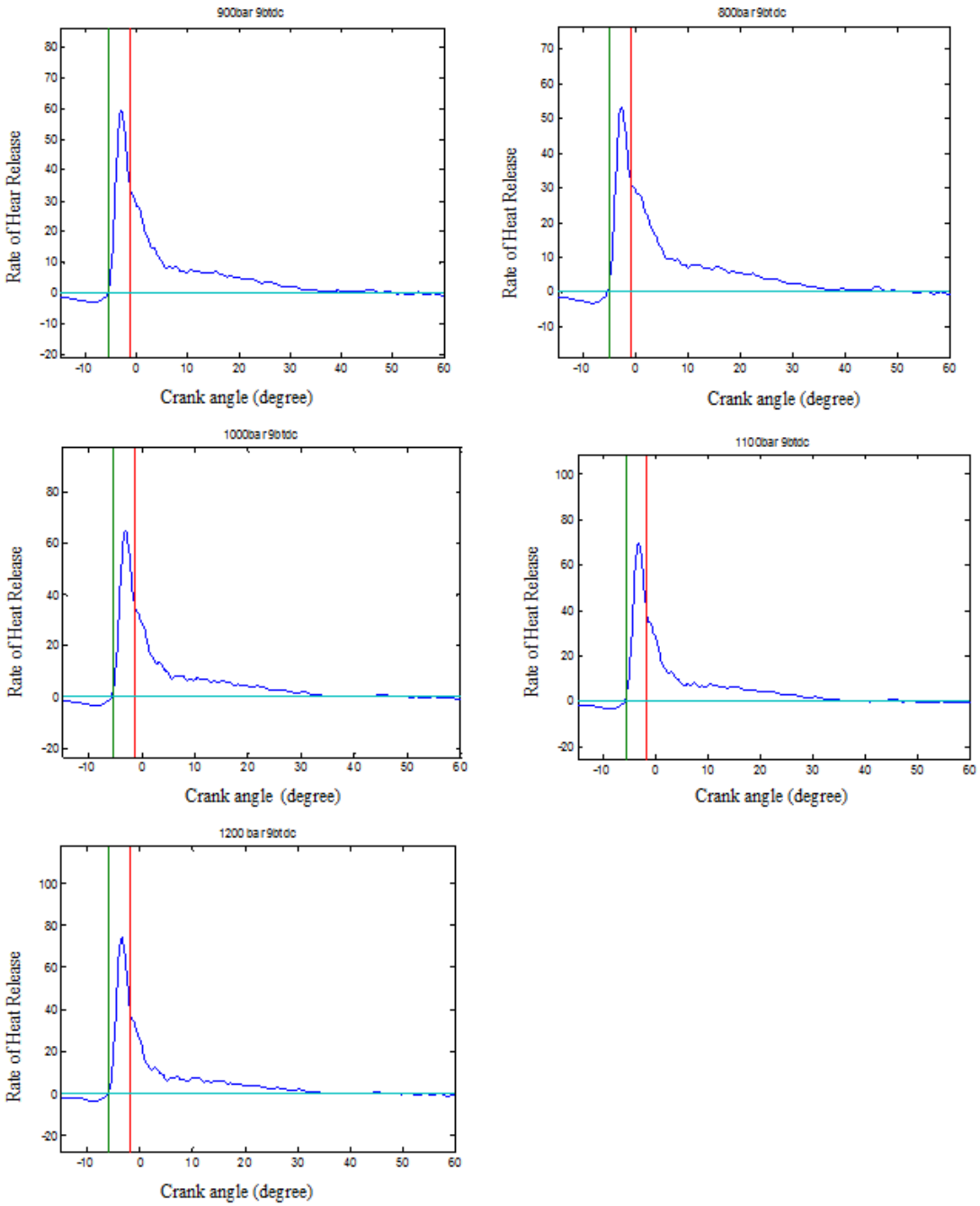

Figure 5.6 Heat release plots for various injection pressures 800 to 1200bars

In Figure 5.5B, specific fuel consumption rate is fairly constant, with slight decrease in air/fuel ratio which in effect, actually means better air utilisation by considering the values of lambda as pressure increased (Figure 5.5C). This is substantiated with decrease in soot emissions as represented by the filter smoke number which decreased as injection pressure increased. Exhaust gas concentrations are plotted in Figure 5.5D, and by reason of scale factor; hidden values of CO_2 and O_2 are zoomed in Figure 5.7A. The marginally reducing value of exhaust oxygen concentration

lends credence to better air utilisation. The CO was fairly constant but with tendency towards reduction, while CO_2 was also fairly constant with tendency towards increment. The THC had a slight increase at 1000 and 1100 Bars and further decreased at 1200Bars as in Figure 5.7B. Considering the narrow band of pressures under consideration, these observations are consistent with combustion chemistry as reviewed in chapter 2. Fuel combustion progresses with formation of host of intermediate products which constitute the THC, so their increase is sign of combustion process. Similarly, the chain reactions lead to formation of CO and subsequent oxidation into CO_2, the trends in Figures 5.7 (A and B) clearly demonstrates this. As more air was utilised, intermediate products are formed and CO oxidation is enhanced. Inherently the combustion temperature remains high and this is responsible for high NOx production (Figure 5.5D). Therefore it is inferred that increase in fuel injection pressure led to decreased soot emission but favoured increase in NOx emission.

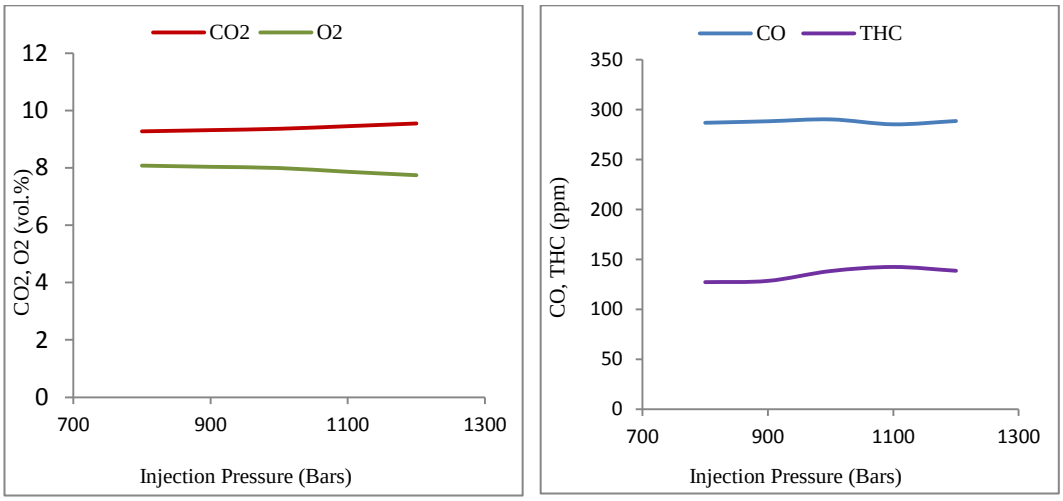

A B

Figure 5.7 A: CO_2 and O_2 emissions; B: CO and THC emissions; with increase in injection pressure at 9^o BTDC, 80Nm and 2000Rpm (5.05 bar BMEP).

5.2.2 Investigation on the influence of Injection Timing on Combustion and Emissions characteristics

Similar to injection pressure, the timing of fuel injection into the combustion chamber has a great influence on combustion and emission characteristics. This is usually expressed in degrees of crank angle. The objective here was also to evaluate relative sooting tendencies at chosen load and speed as the injection time was advanced or retarded.

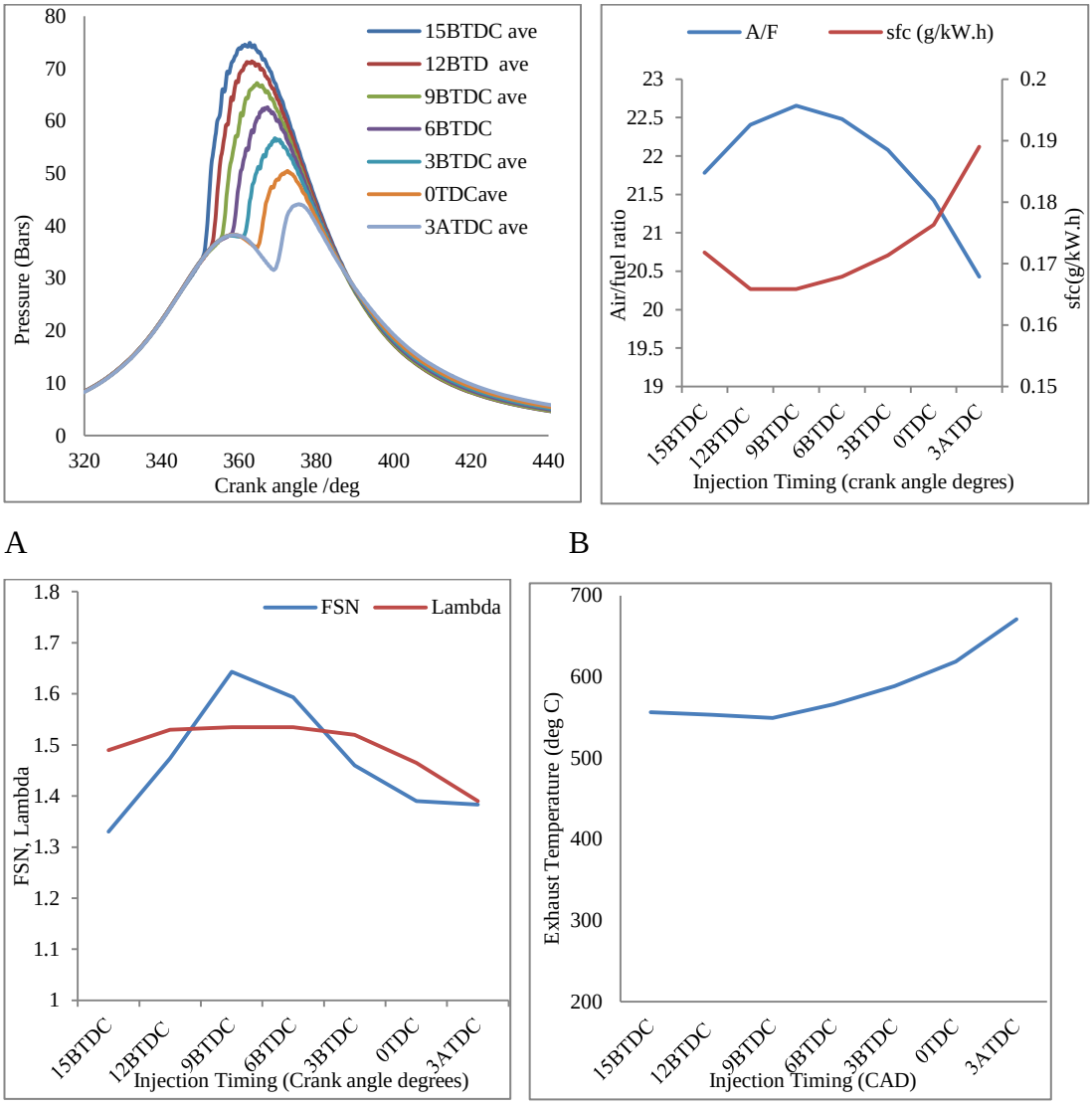

Figure 5.8 Influence of injection timing on combustion and emission characteristic; A: In-cylinder pressures at different injection times at 800 Bars; B: Air/Fuel ratio and Fuel consumption rate; C: Filter smoke number and air utilisation; D: Exhaust Temperature at point extraction to emissions analyser.

The timing was given maximum advance of 15 degrees before top dead centre (BTDC) and there after retarded in steps of 3degrees to a maximum of 3degress after top dead centre (ATDC). Details of combustion and emissions characteristics are presented in Figures 5.8 to 5.10. Advanced injection timing in the range considered has an increasing effect on in-cylinder pressure as seen in 5.8A. This is due to adequate time for mixture formation which enhanced better air utilisation and more kinetic combustion. The air/fuel ratio is observed to increase from 15^{o} BTDC to a maximum at 9^{o} BTDC and afterwards decreased. The fuel consumption rate is a converse or mirror image of the A/F in Figure 5.8B. By implication of better pre-mixed combustion, soot emission from highly advanced timing at 15tdc is low. However it was observed in (Khan, 1969; Majewski, W. A. and Khair, M. K., 2006) that this may be due to more unburnt hydrocarbon if the injection pressure is low. It was linked to longer ignition delay but, this is not likely within the range of timing under consideration here as the difference in both temperature and lambda are not much; it is corroborated with the high cylinder pressure which is a consequence of energy of combustion. The high HRR and concentration of NOx at 15^{o} BTDC compared to other injection times substantiates pure kinetic burning as in Figures 5.9A and 5.10. In the same vein, fuel consumption decreased from 15^{o} BTDC to 12^{o} BTDC and thereafter increased systematically for every injection retard. This observation is matched with decrease in air utilisation and filter smoke number Figure 5.8 (B & C). From the plot of HRR in Figure 5.9, it is evident that the observations are due to increased diffusion burning with injection retard. Despite the increased exhaust temperature (Figure 5.8D), there was significant reduction in NOx confirming that although more fuel was consumed; it was not burnt during premixed combustion process that favours NOx production. Therefore for the purpose of running the engine at a condition of highest sooting propensity in non-boosted operation and without exhaust gas recirculation, injection time of 9^{o} BTDC gave the best compromise.

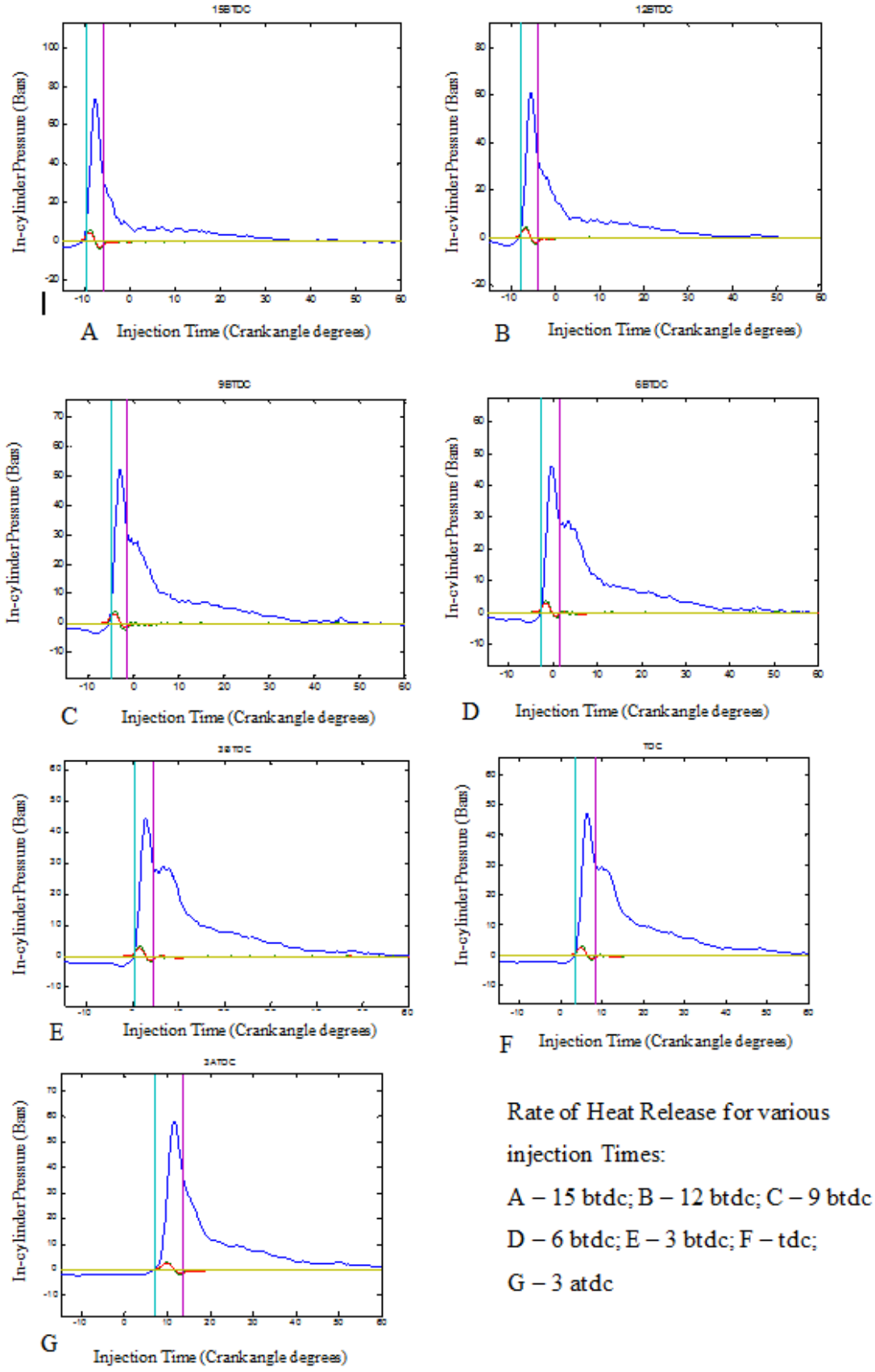

Rate of Heat Release for various injection Times:

A – 15 btdc; B – 12 btdc; C – 9 btdc

D – 6 btdc; E – 3 btdc; F – tdc;

G – 3 atdc

Figure 5.9 Rate of Heat Release at various injection timings

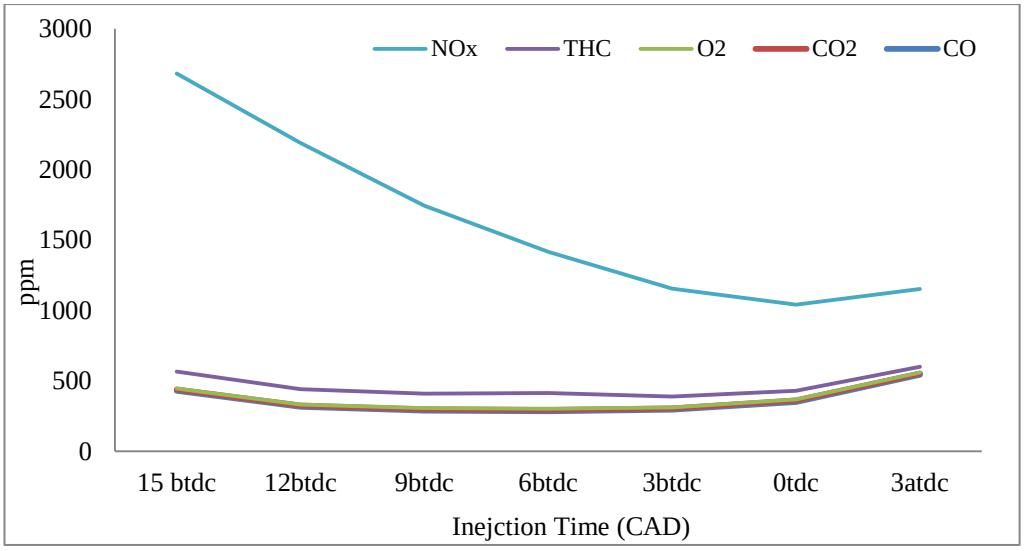

Figure 5.10 Influence of injection timing on gaseous emissions.

5.3 Effect of Engine Operating Conditions on Particle Number and Size Distribution

As a prelude to particle number and size distribution measurements, the effect of engine operating parameters were previewed in line with the established baseline conditions. A dilution ratio of 16.4 was selected from the default calibrations of the electrical mobility spectrometer. To generate samples conceived to contain PM with volatile organics as well as soot particles, engine condition was set at 80Nm and 1500Rpm at injection pressure of 800bars and timing of 9^{o} BTDC. The results are presented in Figure 5.11.

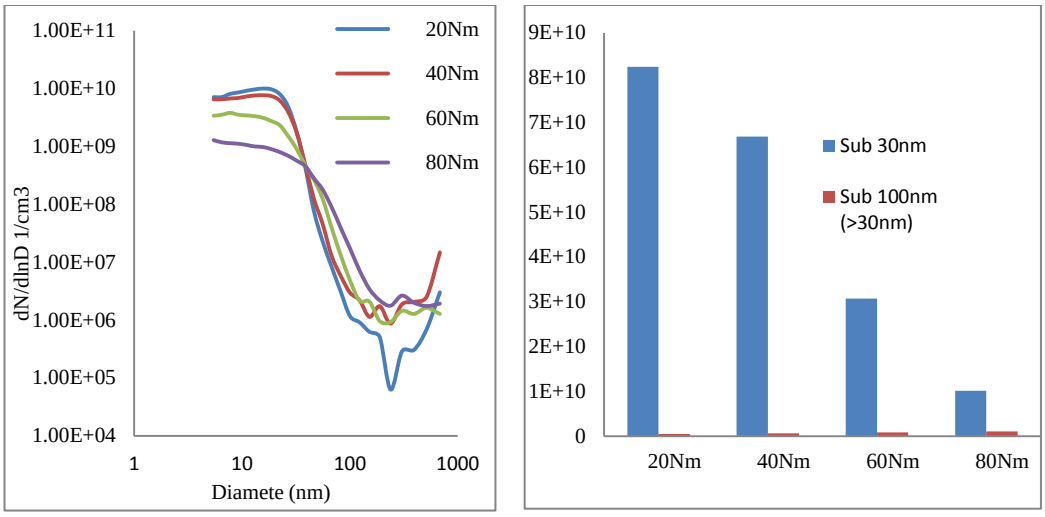

A B

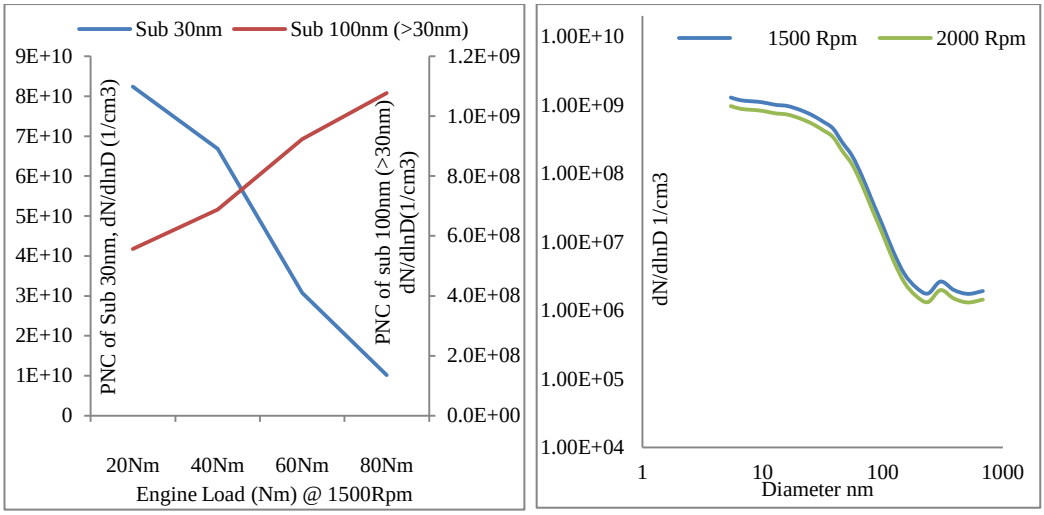

C **D**

Figure 5.11 Effect engine condition on Particle Number concentrations (PNC)

A: Effect of engine load on PNC and size emitted at 1500Rpm and dilution ratio of 16.4, B &C: Effect of engine load on PNC on size distribution {sub 30 nm and (31-100nm)} D: Effect of engine speed on PNC and size distribution

The particle number concentrations (PNC) for the various loads are seen to decrease with increase in engine load within the sub 40nm diameter range; and conversely, increases for particle size greater than 40nm in diameter with increase in load (Figure 5.11). For all the loads, there is an inflexion point at particle size of 40nm diameter on the plots which marked the departure between decreasing and increasing character of the PNC as load increased (Figure 5.11A). This character follows the earlier results with FSN whereby at higher loads, more soot particles are generated which is reflected as the degree of blackness on the filter paper registered as smoke numbers. The smoke number increased with increase in load. Correspondingly, the soot particle number sizes which fall within the range of 50 – 100 nm (Kittelson D. B., 1998.), have an increasing character as load increased in Figure 5.11 B and zoomed in Figure 5.11C. From Figure 5.11A also, it is observed that beyond 100nm, there is fluctuation in the plot of PNCs, and the degree of intensity of fluctuation increases as the load is decreased, this makes the choice of 80Nm more appropriate. Similarly, the influence of engine speed was previewed between 1500 and 2000 Rpm as presented in Figure 5.11D. There is slight increase in PNC at 1500rpm for all the sizes in the distribution but more within the small sizes signifying presence of condensed volatiles that adsorbed on core particles.

5.4 Summary and Engine Baseline conditions

The results so far have shown the combustion and emissions characteristics of the test engine to be consistent with what is known of diesel engine (Heywood, 1988; Majewski, W. A. and Khair, M. K., 2006). The summary of the preliminary observations will be used as established baseline conditions for further tests as reported in the next chapters. These are 800Bars of fuel injection pressure timed at 9^{o} BTDC without any EGR.

1. Low load engine operation has been optimised for stable operation at about 42.7Nm and 1500Rpm which is equals 2.7 bar BMEP. This is taken as a regime for stable low engine operation to generate PM rich in volatile organic matter from the smoke number values.
2. Engine operation at 80Nm and 1500Rpm (5.05 bar BMEP) will be taken as high load low speed that generates PM with good quantities of soot and volatile organic matter.
3. Engine operation at 80Nm and 2000Rpm (5.05 bar BMEP) will be taken as condition for generating PM with high soot within the limit decided on the test engine.
4. The low load (2.7 BMEP @ 1500Rpm) represents about 20% of the maximum power used as operating points for stationary driving cycles in testing automotive diesel engines, while the medium loads (5.05 BMEP @ 1500 and 2000 Rpm) represent 37 – 40%.

CHAPTER 6

MEASUREMENT OF PARTICULATE MATTER EMISSIONS

6.0 Introduction

There is growing concern about the effect of nano particles on human health; particularly with reference to carcinogenicity and cardiovascular diseases which has led to legislation of more stringent limits. Particulate matter (PM) is currently regulated in number metric; therefore its measurement is now better expressed in particle number concentrations (PNC) that occur at different size distributions. By nature, it is composed of particles that condense from volatile matter suspended in the exhaust stream as well as solid carbonaceous particles. In regulation, the carbon or soot particles are of prime significance; therefore the volatile components are first removed before measurements are made in order to determine the real value of the solid carbon particles. The particle measurement programme (PMP) has drafted framework based on hot dilution technique as reviewed in chapter 3 for comparing sampling and measurement efforts irrespective of the methodology adopted. This chapter reports studies made about particulate emissions from measurements made. This is majorly on the influence of dilution conditions on PM measurements and influence of the dilution gas on PM measurements. The measurement facility used is the electrical mobility spectrometer as described in chapter 4. Attempt was made to use an external dilution device that parallels a mixing tube diluter incorporating an evaporator tube together with the manipulation of the dilution system in the EMS to pursue the two stage dilution protocol of the PMP.

6.1 Methodology of Aerosol dilution and measurement with electrical mobility spectrometer (EMS)

The cross-section of the dilution system built jointly with the sample probe was presented in section 4.2.4 and is represented here in Figure 6.1A; and the layout of the dilution flow subsystem is shown in Figure 6.1B. It is a mixing tube diluter connected to the primary probe used to extract raw sample from the engine exhaust line via a high temperature resistant control valve. This arrangement ensures that raw exhaust is mixed at about 12-15 centimetres from the centreline of the main exhaust

line. Therefore the residence time encountered before dilution could only be a matter of milliseconds.

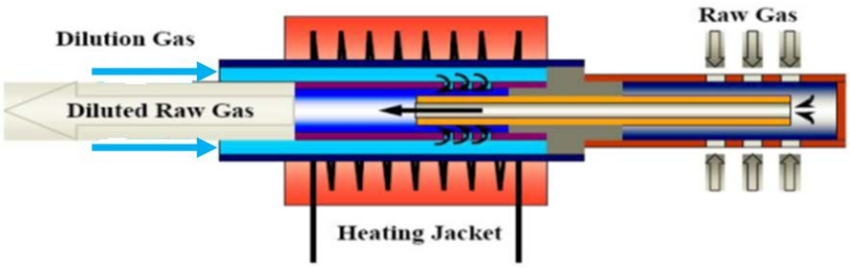

A

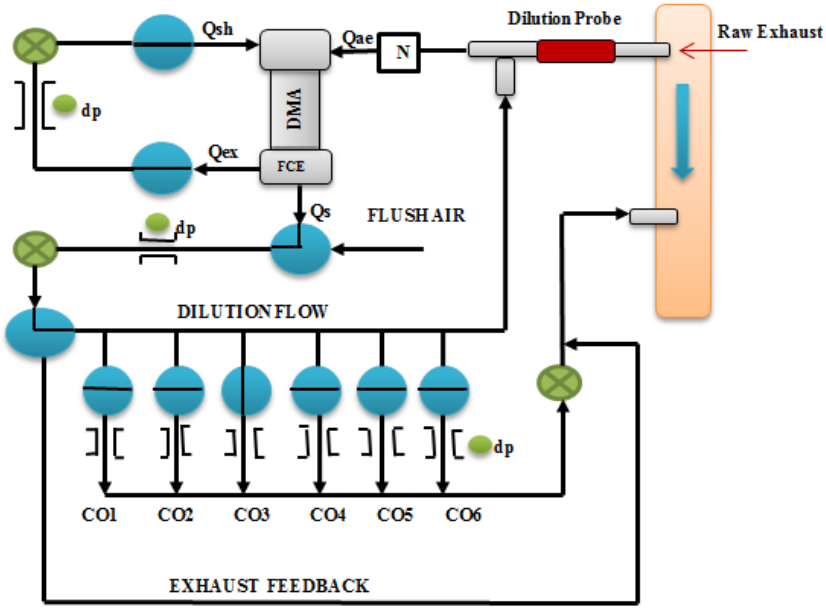

B

Figure 6.1 A: Mixing Tube Diluter, B: Lay-out of the dilution flow system
[N: Neutraliser, DMA: Differential Mobility analyser, FCE: Faraday Cup Electrometer, Qsh: Sheath Air flow, Qex: Excess Air, Qae: Aerosol intake, Qs: Sample Flow, dp: Pressure indicator for sample flow orifice, (Co1 – Co6): Array of critical orifices] (Alozie et al 2014A).

The variable temperature setting of the dilution probe heater and also of the flow control unit were used to vary dilution ratios for various temperatures. The aerosol measurement uses electrostatic technique which involves optimal integration of the DMA and FCE, relying on an idealised relationship of aerosol input-output characteristics. Central to this idealisation is that, consideration of the DMA transfer function was properly made for its operating conditions, geometry, as well as the properties of carrier gas and aerosol particles in the determination of aerosol sizes

measured (Reischl G. P., 1991 B). This is at pre-defined and fixed flow rates which are theoretically optimized for size resolution when sheath air flow (Q_{sh}) = excess air (Q_{ex}). The flow control unit governs Q_{sh} using a critical orifice. The aerosol intake (Q_{ae}) is set to equalise the value of sample drawn (Q_s), which is also determined by the critical orifice. The dilution gas flow is fed back to the sample probe (via an absolute filter) so that Q_{ae} remains constant at the value Q_s. In this way the amount of aerosol taken from the exhaust duct is determined by the amount removed from the dilution feedback through the dilution valves as removed from the dilution feedback flow (Winklmayr, 1991). Secondly, the FCE does not depend on particle size or other particle properties; therefore it represents a near absolute method to measure particle size as well as their concentrations (Reischl G. P., 1991 A). Dilution flows are configured to give ten different dilution ratios by operating critical orifices (CO1-CO6) in different combinations in closed-loop as shown in Figure 6.1B (Analysesyteme, 2008). The dilution ratios achieved with this arrangement as configured in our device are presented in Table 6.1. It is usual to check the calibrations of the aerosol intake by measuring the real flows with a flowmeter coupled to the tip of the probe as a pre-test confirmation.

Table 6.1 List of dilution ratios

Q_s (l/min)	Dilution Ratio	Per cent of Q_{ae}	Aerosol Intake (l/min)	Orifice Combination
2.57	31.5	3.17	0.08	CO1
2.57	24.7	4.05	0.10	CO2
2.57	16.4	6.11	0.16	CO3
2.57	10.8	9.28	0.24	CO1+CO3
2.57	8.0	12.45	0.32	CO4
2.57	5.4	18.56	0.48	CO3+CO4
2.57	4.5	21.98	0.56	CO5
2.57	3.2	31.26	0.80	CO1+CO3+CO5
2.57	2.0	49.42	1.27	CO6
2.57	1.4	71.15	1.83	CO1+CO3+CO4+CO6
2.57	1.0	100.00	2.57	

Flow rates calculated from critical orifice (CO1 – CO6) combinations, according to EMS configuration

Some preliminary tests were carried out to preview the dilution effects at different temperatures when using the instrument dilution probe. In order to have appreciable temperature difference, three temperature ratings of 100^{o}C, 200^{o}C and 300^{o}C were adopted in the closed loop dilution system of the EMS during the experiments**.** Similarly during measurements, four scans were taken and the averages were taken for analysis. Test matrices adopted for the collection of particle number and size data were for the whole range of dilution ratios shown in Table 6.1. The engine was operated as optimised in chapter 5 at 42.7Nm/1500rpm to generate PM well laden with volatile fractions and 80Nm/1500rpm which have substantial mix of volatiles as well as carbonaceous soot. This load conditions represent 2.7bar BMEP and 5bar BMEP respectively without any EGR. The fuel injection pressure was set at 800bar and the fuel was injected at 9^{o} BTDC. These load conditions will simply be referred to as low and high loads. Three temperature settings of the dilution probe heater and also of the flow control unit were used to vary dilution ratios at 100^{o}C, 200^{o}C and 300^{o}C in the closed loop dilution system of the EMS. In each case, four to five scans were taken to monitor stability and repeatability; of which, average of the best three consistent scans were taken for analysis. Test matrices adopted for the collection of particle number and size data sets are shown in Tables 6.2 (A&B) respectively.

Table 6.2A Low load engine operating condition: 42Nm, 1500Rpm, 800Bar, 9^{o} BTDC, and 0% EGR

Temps.	Closed – Loop Dilution Ratios									
[^{0}C]	31.5	24.7	16.4	10.8	8.0	5.4	4.5	3.2	2.0	1.4
100										
200										
300										

Table 6.2B High load engine operating condition: 80Nm, 1500Rpm, 800Bar 9^{o} BTDC and 0% EGR

Temps	Closed – Loop Dilution Ratios									
[^{0}C]	31.5	24.7	16.4	10.8	8.0	5.4	4.5	3.2	2.0	1.4
100										
200										
300										

6.1.2 Particle Mass Estimation from Number Distributions

Besides measurements of PNCs at chosen dilution conditions, mass distributions have also been calculated from the first principles as described in (Eastwood P. , 2008; Andrews et al 2001; Price et al 2006). The model used to calculate mass concentration from the measured number concentration per unit volume of aerosol over a size range is given as:

$$dM/dlogD_p = (dN/dlogD_{p)}\, \rho\, S(D_p{}^{d_f}) \qquad (6.1)$$

Where M is the mass of primary particles, $dN/dlogD_p$ is the number of primary particles per unit volume of gas within the size range, d_f is the fractal dimension of the measured particles, ρ is the density of measured particle, D_p is the particle mobility diameter and S is the shape factor. These parameters are not well defined for the sampled particles, thus it induces uncertainties to the determined mass concentration through the above model. The particle diameter is evaluated in line with the measurement principle of the instrument. For a bipolar charger like the DMA, electrical mobility on the size range associated with diesel particles is obtainable. Therefore, particle diameters D_p could be expressed as mobility diameters (d_m) which are instrument specific relating D_p to macroscopic basic units like volume flow rates, voltage and physical dimensions of the DMA (Reischl G. P., 2006; Reischl G. P., 1991 A). This will also include the perspective of calculating the density and fractal dimension of the particles. The engine-out particles consist of agglomerates of various fractions, so a single density value cannot be confidently adopted. Some studies have been attempted to derive soot density (mainly the density of the assumed solid or carbonaceous particles). In premixed flames, the measured soot density was reported to be 1.8±0.1g/cm^3 when the soot was collected at 30cm above the burner and the density was found to vary with height (Choi et al 1994). In (Abdul-Khalek, I. S., and Kittelson, D., 1995) the value of 2g/cm^3 was adopted. The effective soot density (mass per unit mobility volume) has been reported to vary with size from 1.2g/cm^3 at 30nm to less than 0.3g/cm^3 at 300nm when density was calculated according to a power law, which varied with the fractal dimension that

was itself dependent on the diameter (Maricq, M. M., Xu, N., Chase, R. E., 2006; Maricq, M. M., and Xu, N.,, 2004; Mariq, 2007 B). The density of unburnt hydrocarbons originating from fuel and lubricants are reported to vary from 0.8 – 1.0 g/cm^3 (Choi et al 1994; Baumgard, K. J., and Johnson , J. H.,, 1996; Schneider et al 2005). For sulphate fractions, the densities have been used as 1.5g/cm^3 (Warner et al 2002) and 1.83g/cm^3 in (Schneider et al 2005) respectively.

Detailed theoretical and experimental determination of density for various fractions of engine-out particle emissions and different perspectives for evaluating particle diameter, shape factor and fractal dimension are given in (DeCarlo 2004; Slowik 2004). Studies presented in (Gulijk et al 2004; Shapiro et al 2012; Liang et al 2013) corroborate the that the impacts on soot morphology resulting from these hypothesis are mainly due to the effect of changing density factors influenced by the power law because of changes in fractal dimension. The fractal dimension of soot from diesel exhaust was taken to be 2.3±0.1 in (Maricq, M. M., and Xu, N.,, 2004). The void and the volatile fractions present in the aggregates will also contribute to the variations to the average particle densities. Given these complexities and the need to adopt a simplified approach to achieve a reasonable comparison of number metrics, the ideal characteristics of a standard density value of 1.0 g/cm^3 , a spherical shape factor, and a d_f value assumed to be 3 based on the assertions made in all the above studies cited. Thus the results from this mass analysis should be taken with due regards to these assumptions. Using the uncertainty analysis discussed by (Moffat R. J., 1988), the total uncertainty to the evaluated mass was found to be 5.5% when there was 1% variation in density and fractal dimension.

6.2 Investigation of the influence of dilution conditions on PM measurement

Diesel engine particulates conceptually occur as primary particles called nuclei which undergo surface growth to form spherules of about 20-50 nanometers. These particles agglomerate to form identifiable structures with more primary particles. From the reviews we infer that the study of particulates is complicated with regards to issues like their nature, types, size, shape, transport, transformation and deposition in the course of formation inside the engine, flow through the length of exhaust line and ultimately to the atmosphere+. These complications arise due to complex thermal, chemical and allied flow processes that are inherent in the nature of

combustion and post-combustion reactions (Tree, D. R., and Svensson, K. I., 2007; Dec J. E., 2009). As particulates flow through the exhaust line lower temperatures are encountered and this condition favours nucleation of volatile fractions depending on their concentrations. If the engine exhaust is emitted directly into atmosphere it gets cooled by mixing with ambient air, this leads to infinite dilution and to changes in both number and mass of the particulate matter as it transforms. In order to simulate these physical conditions in laboratory schemes, it is conventional to draw out samples from exhaust stream, mix and cool with dilution gas to a level that the measurement devices can handle. Inherently, additional complications due to artefacts, besides mixing and cooling effects are involved for particle size, mass and number measurements (Kittelson, D. B., Arnold, M. and Watts,W. F. (Jr)., 1999; Khalek I. A., 2007b). The approach to particulate sampling and conditioning prior to measurement has become an established criterion for evaluating the validity of results. The stability of particles in the dilution tunnel are primarily influenced by the temperature of dilution gas, which dictates the state of volatile fractions as they tend to nucleate homogeneously; the dilution ratio, also linked to temperature, which determines how the vapour/condensation pressures of the volatile fractions are at the sampling points; the residence time, which is the time spent by the particles along the sampling path; as well as the relative humidity (Khalek, I. A., Kittelson, D.B., and Bear, F., 2000; Kittelson D. , 2003; Kasper, 2004; Burtscher, 2005; Giechaskiel et al 2008). In effect, the outlook of particle size distribution from any device depends on how the aerosol has been conditioned prior to measurement due to possible condensation of volatile fractions and agglomeration of primary particles. Dilution acts in different ways on aerosol by cooling and mixing, in other words, the heat and mass transfer processes are strongly dependent on the nature and thermal state of the dilution gas. If hot exhaust is mixed with air at low temperature, cooling effect will initially decrease the saturation vapour pressure of the volatile fractions thereby enabling gas-to-particle conversion. With time, mixing will take over and subsequently dominates the process; forcing the partial pressures of the volatile fractions to decrease, thus causing reversal of particle-to-gas transformation. On the other hand, if the exhaust is mixed with hot gas at a close range temperature, there will be no effect on saturation vapour pressure as before; rather the partial pressures of volatile fractions will decrease. Given the interplay between these factors, proper understanding of cooling and mixing of aerosol prior to particle size measurement is

essential. It is deducible that, the way in which aerosol is diluted and how different temperatures cause cooling is more important than the actual dilution ratio itself (Abdul-Khalek, I., Kittelson, D. B., and Bear, F.,, 1999; Kawai, T., Goto, Y., and Odaka, M.,, 2004; Mathis et al 2004; lyyränen et al 2004; Kasper, 2004; Burtscher, 2005; Kumar, 2010; Giechaskiel et al 2012).

The relevant physics that drives the gas to particle conversion of volatile components has been explained in the review with phase diagrams to depict the path which dilution gas at high or low temperature could affect transformation of volatile emissions from engine exhaust as presented in (Kasper, 2004; Burtscher H. , 2005). As the effect of temperature is associated with mixing in the dilution process, there is need to understand how temperature dictates the saturation pressure for various components that constitutes the volatile fractions. It was point out in chapter 2 that diesel like fuels are conventionally distilled at a range of 149^{o}C to 371^{o}C from crude oil from straight run as well as cracking and constitutes of paraffins, olefins, naphthenes, iso-paraffins and aromatic fractions in various compositions. This heterogeneous nature of the generic species imposes different saturation pressures at which condensation of volatile fractions originating from them as well as those of intermediate species due to pyrolytic reactions, will occur. The model for expressing the saturation ratios (the ratio of partial pressure to vapour pressure) for any particular specie could be viewed through the expression of saturation ratios based on the ***Clausius – Clapeyron*** relations which could be expressed as:

$$S = (Y_{HC}/D)\exp((-h_{fg}/R) * (1/T_{mix} - 1/T_{bp}) \qquad 6.2$$

Where:

D - is the dilution ratio

h_{fg} - is the enthalpy of vaporisation [kJ/kg]

R - is the gas constant [kJ/kg]

S - is the saturation ratio

T_{mix} - is the temperature of the air – exhaust mixture [K]

T_b - is the boiling point of hydrocarbon [K]

Y_{HC} - is the hydrocarbon fraction prior to dilution

T_{mix} is a linear interpolation of exhaust gas temperature T_{exh} and dilution gas temperatures $T_{gas,}$ expressed in terms of adiabatic dilution ratio D as:

$$T_{mix} = T_{exh}(1/D) + T_{gas}(1 - 1/D) \qquad 6.3$$

The above equations provide a relationship between the dynamics of phase transformation of volatile fractions and the dilution process; with critical implication for the cooling and mixing of the volatiles. This has been used to describe the saturation characteristic of the volatile species in the sample. In this section, the above theory has been used to investigate the effects of dilution ratio and mixing temperature of dilution gas on particulate number and size distribution from diesel engine using the Electrical Mobility Spectrometer (EMS) connected a closed loop mixing tube diluter which uses filtered exhaust gas as its diluent.

6.2.1 Measurement Results of Particle Number Concentrations

The exhaust soot particle number size distributions were measured at various dilution ratios by maintaining the heater of the dilution probe at different temperatures of 100°C, 200°C and 300°C for both low and high engine loads. Typical data sets of PNC are plots are shown in Figure 6.2.

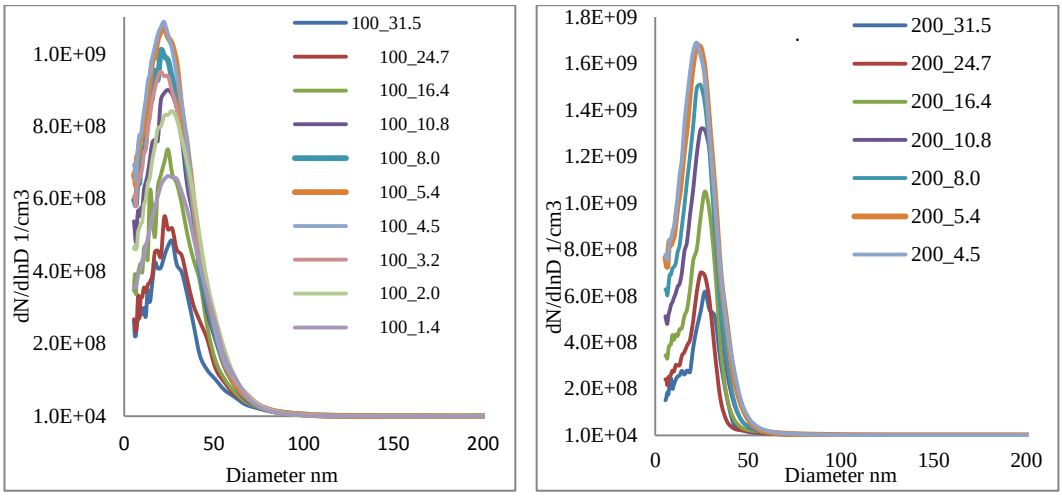

A B

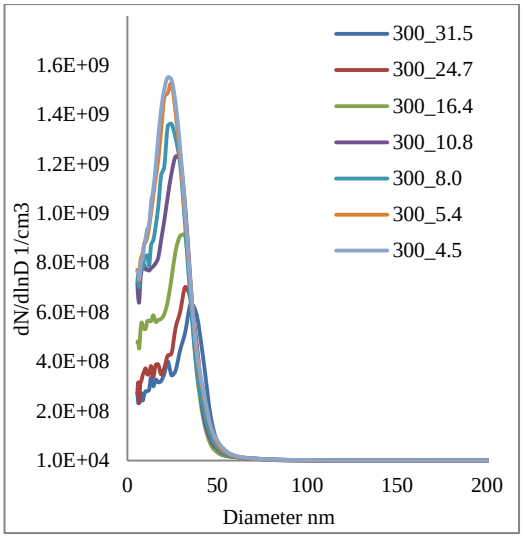

C

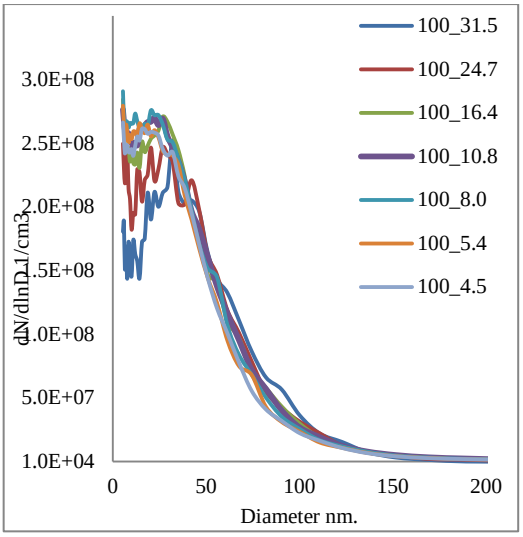

D

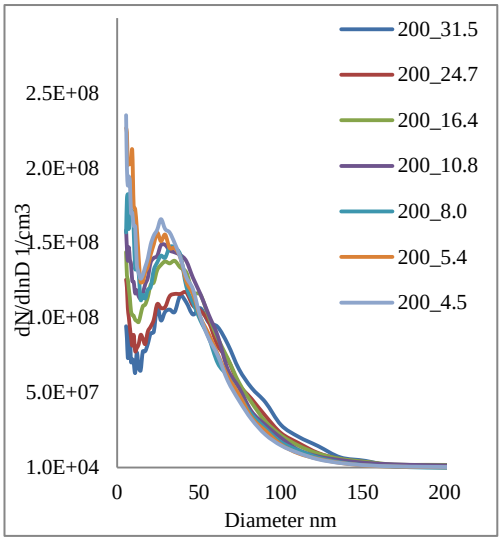

E

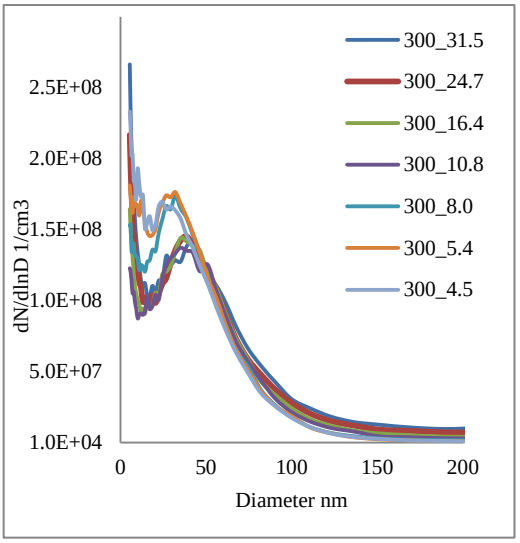

F

Figure 6.2 Particle number concentrations (PNC) at low load engine operations for various dilution ratios A: 100^{o}C, B: 200^{o}C, C: 300^{o}C; and Particle number concentrations (PNC) at high load engine operations for various dilution ratios. D: 100^{o}C, E: 200^{o}C and F: 300^{o}C.

Under low load operation and for the set dilution probe temperature of 100^{o}C, it could be seen in Figure 6.2A that the number concentration of the measured particles increased as the dilution ratio was decreased from 31.5. This trend was observed until the number concentration reached a maximum at the dilution ratio of 5.4, and was coincident with the dilution ratio of 4.5. Thereafter the number concentration decreased with further reduction in dilution ratios such as 3.2, 2.0 and 1.4. This trend

was observed for all other measurements under both engine operating conditions, and at different dilution temperatures. However, the trend was of lesser degree at higher load. For all the set dilution probe temperatures, a clear distinction in the magnitude of measured particle concentration was observed between the two engine operating conditions. The low load registered a higher number concentration compared to high load. The main cause for the observed differences is in the nature of diesel engine combustion. As reviewed in sections 2.6.2 and 3.2.1; and also explained in section 5.1, under low engine load operation and for the chosen injection timing, combustion is more pre-mixed, quantity of injected fuel, the combustion and exhaust temperatures are lower than those encountered at high loads, therefore higher amount of un-burnt hydrocarbons were emitted from the engine due to incomplete oxidation of either diesel fuel or lubricants. Presence of unburnt hydrocarbon in the engine exhaust leads to high nucleation mode particles due to condensation of volatile organic species as temperature decreases. Conversely under high load, more fuel is injected, the engine operating temperature is relatively higher and gives rise to faster fuel vaporisation, this enhances oxidation rates but combustion tends to be more of diffusion burn than premixed. Consequently air/fuel ratio decreases and as there is no sufficient time for proper mixing, this result in localized pockets of fuel lacking sufficient oxygen during the diffusion burning process, which in the presence of high temperature leads to pyrolysis of fuel molecules and formation of carbonaceous nuclei. These carbonaceous nuclei coalesce progressively and form larger aggregates, and become accumulation mode particles during the expansion process, and further aggregation and adsorption of volatile particles on core soot particles occur along the exhaust pipe where the temperature are comparatively lower than in-cylinder. From the data presented in Figures 6.2, it can be seen that there are more nucleation mode particles at low load than at high loads, and more accumulation mode particles at high load compared to low load, these observation are consistent with the outcomes discussed in (Majewski, W. A. and Khair, M. K., 2006).

6.2.2 Effect of dilution conditions on Particle number concentrations and size distributions for PM generated at low load

The effect of dilution on the PNC is investigated by analysing the behaviour of the trends observed in Figure 6.2 at various dilution ratios and temperatures. To eliminate the effect of noise interference, particles below 10nm size in diameter are not considered and it is viewed not to be of significant effect on the results. Figure 6.3 (A), shows the number size distribution of PM measured from the exhaust generated at low load operating conditions for a set dilution ratio of 31.5; and for three different dilution probe temperatures (100^{o}C, 200^{o}C and 300^{o}C). At this dilution ratio (31.5) the measured size distributions exhibited the best spread of the particle diameters for different dilution temperatures. When the aerosol was diluted at 100^{o}C the cooling effect resulted in highest concentrations of larger size particles.

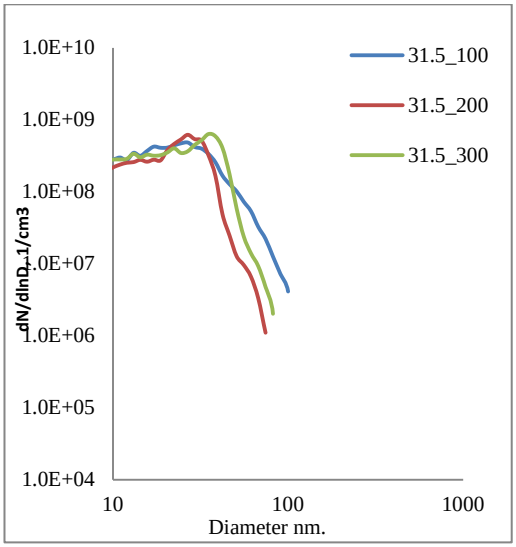

A

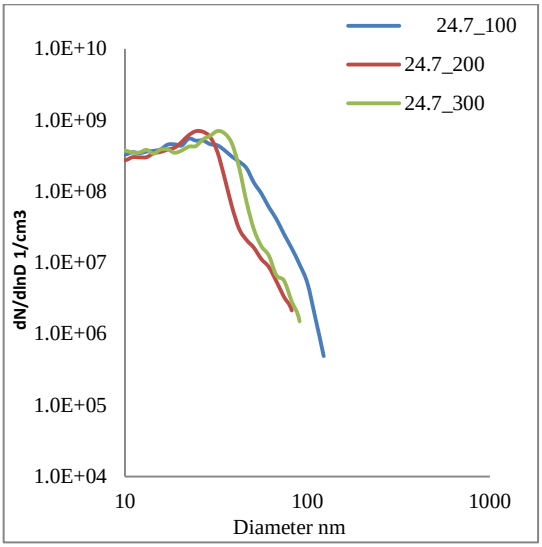

B

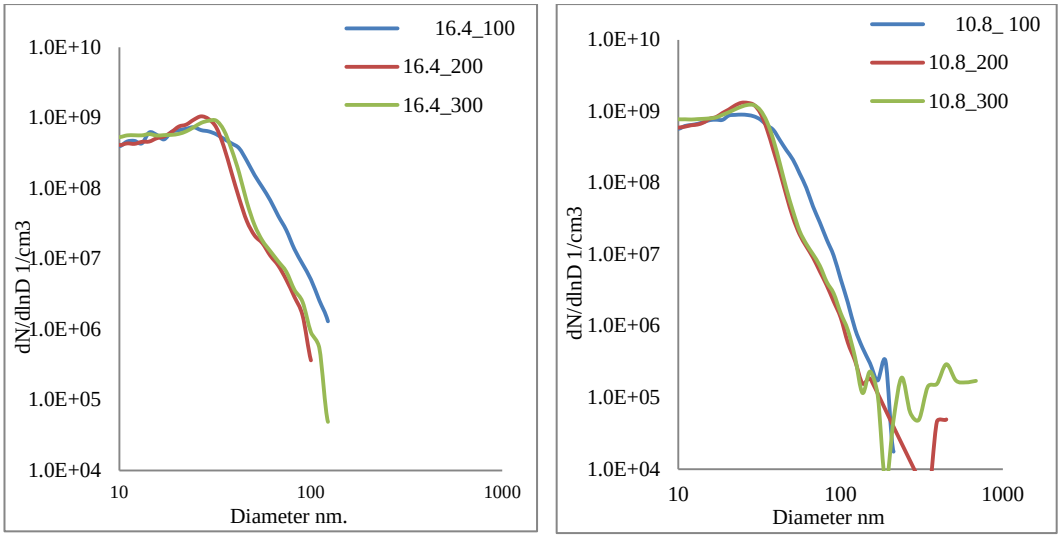

C D

Figure 6.3 Particle size distributions at low load engine operation for various dilution ratios mixing at 100^{o}C, 200^{o}C and 300^{o}C, A – Dilution ratio 31.5; B – Dilution ratio is 24.7; C – Dilution ration is 16.4 and D – Dilution ratio is 10.8

There is a separation hump at 40nm corresponding to concentration range of about 1 × 10^{8} /cm^{3}, while a clearer separation is observed at diameters 50 nm and 60 nm for the dilution temperatures of 200^{o}C and 300^{o}C respectively and corresponding number concentrations of about 1 × 10^{7}/cm^{3}. The explanation is that, at 100^{o}C, more volatiles undergo nucleation (Abdul-Khalek, I., Kittelson, D. B., and Bear, F.,, 1999) (Kawai, T., Goto, Y., and Odaka, M.,, 2004) (Mathis et al 2004). The nucleated volatile particles adsorbed on available solid carbon particles which made them grew bigger. When the aerosol was sampled and diluted at 200^{o}C, volatile fractions still nucleated but as the temperature is relatively higher, the concentration is less ubiquitous and tendency to agglomerate is also relatively less. This explains the growth in nucleation peak and a corresponding decrease in the accumulation mode particles compared to dilution at 100^{o}C. When the aerosol was diluted at 300^{o}C, the saturation pressure of volatile fractions is higher at this condition and the tendency for nucleation is suppressed, occurring rather at a higher temperature signified by a little rightward shift on the size at which nucleation peak occurred. Also the carbonaceous particles on which the volatile particles adsorb have size distributions that tend towards the sizes where the clear humps appear. Evidently, the particle size distributions are limited by the low quantity of aerosol in the sample at this dilution

condition since it is volume controlled. When the aerosol was diluted with dilution ratio of 24.7 Figure 6.3B, the maximum diameter of the measured particle size in the distribution increased and the spread at 200^{o}C and 300^{o}C becomes less separated from sizes more than 40nm. The nucleation peaks occurred at slightly increased diameters with increase in dilution gas temperatures. The plausible reason is increase in aerosol concentration at this dilution ratio, which enhances the growth of particles in line with the trends already described. Decreasing the dilution ratio further to 16.4 as in Figure 6.3C, the difference in particle size distributions is small at 200^{o}C and 300^{o}C. This effect is also reflected for 100^{o}C case, which draws nearer to 200^{o}C and 300^{o}C for larger diameters when compared against the data presented in Figure 6.3B. The nucleation peak for the aerosol diluted at100^{o}C occurs at about 33nm, and the peak at 200^{o}C is higher than that at 300^{o}C. The explanation here goes as before, the increase in aerosol concentration by the volumes of dilution ratios led to more volatile concentrations, while the vapour pressure increased at higher temperature. Decreasing the dilution ratio further to 10.8 caused the temperature to have little effect on particle size distribution beyond 200^{o}C shown in Figure 6.3D. However, dilution at 100^{o}C still holds higher concentration for lager particles signifying more adsorption of volatile particles on core solid particles. The nucleation peak for all the three dilution temperatures occur within the same range between 20 and 30nm. Owing to availability of species, the peak of nucleation is slightly higher at 200^{o}C than 300^{o}C indicating that more volatiles condensates at 200^{o}C. Although not included in the figure, when the dilution ratio was decreased further to 8.0 and 5.4, the temperature effects on the size distribution were very negligible beyond 200^{o}C but still maintaining a strong influence at 100^{o}C, similar to the trend observed in Figure 6.3D. The nucleation peaked at 24nm for 200^{o}C and 300^{o}C, and at 20nm for 100^{o}C for the dilution ratio of 8.0. The nucleation peak was highest at 200^{o}C when the aerosol was diluted at a dilution ratio of 5.4. Peak particle diameters are almost equal for all temperatures and the particle size distributions coincident when mixed at 200^{o}C and 300^{o}C. Mixing at 100^{o}C remained distinctly higher like in other dilution ratios indicating high volatile condensation. Other dilution ratios were left out as the impact of mixing became less significant.

6.2.3 Effect of dilution conditions on Particle number concentrations and size distributions for PM generated at high load

Particle size distributions arising from high load operation, subjected to dilution at various temperatures as before, are shown in Figure 6.4 A-D.

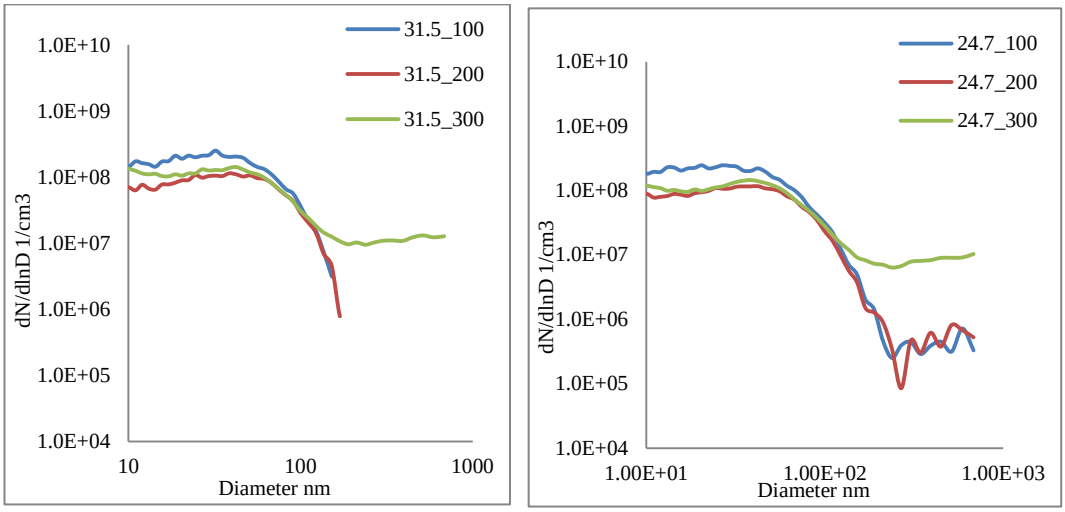

A B

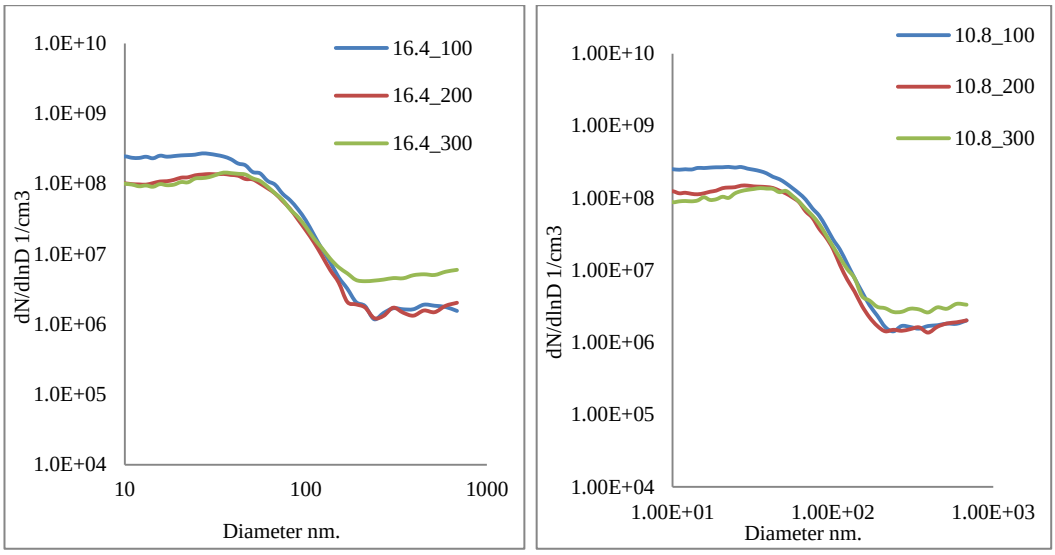

C D

Figure 6.4 Particle size distributions at high load operating condition for various dilution ratios mixing at 100^{o}C, 200^{o}C and 300^{o}C, A – Dilution ratio is 31.5; B – Dilution ratio is 24.7; C – Dilution ration is 16.4 and D – Dilution ratio is 10.8;

Particle size distributions measured under high load operation for the four highest dilution ratios and at the three dilution gas temperatures, are similarly shown in Figures 6.4 A-D. The engine exhaust temperatures from sampling point were within 484^{o}C to 496^{o}C. As determined in chapter 5, diesel combustion characteristics result in more carbonaceous emissions at higher engine loads compared to lower engine loads. Similarly, diluting the aerosol at high temperature helps to suppress nucleation of volatile fractions. Compared to the lower load operation, exhaust temperature was higher than what the diluter heater capacity could give and the plots of PNC are seen to be more unimodal. Similarly, compared to equivalent dilution ratios at the lower load condition, peak PNCs are lower; peaks occur at 30nm for dilution at 100^{o}C, and 40 nm at 200^{o}C and 300^{o}C, respectively, with small differences in PNCs. In addition, particle size distributions extended to the limit of the measurement device with decrease in dilution ratio (implying increased volume of sample measured) as evidence of increase in PM emission at this load condition compared to the lower load. This is also suggestive that larger carbonaceous particles aggregated in this higher load and provided the core particles upon which condensed particles adsorbed. There is a difference in PNC when diluted at 100^{o}C within sub 50 nm, compared to dilution at 200^{o}C and 300^{o}C which are almost coincident indicating the tendency to suppress nucleation of the volatile species at elevated temperature. Diluting the aerosol at the dilution ratio of 24.7 caused the particle size distributions at 100^{o}C and 200^{o}C to extend up to the maximum measurable diameter of the measurement device Figure 6.4B. Diluting the aerosol at the ratios of 16.4 and 10.8 did not have any noticeable difference in the spread of the size distribution Figure 6.4(C-D), but particle sizes beyond 100nm range at 100^{o}C and 200^{o}C caused the number concentration to increase. Similar trends were observed for the dilution ratios of 8.0 and 5.4 except for irregular distribution beyond 150nm at the dilution temperature of 200^{o}C. In effect, all lower dilution ratios did not have significant differences in the spread of the size distribution up to 200nm. However particle sizes extending beyond this range at all temperatures had increased concentrations at various sizes which were quite dependent on dilution temperature, which further indicates increase in species availability in the aerosol. For the two engine load conditions, the assertions made about the influence of dilution conditions on particle size distributions could be further explored by looking at the cumulative particle number concentrations (CPNC) which were obtained by integrating the number

distributions within the range, as well as the cumulative particle mass concentrations (CPMC) obtained by integrating Equation 6.1. In order to achieve a high degree of accuracy, integrations were carried out within the range of particle diameters 10nm to 200nm, where scans of size distributions were most regular. As was stated earlier, in order to avoid possible errors due to noise interferences to FCE in counting the particles, the PNCs of sub-10nm diameter were not considered. In addition, examinations of the variations in scan-to-scan repeatability as well as day-to-day scan repeatability tests were quite low for the three operating temperatures. From the results presented in section 6.2.0 for the two load conditions considered, particle yield from phase transformation was highest during mixing at 100^{o}C with peak concentration occurring at 30 nm. Since particles in nucleation mode (NMP) are around or considerably lower than this diameter, it is convenient to assume that those particles larger than 30nm are associated with growth in both loads conditions. In the higher load condition, the temperature effect at 200^{o}C and 300^{o}C is small at all dilution ratios. Considering the volatility of Diesel fuel, it is also convenient to assume that for most unburnt fuel, the intermediate particle precursors arising from incomplete combustion constituting the VOFs, should condense before 100^{o}C leaving only water and its solubles in the gas phase. Therefore as basis for analysis, particles sizes in the range 10-30nm were accounted as nucleated from volatile species. Since heating did not completely desorb the volatiles in both loads, it is difficult to know the exact size distribution of the accumulation mode particles (AMP). It is reasonable to view it that an intermediate range of sizes exist where nucleation mode particles exists both as independent small particles as well as adsorbing on carbonaceous cores in the accumulation mode. The quantitative measures of these particles based on nucleation activity have been used to examine the effects of mixing and temperature on aerosol at 100^{o}C, 200^{o}C and 300^{o}C of the dilution gas.

6.2.4.1 Effect of Mixing and Temperature on PM generated on Low Engine Load

The results obtained by integration of the number concentrations as CPNCs at low load condition are shown in Figure 6.5 (A&B). The two are plots of the same data but Figure B was separated and zoomed to highlight the concentrations of particles that occurred in the size range of 31-200nm on y-axis which are not properly highlighted on the same scale. At the highest dilution ratio (lowest aerosol concentration), the cumulative number concentration is lowest at all dilution gas temperatures. Accordingly, the cumulative number concentrations increased with decrease in dilution ratio (as aerosol concentrations increase). As already implied, the particle number is higher in the sub 30 nm due to nucleation activity compared to larger particles greater than 30 nm. Figure 6.5B shows the cumulative number concentrations of the larger particles to be highest when aerosol was diluted at 100^{o}C under all dilution ratios. This strengthens the view that particles sampled under low load operation are composed of mainly volatile fractions; and due to their higher concentrations at lower dilution ratios more particles nucleated and condense at this low temperature. The variability of CPNCs at higher temperatures indicates desorption of NMP from existing AMP in this size range. Although the trend shows lower CPNC levels at higher temperatures, the reason for the high values when aerosol was diluted at 300^{o}C in Figure 6B is not clear. It is suspected to be an artefact of uncontrolled cooling between dilution point and measurement since the aerosol was rich in volatiles especially with contributions from water based species. This corresponds to their distributions earlier in Figures 6.3(A-D). This observation is particularly interesting with regards to the phase transformation of the volatile fractions. The character of saturation ratio (S) when aerosol is mixed and cooled goes through initial increases with dilution ratio before reaching a maximum and declining.

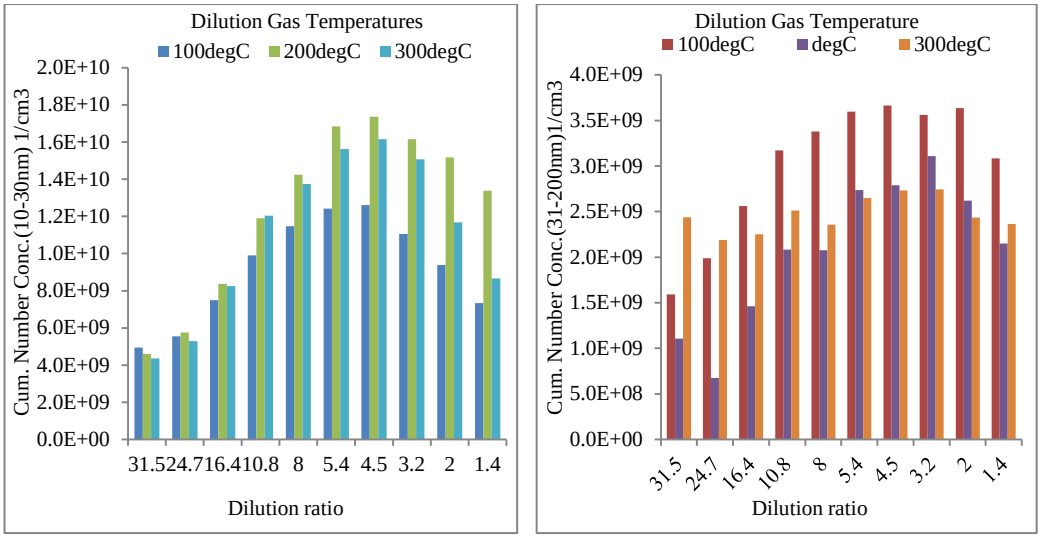

A B

Figure 6.5 Plots of CPNC for various dilution ratios and dilution gas temperatures for lower engine load operation**.** A: A CPNC in the range of 10-30 nm; B: CPNC in the range of 31-200 nm (scales on y-axis was zoomed to highlight these concentrations)

The explanation of this could be viewed through the expression of saturation ratios based on the ***Clausius – Clapeyron*** relations in equations 6.2 and 6.3. The equations reveal the dynamics of phase transformation that occurred with the volatile fractions during the dilution process, with critical implications for cooling and mixing of the volatiles. This describes the saturation characteristic of the volatile species in the sample. It is reasoned that the trend is due to competition between the reciprocal and the exponential functions which express, respectively, the effects of dilution on partial pressure of hydrocarbon and saturation vapour pressure of particular species of hydrocarbon in equation 6.2, (Eastwood P. , 2008). The implication is that at low dilution, condensation is suppressed because T_{mix} is high; similarly, when dilution is high, the hydrocarbon partial pressure is too low to support condensation. This implies that there exists an intermediate range of dilution during which condensation is most likely. The Figures highlight this intermediate range of dilution ratios, during which condensation is most likely at the various dilution temperatures, due to concentrations of volatile species as well as the implications for particle growth. Diluting aerosol at 200^{o}C and 300^{o}C gave lower values of CPNC for the larger particles at dilution ratios lower than 5.4. This supports the assertion that, when mixing is low, condensation of volatile fractions tends to be suppressed due to high temperatures. Further to observations from the integration of PNCs, the mass

concentrations obtained according to equation 6.1 are observed to be similar in the range of particle diameters considered. The effects of dilution ratio on the CPMC in line with the above narratives are shown in Figure 6.6(A and B) respectively. Figure A shows a rise in CPMCs to a maximum at the dilution ratios of 5.4 to 4.5 in the small size range and 3.2 in the larger sizes in Figure B. For all dilution ratios and at all mixing temperatures within the range of particle sizes considered, the values of CPMCs for size range of 31-200 nm are higher than the small sizes of 10-30 nm although the CPNC of the latter is greater as seen in Figure 6.5(A and B). This lends credence to the view that the larger particles are agglomerates with more mass. In Figure 6.6B, there is wide difference in magnitude of the mass concentrations when the aerosol was diluted at 100^{o}C, relative to dilutions at 200^{o}C and 300^{o}C. The explanation is similar to earlier assertion that condensation process usually occurs at temperatures where particles nucleate homogeneously for pure substances which are significantly cooler than those required for evaporation (Kasper, 2004).

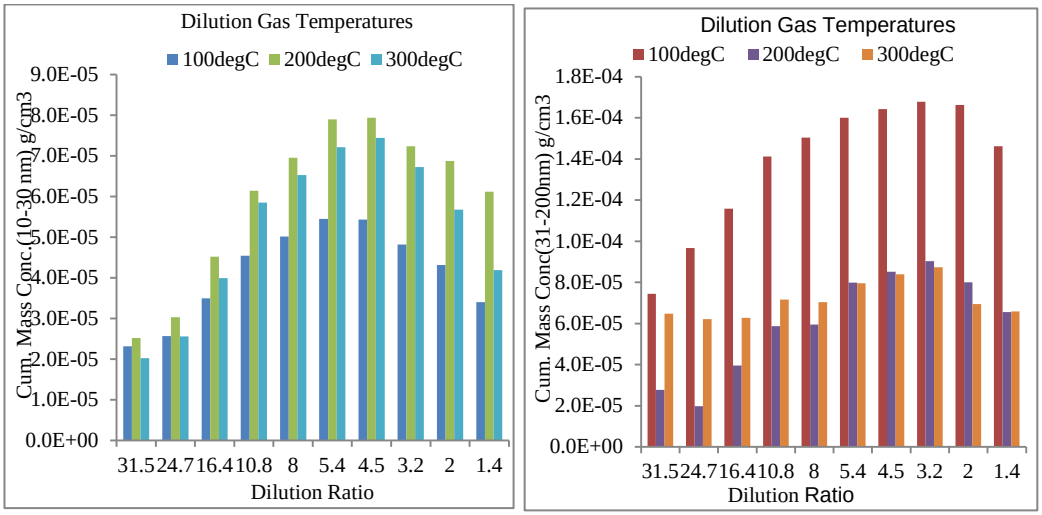

A B

Figure 6.6 CPMC for various dilution ratios and dilution gas temperatures at low engine load operation, A: for particles in the range of 10-30 nm, (scale on y-axis was increased to highlight these concentrations); B: for particles in the range 31-200nm.

The hydrocarbon species could have condensed even before 100^{o}C and contributed to growth of existing carbonaceous particles. However, at high temperatures, the magnitudes are generally lower. It will be noted that volatile components condense differently according to their thermo physical properties. This means that even when

nucleated, they grow at different rates due to saturation phenomenon. Therefore the prevailing temperature determines whether the nucleated particles remain in smaller sizes, grow or adsorb on existing large particles. This is consistent with high PNC observed when aerosol was diluted at 200^{o}C and 300^{o}C as in Figure 6.5A. It corroborates the high CPMC calculated in Figure 6.6B while they are lower in Figures 6.5B and 6.6A, respectively, at the same temperatures. Thus, it is deducible that mixing aerosol at low dilution gas temperature leads to a high cooling rate. The particle growth is high and translates to high CPMC as observed with larger sizes especially with high species concentration at low dilution ratios where PM volume is more.

6.2.4.2 Cumulative Number and Mass Concentration - Mixing and Temperature Effects at Higher Load

Increase in a diesel engine load implies more fuel injection which leads to increased local equivalence ratios in the spray flame. This is coupled with more diffusion burning and intensified pyrolysis at higher temperatures (Tree, D. R. and Svensson, K. I., 2007). Therefore, it is viewed that more carbonaceous nuclei are formed and particle aggregation enhanced. The effect of dilution on PNCs is relevant when accounting for nucleation mode particles which are temperature dependent (Khalek, I. A., Kittelson, D.B., and Bear, F., 2000; Kasper, 2004; Burtscher, 2005). The plot of CPNC is similarly presented in Figure 6.7 (A and B). Considering sizes in the range 10-30 nm in (Figure A), it is observed that mixing the sample at 100^{o}C gave a maximum at the dilution ratio of 8.0, while it occurred between 5.4 and 4.5 when diluting at 200^{o}C and 300^{o}C, (although the cause for high concentration when mixed at 300^{o}C for dilution ratios 31.5 to 16.4 is not clear). The cumulative number concentrations obtained at 100^{o}C are generally higher compared to the values obtained when diluted at gas temperatures of 200^{o}C and 300^{o}C**.** Considering the conversions from volatile fractions, the cooling effect of the dilution gas at 100^{o}C reduced the saturation vapour pressure which enhanced the gas-to-particle conversion as similarly observed at lower load. As the aerosol concentration increases at lower dilution ratios, it leads to an increase in the CPNC, up to a maximum, and then decreases with further decrease in dilution ratio. This rise of CPNC to a maximum with increase in dilution ratio is qualitatively related to equation 2 as discussed. Mixing the sampled aerosol with the dilution gas at 200^{o}C

and 300^{o}C resulted in a relatively lower cumulative number concentrations compared to 100^{o}C. The increase in temperature marginally suppressed condensation and thereby caused portion of volatile species to remain in gas phase. Figure 6.7B shows the CPNC measured for sizes in the range 31-200 nm. As with previous observations it is highest when diluted at 100^{o}C. The trend with respect to dilution ratio is the same for all the three dilution temperatures, showing a general decrease as the dilution ratio decreased. As expected at higher engine load, the aerosol samples are viewed to have more carbonaceous particles. The presence of these particles in the aerosol in high concentration due to low dilution ratios led to extensive particle growth.

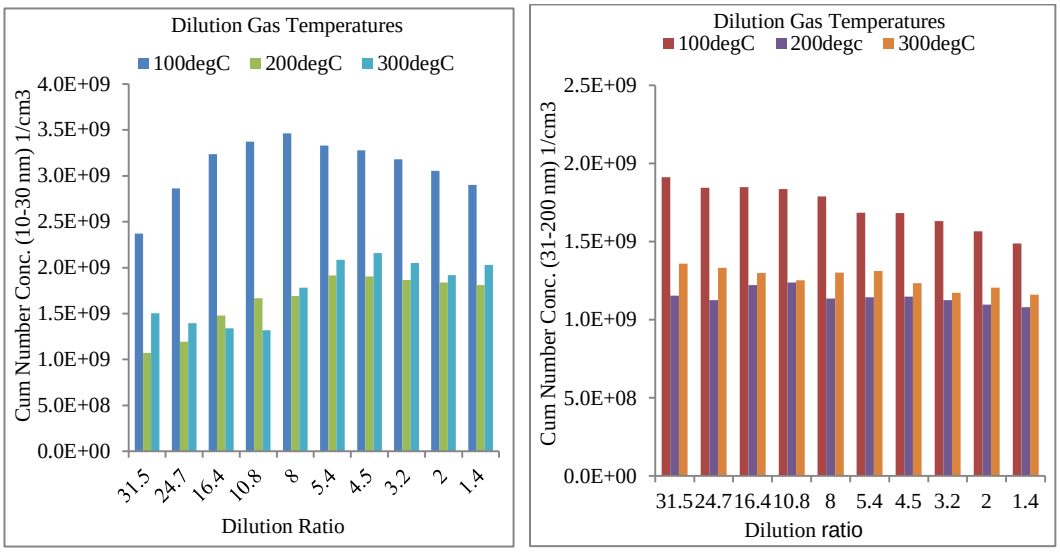

A B

Figure 6.7 Plots for various dilution ratios and dilution gas temperatures at higher engine load operation. A: CPNC for particles in the range of 10-30nm (with scale magnified to highlight the values), 8B CPNC for particles in the range of 31-200 nm

Therefore major portions of the particles agglomerated beyond the diameter range under consideration. This was observed in the size distribution data, which extended to the highest detection limit of the measurement device when plotted beyond the limit of 200nm presented in Figure 6.4. This fact is deducible from the observation that at all temperatures, these reductions tend towards the lowest dilution ratio where aerosol concentration is highest. The CPMCs for the small and large diameters are shown in Figures 6.8 (A and B) respectively. In Figure A it is highest at 100^{o}C

dilution followed by 300°C and 200°C; a trend similar to the number concentration in Figure 6.7A. The masses of nucleation mode particles are known to be very small compared to the accumulation mode particles (Kittelson D. B., 1998.; Heywood, 1988). As stated previously, under higher load operation, some of the larger particles are perceived to consist of a carbonaceous core on which the volatile particles adsorb. Therefore, it is obvious that the CPMC in sizes 31-200 nm are more. The scale in Figure 6.8A has been magnified in order to appreciate this difference in the two sizes. The cumulative mass concentration in Figure 6.8B shows that the estimated mass concentration decreased as the dilution ratio was reduced from 31.5 to 1.4. All the trends observed with mass estimation in this condition replicate those observed with cumulative number integration in Figure 6.7B and therefore the explanations are consistent.

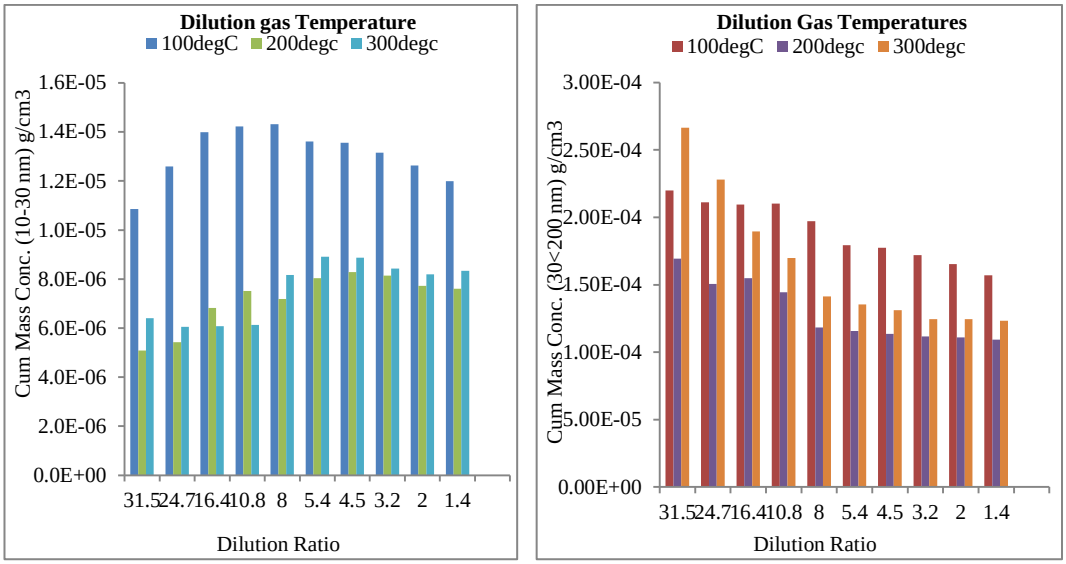

A B

Figure 6.8 CPMC for various dilution ratios and dilution gas temperatures at higher engine load operation. A: for particles in the range of 10-30 nm with scale magnified; B: CPMC for particles in the range 30 < 200 nm

Summary of Results

In this study, the effects of mixing and dilution gas temperature on the particles emitted from the exhaust of diesel engine have been explored using a mixing tube diluter of an electrostatic measurement device at two different engine load conditions. The trends observed about PNCs and their sizes distributions with respect to their dependence on dilution conditions are consistent with the findings published

in literatures cited. In this work, it is further shown that mixing and cooling of exhaust particles depend on the dynamics of phase transformation of the volatile fraction. These are summarised as follows:

Lower Engine Load Operation

Mixing affects particle size distributions in different ways. The rate at which the gas-to-particle conversions occur depends on the ways in which aerosol is diluted. At high dilution ratios, the rate of phase change is different at different temperatures but as the dilution ratio decreases there is less effect of temperature on particle size distribution. In this study, mixing at the lowest temperature of 100^{o}C gave highest PNCs, CPNCs and CPMCs compared to higher dilution gas temperatures at all dilution ratios.

The dynamics of phase change are rooted in the saturation characteristics of volatile components, which are functions of mixing and cooling. Saturation determines how the interplay of concentration and temperature of volatile species, as well as the temperature and quantity of dilution gas, influence nucleation and condensation. Hence, dilution, interpreted in terms of mixing and cooling, affects the partial pressure and saturation vapour pressure of volatile components, of which temperature is the controlling factor. This illustrates the real meaning of dilution ratio.

The particle number concentrations increased with increase in species concentrations (lower dilution ratio), at all dilution gas temperatures. However, this was particularly high when aerosol was diluted at 100^{o}C because it enhanced more condensation of volatile fractions due to the high temperature difference. It also contributed to the growth of existing particles.

The characteristic of saturation ratio (S) when aerosol was mixed and cooled with dilution gas, which go through a maximum has been demonstrated with the CPNC and CPMC. The nucleation mode particles that transformed from VOFs as subjected to different dilution ratios and temperatures, accounted for the observations.

Nucleation mode particles are more prevalent from aerosols generated at very low engine load operation which are viewed to contain more unburnt hydrocarbons. In

our study, aerosols generated at the lower load gave better insight to the influence of temperature and mixing based on phase transformation of volatile fractions. Clear ‘humps’ at high temperatures were observed at high dilution ratios of 31.5, 24.7 and 16.4. This indicates the ease of volatility and tendency to desorb on application of heat.

Higher Engine Load Operation

The peak values of PNCs are lower at higher engine load compared to lower load for all dilution ratios and dilution gas temperatures. However, the size distributions at higher load are larger than those at lower load. This is suggestive of core carbonaceous particle growth as the volatile particles adsorbed on it. This observation is also a measurable effect of cooling and mixing on the conversion of the volatile particles, their contribution to CPNC and CPMC

The growth of particles observed at higher load that extended to the measurement limit, is related to increase in concentrations of aerosol sample (decreasing dilution ratios). The PNCs are highest at the lowest dilution temperature. As a consequence, the CPNCs and CPMCs followed this trend.

6.3 Comparative Influences of Air and Nitrogen as Dilution Gases in Measurement of Diesel Engine Particle Number Concentrations

It is conventional to dilute diesel exhaust gas as a conditioning technique when assessing PM emission to suit the design limitations of the measurement devices. The techniques for conditioning PM samples prior to measurements are outlined in section 3.5.4. These include hot dilution, thermal desorption (denuder) and catalytic stripping. In the application of hot dilution technique, PNC are known to be sensitive to dilution conditions and are considered when evaluating results as laboratories employ different apparatus to dilute exhaust samples before measurements. Different dilution techniques are optimised and customised for several measurement systems by host of manufacturers. Majority use air as dilution gas; our measurement device uses filtered exhaust gas in a closed loop, while others employ nitrogen, where prevention of oxidation reaction is required. In this section, the investigation on the

effect of using air and nitrogen as dilution gases on the PNCs from diesel engine exhausts is reported. The approach explored the use of carbon dioxide (CO_2) concentration ratios in diluted and raw exhaust samples, evaluated by non-dispersive infrared (NDIR) analyser module of HORIBA MEXA 7170D to determine dilution conditions of the measured sample (Labecki et al 2012; Giechaskiel et al 2000). The mixing of exhaust gas with dilution gas was carried out using a bespoke porous tube diluter. The comparative effect of using nitrogen and air as dilution gases was then assessed. Comparison was also made with results obtained from using filtered exhaust as dilution gas in a closed loop system. The particle number concentration reduction factor (PCRF) and volatile removal efficiency (VRE) was used to further extend the evaluation of dilution effect with the use of the different dilution gases. The engine was operated at a stable low load condition to produce aerosol viewed to be laden with volatile fractions. Investigation was made on the relative number concentrations by using different DRs was utilised to compare the relative measured values of PNC when diesel exhaust emissions were diluted with pure nitrogen and air as dilution gases. This was later compared with results obtained with the dilution technique as narrated above and published in (Alozie et al 2014A; Peirce, D and Ganippa, L., 2014B) where filtered exhaust gas passed through an absolute filter in a closed loop was used.

6.3.1 Methodology

The dilution system is locally fabricated which comprises of porous tube diluter (PTD) joined to an evaporator tube (ET). An inlet probe shown in Figure 6.9 was used to extract raw sample from the exhaust line. This has 8 x 4 holes of 1.2mm diameter drilled radially on the small 10mm diameter pipe. Engine-out exhaust sample was drawn through it to flow into the porous tube via a high temperature resistant control valve which enabled optimum volume of aerosol to be drawn at a stable engine operation. Figure 6.10 shows the porous tube diluter (PTD), 180mm in length consisting of two concentrically aligned tubes.

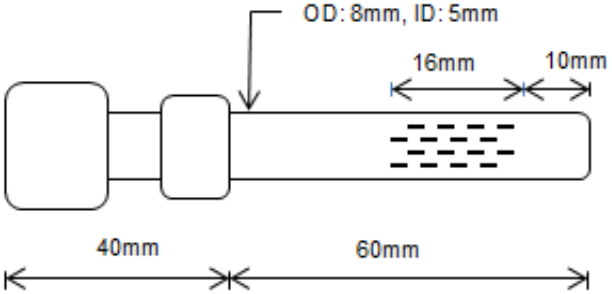

Figure 6.9 Dimensions of Sample Extraction Probe

The inner tube with finely drilled orifices is 10mm in internal diameter while the outer shell is approximately 25mm internal diameter. It is directly welded to a small V-connector and tightly coupled to an evaporator tube (ET) on a flange. Due to space limitation, the ET is elbow-shaped to allow for connection to the measurement device, with larger internal diameter of 40mm and nominal length of 200 mm, located at the left end of the PTD. The V-connector used to fix the PDR with the ET enables direct flow of aerosol without any loss of particles or change of condition as normally associated with a transfer line. The dilution gas was introduced through the perforated tube to mix with the raw aerosol. The PTD design was chosen because it effectively handles aerosols at low DRs and from low engine load operations. It was shown in (Lyyränen et al 2004) that compared to other methods of dilution; the best number size distribution without significant nucleation effects was obtained from a similar design. In addition to being a VPR, the ET damps out pulsations in the diluted sample stream at the end of the PTD and enhances mixing. A relief valve was connected at its base to ensure that inside pressure is only slightly above atmospheric. A thermocouple and a pressure transducer were connected to monitor temperature and pressure in the ET.

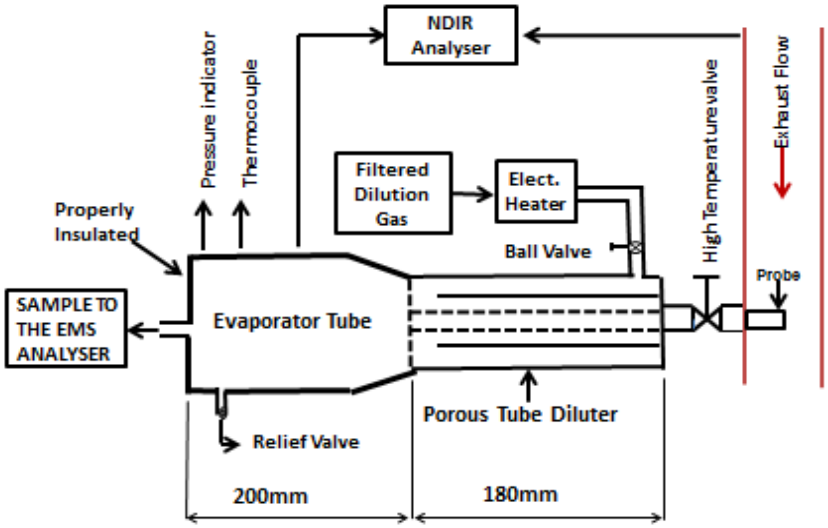

Figure 6.10 Porous Tube-Diluter (PTD) fixed on Evaporator Tube (ET)

A connection was made from the tube to the Horiba exhaust gas analyser whereby exhaust gas recirculation (EGR) port of the Horiba was adapted for sampling of the CO_2 concentration of the diluted sample being measured from the ET. This enabled simultaneous measurements of CO_2 concentrations of the raw exhaust and diluted sample from which the DRs were calculated as:

$$DR = [CO_{2\,(Raw)} - CO_{2\,(Ambient)}] / [CO_{2\,(Diluted)} - CO_{2\,(Ambient)}] \qquad (6.4)$$

This technique is consistent with the many ways DR could be evaluated (Eastwood P. , 2008; Giechaskiel et al 2009; Desantes et al 2011; Giechaskiel et al 2010). Axially from the centre of the ET is the connection of the EMS probe which draws the diluted aerosol into the measurement device as detailed in section 6.1 however, during measurement, the FCU was only used to set the entire critical orifice closed such that, after particles were measured by the FCE, the aerosol sample was discharged to the exhaust as in Figures 6.11 instead of the former closed-loop. In this way the EMS dilution system was not utilised but the spectrometer was only adapted for classifying, analysing and counting of particles as diluted by the porous tube. In order to avoid moisture carry-over into the DMA, a diffusion dryer was installed on the line just before the DMA. The location is the point of lowest

temperature of the diluted sample prior to measurement and therefore, most appropriate for moisture trap.

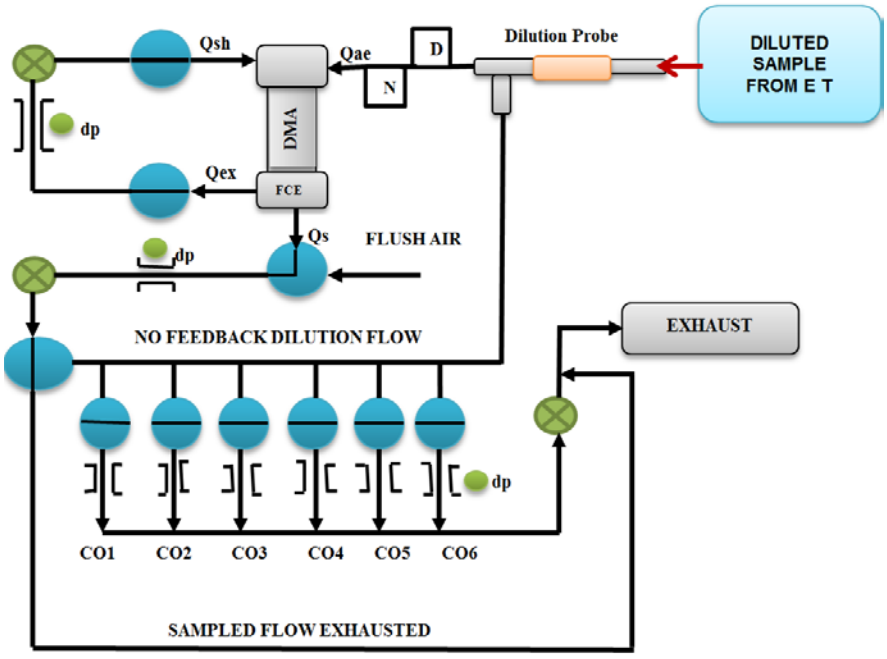

Figure 6.11 EMS layouts as used in conjunction with sample from ET and PTD**.** D: Diffusion Dryer, N: Neutraliser, DMA: Differential Mobility analyser, FCE: Faraday Cup Electrometer, Qsh: Sheath Air flow, Qex: Excess Air, Qae: Aerosol intake, Qs: Sample Flow, dp: Pressure indicator for sample flow orifice, (Co1 – Co6): Closed critical orifices.

6.3.2 Measurements

As criteria to establish base line DRs for comparing the effect of using either pure nitrogen or pure air as dilution gas, known DRs configured in EMS dilution system were calculated and set as targets, and were mimicked using the technique described in equation 6.4. Filtered (Zero Grade) pure nitrogen and air were metered using a flow meter to admit each as heated dilution gas into the porous tube at 125kPa during respective mixing operations. Adjustments were made while the Horiba and the sample analyser were on measurement mode. This was to ensure constant flow from the ET and to avoid aerosol stagnation. These preliminary measurements were not recorded until the set target DRs were stable in the proportions evaluated. Apart from DR, other methods have been described for evaluating a sample pre-conditioning system and the parameters used in characterizing it (Giechaskiel et al

2009). Two of these are particle number concentration reduction factor (PCRF) and volatile removal efficiency (VRE), defined as:

$PCRF_{di} = N_{1,di} / N_{2,di}$ ……. (6.5)

$VRE_{di} = 1- (N_{2,di} / N_{1,di})DR$ …… (6.6)

Where $N_{1,di}$, $N_{2,di}$, are measured PNCs of diameter $d_{i,}$ at inlet and outlet of the sample pre-conditioning system. These definitions were derived on the assumption that the dilution gas has negligible contribution to the particle count. This assumption was adopted given the known quality of dilution gases used. These two parameters were used to evaluate the effect of dilution gas in the porous tube diluter. Correspondingly, during the measurements, $N_{1,di,}$ was adopted as the measured PNC without dilution and $N_{2,di,}$ as the PNC after dilution. The EMS is particularly suited to measure aerosols of relatively very small DRs (Reischl G. P., 2006). Samples utilised for the purpose of this measurement were generated at low load and are perceived to be laden with volatile fractions as already described. Hence their sizes are taken to be more in the sub 50nm range and could be compatible with the device even without dilution.

6.3.3 Results and Discussions

Preliminary data sets were subjected to repeatability tests on scan-to-scan and day-to-day bases. In every measurement, three scans were taken and an average was used for data analysis. Using dilution at 300^{o}C where thermal treatment was more evident, the average coefficient of variation recorded for various dilution conditions calculated according to equation 1 were seen to below 6%. The scans with nitrogen gas were more repeatable on a scan-to-scan basis, while those of air were slightly better on a day to day basis. Comparative plots of the PNC at 300^{o}C are shown in Figures 6.12 (A and B). The plot in linear scale (Figure 6.12A) gives a better appreciation of the difference in number concentrations while the usual log scale presents size distributions better. When the two pairs of results are compared, particle number concentrations are generally observed to be marginally greater in nitrogen than in air, but their peak number concentrations occur at the same

diameters. As a basis for confirming the characteristics of the plots with results formerly obtained when aerosol was diluted using the dilution system of the EMS (which was based on volume proportions that used filtered exhaust as dilution gas); the cumulative particle number concentrations (CPNC) obtained with the different dilution gases were plotted. The characteristics of the plots that showed an initial rise and then declining with increase in DRs were observed as in section 6.2.4 and reported (Alozie et al 2014A).

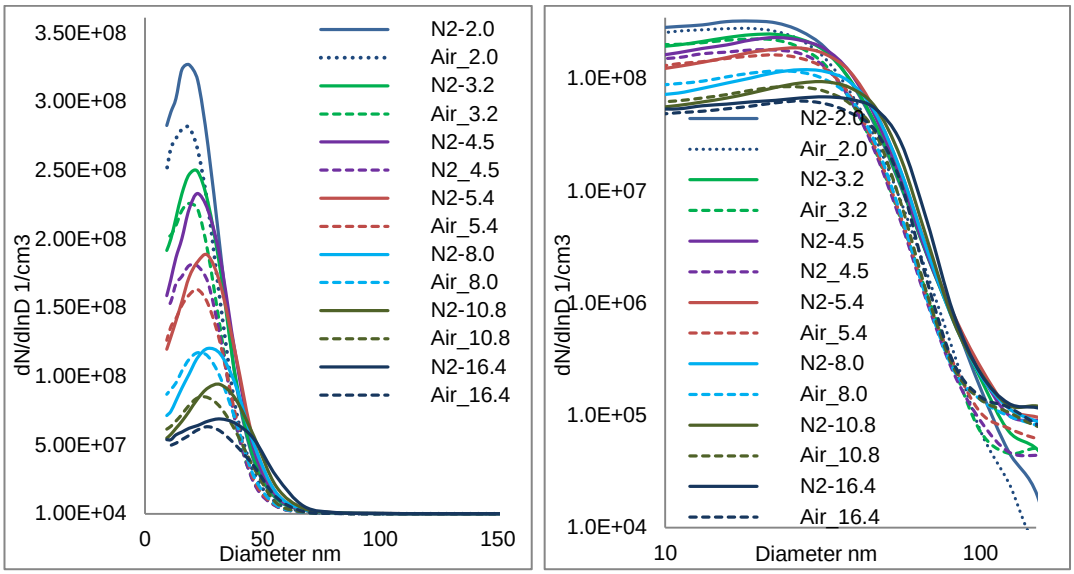

A B

Figure 6.12 Particle number concentrations at various dilution ratios when samples were diluted with nitrogen gas and air respectively at 300^{o}C, A: is in a linear scale; B is in a log scale.

The comparative CPNCs for typical size distributions as measured are shown in Figure 6.13A. There is a little rightward trend in the sizes at which nucleation peaks occur as the dilution ratio is increased which is consistent with trends observed when diluted filtered exhaust of the EMS dilution system reported in section 6.2.4. Not only that similarity exists in characteristic of CPNC with these dilution gases as observed, the plot of the differences at each DR also gave a similar trend like the CPNC plots, Figure 6.13B. However, there are spikes in differences at (very) high and (very) low DRs, therefore only the range of DRs 16.4 to 2.0 was used for further analysis since this appeared to be likely more consistent. The difference PNCs within the range of these DRs at specific peak concentrations are given in in Figure 6.14A.

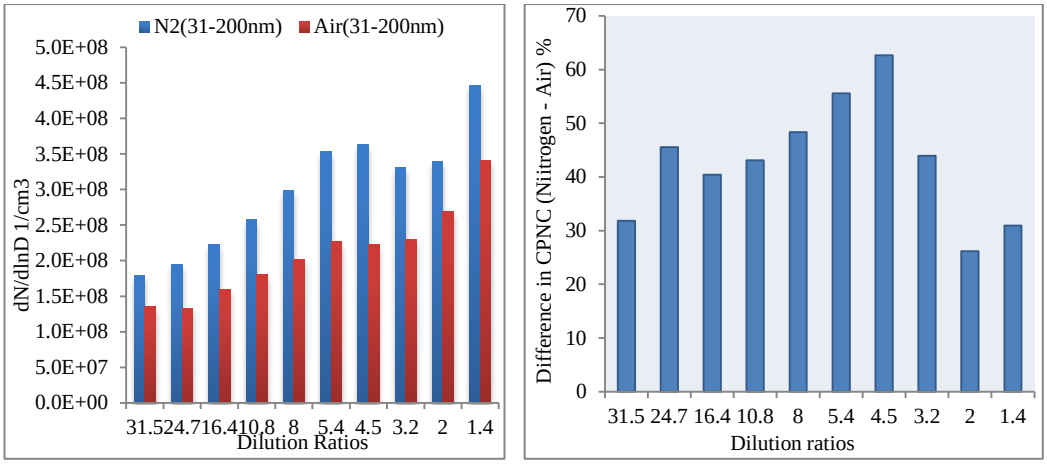

A B

Figure 6.13A Typical plot comparing CPNCs obtained when nitrogen and air were used as dilution gases respectively; Figure 6.13B Percentage Differences in CPNC between using Nitrogen and Air as dilution gases

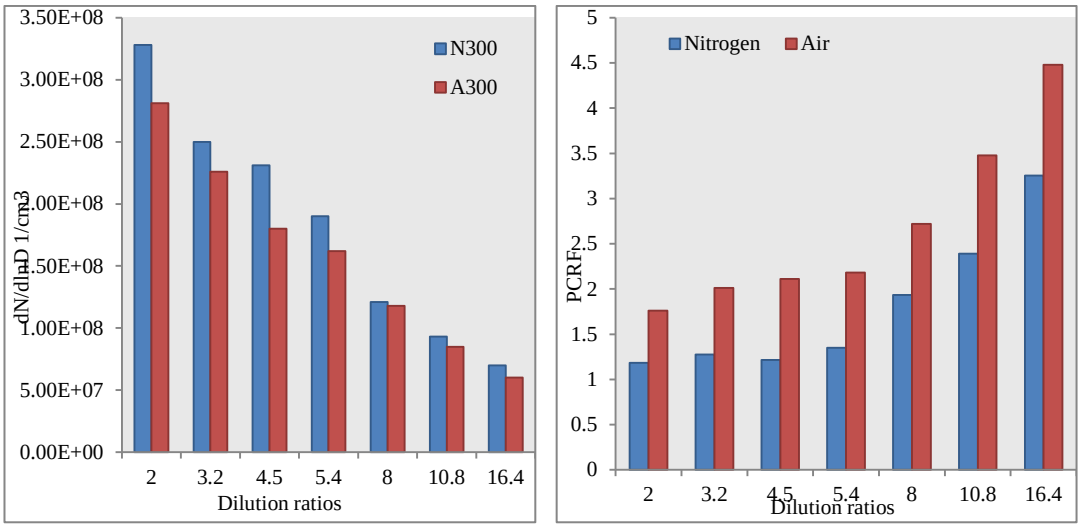

A B

Figure 6.14A Comparison of the magnitudes of particle number concentrations at nucleation peaks of various dilution ratios on low load at 300^{o}C; Figure 6.14B Comparison of the Particle Number Concentration Reduction Factor PCRF with the use of Nitrogen and Air as dilution gases respectively at 300^{o}C, particle diameter (di = 32nm)

Apart from dilution ratio, the particle number concentration reduction factor (PCRF) can be used in the characterization of the dilution system according to (Giechaskiel et al 2009) as presented in equation 6.5. Legislation requires that minimum particle diameter of 30nm be used for PCRF calculation, therefore this was considered at particle diameter 32nm; the comparative PCRFs when nitrogen gas and air were used as dilution gases at 300^{o}C respectively are presented in Figure 6.14B. For the given

DRs, particle reduction factors are obviously greater in air than in nitrogen. The decreasing relationship of PNC with DR in Figure 614A conforms to the increase in PCRF as DR was increased; which in essence shows good agreement. The difference in percantage reduction between the use of the two gases could as well strengthen the view held with PNC and the overall CPNC. In effect, the difference in number concentrations is a mirror image of the extent to which volaticle reduction occurred in the two gas media. Figure 6.15A shows a near repeat of Figure 6.13B for the DRs considered. In general, the plot of percentage difference in PCRF follow the initial rising and then declining with DRs except at 8.0. Similarly, another parameter discussed in (Giechaskiel et al 2009) is the volatile removal (VRE) expressed as in equation 6.6. It was similarly considered at the particle diameter of 32nm. Comparative analysis when the two gases are used is shown in Figure 6.15B. It shows that although both gases could eventually achieve the same effect of volatile reduction at high DRs, efficiency of volatile reduction is higher with air at low DRs. At this dilution temperature, the thermal properties of air and nitrogen are marginally different. The mass and density of air is 3.4% higher than nitrogen; thermal diffusivity is 1.7% higher and thermal conductivity higher by 0.6%. On the other hand, nitrogen has about 2.5% higher specific heat capacity, making it a slightly more significant thermal sink. This is viewed to invariably affect the saturation vapour pressures of the volatile species in the different dilution media.

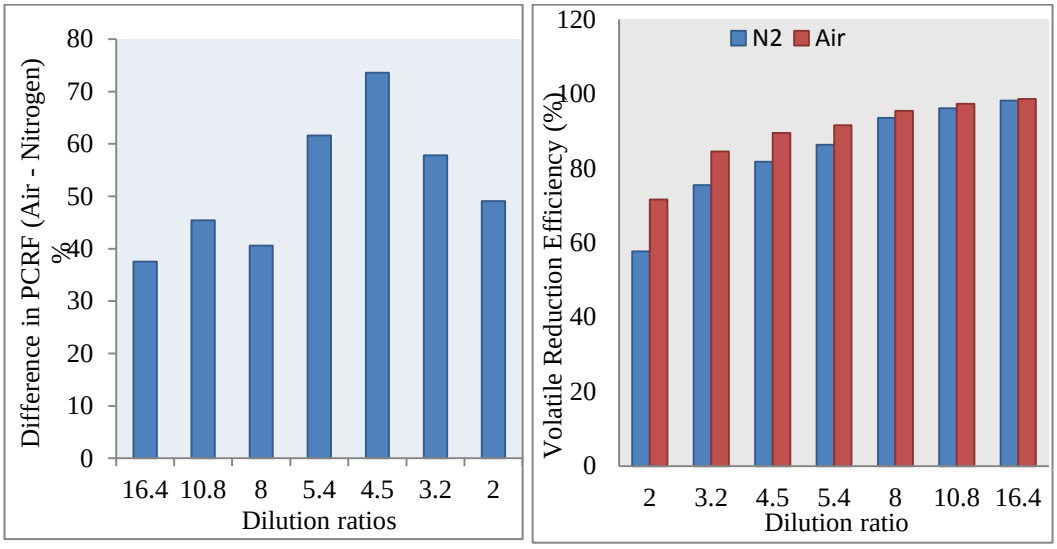

Figure 6.15, A: Percentage difference in PCRF; B: Volatile Removal Efficiency compared with the use of Nitrogen and Air as dilution gas at particle size of 32 nm.

As an extension, the VRE evaluated at nucleation mode peaks for the three dilution media are presented in Figure 6.16. It is seen that VRE is least in filtered exhaust followed by nitrogen and highest with air with decrease in DR. This result is obvious when reasoned that with the use of filtered exhaust, all volatile species as metered could be carried over to the next dilution process if the vapour pressure is quite low and then re-nucleate if the condition becomes favourable. Herein is the possible reason for the artefact of measurement as encountered when the EMS only dilution system was employed in addition to limited temperature to vaporise volatile species in the sample.

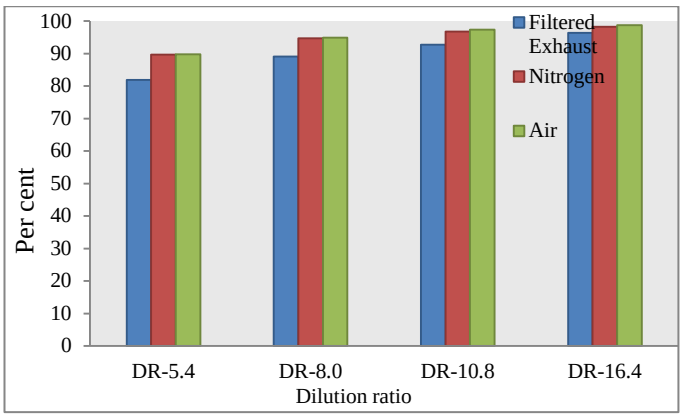

Figure 6.16 Extension of VRE evaluations on three dilution gas media at nucleation mode peaks

At the nano meter range, the particle size is viewed to be affected by its interaction with the surrounding medium (Kittelson, D .B., Arnold, M., Watts, W. F, 1999). Considering the molecular interactions of the volatile species, since the mean free path is still high, the physical property of the surrounding medium is relevant to the nucleation/condensation as well as the adsorption /desorption processes. Also at the dilution temperature of 300^{o}C, the dynamic viscosity of air is about 3.7% higher than that on nitrogen. These attributes in thermal and flow properties are viewed to be related to the differences in vapour pressure that the volatile fractions could exercise in the different dilution media. They make the initial formation of the droplet from volatile species more complicated and therefore accounts for the variations in particle counts observed. Comparing information summarised in Table 6.3, one could deduce that the expression of DR is indeed not adequate, as it does not give detailed information on the dilution effect as could be inferred from PCRF and VRE with

regards to particle reduction and removal of volatiles due to mixing and temperature effects.

Table 6.3 Summary of observations with dilution gases

DILUTION RATIO	NITROGEN		AIR	
	PCRF At 32 nm	VRE at 32 nm	PCRF at 32 nm	VRE at 32 nm
2.0	1.81	0.57	1.76	0.72
3.2	1.27	0.75	2.01	0.85
4.5	1.22	0.82	2.11	0.89
5.4	1.35	0.86	2.18	0.92
8.0	1.94	0.94	2.72	0.95
10.8	2.39	0.96	3.48	0.97
16.4	3.26	0.98	4.48	0.99

This is particularly important when considering various uncertainties that could arise in using pre-conditioning apparatus with non-standardized calibrations as in this small scale direct laboratory measurement (Giechaskiel et al 2007; Giechaskiel et al 2012A). The observations from this study will have implications for the use of nitrogen in systems that involve the use of CS. The use of nitrogen as dilution gas will not work since there will be no oxygen required for oxidation. Similarly, since the use of TD is size dependent, information from this study can be utilised for appropriate scaling of units involving thermo-desorption.

Summary

(1) The use of any suitable dilution gas will give similar trends in particle number concentrations. However in comparative terms, this study shows the need to consider the type of carrier gas used in dilution along with other parameters when interpreting results.

(2) The use of PCRF gives better information on dilution condition compared to dilution ratio. It clearly distinguishes the effect of mixing and heating or

cooling of aerosol laden with volatile/semi-volatile particles. For most systems where reduction of particle number concentrations and removal of volatile particles are the objective, then PCRF and VRE are essential and air is a superior dilution gas compared to nitrogen as seen through the results obtained.

(3) The effect of the difference in the two gases is more important when low dilution ratios are involved. At low dilution ratios, air has superior volatile removal efficiency, but as both gases approach high dilution ratios similar efficiencies are achieved. This has design implications in terms of the residence time at low dilution ratios when nitrogen is used.

(4) The PCRF and VRE values when air is used are suggestive of further oxidation reaction. Therefore nitrogen will be better carrier gas where there is need to freeze further oxidation of an exhaust sample, but adequate mixing is necessary.

6.4 Mimicked two-stage hot dilution technique to pursue PMP prescriptions

Having established the superiority of air as dilution gas, attempts have been made to adopt it to pursue the two stage dilution technique to mimic PMP dilution prescription.

6.4.1 Methodology

In the process, the external dilution as described with Figure 6.10 was used for primary dilution and afterwards the sample was drawn into dilution system of the EMS and diluted again using a modified dilution feedback as a secondary dilution. Metered air was fed to the dilution feedback flow as shown in Figure 6.17(A) to dilute the aerosol diluted previously (as achieved from the porous tube diluter taken as primary). As implied earlier, the primary dilution made use of porous tube diluter (PTD) design which is effective in handling aerosols at low DRs and from low engine load operations and has shown to exhibit good number size distributions without significant nucleation effects in the dilution process (Lyyränen et al 2004). By using the dilution probe of the EMS (the cross-section of which is re-presented in

Figure 6.16B), which has a mixing tube diluter similar to the PTD; the aerosol is given a second stage dilution. The procedures for measuring non-volatile particle number emissions as drafted by the Particle Measurement Programme (PMP) (Andersson et al 2007) emphasised the use of two stage dilutions as mimicked. This is in order to assess good repeatability and reproducibility; whereby the two stage technique was described as volatile particles remover (VPR) consisting of a primary hot diluter (PND1), an evaporation tube (ET) and a secondary cold diluter (PND2) in series (Giechaskiel, B., Dilara, P., and Anderson, J., 2008B; Giechaskiel et al 2007). Initial aerosol dilution is prescribed at a temperature more than 150^{o}C and at dilution ratio (DR) of at least 10:1. Further heating in the ET is at a temperature of 300-400^{o}C to vaporise condensed volatile fractions before diluting again at the PND2. By implication of the theory of dilution as already presented, the two stage dilution reduces the partial pressures of the volatile species to a level that cannot support their condensation and therefore suppresses nucleation of new particles as aerosol cools. The thermodynamic path can be traced through the phase diagram as described in 3.5.4. In recognising the diversity of measurement techniques and huge cost of a full flow dilution tunnel with constant volume sampling (CVS) or partial flow dilution system (PFDS), in which the procedures have been based, a simplified guide to avoid measurement errors involving direct measurements from raw exhaust as in small research and development laboratories like this, is presented (Giechaskiel et al 2012).

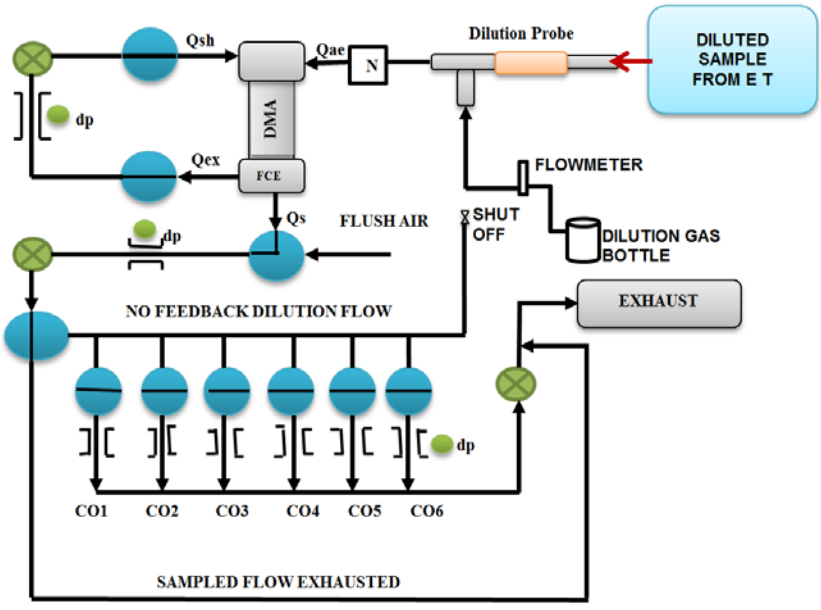

A

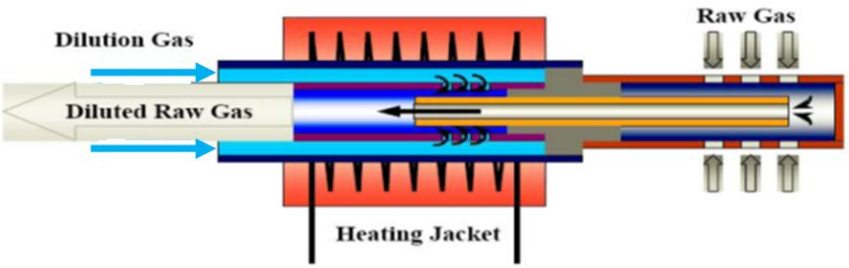

B

Figure 6.17 Second stage dilution of diluted gas from set-up in Figure 6.10. A: shows scheme for metering dilution gas into the dilution probe via the feedback dilution line; B: is re-presentation of the dilution probe section

In this scheme, aerosol sample was drawn directly from the exhaust as emitted immediately after the turbocharger at a temperature of 300-305^{o}C for low load and 480-496^{o}C at high load. Therefore there was no need for primary warm-up heating rather primary dilution air was heated to about 170-180^{o}C and the temperature of the ET was kept about 380-390. Then the EMS dilution probe temperature was maintained at 150^{o}C. This set up is technically the same with the PMP prescription only that both primary and secondary dilution were manually manipulated, which was considered as possible source of error. However when coefficient of variation of scan-to-scan measurement average was taken, it was seen to be below 10%.

6.4.2 Results

Results obtained for low load engine operation is presented in Table 6.4 and Figure 6.17 on a log scale in order to give better view of the particle diameters. As highlighted in the Table the dilution parameters used in assessing the pre-conditioning process were pursued using known dilution ratio of 8.0 of the EMS system in the primary dilution as given. The target DRs in second stage were also pursued to achieve known DRs of the EMS for comparison purposes; but the total values where stable readings were achieved were not entirely coincident as seen in the total DRs obtained as the product of dilution ratios from the two stages.

Table 6.4 Dilution Parameters on low load engine operation.

Target DR	2-stage DR	Total DR	PCRF@ 30nm	VRE@ 30nm
0	0	0	0	0
8.0	8.0(0)	8.0	43.5	81.39
10.8	8.0(1.3)	10.4	100	89.6
16.4	8.0(2.03)	16.24	508	96.8
24.7	8.0(3.65)	29.2	1000	97.08

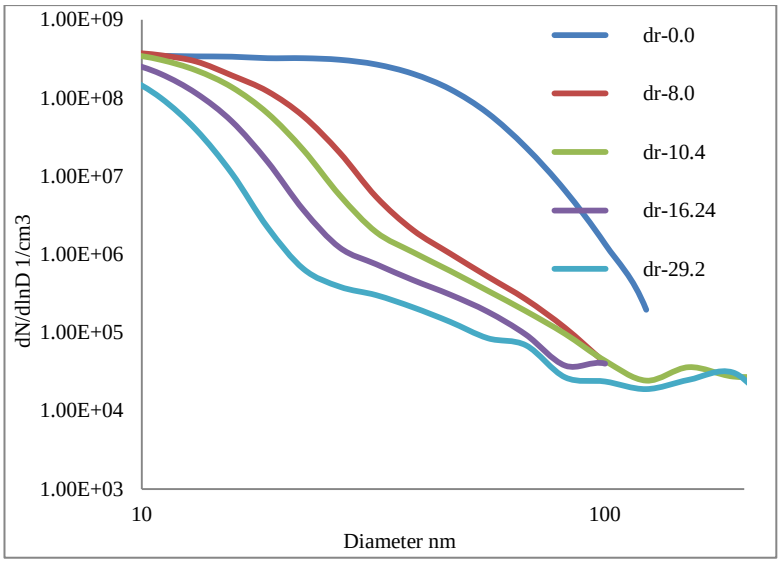

Figure 6.18 Particle number size distributions for two stage dilutions taken at various proportions of DR-8 at low load.

In order to appreciate the impact of the two stage dilution, comparative values of the dilution ratios from the EMS system that used filtered exhaust presented in section 6.2.1 and the mimicked two-stage dilution using air are plotted as in Figure 6.18 (A and B).

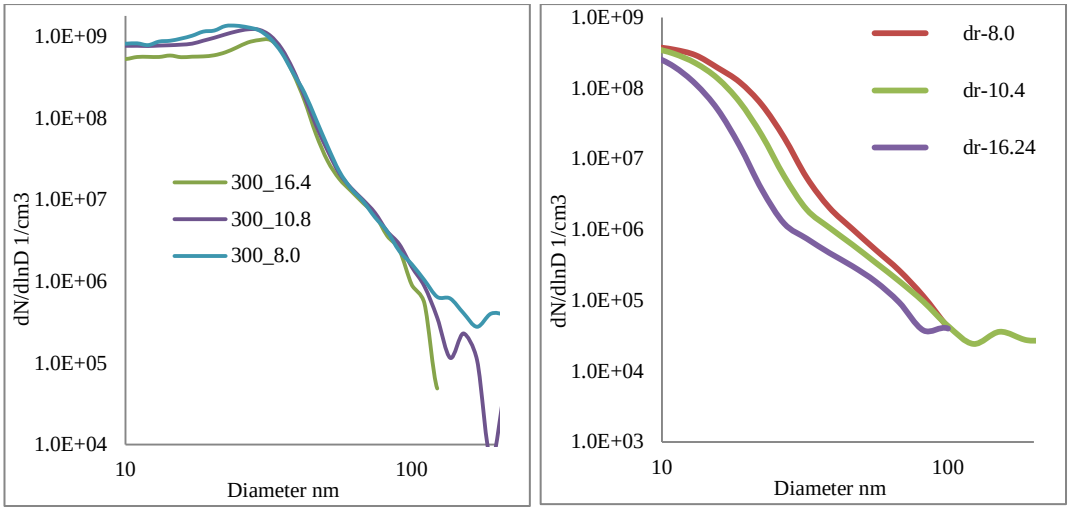

A B

Figure 6.19 Comparison of PNC of PM generated at low load condition sampled under two dilution systems. A: Closed loop dilution system using filtered exhaust at 300^{o}C; B: Two-stage dilution with air to mimic PMP prescription, 1st stage dilution gas temperature is 170-180^{o}C, ET temperature kept at 390^{o}C and 2nd stage dilution at 150^{o}C.

Obviously the dilution temperatures are not the same due to limitation of the heater used in the former and also there seems to be artefact of measurement with the apparatus with regards to the nucleation mode particles which did not properly strip even at higher temperature with the two-stage dilution. However, some deductions are visibly present from the two plots without rigorous analysis. One, the PNC concentrations are higher with the use of filtered exhaust compare to the use of air. Similar to the assertion made when compared with the use of nitrogen, the use of air as dilution gas gives better volatile removal efficiency and by implication, more particle number reduction factor. This is evident by the PNCs of the size distributions at which the particles associated with the accumulation mode represented by the 'humps' appear. At the highest dilution ratios of 16.4 compared in Figure 6.18, the hump started after 50nm when filtered exhaust was used at a PNC of 2x10^{7}/cm^{3}. Comparatively it started at 30nm and after a concentration of about 1x10^{6}nm/cm^{3}. Similarly the PCRF and VRE were calculated in Table 6.4 and plotted for in Figure 6.19 (A and B). Evidently, they followed the trends already seen in the first part of dilution scheme in one stage however; two-stage dilutions are seen to have a better particle reduction effect than single stage dilution. This demonstrates that the expression 'dilution ratio' is indeed incomplete as it does not give enough information on the dilution effect as could be inferred from PCRF and VRE. This is

particularly important when considering various uncertainties that could arise in using pre-conditioning apparatus with non-standardized calibrations as in this small scale direct laboratory measurement.

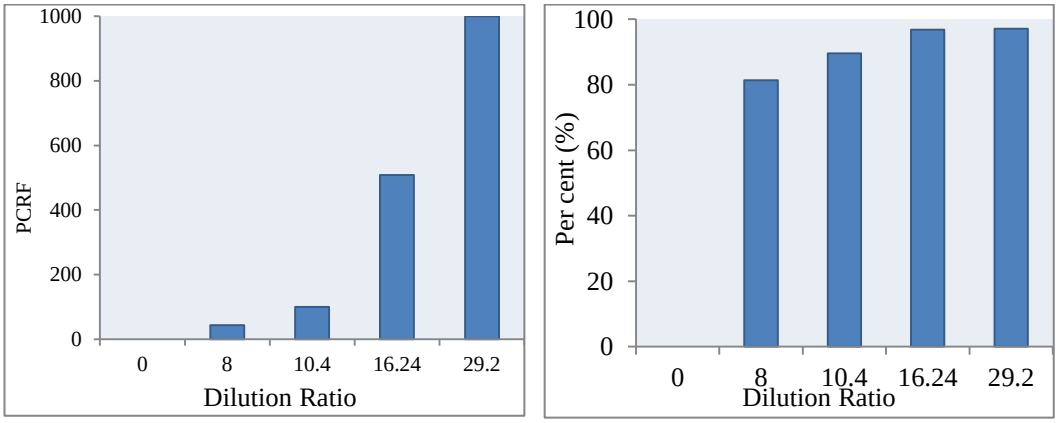

Figure 6.20 A: PCRF at 30nm, 2-stage dilution for low load; B: VRE at 30nm, 2-stage dilution for low load

Similarly, the particle number size distributions obtained at high load engine operations are presented in Figure 6.20 and the evolving PCRFs are calculated at 30nm as shown in Table 6.5. Compared to low load, the PCRF values are very low at similar dilution ratios showing that the aerosol had far lower volatile fractions whose condensation could be suppressed by heating as with aerosol generated at low load engine operation. In fact when plots are viewed beyond 100nm, it is deducible that particle reduction due to increased dilution simply encouraged particle growth as nucleation mode adsorb on core solid particles.

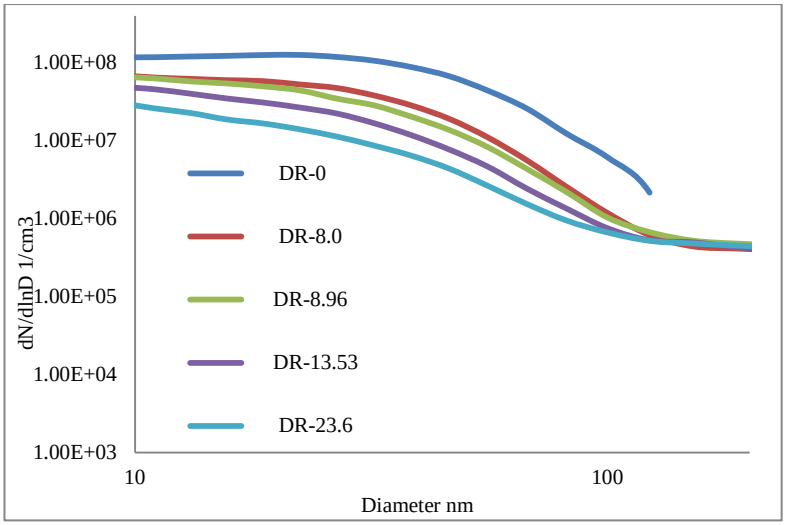

Figure 6.21 Particle number size distributions for two stage dilutions taken at various proportions of DR-8.0 at high load.

Table 6.5 Dilution Parameters on high load engine operation

Target DR	2-stageDR	Total DR	PCRF@30nm
0	0	0	0
8.0	8.0(0)	8.0	2.5
10.8	8.0(1.12)	9.0	3.3
16.4	8.0(1.69)	13.5	5.0
24.7	8.0(2.95)	23.6	10.0

Discussions and Summary

As already implied, the PCRF parameter gives better information about the dilution condition compared to the dilution ratio. Operationally, the constant-pressure volume flowrates of dilution gas that gave the various proportions of CO_2 cannot be seen as a source of perfect relationship with calculated dilution levels. Looking at the values obtained for low and high loads, CO_2 concentrations at high load are quite more than that of low load as should be expected. Therefore the dilution condition expressed in either volume flow rates of the dilution gas or the ratio of emission gas concentrations as measured could be limiting. For low load, the high PCRF values obtained for the various total dilution ratios reveal possible error in the pressure

calibration inside the ET. It is viewed that the flows through the porous tube orifices could have been choked downstream, while the dilution gas mass flowrate was on the increase. Thus given the volume of the ET, dilution proportion could have been more than values measured, since some volatiles could as well oxidise at the high temperature in presence of air. Here lies the superiority of PCRF parameter in revealing the true dilution condition. This assertion is complemented by the VRE as shown Figures 6.19 (A and B). The obvious implication is that aerosol generated on high load has low values of PCRF upon similar dilution values. These values were achieved even with higher dilution gas flowrates and temperatures. Therefore it is conclusive that there were low volatile fractions. While the particle concentration reduction in low load spanned through three orders of magnitude at 30nm, it was only within one order of magnitude at high load. It is therefore established that given better understanding of dilution condition through parameter like PCRF and VRE, errors due to artefacts and uncertainties could be highlighted in measurements.

6.5 Use of two-stage dilution technique to measure PM from different biodiesels

Biodiesel is produced by transesterification of plant oils and animal fats and have been in active use as alternative to petrodiesel or partly used in blending petrodiesel. It possesses fuel oxygen which impacts the characteristic tendency to reduce engine soot emission compared to petrodiesel (Song et al 2006; Williams, A., Black, S., McCormick, R. L., 2010; Andersson, Jon, 2011; Bhardwaj et al 2013A; Boehman, A. L., Song, J., and Alam, M., 2005). The objective here is complementary to another study at a time when the two-stage dilution rig was on the engine while biodiesel fuels were used (Peirce D. , 2015). Since the two-stage dilution set-up was a novel fabrication, it became expedient to test its performance on PM generated with other fuels. Reviews about biodiesel fuels are presented in chapter 7 and more details about the specific biodiesel fuels used here are also presented in the study published in (Peirce D. , 2015).

6.5.1 Methodology

The set up used remains same as presented in section 6.5 and the engine was ran at 80Nm and 2000 rpm. Warm up time of 60 minutes was allowed and another 90

minutes run was allowed at the chosen nominal condition on diesel fuel before baseline measurement was taken. Then the test fuel was switched on and allowed for another 90 minutes in order to stabilise all operating parameters before baseline measurements were taken for the fuel. Afterwards, exhaust emission was diluted as presented in section 6.5 for targeted dilution ratios that were mimicked.

6.5.2 Results

After measuring the PM for a given fuel baseline, the dilution ratio of 8.0 was set in the primary dilution and subsequent second stage dilutions were manually pursed while scanning to avoid stagnation in the ET until stable reading was achieved in the CO_2 concentration proportion. After stable dilution ratios were achieved at given flow rate, measure values were subsequently recorded.

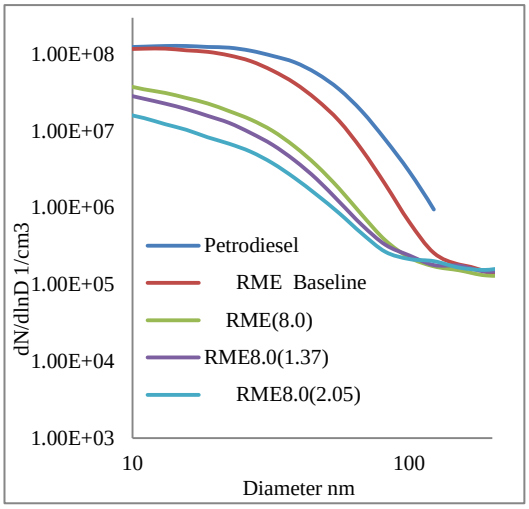

A

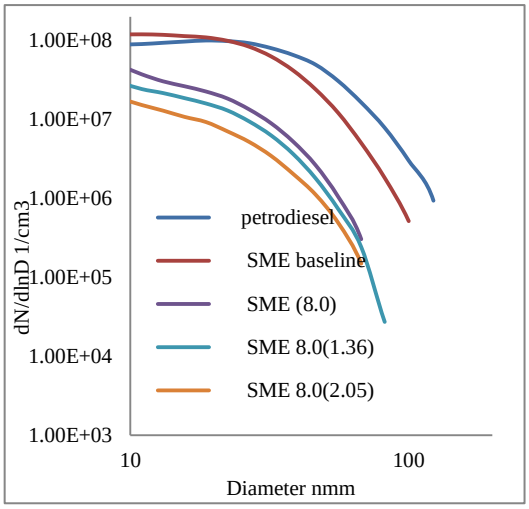

B

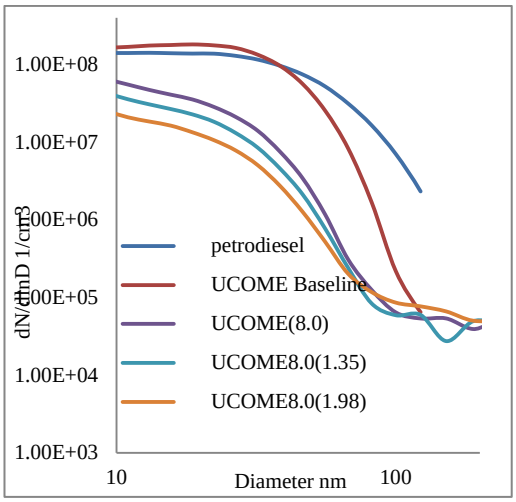

C

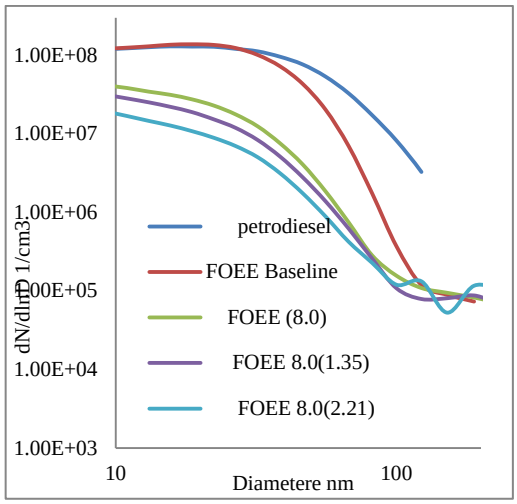

D

Figure 6.22 PNCs exhibited by various biodiesel fuels with consequent first stage DR of 8.0 and set of second stage DRs in brackets. [A: RME; B: SME; C: UCOME; and D: FOEE]

Although exact secondary dilution ratios could not be established for the entire tests, measured values give convenient outlook for assessment to be made (they are terms in the bracket in the Figure 6.22 legends). It is observed that petrodiesel baseline concentrations are reasonably constant. The baseline concentrations of the biodiesels are marginally higher than that of the petrodiesel at sub 30nm diameter range (except RME); but are generally lower than the petrodiesel at diameters beyond 30nm. This is quite expected as biodiesels are known to reduce soot while producing more water-bound volatiles particles. The nucleated volatiles give rise to higher concentrations observed within the nucleation mode size range. To check for reliability of the results in terms of scan-to-scan and day-to-day variability, average scans for three different days were evaluated and it was found that average coefficient of variation for particle sizes 10-100nm was about ±6%. Typical average of measurements made on three different days is shown in Figure 6.23A. Similarly, the average of three readings of filter smoke number taken per fuel at its baseline condition and their corresponding temperature at the point of extracting exhaust samples are presented in Figures 6.23 B and C. The low FSN with blends of biodiesel compared to petrodiesel shows that soot emission is quite reduced; and corroborate the measurements of PNCs respectively.

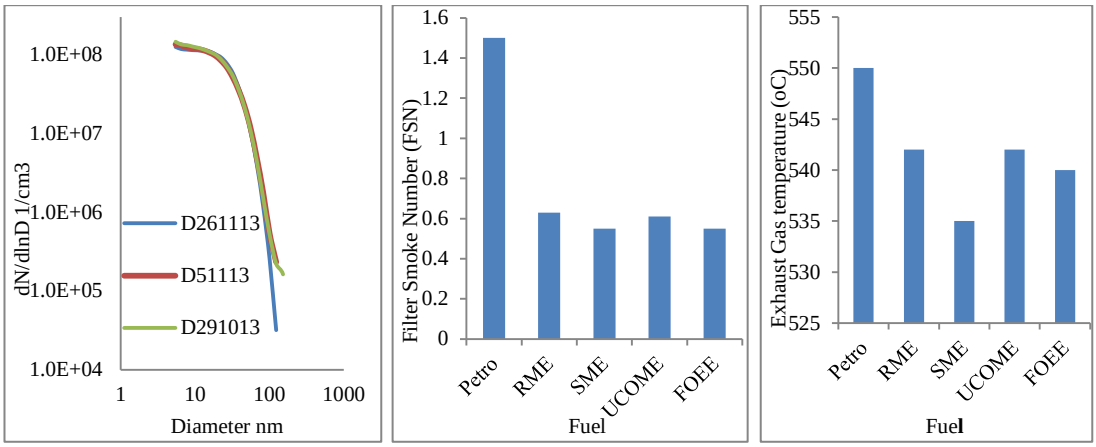

A B C

Figure 6.23, [A: Repeatability test with RME at three different days; B: Filter smoke number (FSN) and C: the exhaust gas temperatures at point of extraction for the three fuels].

With the confidence from the above data based on known relationship between FSN and PNC, further analysis of the dilution condition is conducted following the convention used in section 6.5 for two-stage dilution. Target DRs are compared with measured DRs and the PCRFs evaluated at 30nm and presented in Table 6.6

Table 6.6 Comparison of Target DRs and measured DRs and PCRFs

Fuel	1st-stage DR	2-stage DRs	Total DR (Targets=10.8 and 16.4)	PCRF @8.0	DRs 10.8	DRs 16.4	FSN	Exhaust Temp. (°C)
Petro	8.0	8.0(1.12; 1.69)	10.8; 16.4	2.5	3.3	5.0	1.5	550
RME	8.0	8.0(1.37; 2.05)	10.96;16.4	7.6	10.86	25	0.63	542
SME	8.0	8.0(1.36; 2.05)	10.88;16.4	7.6	10.86	25	0.55	535
UCOME	8.0	8.0(1.35; 1.98)	10.8;15.84	9.63	10.5	21	0.61	542
FOEE	8.0	8.0(1.35; 2.21)	10.8;17.68	9.52	10	20	0.55	540

The true implication of viewing dilution effects with PCRF is demonstrated here. Dilution of exhaust sample is known to reduce PM concentration and conventional approach of expressing dilution effects by DRs has got limitations that are demonstrated from Table 6.6.

The variations between the target DRs and the measured DRs are minor in both primary and secondary dilutions however, the true dilution effect are obtained by considering he PCRFs. At the primary dilution stage, petrodiesel has a particle reduction factor of 2.5 while RME and SME have 7.6. This indicates high nucleation activity in PM formation or high index of volatile stripping during dilution from PM generated with biodiesels. RME and SME are good examples of first generation biodiesels and exhibit similar qualities. In the same way, UCOME and FOEE has equal first stage dilution ratio but the PCRF are different; and different second stage DR but close PCRF. These again show how the parameter of PCRF defines dilution effects due to stripping of volatile particles. As a confirmatory check, cumulative particle number concentrations (CPNC) of the different fuel were checked in line with the explanations given in section 6.2.4.2 and the ratios of sub 30 nm particles (which defines the nucleation mode particles) to the total CPNC is reasonably correlated to

the first stage dilutions. This is shown in Figure 6.24 and although it is not possible to say the exact sizes of the accumulation mode particles since Figure 6.22 is not bimodal, the concentration of sizes within 30-100nm point to it and confirms that petrodiesel emits more soot compared to biodiesels.

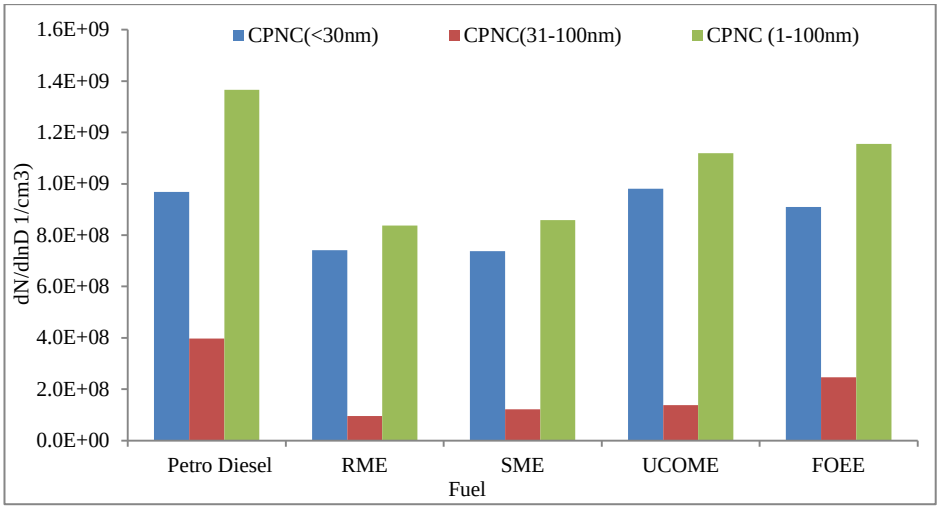

Figure 6.24 Cumulative particle number concentrations (CPNC) from various fuels.

Summary and conclusion

In line with the discussions given in section 6.5, two points of conclusion emanates from this study. The two stage dilution scheme has given the same account when examined with PM from different fuels showing its functionality of the set-up. Although perfect calibrations cannot be claimed, the results are consistent and therefore are reliable. It is also conclusive that better understanding of dilution condition is deducible through a parameter like PCRF as already pointed out; errors due to artefacts and uncertainties could be better highlighted in measurements compared to the use of dilution ratios.

CHAPTER 7

INVESTIGATION OF THE OXIDATION CHARACTERISTICS OF DIESEL PARTICULATE MATTER

7.0 Introduction

The emissions of particulate matter from diesel engines have been of concern to human health and investigations are made on how to reduce it through several options. These options include: improvements in engine design and operating conditions like optimal fuel injection schedule, fuel quality improvements, combustion chamber designs and use of after treatment devices. Considerations for fuel improvement among others, have involved the use of bio-fuels or their blends with petro-diesel. These have proved to reduce soot emissions (Andersson, Jon, 2011; Williams, A., Black, S., McCormick, R. L., 2010); while after-treatments basically involve the use of oxidation catalyst to further oxidise exhaust gases and filtration of soot particles emitted from the engine (Lemon, 2014). The use of diesel particulate filter (DPF) causes soot build-up that clogs and prevents free flow of exhaust gases leading to undesirable pressure drop across the DPF. The soot build-up on the DPF therefore requires regular and fast burn-out (regeneration) in order to ensure good engine performance. Experimental studies on combustion schemes are costly and fraught with difficulties during measurements at high temperatures, and for the engine-generated soot, regeneration process is also demanding but depends on the engine design and operations. Therefore small scale thermal investigations are effectively used to gain understanding of many combustion phenomena. In this chapter, a fundamental study of the oxidation characteristics of soot generated from a high speed direct injection diesel engine is made using results from combined thermogravimetric analyser (TGA) and Differential Scanning Calorimeter (DSC).

7.1 Objectives

The objectives of this chapter are:

1. To investigate the oxidation characteristic of diesel generated PM using some Arrhenius kinetic parameters.

2. To investigate the effect of fuel blending with bio-diesel as example of fuel quality improvement on soot oxidation characteristics

7.2 Soot Sample Collection

The choice of engine operating condition was set at 80Nm, 2000Rpm, 800bars of injection pressure and 9^{o}BTDC. This was based on the preliminary investigation of filter smoke number (FSN) when engine was operated at different injection timings and injection pressures as highlighted in chapter 5. In the typical engine operation using petro diesel, fuel was fed through the normal laboratory diesel supply line but when fuel blends were used, fuel was supplied through a blend-fuel tank coupled with a two-way valve to enable change in supply from the central diesel supply line to the blend tank and vice versa as in Figure 4.1. Soot samples were collected on a high temperature filter element, (Pall Tissuquartz filter, 2500 QAT-UP) 47mm in diameter, secured in a cartridge and the fitted into a modified holder which allowed for quick connection or removal of the filter cartridge as necessary Figures 7.1 (A & B). The cartridge was installed on a by-pass exhaust line connected to a BECKER U4.20 vacuum pump downstream as in Figure 7.2. A check valve downstream of the filter cartridge and open to the atmosphere was set to crack at 500 milibar of vacuum, to protect the vacuum pump from excessive vacuum as soot accumulation on the filter obstructs exhaust flow and was used to set the limit of soot collection. By the rating of the vacuum pump, maximum suction air flow rate at this crack pressure is 16.9m^3/hr at intake pressure (8.5m^3/hr at atmospheric pressure) for a motor capacity of 0.55kW/50Hz. A thermocouple, attached to sense the temperature of the exhaust flow immediately after the filter cartridge enabled direct measurement using a hand held meter at the point of collection. A valve was used to shut-off flow on the by-pass line when not in use; therefore it was convenient to allow exhaust flow to the filter when the required engine operating conditions were reached. At the end of each loading session, the filter cartridge was quickly transferred to a desiccator and afterwards soot was carefully scrapped into a specimen tub for thermogravimetric analysis. The schedule of samples generated as in Table 7.1.

Figure7.1, A: Cartridge holder modified on line, B: Filter element loaded with soot

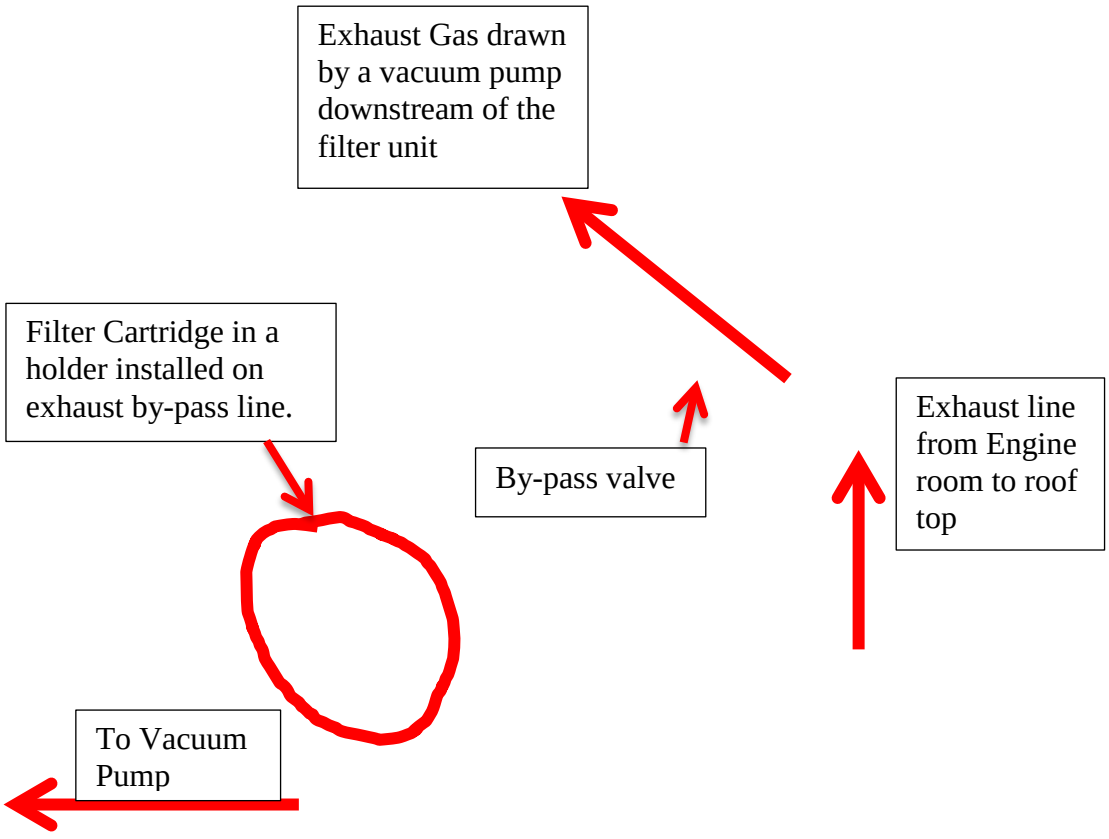

Figure 7.2 Layout of the soot collection set-up

Table 7.1 Samples generation schedule

Batch 1(Baseline)	Batch 2(Blend 1)	Batch 3 (Blend 2)
	B20 (RME)	B40 (RME)
B(0) Petrodiesel	B20 (SME)	B40 (SME)
	B20 (UCOME)	B40 (UCOME)

7.3 Methodology

Soot samples were oxidised using a SDT 600 for simultaneous TGA/DSC analysis. The technical specifications with regards to sensitivity, accuracy and precision of signal measurements are as in Table 7.2. It was used to measure change in weight (TGA) and the accurate differential heat flow (DSC) on the soot sample from ambient to the oxidation temperatures during sets of isothermal and non-isothermal oxidation tests. The balance/thermocouple beams bear the sample and reference cups Figure 7.3. The reference cup was empty while the sample cup was loaded with soot samples; the relative differences with changes in weight and thermal flows were used to measure the oxidation behaviours of the soot at any instance of time or temperature.

Table 7.2 SDT 600 Technical Specifications

System Design	Horizontal Balance and Furnace
Balance Design	Dual Beam (growth compensated)
Sample Capacity	200mg (350mg including sample holder)
Balance Sensitivity	0.1µg
Furnace Type	Bifilar Wound
Temperature Range	Ambient to 1500 ^{o}C
Heating Rate – Ambient to 1000 ^{o}C	0.1 to 100 ^{o}C/min
Heating Rate - Ambient to 1500 ^{o}C	0.1 to 25 ^{o}C/min
Furnace Cooling	Forced Air (1500 ^{o}C to 50 ^{o}C in < 30 min' 1000 ^{o}C to 50 ^{o}C in < 20 min)
Thermocouples	Platinum/Platinum-Rhodium (Type R)
Temperature Calibration	Curie Point or Metal Standards (1 to Points)
DTA Sensitivity	0.001 ^{o}C
Calorimetric Accuracy/Protection	± 2% (Based on Metal Standards)
Mass Flow controller with Automatic Gas Switching	Included
Vacuum	Included – Separate gas tube
Dual Sample TGA	Included
Auto Separate TGA	Included
Sample Pans	Platinum: 40 µl, 100 µl Alumina: 40µl, 90µl

The effects of ramping and mass of sample in a typical TGA study have been studied by (Lupuerta, M., Ballesteros, R., and Rodriguez-Fernandea, J., 2007), the experimental factors that could affect good account of soot oxidation were optimised in the work of (Rodriguez-Fernandez, J., Oliva, F., and Vazquez, R. A., 2011) and were further studied in (Sharma et al 2012). These include the oxidant flow rate, initial sample mass, ramp rate. These factors directly affect diffusion and could limit the oxidation kinetics of the soot sample.

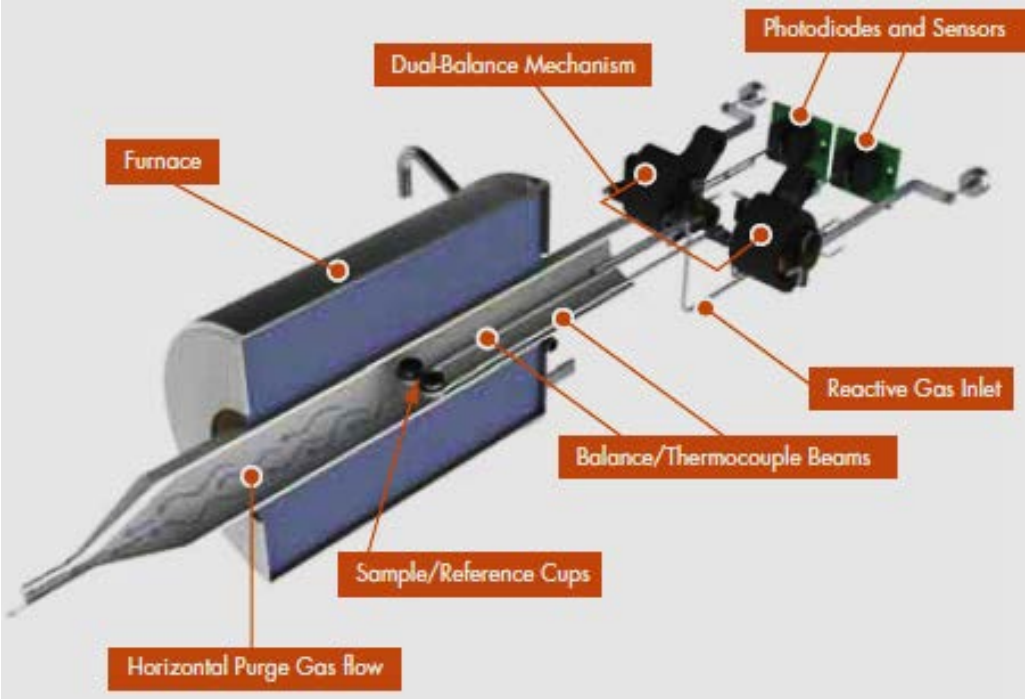

Figure 7.3 SDT 600 Measurement Technologies

The influence of oxygen, a naturally occurring element in the air is known to be critical in soot oxidation. However the air flow rate has been shown to be of minimal effect except for values below 40mL/min in TGA studies where it can slow down reaction especially at high temperatures where reaction are faster. Thus, the effect of oxygen diffusion is negligible compared to oxidation kinetics which controls reaction (Rodriguez-Fernandez, J., Oliva, F., and Vazquez, R. A., 2011). As no optimal flowrate is recommended, air flow rate of 100mL/min was selected from the manufacturer's options. The effect of initial sample mass has been shown to affect TGA analysis (Stanmore, B. R., and Gilot, P., 1995; Gilot, P., Brillard, A., and Stanmore, B. R., 1995; Stanmore B. R., 2001; Zouaoui et al 2010). Most studies used

commercial soot or dry soot from diesel particulate filters (after driving off volatile matter) instead of the total PM as collected on the filter paper. Large initial mass could limit diffusion of oxygen into the sample core, affect the programmed heating rates due to deviations that results from localised endothermic or exothermic reactions in small parcels of the sample (Stanmore, B. R., and Gilot, P., 1995; Sharma et al 2012; Rodriguez-Fernandez, J., Oliva, F., and Vazquez, R. A., 2011). Conversely, small initial mass may induce reproducibility problems due to possible inaccurate measurements and instrument calibration limits. It was recommended that a minimum of 3mg (Rodriguez-Fernandez, J., Oliva, F., and Vazquez, R. A., 2011; Chong et al 2013) of sample be used; and bearing in mind that some small quantities of the filter paper could as well be scrapped into the soot, initial mass of more than 4.0mg was deliberately measured into the TGA sample cup during each oxidation test. Similarly, the nature and shape of the crucible were identified to bear influence on the oxidation kinetic due to limitations imposed by diffusion and mass transfer. Conventionally, short and wide crucible minimizes stagnation points and therefore prevents such limitations. The SDT600 used in the experiment has a Q600 thermobalance with ceramic (alumina) crucibles that offer high thermal stability in excess of 1000^{o}C. Heating ramp rate and initial mass have overlapping effects. Ramp rate was also identified in the above studies to be associated with limitations inherent in heat and mass transfer processes and therefore the overall repeatability of results. Using low ramp rates improve the resolution of the oxidation process and its reproducibility. Therefore low ramp rates were adopted: 5^{o}C/minute for non-isothermal and 10^{o}C/minute for isothermal oxidation protocol as follows:

(i) For Iso-thermal test:

It is known that soot oxidation can starts from 500^{o}C but perfectly at 600^{o}C;
therefore reference soot generated from petro-diesel fuel was oxidised at three iso-thermal temperatures of 500, 550 and 600^{o}C as follows:

- Start with Nitrogen 100ml/minute
- Ramp 10 ^{o}C/minute to 30 ^{o}C
- Isothermal for 30 minutes to stabilize sample
- Ramp 10 ^{o}C/minute to 400^{o}C

- Isothermal for 60 minutes to remove VOF
- Ramp the sample 10 ^{o}C/min to 500 ^{o}C in nitrogen ,
- Switch to air for oxidation
- Isothermal for 60 minutes.

The process was repeated for devolatilization in nitrogen and then oxidised isothermally at 550 ^{o}C and 600 ^{o}C respectively.

(ii) For non-isothermal test:

This involved all soot samples in the schedule:

- Use pure air from atmospheric condition.
- Ramp 5 ^{o}C/min to 700 ^{o}C
- Isothermal for 60 minutes.

7.4 Results

In line with the objectives, the particulate matter (comprising of volatiles and soot) as generated under the given operating condition using petro-diesel was first devolatilised using nitrogen and then the reaction kinetics of the dry soot examined through isothermal oxidation in 100% pure air. Then non isothermal oxidation was adopted to study the effects of fuel blending with bio-diesel. Several tests are usually required to extract information about the kinetic parameters from isothermal oxidation which ultimately gives better repeatability but will require generating more samples, and is also time and energy consuming. However, if experimental parameters are properly optimised, same information could be extracted through sweep of the whole temperature window in a non-isothermal process. This accounts for the considerations outlined in the methodology. There can be no real dry soot without some portions of condensed volatile organic fractions in engine-generated PM neither can there be ideal isothermal oxidation in the regeneration process. Exhaust temperatures around the upstream of the DPF in typical automotive applications are above 200°C and it can be taken that most volatile organics that originate from diesel fuel and the intermediates vaporise within the 200 - 400°C temperature window (Stratakis, G. A., Konstantas, G. S., and Stamatelos, A. M, 2003; Stratakis, G. A. and Stematelos, A. M., 2003b). However from 400°C, some traces of high density volatile species originating from the lubricant which could have been trapped in the inner core of the soot mass could ignite in the presence of

air. Similarly, smaller sizes of the soot particles with localised high porosity will preferentially ignite ahead of the bulk mass (Lopez-Fonseca et al 2006). The oxidation temperature that will trigger complete burn-out of PM is of paramount interest in the design of particulate filters (Rodriguez-Fernandez, J., Oliva, F., and Vazquez, R. A., 2011). By implication, the temperature of the PM oxidation kinetics that will fit the ideal Arrhenius curve is within the trigger oxidation temperature region. Therefore the temperature window at which the active oxidation occurs should be representative for design considerations. Classic investigations for pure isothermal treatments have been described in (Chong et al 2013). Insights from this strategy together with considerations for non-isothermal treatments (Sharma et al 2012; Rodriguez-Fernandez, J., Oliva, F., and Vazquez, R. A., 2011) informed a comparison of purely isothermal oxidation when temperature has been ramped to 500 ^{o}C, 550 ^{o}C and 600 ^{o}C respectively before introduction of air; and a 'hybrid' treatment in which air was introduced from 400 ^{o}C while ramping to, and then oxidised isothermally at the respective oxidation temperatures. The aim is to see the contribution of oxidation process from 400-500 ^{o}C, - a period not normally considered for oxidation of volatiles nor oxidation of real soot (usually considered from 500 ^{o}C). Some studies have used mixture of inert gas with air for oxidation probably to simulate likely air proportion in the engine exhaust however (Chong et al 2013; Neeft et al 1997), in this study use of 100% air to oxidise PM have been purposefully chosen to limit the number of unknowns.

7.4.1 Oxidation characteristics of petro-diesel generated PM using isothermal oxidation protocol.

This aspect of the study has been conducted to evaluate the reaction order, soot oxidation rate and the activation energy. The aim is to compare these oxidation kinetics parameters of the soot samples with those obtained from known protocols in literature. The periodic burn-off or regeneration of soot accumulated in DPF requires good thermal management in order to avoid thermal runaway. It requires adequate understanding of soot oxidation kinetics relevant to the manufacture of efficient filter traps that can withstand thermal stresses within the confined space of the engine exhaust system. The oxidation rate for oxidising materials is evaluated from the kinetic parameters using Arrhenius concept:

$$-\frac{dm}{dt} = k_c m^n {po_2}^r = Aexp(\frac{-E_a}{RT}) m^n {po_2}^r \qquad 7.1$$

Where m is sample mass, t is time, k_c is the reaction rate, A is the pre-exponential factor, E_a is the activation energy, R is the universal gas constant (8.31447 J mol^{-1} K^{-1}); T is the temperature in kelvin; n is the reaction order of soot, P_{O_2} is the partial pressure of oxygen, r is the reaction order of oxygen. It is usual to assume that the reaction order for soot is approximately unity however here; the reaction order is first determined using experimental data and then it was used to evaluate oxidation rate of the soot.

7.4.1.1 Panoramic view of oxidation profiles at different temperatures

The instantaneous mass with temperature variations for two sets of data as soot was isothermally oxidised at 500, 550 and 600 ^{o}C respectively are shown in Figures 7.4.

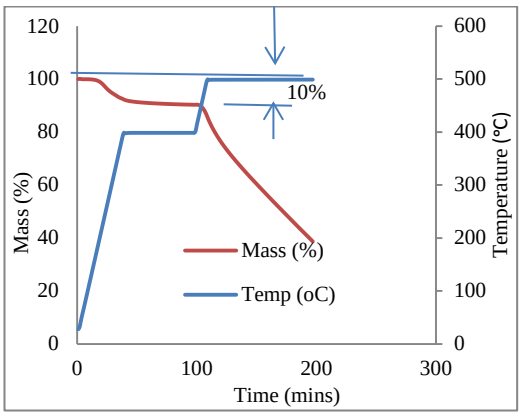

Set [A1] Isothermal oxidation profile at 500°C

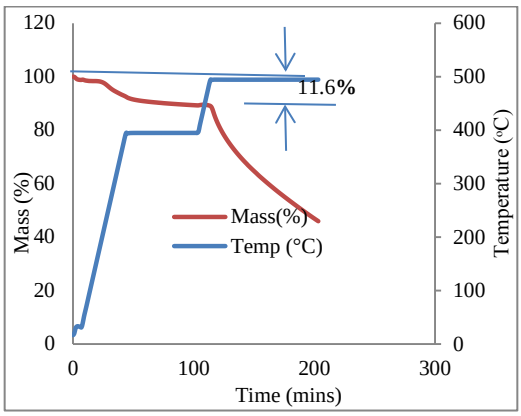

Set [B1] Isothermal oxidation profile at 500°C

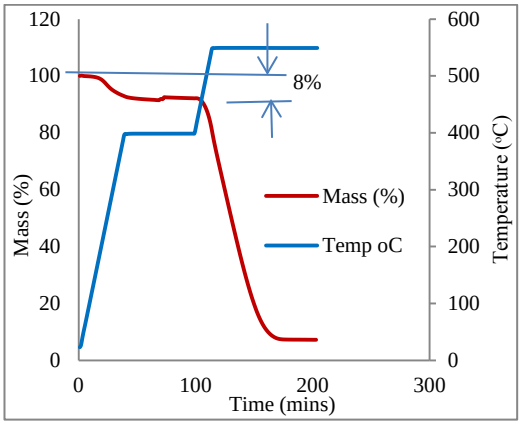

Set [A2] Isothermal oxidation profile at 550°C

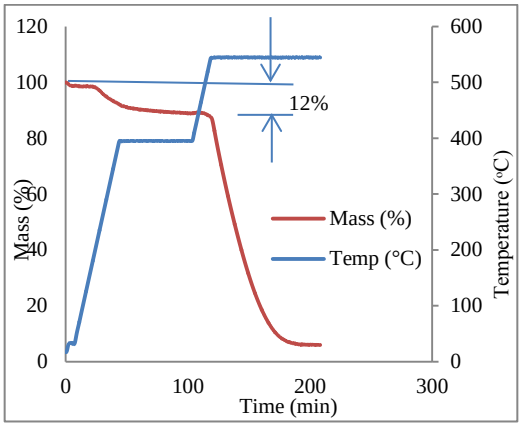

Set [B2] Isothermal oxidation profile at 550°C

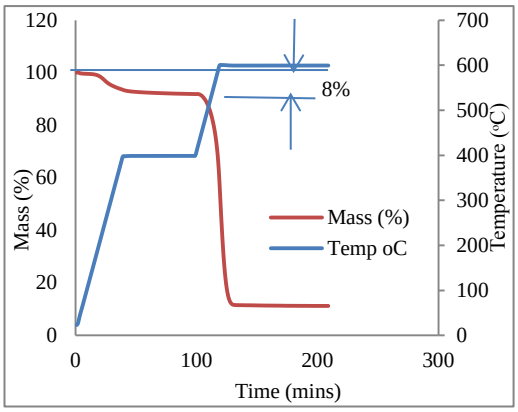

Set [A3] Isothermal oxidation profile at 600°C

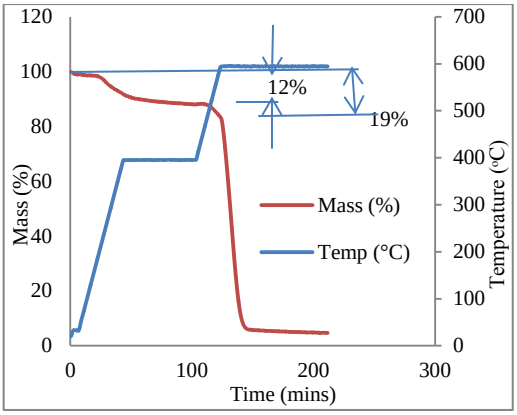

Set [B3] Isothermal oxidation profile at 600°C

Figure 7.4 mass and Temperature profiles Verses Time for oxidation at three isothermal temperatures of 500°C, B: 550°C, C: 600°C. Set A profiles were ramped to and oxidised from 400°C to respective temperatures and oxidised isothermally, while set B profiles were ramped to and oxidised at their respective isothermal temperatures.

In the first series of plots [Set A] three samples were treated with nitrogen from ambient, ramped 10°C/minute to 400°C and dried for 60 minutes to drive off VOF. Then pure air was introduced at 400°C and ramped respectively to 500°C, 550°C and 600°C differently on the three samples and oxidised isothermally at these temperatures. In another set of three samples [Set B], each was also dried with nitrogen while ramping at the same rate but up to their respective oxidation temperatures before introduction of air and then isothermally oxidised. The initial slight drop in sample masses in the two sets of data (less than 4%) corresponding to temperatures below 140°C signifies vaporisation of low vapour pressure volatile components in the sample. Afterwards, there is a drop to constant plateau which signifies vaporisation of organic fractions before the steady mass reduction that was due to the soot oxidation process. There is a difference in the level of VOF in the two sets of data signifying more devolatilization of the samples beyond 400°C. The level of VOF removed in the first set of data ramped only to 400°C before introduction of air could be taken as 8% (except on the first sample) and those ramped to their respective oxidation temperatures as 12%. In the last sample of set B oxidised at 600°C, a further mass decrease of 7% was noticed, it is viewed not only as loss due to VOF but suspected that some mass of soot oxidised during displacement of nitrogen from the pores as oxidation commenced. Nitrogen is a diluent as well as a

thermal sink; therefore energy release upon initial contact with air was not immediate but momentarily delayed as seen for the oxidation rate curve (Figure 7.5B). The effect is more noticeable at 600°C than 550°C and 500°C in the plots of mass loss rate just as in those of instantaneous mass. It is known that volatile fractions are generated more at low load and also depend on the torque/speed relationship. The condition under which these samples were generated could be taken as medium load for a diesel engine (80Nm/2000Rpm ~ 5.05Bar BMEP). Some authors have reported different levels of VOF contents in samples which depend on many factors.

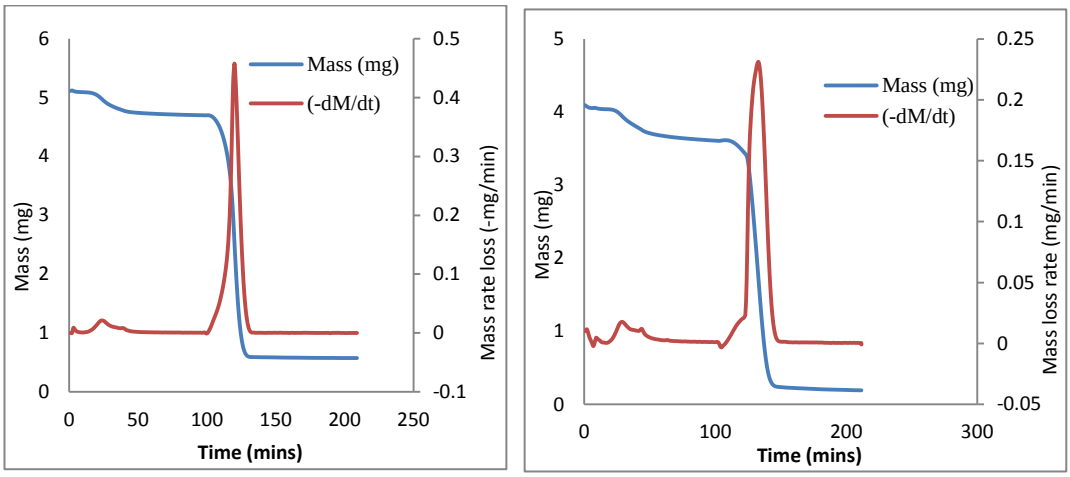

Set [A] Set [B]

Figure 7.5 Mass and Mass loss rate profiles for oxidation at isothermal temperature of 600 for Sets [A&B]

The method of sample collection and condition of engine operation for instance, affects the nature of soot sample. Samples collected from a DPF trap will contain PM that arises from wide range of engine operating conditions: transient and steady conditions, low and high loads, low and high speeds, - and all affect the exhaust gas temperature at the point of soot trap. Also are engine design characteristics: the injection systems, boosting and exhaust gas recirculation (EGR). These will emit varying degrees of VOFs which will characterise the soot oxidation (Stratakis, G. A. and Stematelos, A. M., 2003b; Kandylas, I. P. and Stamatelos, A. M., 1999; Stratakis, G. A., Konstantas, G. S., and Stamatelos, A. M, 2003; Stanmore, B., Brilhac, J. F., and Gilot, P., 1999). This will be different from a sample collected from a DPF trap after a DOC has oxidised the gaseous emissions and leave only dry soot on the filter (Martyn, V. T. and Phillips, P. R., 2009; Prassad, R. and Bella V. R., 2010). Other factors that influence the level of VOF in TGA analysis reported by

authors are based on the oxidation protocols used. These are rate of temperature ramping, the maximum temperature attained, and the duration of isothermal devolatilization at the chosen temperature. Smaller ramp rates will lead to delayed oxidation but more uniform heating of the sample thereby leading to better expulsion of the VOF particularly if the maximum limit is high, though this takes more time and also related to the quantity of the sample (Sharma et al 2012; Lupuerta, M., Ballesteros, R., and Rodriguez-Fernandea, J., 2007; Chong et al 2013). The level of VOF from this test is similar to those published in literature: it was shown to vary from 2 -11% (Stratakis, G. A., Konstantas, G. S., and Stamatelos, A. M, 2003; Stratakis, G. A. and Stematelos, A. M., 2003b) from a sample collected on a silicon carbide filter at low to medium load, showed dependency on load and the torque/speed relationship. Similarly, in (Lupuerta, M., Ballesteros, R., and Rodriguez-Fernandea, J., 2007) samples collected at a comparative medium load (110NM/1853Rpm) gave VOF of 14-15.5% when analysed on a TGA. Correspondingly, oxidation rates were highest at 600°C, followed by 550°C and 500°C. During isothermal oxidations at 500°C, the process was terminated prior to completion (due to oversight in programming the oxidation protocol in the TGA). By taking the natural logarithm of equation 7.1 and re-arranging, it gives equation 7.2.

$$\ln\left[-\frac{dm}{dt}\right] = nln[m] - \frac{E_a}{R} * \frac{1}{T} + n_{O_2} \ln\left[P_{O_2}\right] + \ln[A] \qquad 7.2$$

From the three isothermal experiments, the mass rate losses were determined from the mass data. Then the logarithms of mass and mass rate losses were evaluated for the each data set. The plot of logarithm of mass loss rate as a function of the logarithm of mass for each set of data is plotted in Figure 7.6 (note that oxidation processes were not complete at 500° C in sets [A] and [B]) and the gradient of the linear regression line taken for each plot. These were taken within the limits where instabilities are not high. The gradient of the regression lines give the reaction order ‘n’ according to equation 7.2. Then the average values of the gradients of plots at the three oxidation temperatures were taken for each set and the comparison is presented in Table 7.3. The value of ‘n’ for set [A] data is **0.68** while it is **0.75** for set [B] data and these were separately used to substitute back in the equation 7.2, to achieve equation 7.3 for two the sets of experiments.

$$\ln\left[-\frac{dm}{dt}\right] - 0.68\ln[m] = -\frac{E_a}{R} * \frac{1}{T} + n_{O_2}\ln\left[P_{O_2}\right] + \ln[A] \qquad (7.3A)$$

$$\ln\left[-\frac{dm}{dt}\right] - 0.75\ln[m] = -\frac{E_a}{R} * \frac{1}{T} + n_{O_2}\ln\left[P_{O_2}\right] + \ln[A] \qquad (7.3B)$$

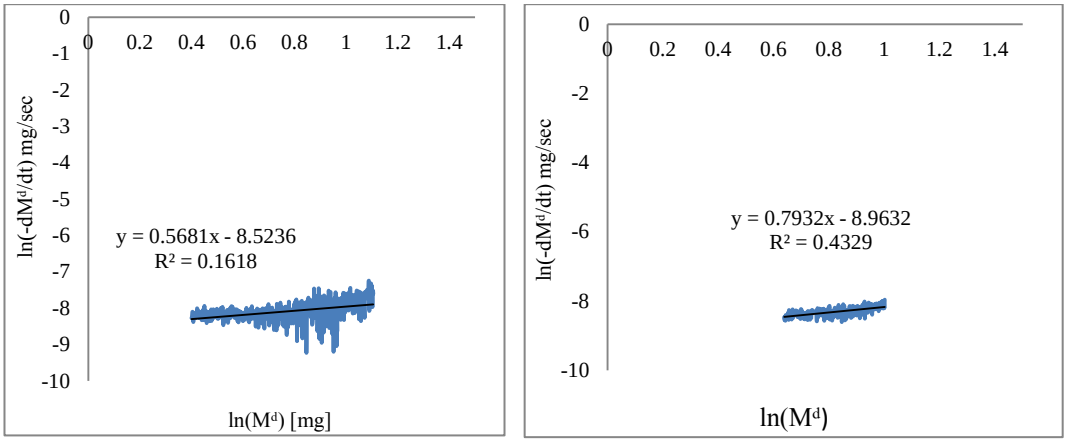

(A) Evaluation of reaction order at 500°C: Set [A] range of steady oxidation is 5-51%; set [B] range of steady oxidation is 5-48%.

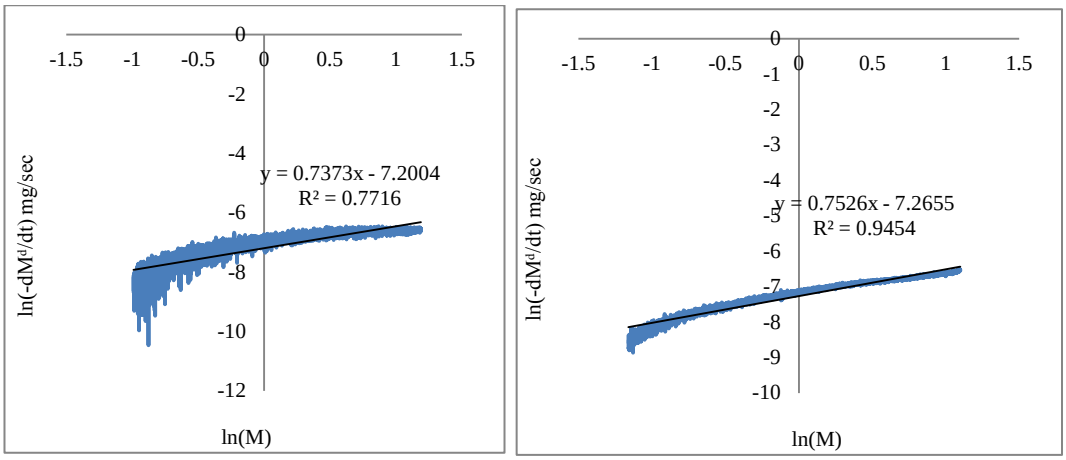

(B) Evaluation of reaction order at 550°C: Set [A] range of steady oxidation is 18-90%; set [B] range of steady oxidation is 10-90%

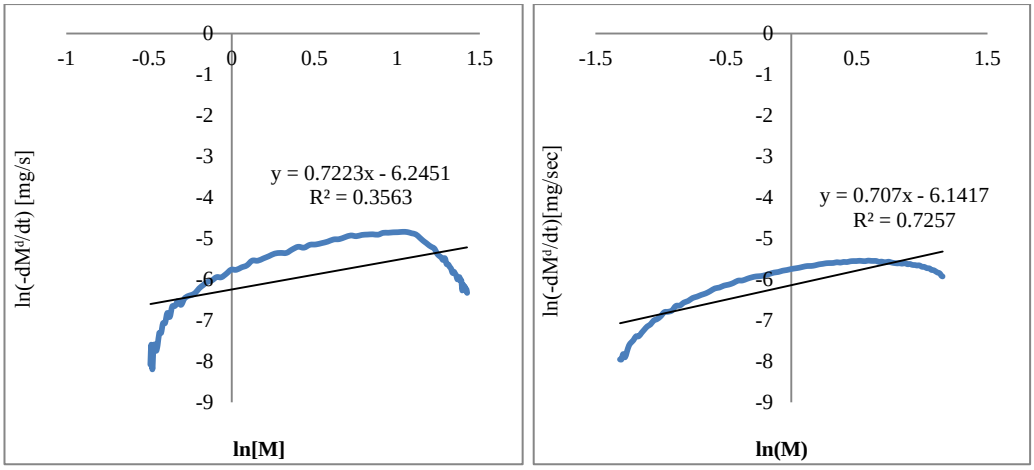

(C) Evaluation of reaction order at 600°C: Set [A] range of steady oxidation is 11- 88%; set [B] range of steady oxidation is 10-93%

Figure 7.6 (A-C) Evaluation of Reaction order for the two sets of data at 500, 550 and 600°C respectively.

Table 7 .3 reaction order for the two data sets

Temperature [°C]	Reaction order [Set A]	Reaction order [Set B]
500	0.57	0.79
550	0.74	0.75
600	0.72	0.71
Mean	**~ 0.68±11**	**0.75±0.04**

It was observed that oxidation temperature window within which the reaction was steady without much instability was smaller in samples sets [A] than [B] using complete oxidations processes at 550°C and 600°C as reference. The range for stable reaction used in determination of the reaction order started earlier and also ended earlier in set [A] compared to set [B] however, the value of mass percent of stable oxidation was higher in set [B] than set [A]. This clearly demonstrates the effect of higher heating period for devolatilization prior to oxidation. Set A must therefore possess some VOF that enhanced earlier start of oxidation but had higher level of instabilities at the commencement and towards the end of oxidation. The value of reaction order derived with set [A] is (0.68±11) and in set B data, (0.75±04). Compare to that obtained in (Chong et al 2013; Yang, S., Lee, K., and Chong, H., 2010), they calculated the reaction order for two reaction zones as 0.24±0.05 and

0.74±0.08 for the zone of early oxidation; 0.00 and 0.80 for the zone of later oxidation respectively. This gives a clue that early part of the oxidation has lower reaction order compared to the later part, which is similar to the lower reaction order from set [A] data where oxidation started earlier when comparing the characteristics of the two data sets.

The evaluation of activation energy (E_a) was pursued by plotting values of the terms on the left side of equation 7.3 as a function of reciprocal of the temperature at the three oxidation temperatures. The slope of the line obtained by plotting the values obtained when m = 0 at the three oxidation temperatures are shown in Table 7.4 and Figure 7.7.

Table 7.4A Determination of Activation Energy using the dry soot for set [A] data

Oxidation Temp(°C)	**1000/T (k^{-1})**	**ln(-dM/dt) - 0.68 ln(M) [when M= 0]**	**R**	**Slope**	**Intercept**	**Activation Energy (E) kJ mol^{-1}**
500	1.293661061	-8.55	8.314	18.53	15.4	**~ 154**
550	1.215066829	-7.2				
600	1.145475372	-5.8				

Table 7.4B Determination of Activation Energy using dry soot for set [B] data

Oxidation Temp (°C)	**1000/T(K^{-1})**	**ln(-dM/dt) – 0.75ln(M) [when M =0]**	**R**	**Slope**	**Intercept**	**Activation Energy (E) kJ mol^{-1}**
500	1.293661061	-8.97	8.314	19.41	16.2	**~ 161**
550	1.215066829	-7.3				
600	1.145475372	-6.1				

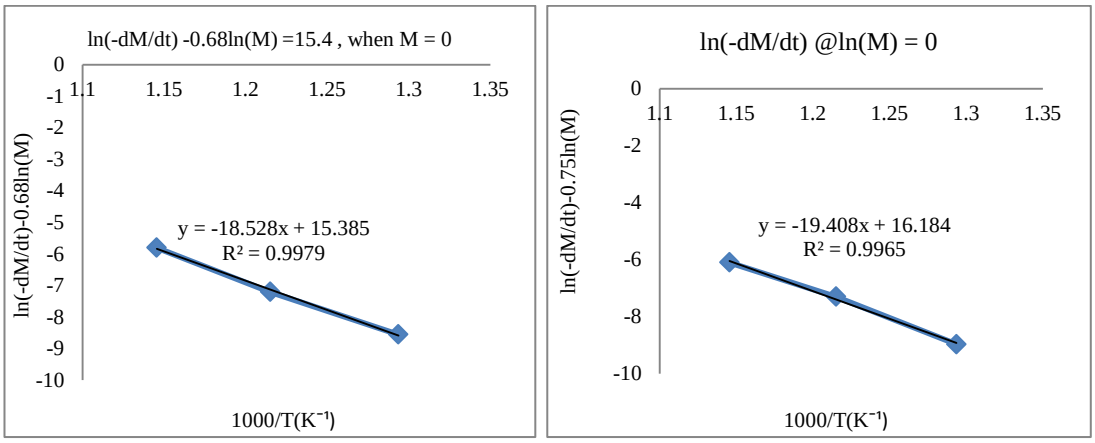

Set [A] Set [B]

Figure 7.7 Activation Energy evaluated for two sets of data at three oxidation temperatures and associated reaction order 'n'

The values of the activation energy evaluated with the two data sets are also consistent with many in literature. Similar isothermal treatment of diesel soot with air gave activation energy as 152 -169 kJ mol^{-1} and with 10% oxygen in Argon as154 – 172kJ mol^{-1}; in each case, it depended on the ramping used (Sharma et al 2012). The low values correspond to ramping at 20°C/minute and the high values, 5°C/minute. Also, soot generated from 1.9 litre engine on multiple operating conditions, dried with helium and oxidised with air, gave E_a as 139.55 kJ mol^{-1} and 136.26 kJ mol^{-1} (Chong et al 2013); 154 ± 25 and 153 ± 34 kJ mol^{-1} (Yang, S., Lee, K., and Chong, H., 2010) for the early and latter parts of the combustion zones respectively. In (Stanmore, B., Brilhac, J. F., and Gilot, P., 1999) activation energy was evaluated as 210 kJ mol^{-1} for non-catalysed and catalysed diesel soot (doped) with Cerium.

Pure air contains 21% oxygen; therefore the partial pressure it can exercise is 0.21. The determination of reaction order of oxygen need separate sets of experiments but were not intended in this work though necessary to describe detailed kinetics of soot oxidation. However from equation 7.3 (A&B), the slope (Ea/R) from where the activation energy was calculated equals 18.53 and 19.41 respectively. The intercept for the two sets of data are also 15.4 and 16.2 respectively. Since the plot was made with respect to terms that are functions of mass and temperature, the intercept represents the sum of the terms on the right hand side:

$n_{O_2} \ln[P_{O_2}] + \ln[A] = 15.4$ - For sample set [A]

$n_{O_2} \ln[P_{O_2}] + \ln[A] = 16.2$ - For sample set [B]

By substituting these terms and evaluating back to equation 1, the oxidation rate equation within the limits where stable oxidations were considered is expressed as:

$\left(-\frac{dm}{dt}(mg/\text{sec}) = 4.877 \times 10^3 \exp[-\frac{18528}{T\,(K)}] * [m]^{0.68}\ (mg)\right.$ - Set [A]

$(-\frac{dm}{dt}(mg/\text{sec}) = 1.0854\ \times 10^4 \exp\left[-\frac{19408}{T\,(K)}\right] * [m]^{0.75}\ (mg)$ -Set [B]

The difference in these equations show the effect of the oxidation protocols adopted. The equations as derived with the two sample sets show that with set [A], oxidation started from 400℃ and continued with attainment of the respective iso-thermal temperatures; while in set [B], the samples were dried up to their respective iso-thermal temperatures. This is viewed to be responsible for the difference in reaction orders and activation energies thereby affecting the overall oxidation processes in the two sets of samples. It is considered that early start and end of combustion and also higher scale of oxidation instabilities especially at lower oxidation temperatures gave the difference. Similarly, it could be viewed that slight thermal aging of the soot could have also affected their internal structures as explained in (Chong et al 2013) where two sets samples were subjected to two time frames of iso-thermal heating. It was observed that kinetic parameters were affected by thermal aging with consequent reduction in reactivity of diesel soot. The graphitic structure of soot has been shown to have strong influence on the oxidation characteristics of diesel generated soot (Vander Wal, R. L. and Mueller, C.J., 2006; Vander Wal, R. L., Aaron, T., and Tomasek, A. J, 2003; Boehman, 2013; Song et al 2006) because with more ordered structure due to increased graphitization, soot reactivity has been shown to decrease (Müller et al 2005; Yehliu et al 2012; Bhardwaj et al 2013A). However in this study, full reactivity examinations could not be carried out as the aim is to have baseline

values of the basic kinetic parameters, and these were even derived within limits where oxidation instabilities was minimal. Therefore the models are not fully representative for the whole oxidation process.

7.4.2 Investigation of the effect of different biodiesel blends on soot oxidation using non-isothermal protocol.

It is known that biodiesels have characteristic tendency to reduce engine soot emission due to their oxygen content compared to petrodiesel (Song et al 2006; Williams, A., Black, S., McCormick, R. L., 2010; Andersson, Jon, 2011; Bhardwaj et al 2013A; Boehman, A. L., Song, J., and Alam, M., 2005). In this section, the aim is to investigate the influence of biodiesel content in soot (or PM) oxidation. This is relevant in particulate filter design since PM oxidation at lower temperature will imply faster and better DPF regeneration process. The temperature windows at which the oxidations occur due volatile components and soot as well as associated mass losses have been considered.

7.4.2.1 Investigation of the VOF contents in different blends of B20 and B40 compared to petro diesel

The amount of VOF in PM like other emission candidates is related to the engine operating condition as well as the type of fuel used. Engine operating conditions were optimised for highest sooting tendency without any EGR at 9° BTDC, speed of 2000Rpm and 80Nm load under stable operation. Petrodiesel used in engine is a commercial ULSD which meets Euro EN 590 specifications and therefore may contain about 7% of biodiesel which impacts only small difference in the physical properties when compared to the properties of a 100% petro diesel. The use of 2% to 20% blend of biodiesel in automotive diesel by volume is common in the U. S. market and is made to conform to ASTM D7467 requirement (Williams, A., Black, S., McCormick, R. L., 2010; Bhardwaj et al 2013A). Although some species of hydrocarbons with low vapour pressure may not nucleate into particles, it is conventional to relate condensed particles from volatile organic fractions (VOF) or more specifically soluble organic fractions (SOF), to unburnt hydrocarbon. Deliberate efforts were made to collect samples at temperatures above 100 ^{o}C, therefore water particles and acids bound to it were excluded. Results in Figures 7.8

and Tables 7.5 show a general trend in the reduction of VOF in PM from the RME and SME blends compared to that of petro diesel. The effect of blending petro diesel with biodiesel with regards to its influence on lowering the VOF (VOF here is attributed to UHC) in PM emission did not give a clear relationship. This is similar to the observations in (Lu, T., Cheung, C.S., Huang, Z., 2013; Andersson, Jon, 2011). RME and SME are extensively studied first generation biodiesels with physical properties comparable to petrodiesel. The UCOME used here has a degree of similarity with RME and SME from their estimated physical properties but the cetane number is slightly higher (Table 7.6A). Many authors have attributed different reasons for low UHC with the use of biodiesel as reviewed in (Lapuerta, M., Armas, O., and Rodrıguez-Fernandez, J., 2008). This non-linear decrease in UHC can be attributable to some differences in some of the physical properties of biodiesel depending on the feedstock from where it is derived. The following remarkable properties are viewed to account for some observations made:

Oxygen content

Biodiesel burns more rapidly during engine combustion by virtue of its oxygen content when compared to petro diesel, and therefore can leave soot drier. This feature is remarkable with soot from RME and SME blends compared to that of petro diesel. RME and SME are good examples of first generation biodiesels and contain about 10.8% oxygen (Bhardwaj et al 2013A; Andersson, Jon, 2011; Lapuerta, M., Armas, O., and Rodrıguez-Fernandez, J., 2008; Bhardwaj et al 2013B; Song et al 2006). The presence of oxygen in fuel is an indirect enhancement of the fuel - air mixing which leaves the soot with less UHC and by implication less condensed volatile particles from the exhaust samples.

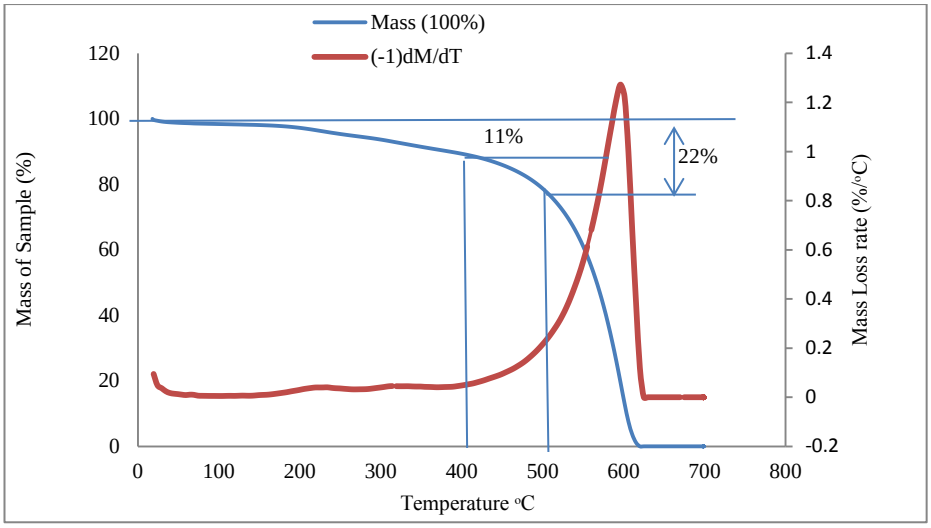

A: Mass and mass lost rate for PM generated with petro-diesel; Mass lost at 400°C is 11% and 22% at 500°C.

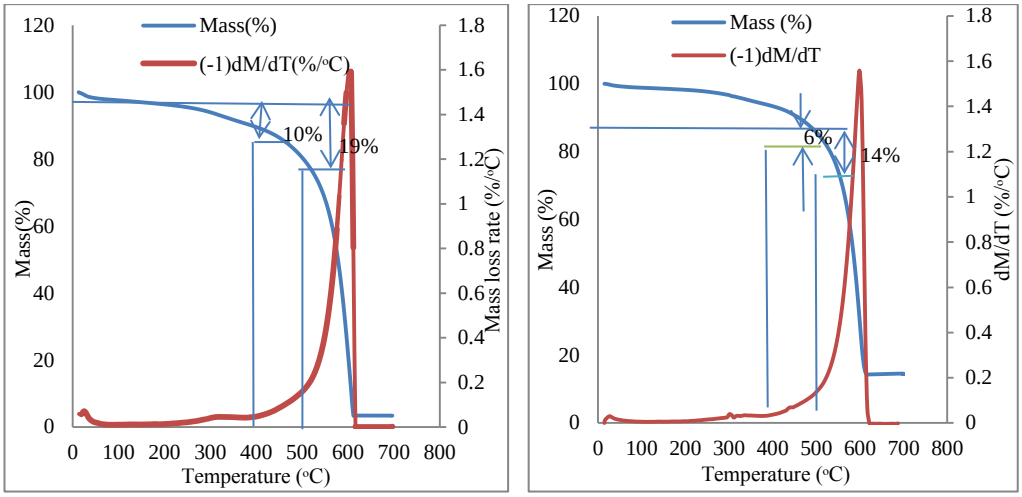

B1 B2

B1: Mass and mass loss rate for PM generated with B20 RME, Mass lost at 400°C is 10% and 19% at 500°C; B2: Mass and mass loss rate for PM generated with B40 RME, Mass lost at 400°C is 6% and 14% at 500°C.

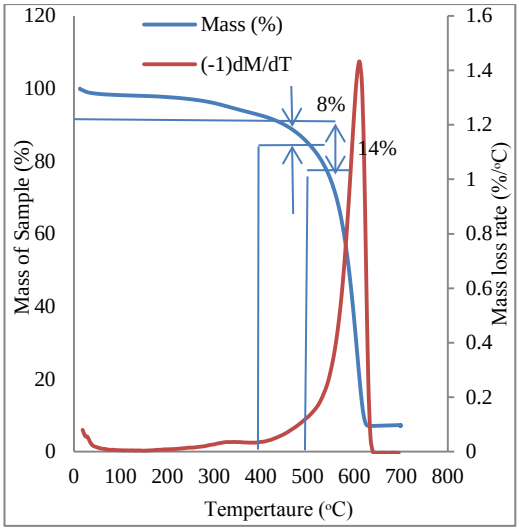

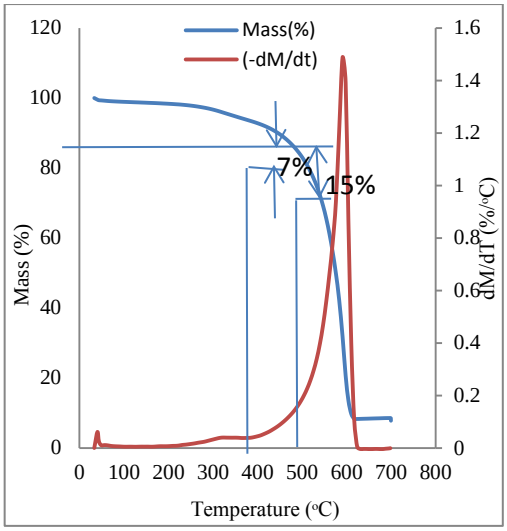

C1 C2

C1: Mass and mass loss rate for PM generated with B20 SME. Mass lost at 400°C is 8% and 14% at 500°C; C2: Mass and mass loss rate for PM generated with B40 SME. Mass lost at 400°C is 7% and 15% at 500°C

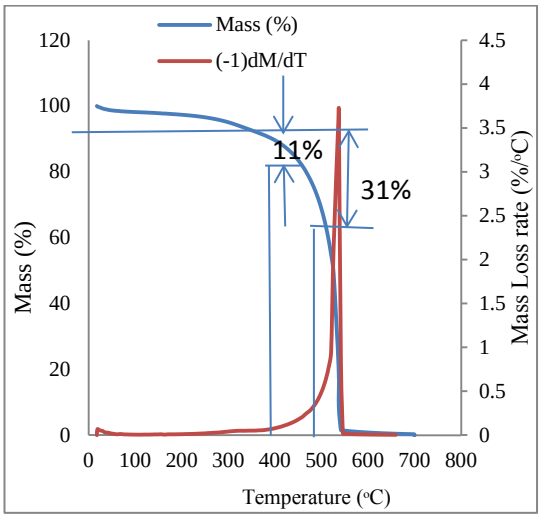

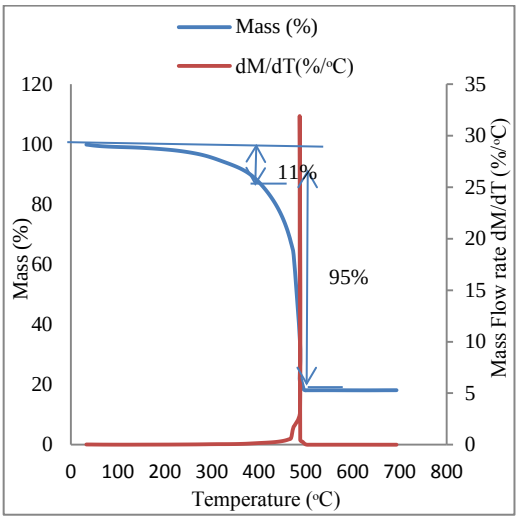

D1 D2

D1: Mass and mass loss rate for PM generated with B20 UCOME. Mass lost is 11% at 400°C and 31% at 500°C; D2: Mass and mass loss rate for PM generated with B20 UCOME. Mass lost is 11% at 400°C and 95% at 500°C

Figure 7.8 Mass and mass loss rate for PM generated with petrodiesel and blends of biodiesel

Table 7.5 Comparison of oxidation characteristics of PM generated from Petro, 20% and 40% biodiesel blends

A – Comparison with B20

Sample	Initial Mass (mg)	Initial Mass (%)	Mass after devolatilization (% @°C)	Mass lost @400°C	Mass lost @ 500°C	Residual Mass	Minimum Mass of PM oxidised (mg)
B(0) Petro	4.00	100	89@400, 79@500	11	21	0.00	4.00
B20 RME	4.713	100	90@400; 81@500	10	19	0.002	4.711
B20 SME	4.713	100	92@400; 86@500	8	14	0.338	4.375
B20 UCOME	4.151	100	95@300; 89@400; 69@500	11	31	0.00	4.151

B - Comparison with B40

Sample	Initial Mass (mg)	Initial Mass (%)	Mass after devolatilization %@ (°C)	Mass lost @ 400(%)	Mass lost @ 500(%)	Residual Mass (mg)	Minimum Mass of PM oxidised (mg)
B (0)	4	100	89.3 @400	11	21	0	4
B40 RME	5.462	100	94@400; 86@500	6	14	0.788	4.674
B40 SME	4.73	100	93@400; 85@500	7	15	0.369	4.361
B40 UCOME	5.442	100	96@300; 89@400; 0.48@500	11	99.5	0.963	4.480

Table 7.6A Estimated properties of biodiesel from their fatty acids compositions **(Peirce D. , 2015)**

Fuel	Density @ 20°C (kg/m³)	Cetane Number (kg/m³@20°C)	Viscosity (mm²/s @40°C)	Double Bond Number	Average main Chain Length
Rape seed methyl ester (RME)	879	54	4.3	137	17.94
Sunflower Methyl Ester (SME)	881	50	4.1	152.5	17.86
Used Cooking Oil Methyl Esther (UCOME)	878	55	4.3	127	17.81

Table 7.6B Biodiesel Structural properties evaluated with a Gas Chromatograph **(Peirce D. , 2015)**

Fuel	C16.0	C18.0	C18.1	C18.2	C18.3	C20.1
RME	4.5	1.5	60.5	21	11	1.5
SME	6.5	3.5	27	62.5	-	-
UCOME	10.5	3.5	48	32.5	4.5	1

Volatility

Although it is conventionally taken that petrodiesel is more volatile than biodiesel, evidence from differential boiling curve show that biodiesel has a narrow distillation temperature range at about 300℃. In comparison, petrodiesel has a wide possible range of distillation from 180℃ to 380℃ (Bhardwaj et al 2013A; Bhardwaj et al 2013B). The implication is that petro diesel may contain fractions with higher volatile points which could remain in the PM inner core and contributes to higher VOF as observed in the TGA oxidation profile at higher temperatures.

Cetane number

Similarly, biodiesel has a higher cetane number (Hansen, 1997; Lapuerta, M., Armas, O., and Rodrıguez-Fernandez, J., 2008; Bhardwaj et al 2013A; Bhardwaj et al 2013B; Jung H., Kittleson, D. B., and Zachariah, M. R., 2006), a property that enhances ignition quality thereby reducing delay in combustion. This has positive implication for PM emissions and has been linked to reduction in UHC (Monyem, A., Van-Gerpen, J. H., and Canakci, M., 2001). The cetane number of UCOME is highest among the three biodiesels tested and it may appear that observations made are contradictory however at 500℃, the PM oxidation was over 95% complete; this gave an unusual high oxidation rate, but by the same view may likely involved the presence of VOF fractions with high volatile points that could have been present in it; however many other reasons are superior.

The observation of decreasing trends in VOF reduction when the quantities of biodiesel blends were increased from 20% to 40% is same but did not give linear

relationship due to increase in quantity – Tables 7.5 (A & B). However it is plausible to consider that, surface characteristics like density, higher bulk modulus, speed of sound and viscosity is higher with bio diesel than petro diesel. These have been suggested to have effect on ignition timing in addition to higher cetane number of biodiesel. It was shown that shorter ignition delay led to reduction in UHC (Monyem, A., Van-Gerpen, J. H., and Canakci, M., 2001). Similarly it was shown that UHC emission is lower in biodiesel to which an oxidiser was added. This implies that the presence of peroxides as a consequence of biodiesel oxidation leads to reduction in VOF emission (Lapuerta, M., Armas, O., and Rodrıguez-Fernandez, J., 2008; Monyem, A., Van-Gerpen, J. H., and Canakci, M., 2001). These could explain the reductions in VOF witnessed in the use of B40 blends. The effect of the blend which could not be fully established at B20 increased to a threshold value with B40 where there could have been more peroxides, thereby decreasing the VOF more. As an extension, effect that could not be fully established at 400^{o}C was also possible when considered up to 500^{o}C. Summing up, the presence of oxygen in biodiesel and its physical properties has a cumulative effect of reducing VOF (attributed to UHC) content in the PM.

7.4.2.2 Investigation of oxidation temperatures of PM generated with B20 and B40 blends compared to PM from petro diesel

The oxidative reactivity of any combustible material is conventionally monitored with oxidation rate data as matter is oxidised. In all soot samples used in the test, the oxidised dry mass was more than 3.0mg – Tables 7.5 (A&B) which was a criterion that conforms to the minimal quantity optimised for determination of accurate oxidation characteristic temperatures, as defined in (Rodriguez-Fernandez, J., Oliva, F., and Vazquez, R. A., 2011) as follows:

(i) Starting oxidation temperature (SOT) signals the beginning of measurable temperature rise as oxidation commenced

(ii) Triggering oxidation temperature (TOT) signifies temperature of turning or inflection point on the mass loss rate curve, from where the oxidation rate becomes self-sustaining

(iii) Maximum mass loss rate temperature (MLRT) is the maximum temperature when oxidation rate is highest. In typical diesel soot, there could be two peaks giving first and second maximum, but from these samples, only one

peak is obtained. This is due to the engine operation on low load which gives more of premixed burning that diffusional burning (Chapter 5); and in addition, the samples were collected under steady operating condition

(iv) Final oxidation temperature (FOT) signifies the end of measurable heat release and in effect, the end of oxidation process.

Similarly, consideration for heating ramp of 5°C/minute was based on the same optimised study whereby it was observed that the soot sample contact time with air is reduced at high heating rate than at a lower heating rate; and increased contact time reduced oxidation temperature. The instantaneous mass and mass loss rate have been plotted as functions of temperature Figures7.9 (A-D). The summary of the characteristic temperatures as obtained is presented in Table 7.7 (A & B).

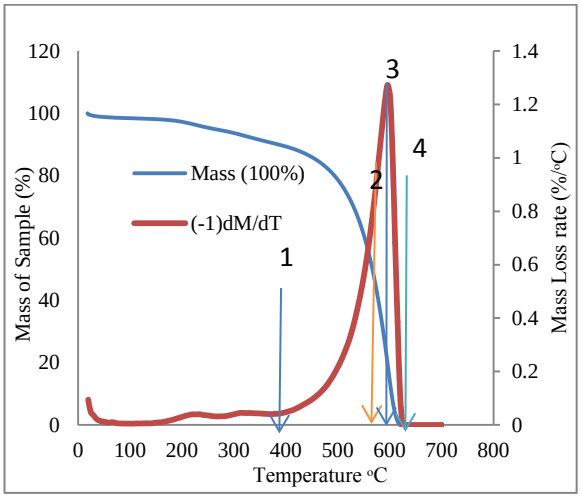

A:

Oxidation Temperatures for soot generated with petrodiesel; 1: Starting oxidation temperature (SOT: 400°C), 2: Triggering oxidation temperature (TOT: 580.5°C), 3: Maximum mass loss rate temperature (MLRT: 595.98°C), Final Oxidation Temperature (FOT: 615°C).

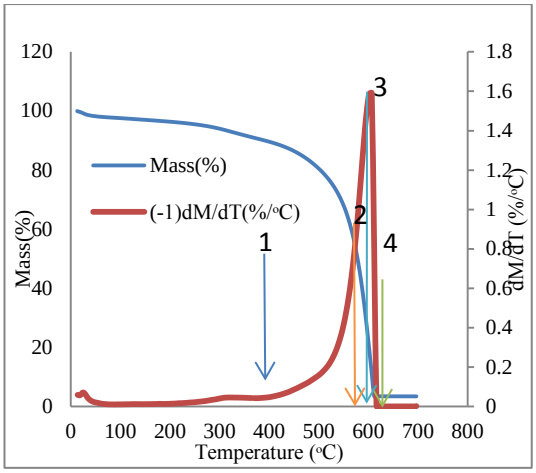

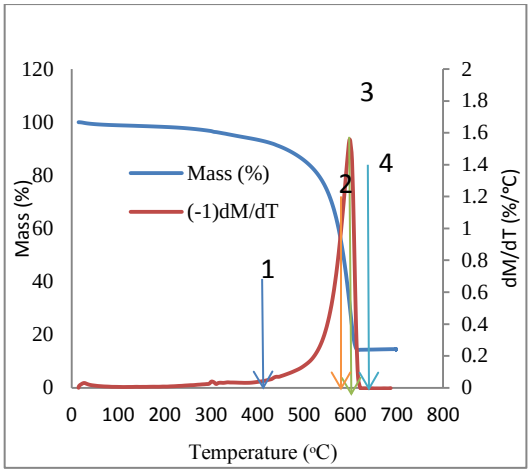

B1 B2

B1: B20 RME: Starting oxidation temperature (SOT: 409°C), 2: Triggering oxidation temperature (TOT: 586°C), 3: Maximum mass loss rate temperature (MLRT: 602°C), Final Oxidation Temperature (FOT: 616°C). B2: Mass and mass loss rate for soot generated with B40 RME at 9° BTDC, 800bar. 1: Starting oxidation temperature (SOT: 411°C), 2: Triggering oxidation temperature (TOT: 583°C), 3: Maximum mass loss rate temperature (MLRT: 600°C), Final Oxidation Temperature (FOT: 622°C)

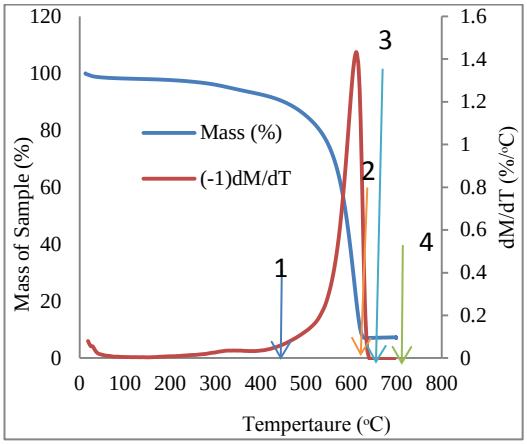

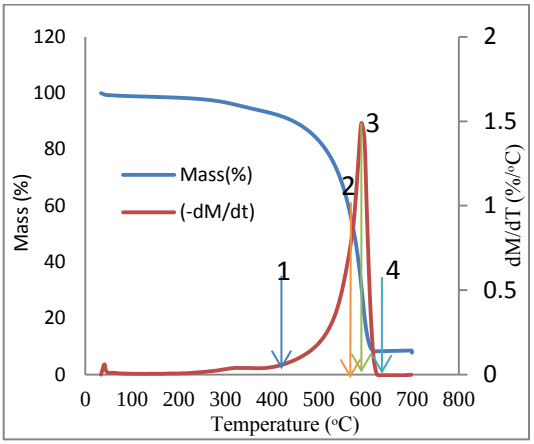

C1 C2

C1: Mass and mass loss rate for soot generated with B20 SME; 1: Starting oxidation temperature (SOT: 420°C), 2: Triggering oxidation temperature (TOT: 586°C), 3: Maximum mass loss rate temperature (MLRT: 611°C), Final Oxidation Temperature (FOT: 634°C). C2: Mass and mass loss rate for soot generated with B40 SME at 9° BTDC, 800bar. 1: Starting oxidation temperature (SOT: 413°C), 2: Triggering oxidation temperature (TOT: 583°C), 3: Maximum mass loss rate temperature (MLRT: 598°C), 4: Final Oxidation Temperature (FOT: 624°C)

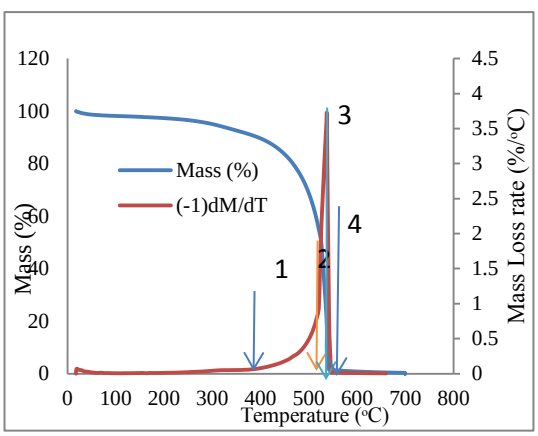

D1

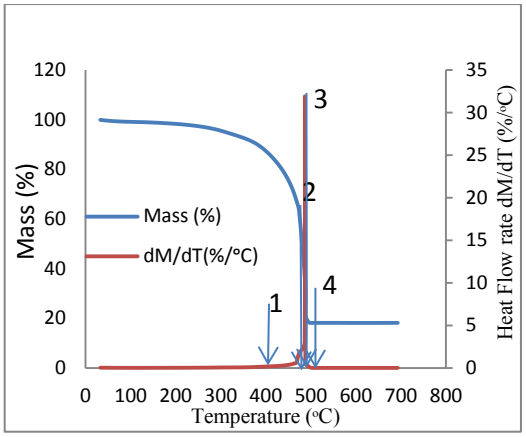

D2

D1: Mass and mass loss rate for soot generated with B20 UCOME at 9° BTDC, 800bar. 1: Starting oxidation temperature (SOT: 380°C), 2: Triggering oxidation temperature (TOT: 526°C), 3: Maximum mass loss rate temperature (MLRT: 537°C), Final Oxidation Temperature (FOT: 546°C). D2: Mass and mass loss rate for soot generated with B40 UCOME at 9° BTDC, 800bar. 1: Starting oxidation temperature (SOT: 372°C), 2: Triggering oxidation temperature (TOT: 487°C), 3: Maximum mass loss rate temperature (MLRT: 487°C), 4: Final Oxidation Temperature (FOT: 502°C

Figure 7.9 Plots of Oxidation Temperatures of PM obtained with petrodiesel and blends of biodiesel

Table 7.7A Comparison of Oxidation characteristics of PM

A - Comparison of PM generated from Petro and 20% Bio-diesel blends

Sample	**FOT (°C)**	**SOT (°C)**	**H (°C/min)**	**Oxidation Time (t_{ox})**	**TOT**	**MLRT [°C]**
B(0) Petro	624	190/400	5	44.8	581	596
B20 RME	616	280/420	5	39.2	586	602
B20 SME	630	300/420	5	42.0	586	611
B20 UCOME	546	380/400	5	33.2	526	537

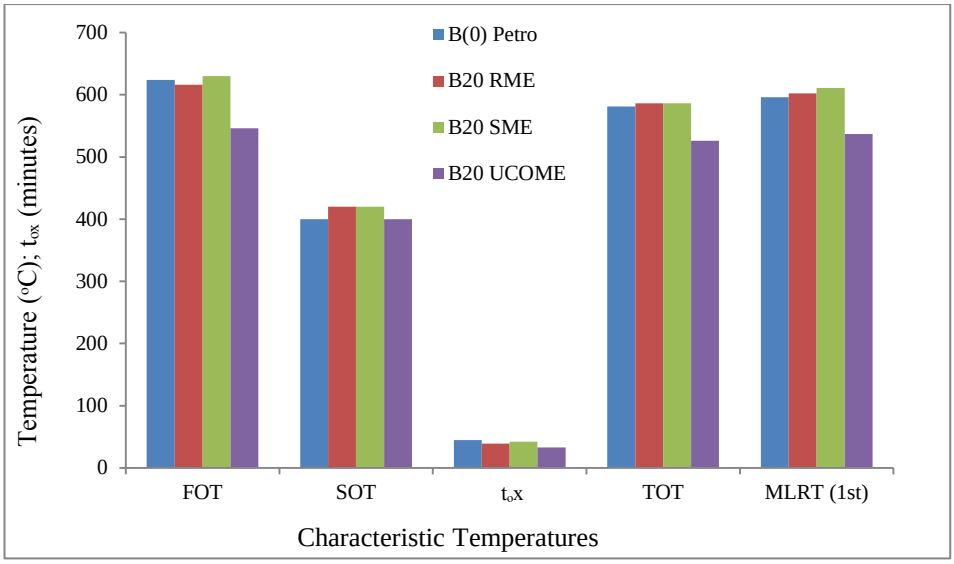

Figure 7.10A Comparative characteristic temperatures with B (20) PM

Table 7.7B Comparison of PM generated from Petro and 40% Biodiesel blends

Sample	FOT (°C)	SOT (°C)	h	t_{ox} (°C)	TOT (°C)	MLRT [°C]
B (0)	624	190/400	5	44.8	581	596
B40 RME	622	300/410	5	42.2	583	600
B40 SME	624	305/413	5	42.2	583	598
B40 UCOME	504	372	5	26	487	487

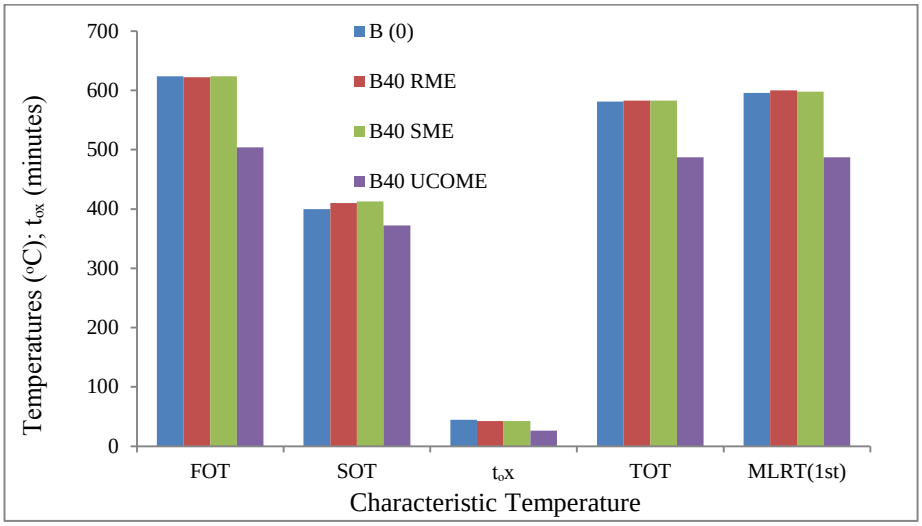

Figure 7.10B Comparative characteristic temperatures with B (40) PM

The effect of blending with 20% and 40% portions of different biodiesels on the oxidation characteristics of PM could equally be interpreted in line with the fuel properties. The starting oxidation temperatures for the blends significantly followed the trend observed with presence of VOF and have no linear effect due to increase in quantity. The effect of VOF could be seen to be momentary in the early part of the rate curves (Figures 7.8 and the first values of SOT – Table 7.7A) and real rise in rates were observed as from 400°C. The SOT of PM from UCOME was least, however using SME and RME as comparatives; similar observations are made as stated. The SOT due to VOF was lower in petro diesel compared to 20% blends of biodiesel. The final oxidation temperatures have no extrapolations but the time taken for oxidation to complete is slightly higher in PM from petro diesel than with B20 blends. The observation with B40 is similar in trends about SOT and FOT but with slightly lower values that are almost equal for RME and SME. Generally, the oxidation times are lower in soot with blends and the trigger oxidation temperatures are marginally higher (though slightly lower with increased blend) compared to petro diesel. The PM from biodiesel blends had similar but slight higher MLRT than petro diesel. In all these observations, the PM from blends of RME and SME show common trends in their oxidation characteristics. However, those from UCOME blends have remarkable difference, with low characteristic oxidation temperatures. This is ascribed to the bio diesel feedstock. It was sourced from prison kitchens waste cooking oils processed into clean biodiesel by 'Work This Way Oil Works' (Works). The chromatographic analysis in Table 7.6B shows that UCOME has more palmitic content [C16.0] than RME and SME and also comparatively lower in [C18.1] and [C18.2] respectively. It has been reported in (Knothe, 2006) that UHC emissions reduced with increase in chain length of biodiesel when methyl esters – lauric (C12.0), palmitic (C16.0) and oleic (C18.1) were used in a 6-cylinder engine. A plausible reason for the observation therefore is that RME and SME have reduced UHC due to more fractions with increased chain length compared to UCOME. It is reasonable to view that VOF in the PM from UCOME will have a narrower temperature window at which volatilization occur as this contributed to its fast oxidation. However the observation can be attributed more to the soot micro-structure (Vander Wal, R. L. and Mueller, C.J., 2006; Vander Wal, R. L., Aaron, T., and Tomasek, A. J, 2003). The implication is that PM with UCOME blends had late

starting oxidation temperature and quick burn out time. As reviewed in (Lapuerta, M., Armas, O., and Rodrıguez-Fernandez, J., 2008), some authors postulated that biodiesel feedstock has no effect on the UHC emissions (relevant to VOF) except on the use of pure esters. However in the work of (Rodriguez-Fernandez, J., Oliva, F., and Vazquez, R. A., 2011) oxidation of soot from pure biodiesel prepared from animal fat was used to compare soot oxidation from a reference petrodiesel and deduced that oxidation of soot from the biodiesel occurred at a lower temperature. Although the oxidation rate of the PM generated with UCOME is unusually high, it is viewed that since it was sourced from 'used kitchen oil', there is a likelihood of animal fat content leading more credence to our observation in its characteristic temperatures. Relevant to soot regeneration in engine application, the effect of biodiesel blending from these observations is significant only in the very small difference in oxidation time. This faster oxidation is related to the biofuel's natural faster reactivity than petro diesel due to other factors inherent in the chemical and physical properties.

7.4.2.3 Investigation of oxidation kinetics of PM generated with B20 and B40 blends compared to PM from petro diesel

The composite plots for instantaneous mass loss with temperature for B (0) compared to B (20) is shown in Figure 7.11, which strengthen the observations made in section 7.4.2.2. The trend was same for B (40) without tangible effect due to quantity increase. In addition to the characteristic temperatures, the Arrhenius kinetic parameters offer more understanding of the oxidation process of the PM. The model used to describe PM oxidation was given in equation 1 as:

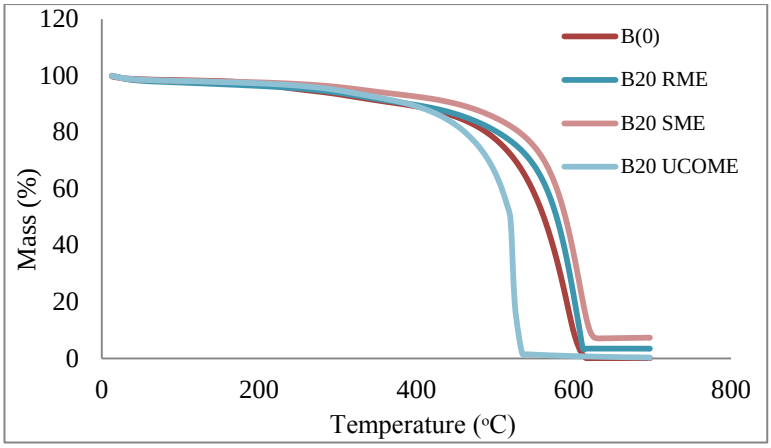

Figure 7.11 Instantaneous mass loss with B (0) PM compared to B (20) blends

$$-\frac{dm}{dt} = k_c m^n {po_2}^r = Aexp(\frac{-E_a}{RT}) m^n {po_2}^r \qquad 7.1$$

By taking logarithm of both sides, equation 7.4 is obtained.

$$\ln\left(-\frac{dm}{mdt}\right) = \ln(Apo_2) - \frac{E_a}{R}\frac{1}{T} \qquad 7.4$$

A plot of the left side of equation 7.4 versus the reciprocal of the absolute temperature is used to determine the slope which represents the term (E_a/R) from where the activation energy is derived knowing the universal gas constant. Typical Arrhenius plot obtained from B (0) PM is presented in Figure 7.12A. It could be observed that plot has two bands of oxidation regimes signifying oxidation periods due to VOF and soot. Each band is preceded by period of instabilities represented by zones 1 and 3, while the stable periods were zones 2 and 4 during VOF and soot oxidations respectively. In effect the parameters were determined during the stable periods in zones 2 and 4 as shown in Figures 7.12 B and C.

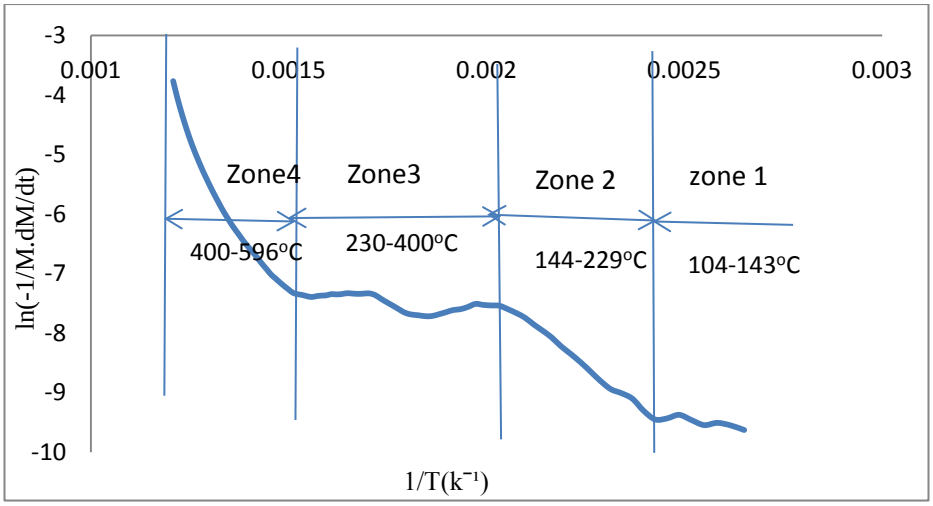

Figure 7.12A Oxidation (Arrhenius) plot of B (0) PM

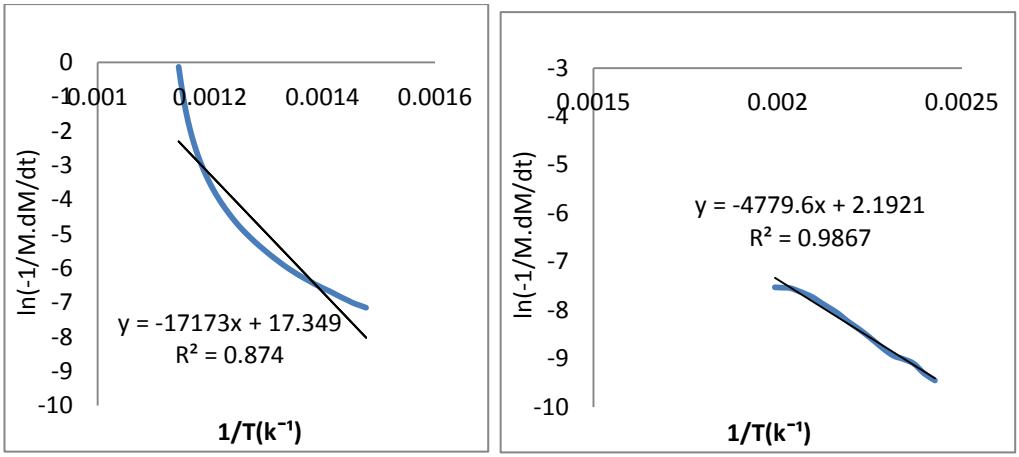

B C

Figure 7.12; B: Plot of stable soot oxidation; C: Plot of stable VOF oxidation from B (0) PM

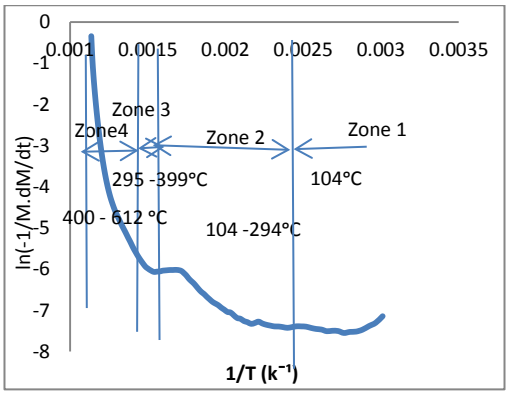

A1: B20 RME

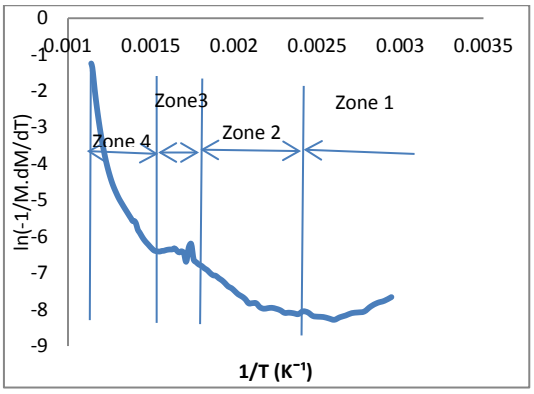

A2: B40 RME

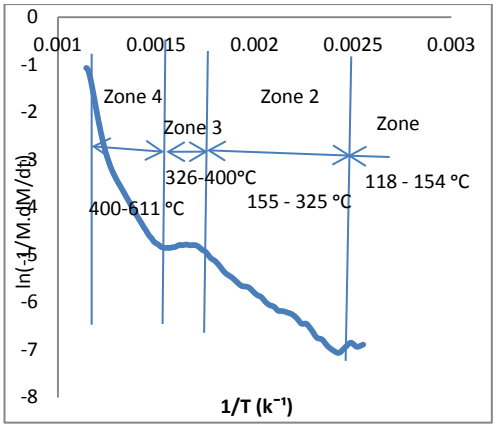

B1: B20 SME

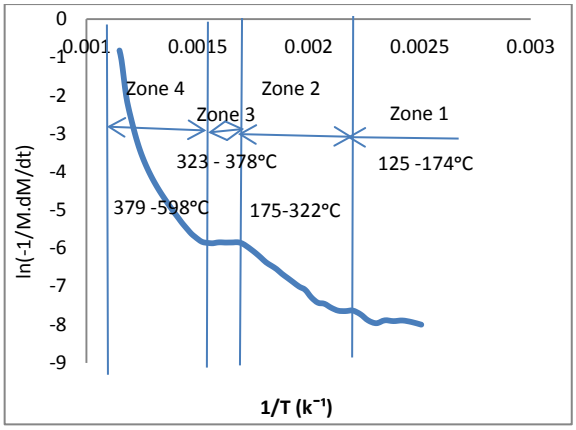

B2: B40 SME

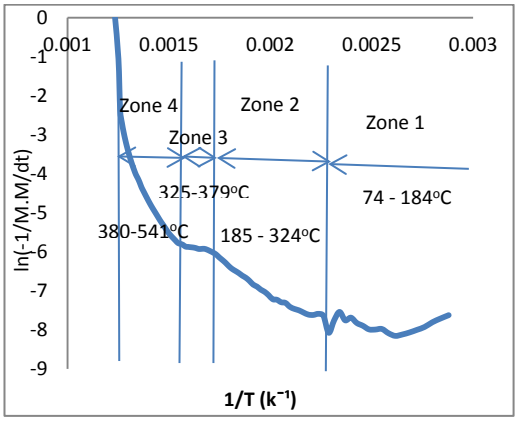

C1:B20 UCOME

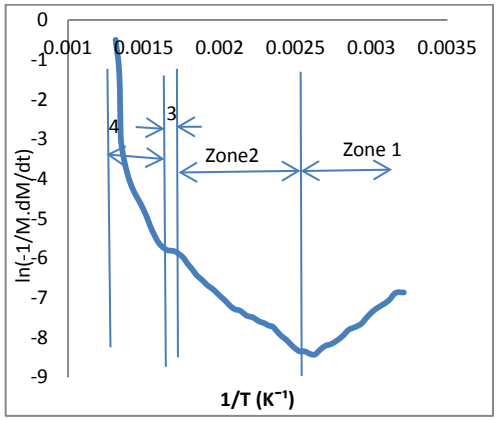

C2: B40 UCOME

Figure 7.13 Oxidation (Arrhenius) plot of A: B20 and B40 RME; B: B20and B40 SME; C: B20 and B40 UCOME

Table 7.8A1 Summary of the oxidation statistics with B20

Fuel Blend	Initial Mass (mg)	Mass at 400°C	Trigger Oxidation Temp (TOT)(°C)	Mass at TOT (mg)	Final Mass (M^f) (mg)	Mass of Dry soot ($M_{400} - M^f$)	% Mass of Soot Oxidised at TOT	% Mass of Soot Oxidised at FOT	% mass of Ash Residue
B (0)	4.00041	3.5738	581	1.50414	0.000230	3.573592	58	99.994	0.0
B (20) RME	4.71322	4.2249	586	1.95369	0.160690	4.064194	55.88	96	4
B (20) SME	4.71282	4.3637	586	2.48622	0.332784	4.030887	46.58	92	8
B (20) UCOME	4.15115	3.7194	526	2.04490	0.000591	3.718828	45.03	99.98	0.0002

Table 7.8A2 Summary of Arrhenius plot [ln (-1/M.dM/dt) vs 1/T (k^{-1})] Soot oxidation

Fuel Blend	Slope = E_a/R	Intercept: [ln(Apo_2)]	E_a = Slope* 8.314 (kJ/mol)	R^2	% of E_a with Petro diesel
B (0)	-17173	17.349	143	0.874	-
B (20) RME	-12.316	11.7.31	102	0.894	71.33
B (20) SME	-11.367	11.512	95	0.948	66.43
B (20) UCOME	-10.899	10.739	91	0.954	63.63

Table 7.8A3 Summary of the Arrhenius plot [ln (-1/M.dM/dt) vs 1/T (k^{-1})] for VOF oxidation

Fuel Blend	Slope = E_a/R	Intercept: [ln(Apo_2)]	E_a = Slope* 8.314 (kJ/mol)	R^2	% of E_a with Petro diesel
B (0)	-4.7796	2.1921	40	0.987	-
B (20) RME	-1.3105	-4.2554	11	0.8133	27.5
B (20) SME	2.9126	0.0	24	0.9889	60
B (20) UCOME	-3.466	0.1379	29	0.9909	72.5

Table 7.8B1 Summary of the oxidation statistics with B40

Fuel Blend	Initial Mass (mg)	Mass at 400°C	Trigger oxidation Temp (TOT) (°C)	Mass at TOT (mg)	Final Mass (M^f) (mg)	Mass of Dry soot ($M_{400} - M^f$)	% Mass of Soot Oxidised at TOT	% Mass of Soot Oxidised at FOT	% mass of Ash Residue
B (0)	4.00041	3.57382	581	1.50414	0.000230	3.573592	58	99.994	0.0
B (40) RME	5.46204	5.10230	583	2.86087	0.787849	4.314453	51.96	84.56	15.44
B (40) SME	4.72999	4.69662	583	2.01634	0.368819	4.327797	61.93	92.15	7.85
B (40) UCOME	5.44243	4.75965	487	1.84426	0.961948	3.797698	77.38	79.79	20.21

Table 7.8B2 Summary of Arrhenius plot [ln (-1/M.dM/dt) vs 1/T (k^{-1})] Soot Oxidation

Fuel Blend	Slope = E_a/R	Intercept: [ln(Apo_2)]	E_a = Slope * 8.314 (kJ/mol)	R^2	Difference of E_a between B20 and B40	% of E_a with Petro diesel
B (0)	-17.173	17.349	143	0.874	-	-
B (40) RME	-11.381	11.381	95	0.90	(-) 7	66.43
B (40) SME	-11.034	10.466	92	0.935	(-) 3	64.33
B (40) UCOME	-9.689	9.716	81	0.968	(-) 10	54.48

Table 7.8B3 Summary of Arrhenius plot [ln (-1/M.dM/dt) vs 1/T (k^{-1})] VOF Oxidation

Fuel Blend	Slope = E_a/R	Intercept: [ln(Apo_2)]	E_a = Slope * 8.314 (kJ/mol)	R^2	Difference of E_a between B20 and B40	% of E_a with Petro diesel
B (0)	-4.4496	2.1921	40	0.987	-	-
B (40) RME	-2.794	1.8223	23	0.965	(-) 17	57.5
B (40) SME	-3.783	0.4781	31	0.975	(-) 9	77.5
B (40) UCOME	-2.964	0.9057	25	0.983	(-) 15	62.5

The plots obtained from the blends are presented in in Figures 7.13 (A – C) and the summary of the comparative parameters during respective soot and VOF oxidations are presented in Table 7.8 (A & B). In addition to the oxidation behaviours for various blends presented above with reference to the physical properties (particularly the fuel oxygen contents and consequent VOF proportion in the PM), the starting oxidation temperature was not much different for PM generated from petro and blends of RME & SME but was outstanding for UCOME. Oxidation rates are synonymous to the activation energy needed to distort or even destroy intermolecular bonds of reacting species (reactants) into burnt products in the oxidisation process. As the PM is composed of different intermediaries of the fuel combustion products, it is inevitable that the PM oxidation followed different chemical reaction pathways which defined their activation energies as exhibited. In addition, the activation

energies obtained in oxidation of PM from various blends could partly be supplied through the energy release from earlier combustion of the VOF. Oxidation process is a progressive event owing to the soot internal structure as the differences in soot oxidation rates have been related to initial properties and the associated structural changes as viewed with high resolution transmission electron microscope (HRTEM) (Song, J., Alam, M., Boehman, A. L., and Kim, U., 2006). Similarly, the frequency of collision of the reacting species is another factor shaped by molecular bond and orientation. The values as presented in Tables 7.8A2 and 7.8B2 are in line with the other characteristics earlier considered according to the blend feedstock. The activation energy is least with PM from UCOME blends while the values obtained with RME and SME are quite close. There is marginal reduction in activation energy with increase in blend from 20% to 40% without a correlation. Compared to the activation energy of petrodiesel PM, it is obvious that the stronger argument for reduction in value will be in the soot microstructure than the VOF content as attested by many authors (Boehman, A. L., Song, J., and Alam, M., 2005; Bhardwaj et al 2013A; Boehman, 2013; Yehliu et al 2012; Chong et al 2013; Song et al 2006). This means, soot from biodiesel blends have greater rate of oxidation due to higher rate of structural transformation during oxidation and therefore will require less activation energy in the process. The soot generated from biodiesel fuels in many of the studies have been shown to exhibit amorphous and shorter microstructures that give rise to more reaction sites compared to soot from petro diesel. This has been linked to biodiesel high reactivity and reduction in activation energy. There is similarity in this regards with the results obtained here. The increase in reactivity depicted by lower activation energy values and minor reduction in oxidation times with biodiesel blends is viewed to be due to soot initial microstructure considered a key factor (which however did not give a linear correlation with increase in quantity), whereas same cannot be said of the VOF component where oxygen content is a strong factor. It was not feasible to conduct full image studies with devolatilized and heated diesel soot to compare results, however only images of the PM as generated were taken as presented in Appendix to chapter 7.

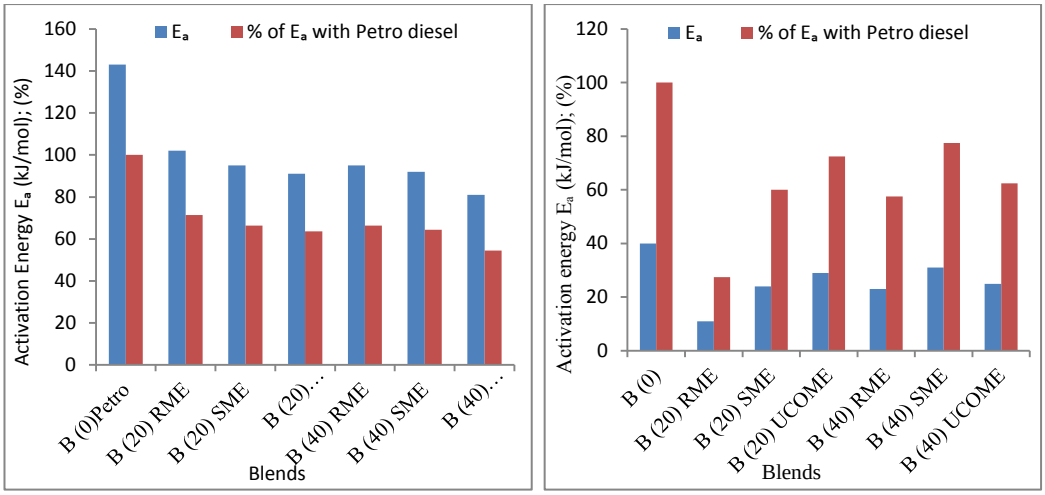

A B

Figure 7.14; Comparison of the Activation energy values for A: soot oxidation; B: VOF oxidation

The degree of material conversion is another pointer to the reactivity of biodiesel soot. However, rigorous extrapolation could not be made on this as some filter paper scraps of collected along with PM samples could not be quantified. Therefore percent of soot mass oxidised at final oxidation temperatures and those ash residues could not be correlated. Though this may limit the accuracy in deduction that could have been made with percent of E_a from the blends compared to with Petro diesel, it is however deductible that this decreased with increase in biodiesel blend in the different feedstock – Figure 7.15.

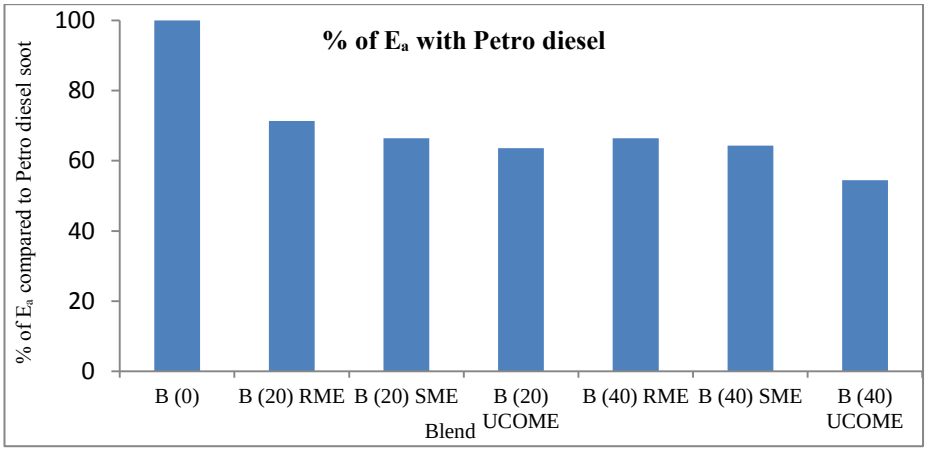

Figure 7.15 Comparative percent of activation energy obtained with petro diesel and blends

Relevant to regeneration, this implies that the energy required to burn PM generated with biodiesel blends is less than with petro diesel. This in effect, is the energy required to bring the PM to the trigger oxidation temperature where oxidation becomes self-sustaining and could impact on the total oxidation time which are slightly lower with biodiesel PM compared to petro diesel. This study therefore conclude that blending of petro diesel with biodiesel will improve the regeneration of diesel particulate filters and consequently reduce its back pressure compared to conventional petro diesel when engine is operated at the same condition.

7.5 Summary and Conclusion

(i) The kinetic parameters evaluated for the soot generated with petrodiesel is consistent with those published in literature.

(ii) The degree of devolatilization before oxidation affected the diesel PM combustion characteristics and its stability.

(iii) By implication, the PM oxidised by non-isothermal process exhibited lower values of activation energy. This is attributed to the contribution of the energy contributed by oxidation of VOF

(iv) The oxidation of PM with biodiesel blends is faster than that from petro diesel. When considered in line with some published works, this is attributable to two factors: - the oxygen content of the biodiesel which impacts on the oxidising quality and the microstructure which is more disordered in biodiesel and therefore provides more sites for oxidation event than the more orderly graphitic structures of petro diesel soot.

CHAPTER 8

MITIGATION OF PARTICULATE MATTER EMISSIONS USING FILTER TRAPS AND FEASIBILITY OF REGENERATING DIESEL PARTICULATE FILTER (DPF) USING MICROWAVE POWER

8.0 Introduction

Mitigation of diesel exhaust emissions with the use of DOC and DPF have become established after-treatment techniques in modern diesel engine technology. The DOC oxidises CO to CO_2, UHC to CO_2 and H_2O; while with the conventional wall flow DPF, particulate matter (PM) is trapped in the filter and gaseous species flow past the walls of the channels which are alternately closed at opposite ends. These devices can achieve 99% PM trapping efficiency and have enabled the PM emission bench-mark of EURO 6 standard to be met. In application, the technical issue that arises is the pressure drop (ΔP) across the DPF as it is loaded with PM, which prevents free flow of exhaust stream. It creates the need for prompt burn-off of the accumulated PM on the filter as threshold limit of ΔP is reached (Eastwood P. , 2001; Eastwood P. , 2008; Lemon, 2014; Murtagh, M. J., and Johnson T. V., 2014). In addition, the process of burning off the accumulated PM in the filter (regeneration) requires the DPF upstream surface be raised to the soot oxidation temperature of about 550^{o} - 600^{o}C for combustion to be initiated and sustained. A positive introduction of heat for this purpose demands additional energy input; and therefore, avenues are being sort to reduce such energy requirement. One of such avenue is the use of Microwave energy (An, H., Kilroy, C., McGinn, P. J., 2005; Palma et al 2010; Palma et al 2013; Palma et al 2015). In this chapter, the removal PM emitted by diesel engine using DPF is highlighted through measurement of particle number concentration at upstream and downstream of the DPF. Concurrently, measurement of the back pressure upstream of the DPF as PM builds-up was made. Afterwards, investigation on the use of microwave energy to study the feasibility of regenerating DPF was carried out. This was carried out for non-catalysed and for catalysed DPFs using an available multi-mode laboratory-scale microwave cavity.

8.1 Objectives

The objective of this chapter is to explore the feasibility of using microwave technology in the regeneration of diesel particulate filter. A wider interest is to incorporate this preliminary result into design of optimal system for investigation of possible energy savings in adopting the technique over current regeneration schemes in large marine engines. This is part of Marine Diesel Exhaust Gas Treatment System (MAGS), a joint project between Brunel University London and Innovate UK (Technology Strategy Board) No 42471-295209. The investigations carried out include:

Investigation of the back pressure build-up on exhaust line due to use of DPF.

Investigation of the effect of using DPF in reduction of PM from a diesel engine.

Preliminary test of DPF regeneration using laboratory-scale non thermal plasma reactor (NTPR) based micro-wave technology for catalysed and non-catalysed units.

From the results of the preliminary tests, design a model of optimal cavity to be used in the study DPF regeneration using MW energy for comparison with conventional resistive approach.

8.2 Methodology

The 2.0 litre HSDI Ford engine was used to generate PM at an optimised sooting condition of 80Nm/2000Rpm without EGR. The PM was trapped by a silicon carbide DPF and then taken to NTPR based microwave cavity for regeneration. Modification jobs were done on both the exhaust line and the MW cavity before they could be used.

8.2.1 Exhaust line and MW cavity modifications

The exhaust line was modified to accommodate the DPF supplied by Johnson Matthey. Typical dimension of the unit supplied is 182 cm length and 143cm diameter; it contains 49 channels per square centimetre or 289 channels per square inch. The channels are alternately plugged at opposite ends; therefore filtration of exhaust particles is through the walls of the channels as the exhaust gas flows (Twigg, M. V., and Phillips, P. R., 2015). It was placed in a steel canister with pressure sensors and gas measurement ports at the upstream and downstream of the canister. The pressure sensors are important as they were used to monitor back pressure in the exhaust line as soot was accumulated in the DPF. A limit of 500 milibar was set as the maximum pressure upstream of the DPF and was used as safety measure for the permissible level of soot accumulation before regenerating the DPF in order to prevent possible damage to the engine. On the upstream and downstream of the canister, ports are drilled and tapped for exhaust gas to be drawn for concurrent measurements of gaseous emissions using the Horiba Gas analyser, filter smoke number (FSN) using the smoke meter and the number concentrations using the Electrical mobility analyser. Other real time measurements were engine pressure data, exhaust temperature, fuel consumption, oil pressure, coolant inlet and outlet temperatures, air/fuel ratio and Lambda. Based on experience, these were used to monitor safe engine operating condition. The set-up is as shown in Figure 8.1A&B (make one picture). Initially, there were leakages from the top short section bearing the flexible pipe. This made it difficult to have reliable back pressure measurements. It was modified with a leak proof flexible pipe section and a low pressure gauge was incorporated upstream of the canister line to corroborate the readings obtained from the engine console. Afterwards, reliable back pressure measurements were achieved as the leakages got sealed off.

Modification was also carried out on the existing multi-mode microwave (MW) cavity. On a preliminary trial, there was large thermal loss due radiation to the cavity walls and also due to the sheer size of the cavity compared to the DPF.

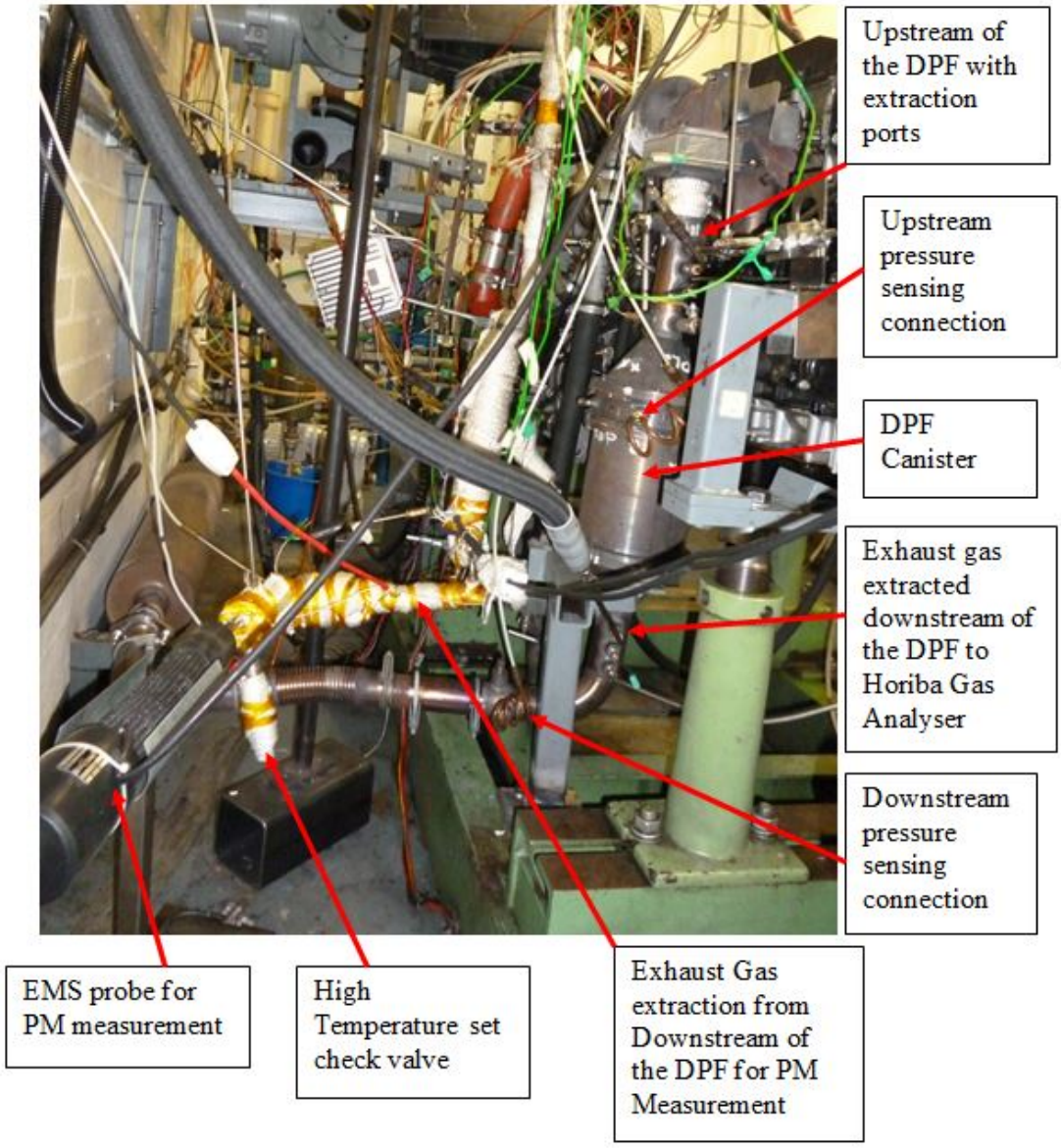

Figure 8.1A Modified engine exhaust line bearing the DPF canister.

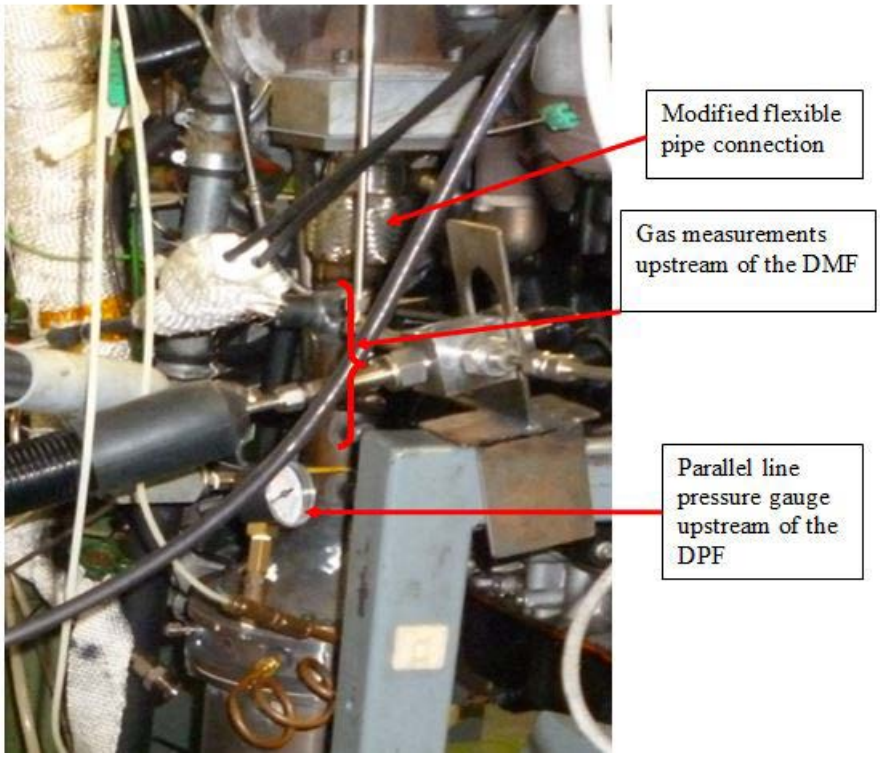

Figure 8.1B

A thermal insulating material (Fiberfrax Durablanket) that is susceptible to microwave irradiation was used to wrap inside the cavity in order to minimise thermal losses to the walls. The Durablanket insulator is made of 50% SiO_2 and 50% Al_2O_3 and the manufactures published that its thermal conductivity is below 0.15 W/m. K for temperatures up to 600 °C, which was sufficient for the temperature regime associated with DPF regeneration. In the tests, this material minimised formerly encountered heat losses and thereby improved the efficiency of regeneration. As conventional metallic thermocouples could not be used in a MW field it was a challenge to carry out real time temperature measurements. Infrared thermometer was used to measure only the DPF surface temperature on real time which was limited to 500°C; however a hole was drilled on top of the cavity and close with a high temperature masking tape for quick intermittent temperature measurements of the DPF when the magnetrons were switched off in the course of the regeneration.

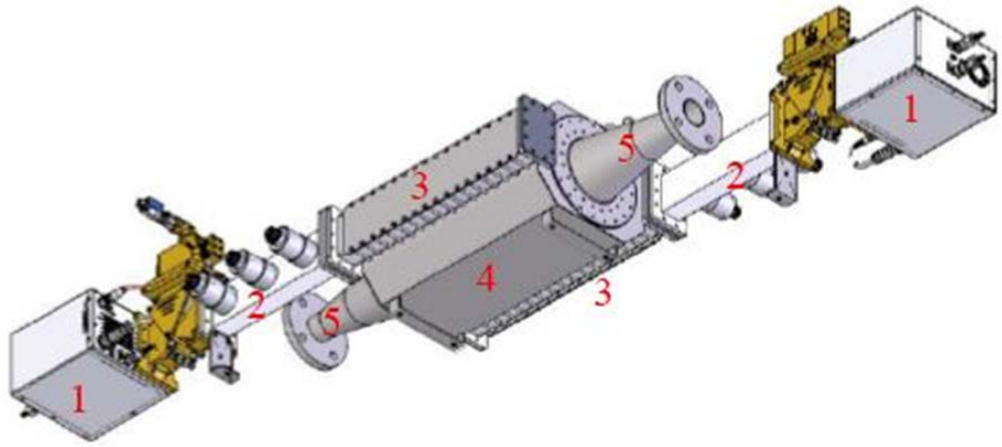

Figure 8.2A Schematic of the Multimode Microwave generation and Cavity

(1- Microwave generators (Magnetron, Isolator, Water cooling and MW power measurement); 2-Stub Tuners; 3- Waveguides; 4 -Multi-Mode Cavity; 5 -Gas inlet/outlet)

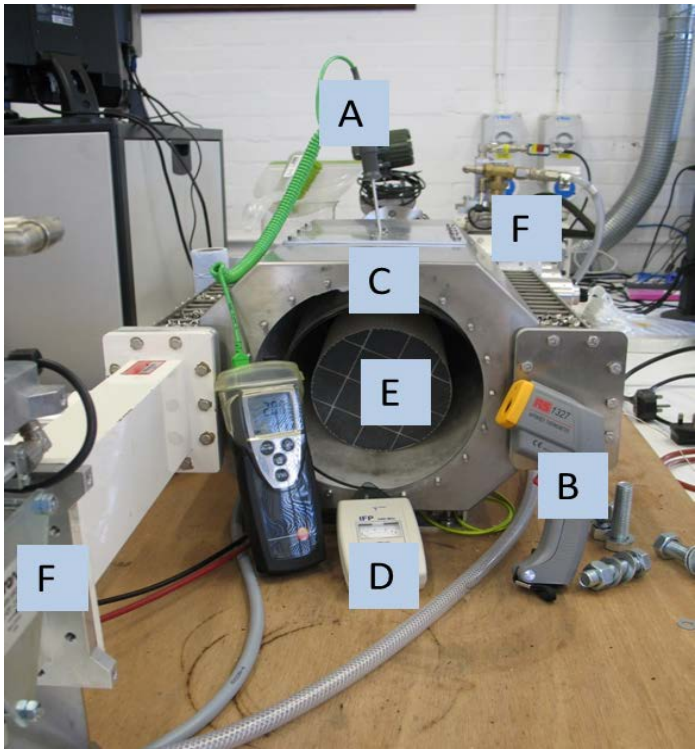

Figure 8.2B Microwave cavity opened to show insulated interior bearing the DPF.

A - Surface probe temperature measurement; B - Infrared temperature measurement (RS137); C - Microwave multi-mode cavity (insulated with Durablanket Insulator, Quartz tube + DPF); D- Microwave leak measurement; E- DPF positioned within quartz tube; F- MW sources

The schematic diagram of the multi-mode microwave cavity is shown in figure 8.2A while the open section of the cavity and the measurement accessories are shown in Figure 8.2B. The available MW cavity is fed by two MW magnetrons; each feed is deployed into the waveguide through 3-stud stub tuners. The microwave energy is then fed into the multi-mode cavity via six slots on each waveguides. Each magnetron can generate up to 2 kW of microwave power. Each magnetron has a dedicated controller, by which forward power and reflected power are monitored and controlled. Cooling water cooling is supplied to each magnetron for absorption of any reflected MW energy.

8.2.2 Loading of the DPF with PM

The scheme of loading the non-catalysed DPF with soot was done in the university's engine test cell while the loading of the catalysed DPF was done at CAMBUSTION (Cambridge), which has the facility for (non-engine) diesel particulate generation (DPG). The use of their facility to fill the catalysed unit was due to the low temperature involved in the operation of catalysed DPF as it can switch to continuous regeneration as from 270 ℃ if the catalyst light-off temperature is attained depending on the catalyst genre (Eastwood P. , 2001). The catalysed DPF was only used on engine to demonstrate the continuous regeneration mode when the catalyst light-off temperature was attained. In operation, the engine was set to the base line of 80Nm/2000Rpm, 800bar of injection pressure, 9^{o} BTDC and 0% EGR. However as there was no exhaust by-pass line during engine transient operation, exhaust emissions generated during start-up, idle and gradual loading times as well as waiting times for stable engine operation all passed through the DPF; so it is difficult to account for the PM loaded exclusively when the engine was running on steady condition. Similarly, it was not possible to de-green the filter before loading in the PM however meticulous back flushing of ash content with filtered air after each regeneration exercise was undertaken.

8.3 Results

The results obtained in the series of tests conducted are presented according to the observations made from monitoring the engine operations and regeneration of DPF using in the MW cavity.

8.3.1 Investigation of the effect of PM load on pressure drop across the DPF using a non-catalysed unit.

The pressure drop across the DPF due to build-up of PM is critical for continuous safe engine operation. This is conventionally regarded as exhaust back pressure in a relaxed scientific sense. The gas flow mechanics of the exhaust line is such that exhaust gas is driven by positive compression pressure of the engine, sufficiently high to overcome any obstruction along the exhaust flow line. In a strict sense therefore, the term 'back pressure' is more suitable to express the pressure drop across the entire exhaust line which is numerically equal to the exhaust pressure at the turbo (or exhaust manifold) outlet, not just the pressure drop across a component of the exhaust system (Jääskeläinen, 2007). The factors that contribute to pressure drop across the filter can be classified into four perspectives: the geometrical properties where the length, frontal area, wall thickness and channel dimensions are considered; the substrate material properties whereby the porosity, permeability and pore size are considered; the exhaust gas flow characteristics where the temperature, flowrate and viscosity are considered; and the nature of PM membrane, where the particle size distribution, density and permeability are considered (Eastwood P. , 2001; Murtagh, M. J., and Johnson T. V., 2014). These considerations are normally used to study pressure drop across DPF in both modelling and experimental efforts. With regards to engine operations, engine load and speed determines the exhaust flow rate whereby, increase in load and speed increase the pressure upstream of the filter (Stobart, R., and Wijewardane, A., 2011; Hinds, T., Twigg, M., and Gallinger, M., 2010; Bermudez et al 2012; Jaussi, 2008). As the engine was operated at constant speed variable load, the set engine speed is of significance. It was observed that at high speed of 2000Rpm, the upstream pressure increased fast during the transient period and also at a high rate after the operating condition was reached (Table 8.1). At a reduced speed of 1500 RPM, the upstream pressure was low at the same load (Table 8.2). The rate of increase was moderate at this speed as load was gradually increased. This observation was significant in managing the engine transient period which allowed for warm up and gradual load increase. Three engine speeds were compared as shown in Table 8.2 and in line with the manufacturer's guideline; the upstream pressure rise was limited to 500milibar which became the criterion for setting the limit of PM loading.

Table 8.1The trend of quick build-up of DPF upstream pressure at high speed (2000Rpm)

Engine operating conditions (Nm/Rpm)	**Time**	**DPF Upstream pressure P1(milibar)**	**DPF Downstream pressure P2(milibar)**	**Pressure drop (ΔP) (milibar)**	**Exhaust Temp. (^{o}C)**
Start	13.05	200	-	-	
N10	13.10	250	150	100	175
N20	13.14	250	150	100	215
N30	13.18	260	150	110	245
N40	13.22	280	160	120	283
N50	13.24	300	160	140	313
N60	13.27	330	170	160	348
N70	13.30	370	180	190	388
N80	13.34	410	190	220	426
N80	13.40	460	200	240	442
N80	13.44	470	210	260	450
N80	13.48	490	210	280	488

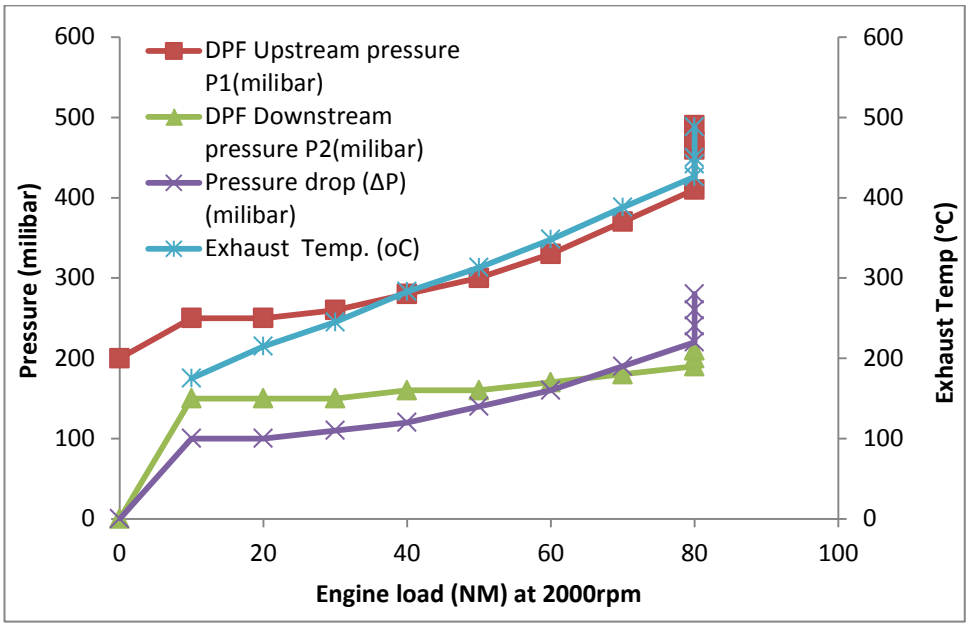

Figure 8.3A Exhaust line pressure conditions during transient loads and at full load of 80Nm/2000Rpm with non-catalysed DPF.

Table 8.2 Comparison of DPF upstream pressure build-up at three engine speeds: (1500, 1800 and 2000Rpm)

Engine operating conditions (Nm/Rpm)		Time (Hours)	DPF Upstream pressure P1(milibar)	DPF Downstream pressure P2(milibar)	Pressure drop (ΔP) (milibar)	Exhaust Temp. (°C)
Start		11.40	-	-	-	
Transient Period	10/1500	11.45	120	70	50	191
	20/1500	11.53	140	80	60	197
	30/1500	12.25	140	80	60	220
	40/1500	12.33	140	80	60	237
	50/1500	12.50	150	80	70	250
	60/1500	13.00	160	90	70	294
	70/1500	13.10	180	90	90	322
80/1500		13.25	190	100	90	356
80/1800		13.40	270	150	120	377
80/1800		13.50	340	170	170	392
80/2000		13.57	380	180	200	441
80/2000		13.58	400	200	200	443
80/2000		13.59	420	210	210	448
80/2000		14.01	450	210	230	450
80/2000		14.03	450	210	230	450

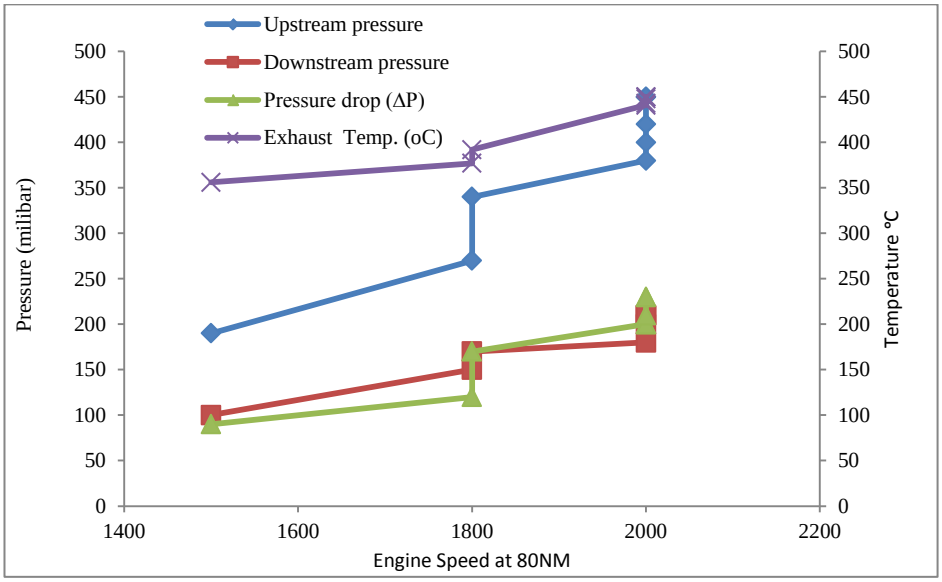

Figure 8.3B Exhaust line pressure conditions at different speeds with non-catalysed DPF

The pressure downstream of the filter is significantly different from that of typical automotive application which is usually close to ambient because the flow is on the same datum and without bends. In this set-up, three significant bends are present (Figure 8.1A): from the canister to the flexible pipe, from the flexible pipe to the muffler, and then the exhaust pipe is bent upwards and vented at the roof top outside. These bends and the additional column of about 5 meters to roof top, built up additional pressure downstream of the DPF. These factors contributed to discrepancy between this result and soot load calibrations of the filter manufacturer that loaded particulates from a setup where the inlet and outlet of the exhaust gases are on the same datum. In effect, these accounted for low quantity of soot captured from our set up, but were adequate for the experimental studies. The pressure drop is synonymous with PM load at a given time interval. In effect, Figures 8.3 (A and B) could have been better presented with respect to time or mass of PM however, it was not possible to isolate transient loads, and therefore extrapolation based on time will not be strictly correct. However, the pressure drop could still be inferred to follow typical ΔP vs Time and ΔP vs Mass plot as seen in Figure 8.4 A where parameters were properly measured with good instrumentation.

8.3.1.2 Loading the Catalysed DPF with PM

Two un-canned catalysed DPFs were sent to CAMBUSTION to be filled with PM using their Filter Test Housing (FTH) on the CAMBUSTION Diesel Particulate Generator (DPG). Prior to testing, the DPFs were de-greened in an oven for 2 hours at 700°C and afterwards loaded with 23.8g of PM. The flowrate used was 250kg per hour which yielded PM loading rate of 10 grams per hour at inlet temperature of 240 °C. The mass was confirmed by weighing the filters at temperatures greater than 200 °C before and after loading. The backpressure and filtration efficiency of PM measured in mass metric are as plotted in Figure 8.4A & B. Two units were filled with identification numbers 1575 and 1576 respectively, and they show identical loading sequence. Loading of a ‘de-greened’ DPF as in this case enables proper evaluation of filling characteristics at a stable engine operation. The plot has three characteristic regions on the ΔP vs Time or Mass. First is the period of filling the pores for a typical fresh DPF which is represented as the short period of sharp pressure rise in Figure 8.4A. The second is the period of blocking the pores

represented by the bent portion of the plot (prior to the linear portions). This subsequently gives way to cake formation period as the PM builds up.

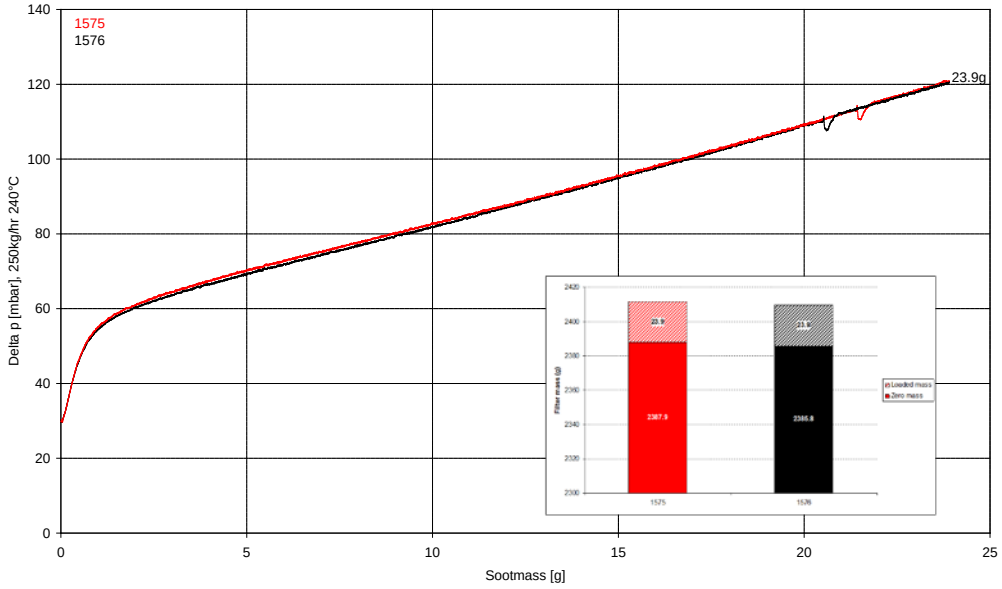

Figure 8.4A: Pressure drop due to soot load in the catalysed DPF using diesel particulate generator (DPG) as supplied by Cambustion**.**

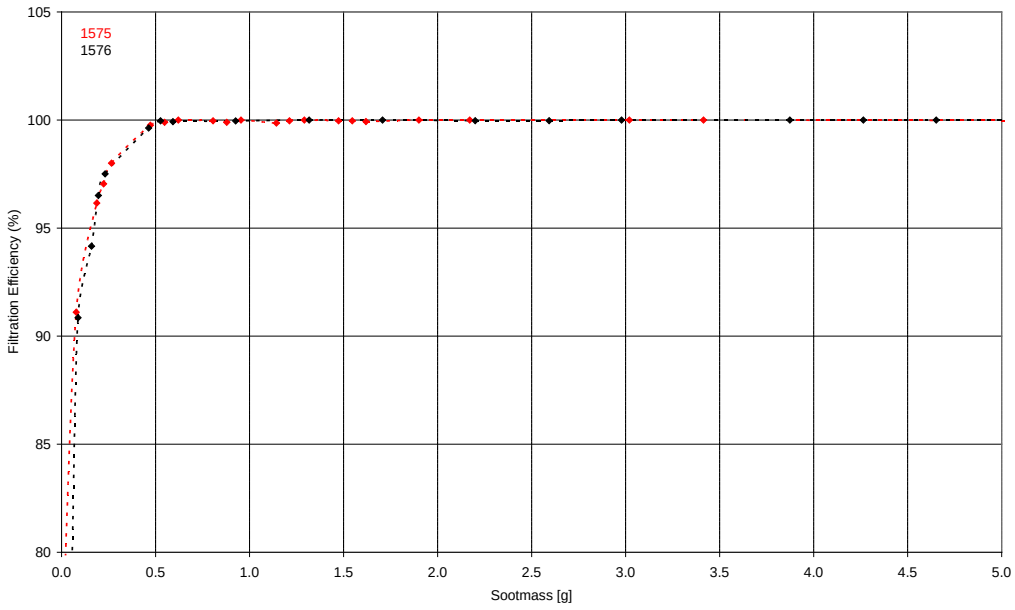

Figure 8.4B: The efficiency of soot filtration with the catalysed DPF using diesel particulate generator (DPG) as supplied by Cambustion**.**

8.3.2 Investigation of the effect of using DPF in reduction of PM from a diesel engine

Particulate emission is currently regulated in particle number metric – Table 3.1. To investigate the efficiency of PM reduction, the particle number concentrations (PNC) were measured using the electrical mobility spectrometer at an optimised dilution ratio of 16.4 at the upstream and downstream sides of the DPF. The PM was collected using the set up described in chapter six at temperature measures ranging from 530 -550 ^{o}C, and transferred via the mixing tube diluter maintained at 400 ^{o}C without any primary dilution and measurement after dilution with the EMS system maintained at 300 ^{o}C. A typical result obtained at the upstream and downstream of the filter is shown in Figure 8.5 A., while the efficiency of PM filtration based on the instrument scanning diameters is presented in Figure 8.5 B. It is seen that particles greater than 40 nm were all trapped by the DPF while some particles less than 30 nm passed through the filter.

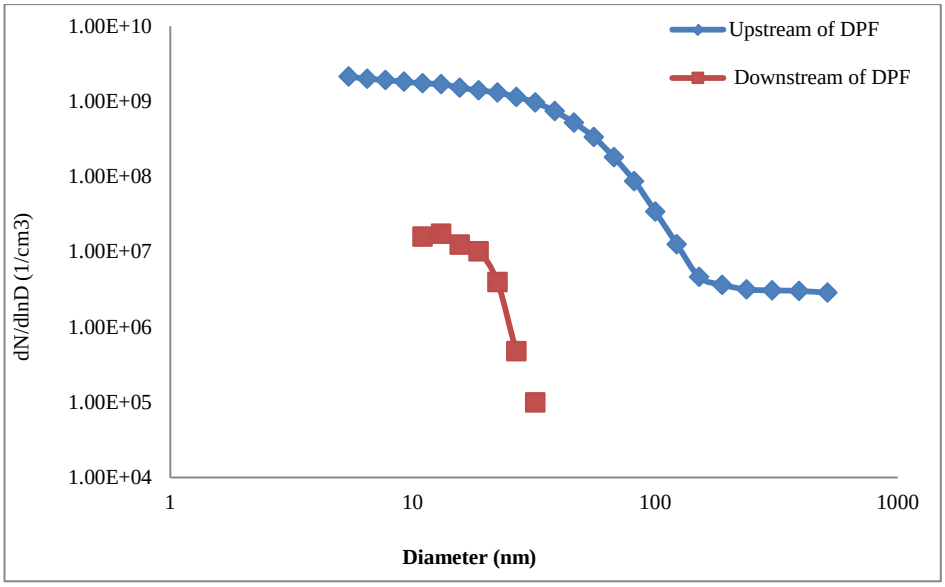

Figure 8.5A: Particle number concentrations (PNC) at the upstream and downstream sides of the DPF showing total trap of particle sizes from 30nm.

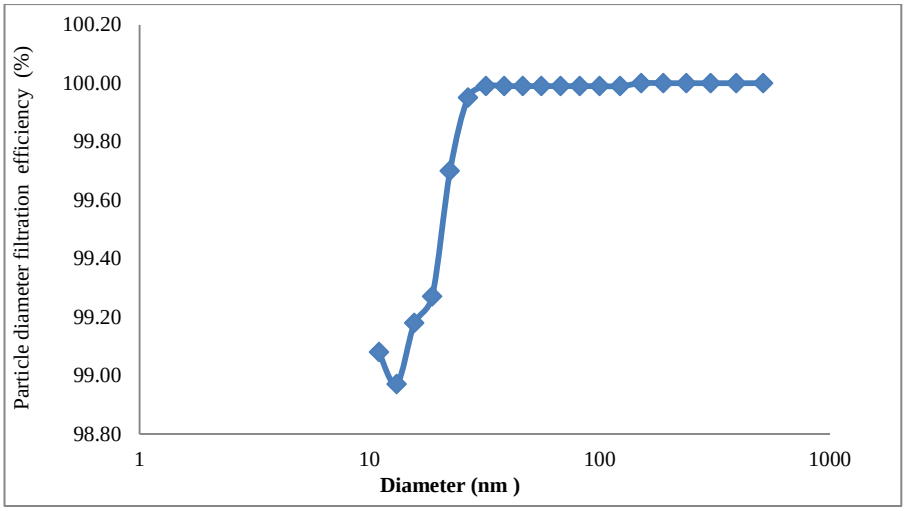

Figure 8.5B: Efficiency of PM reduction by DPF by particle number concentrations

The sub 30 nm particles are known to be the nucleation mode particles which are condensates of volatile matter; while the particles greater than 40 nm could be regarded as those that likely have solid soot particle at the core upon which volatile matter adsorbed. A clear sharp increase in efficiency was obtained from 13 nm reaching 100% from 40 nm. This result is corroborated with simultaneous measurement of filter smoke number which gave average of 1.88 and 0.04 at upstream and downstream respectively – Figure 8.6.

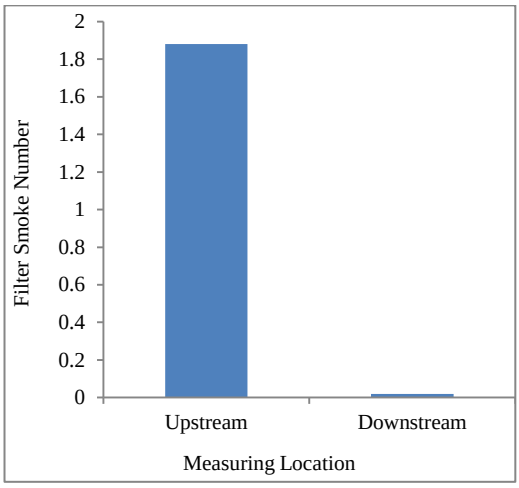

Figure 8.6 Filter Smoke number up and downstream of the DPF.

8.4 DPF regeneration using laboratory-scale non thermal plasma reactor (NTPR) based micro-wave technology.

The aim of studying regeneration DPF in diesel engine is aimed at reducing energy and operational demands while avoiding thermal runaway to ensure filter integrity. Conventionally, engine PM is known to burn from 500 ℃ to 600 ℃ by taking reference from oxidation of pure soot devoid of volatile organic components (VOCs) and could be reduced with the aid of catalyst. Developments in the adoption of after-treatment technologies in diesel engines have been generic due to the distinct requirements of the various species emitted. The current state of technology in automotive application is a composite train consisting of the following units (Majewski, W. A. and Khair, M. K., 2006; Lemon, 2014):

i. Oxidation catalyst that convert carbonaceous gases into their full oxides
ii. DPF that traps and continually burn soot in the presence of a catalyst if the light-off temperature is attained.
iii. A Reductant to decompose NOx into NO or N_2.

The objective of this section is to regenerate DPF using the Microwave energy for both catalysed and non-catalysed versions. Temperature is an important factor in the regeneration process, therefore dosing the DPF substrate with catalyst is aimed at lowering regeneration temperature. The first set of experiments was performed to characterize the thermal profile of the DPF (without any soot) within the microwave cavity. The MW regeneration tests were then performed for both catalysed and non-catalysed DPF filled with soot. The following sub-sections present the details of these experiments and results.

8.4.1 DPF Heating Measurements

The measurement of DPF temperature within the microwave field could not be done with conductive probe while in operation in order to avoid changing the field pattern and electric discharge at the tip of the probe. The schematic diagram of the experimental facility used for soot regeneration is shown in Figure 8.2. Therefore two temperature measurements were made at regular intervals. Surface temperature

probe (with thermocouple) was used to measure the DPF through the small hole of about 10 mm diameter, located top of the cavity intermittently when the microwave was switched off. The second one was non-intrusive infrared (IR) temperature measurement through the opening of inlet pipe to the MW cavity as shown in Figure 8.7. These temperature measurements were performed at regular intervals when MW was switched off for a short period (<30 s). From them, an indication of the actual DPF temperature was estimated.

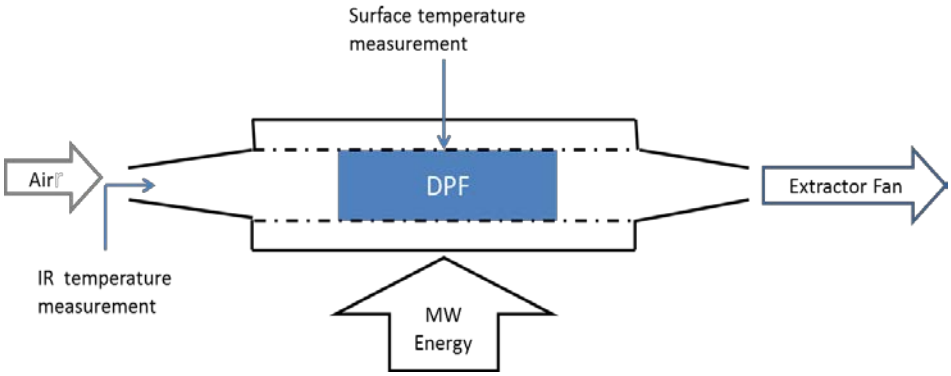

Figure 8.7 Concept of DPF temperature measurements in the cavity

The experimental matrix initiated to study the DPF thermal profile during microwave heating at various power supplies and gas flow rates is shown in Table 8.3A. The gas flow rate was controlled using the extractor fan speed. The flow rate was estimated by measuring the air flow through a 55mm diameter pipe using an anemometer. Since higher fan speed implies more energy requirement for heating air mass at the expense of heat supply to DPF; the fan speed was initially well reduced to the extent that it only enabled draft from indoor to outdoor. This was tested with a 'skin-thick' tissue membrane to monitor the direction of flow. In this way, more MW power was available to initially heat-up the DPF. Successive trials were made and eventually limited to two gas flows and three MW power ratings as presented in Table 8.3 B. The summary of results is presented in Table 8.3 C.

Table 8.3A: Proposed Experimental matrix for DPF heating

Fan Speed (Hz)	Flow rate (~l/s)	Microwave Power (W) 1000	1500	2000
10	3.7			
20	12.3			
40	18.5			

Table 8.3B: Matrix if Experiments performed during DPF Heating

Fan Speed (Hz)	Flow rate (~l/s)	Microwave Power (W) 1000	1500	2000
10	3.7			
20	12.3			

Table 8.3C: DPF heating summary results

MW power (W)	Air flow (l/s)	IR Temperature measurement (°C)	Time taken (min)
1000	3.7	280	55
1500	3.7	306	55
1980	3.7	460	65
1980	12.3	430	60

The results of these measurements are shown in Figure 8.8 which indicates that the DPF temperature becomes steady after about an hour. There is significant difference between the temperatures measured from IR and thermocouple sensors, and the values depended on the combinations of the MW power applied and the air flow rate. These heating values are taken as indicative since temperatures must have been quite higher than measured as was inferred when PM was successfully regenerated. The results show that DPF heating was not homogenous in the multi-mode cavity.

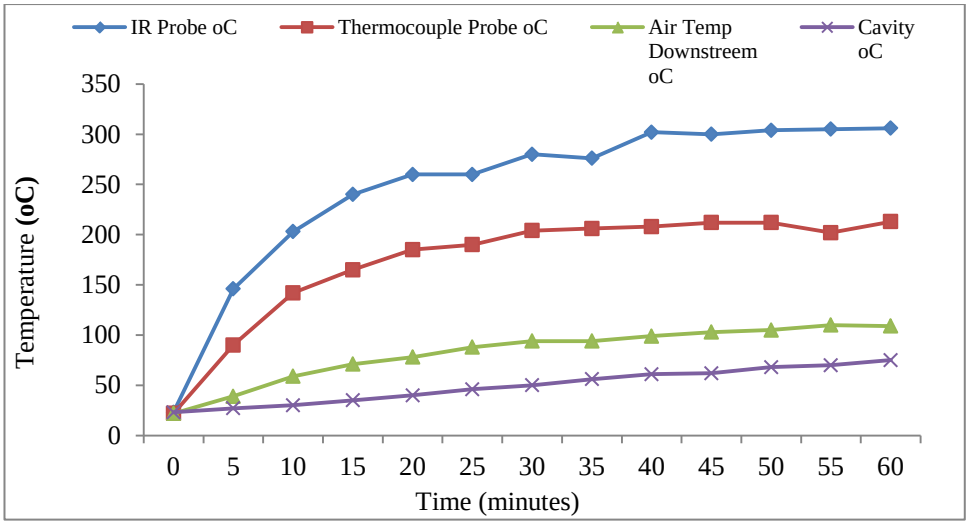

A: 10 Hz, 1.5kW {Air flow ~ 3.7 (l/s)}

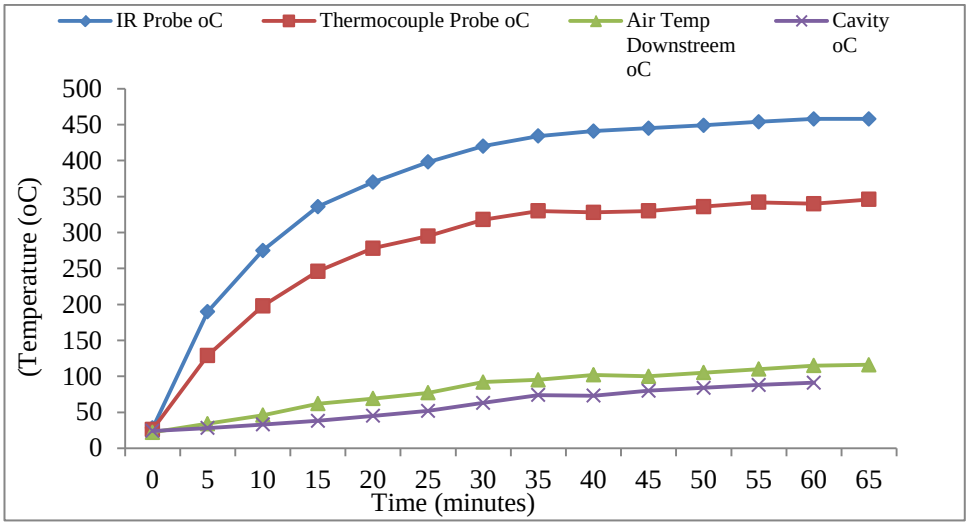

B: 10Hz, 1.98 kW {Air flow ~ 3.7 (l/s)}

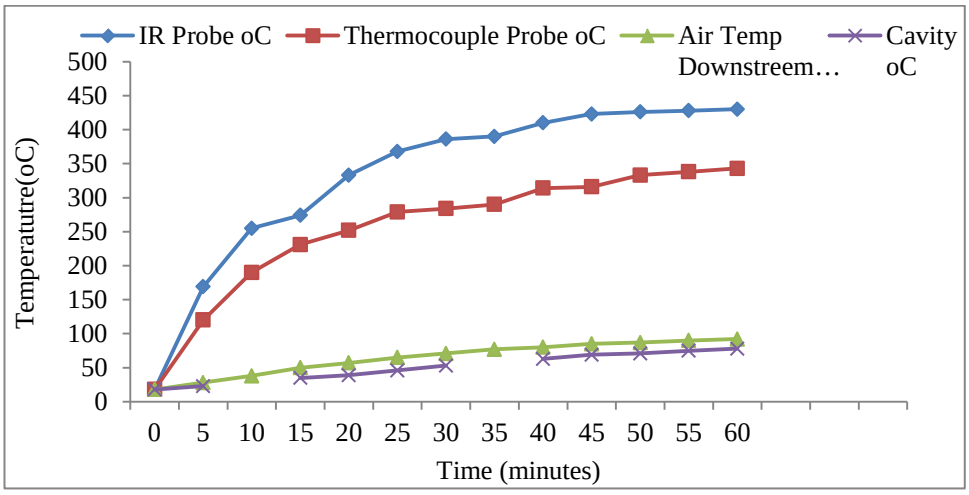

C: 20Hz, 1.98 kW {Air flow ~ 12.7 (l/s)}

Figure 8.8 DPF heating profile against time for various MW power and air flow rate

8.4.2 DPF Regeneration

The results obtained from the DPF regeneration for both catalysed and non-catalysed units are presented in this section. Measurements made during the regeneration tests include: mass of fresh DPF (M_{dpf}), mass of filled DPF (M_{dpf_pm}), mass of regenerated DPF (M_{dpf_regen}), MW energy supplied for regeneration (power × duration), temperature of DPF during regeneration at regular intervals and air flow rate into the cavity. PM removal efficiency was calculated as the percentage of the mass of PM removed (M_{dpf_pm} - $Mdpf_{\_regen}$) to the mass of the PM captured in the DPF (M_{dpf_pm} - M_{dpf}). The mass measurements were done on a high sensitive weighing scale (KERN ems), with scale up to 6000 grams and a resolution of 0.1 gram. Successive trials were also made by dwelling on the insight gained by heating ordinary DPF in the cavity, but there was no effective regeneration when the DPF was place along the flow axis of the cavity. However regeneration of PM became effective when the DPF was placed in a cross-flow direction making it to face the slanted slot through which MW energy is deployed into the cavity. A careful observation inside the MW cavity on the left side of Figure 8.9 shows the slanted slots. The soot filled face of the DPF is directly opposite and very close to the slanted slots (2mm width and slanted at 19 °C to horizontal) through which microwave energy is launched into the cavity from the waveguide; thereby ensuring maximum exposure of MW power to the side of DPF filled with PM. The top side of the insulation material (susceptible to MW irradiation) was purposefully removed to show the slant (inside the cavity). The DPF was similarly wrapped with the insulation material to help contain the thermal energy within the DPF substrate thereby reducing thermal radiation from it.

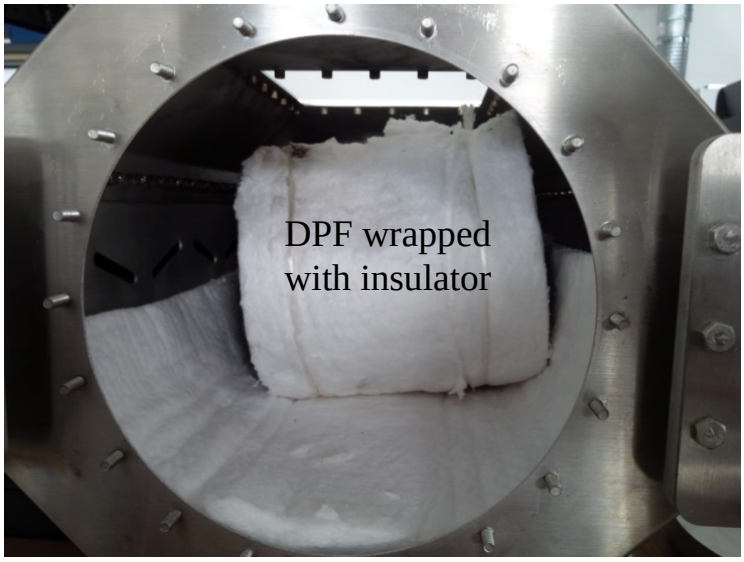

Figure 8.9 Non-catalysed DPF inside the MW cavity

In line with the matrix used to heat ordinary DPF, the MW power and flow combination that gave successful DPF regeneration during preliminary trials is as in Table 8.4 and Figure 8.10 shows the DPF before and after regeneration, showing complete soot removal.

Table 8.4 Regeneration matrix

Fan speed (Hz)	Flow rate (~l/s)	Microwave Power (W)		
		1000	1500	2000
10	3.7	-	-	
20	12.7	-	-	

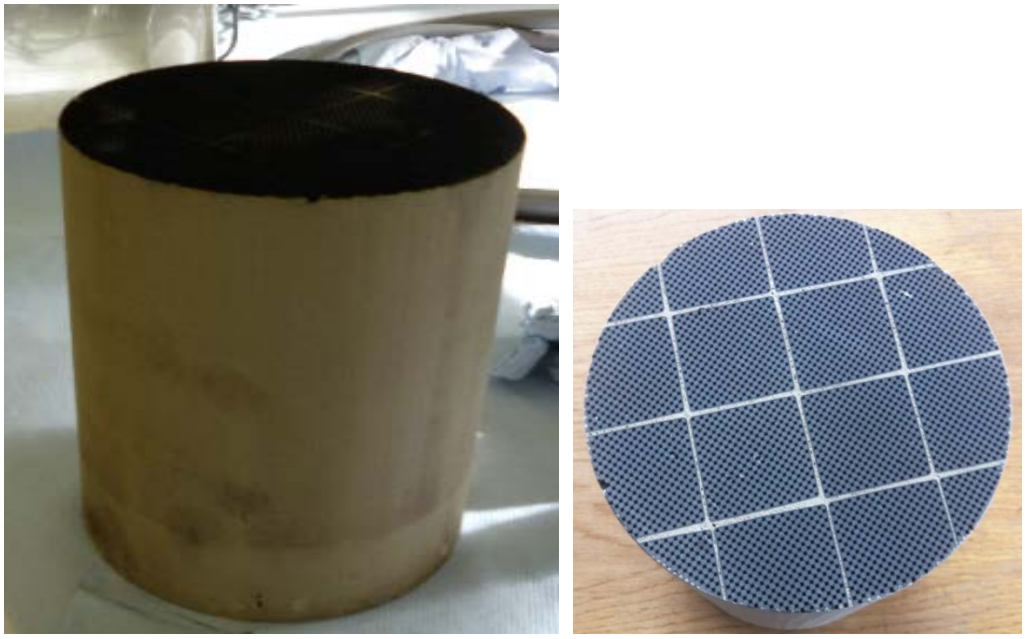

A B

Figure 8.10 SiC DPF, A: Filled with PM; B: Clean surface after successful MW regeneration

8.4.2.1 Feasibility results on regeneration of non-catalysed DPF

The temperature required to achieve regeneration of non-catalysed DPF is taken to be from about least 550℃ to 600℃. This projection was made from the oxidative studies of chapter 7 and as commonly regarded for diesel soot. Preliminary tests were done to determine the times taken for warming up (to raise the DPF temperature to 550 ℃) and to burn-off the PM for the un-insulated cavity and insulated cavity when 2000 W MW power was used. During this experiments 9 grams soot were removed in each case. It is clear from the results that insulation improved the efficiency of regeneration. Simple evaluation shows that, the cavity without insulation had regeneration efficiency of about 5% while with insulation, it was about 20%, a great improvement by factor of 4. There was very low utilisation of MW power directly on the DPF due to non-homogeneous distribution of electric field within the multimode cavity and also, the cavity material itself (stainless steel) is a large thermal sink conducting away substantial portion of the heat energy radiated to it by the DPF. However the real efficiency of soot regeneration using this technique is only properly evaluated with consideration of these loss factors.

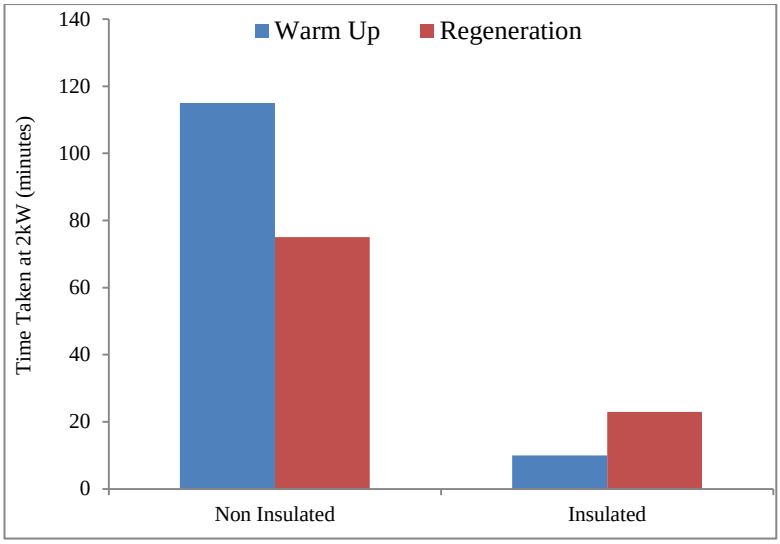

Figure 8.11 DPF Regeneration results with and without insulation

The second sets of experiments were carried out to understand the heating duration/ final temperatures against the removal PM with the fully insulated cavity. The results are tabulated in the Table 8.5.

Table 8.5 DPF (Non-catalysed) regeneration test results

	MW power (W)	Time from beginning of heating/ regeneration (minutes)	Temperature reached (°C)	Fan frequency (Hz)	Mass of PM removed (g)	Efficiency of regeneration (%)
Test 1	1500	28	260	10	3	13
Test 2	1500	29	310	10	1.8	7.8
Test3	1980	30	370	10	0	0
Test4	1980	40	>550	0	1.3	7
Test5	1980	40/10	>550	0 (before 40 min)	14.5	90
Test 6	1980	40/10	>550	20 (after 40 min)	6.3	90

Test one carried was out for 28 minutes where the temperature of 260 °C was reached and only 3 g of PM removed. This minor loss in mass was attributed to vaporization of VOCs at the prevailing temperature. Tests 2 further removed 1.8g of PM while test 3 did not record any weight loss despite the increase in power that achieved higher temperature. This demonstrated that all the volatiles had been

removed but as the temperature was still below 550°C, soot could not oxidise. In the Test 4, the extractor fan was switched off and the temperature reached required 550 °C, but there was no air flow through the DPF and therefore oxidation reaction that took place would have only used air previously in the cavity. Although no significant amount of soot was removed, insight was gained on the approach to reach regeneration temperature. Based on this, Test 5 produced interesting result as the PM was completely removed. DPF was first heated for 40minutes to bring the temperature above 550 °C without air flow as indicated by the IR probe. Air was then introduced for another 10 minutes and DPF fully regenerated. During this process 14.5 g of soot was removed. Test 6 is a repeat of test 5 with another DPF that had only 6.3 g of PM and again the DPF was fully regenerated. With these results, the feasibility of microwave regeneration was established.

8.4.2.2 Comparative of DPF regeneration using the microwave cavity: (estimates from electrical heated oven)

Rigorous analytical evaluations of energy efficiency cannot be pursued from the feasibility results obtained so far due to many unknowns associated with cavity size, accurate air flow rate and heat loss to cavity walls. . However in order to get a fair characterisation of the microwave power used for regeneration, compared to the power utilisation from electrically heated furnace from known technical specifications, the experiment was repeated based on the insight gained. The same Silicon carbide DPF was loaded with PM on the same engine operating condition. Empty mass of the DPF was 1830g and filled mass was 1847.9g, giving a PM mass of 17.9g. The model of electrical furnace from the range of Carbolite furnaces suitable for the size of PDF in use is BWF 11/13 (Carbolite). The chamber is electrically heated and air flow is vented through a chimney as soot is oxidised. The air flow scheme of the furnace is shown in Figure 8.12 and technical data from the manufacturer that gives enough insight towards estimating the heating requirements is as in Table 8.6.

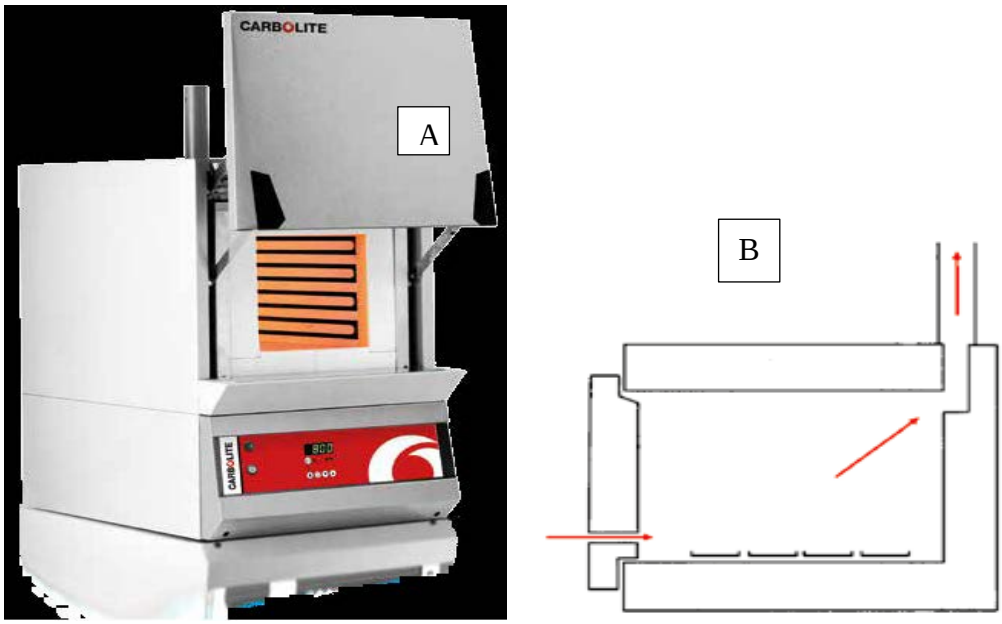

Figure 8.12 Carbolite Furnaces (A: Model BWF 11/3), (B: Air flow in model BWF)

Table 8.6 Technical data for BWF Carbolite Furnace

Model	Max Temp (^{o}C)	Heat-up time (mins)	Max continuous operating temperature (^{o}C)	Internal dimensions HxWxD (mm)	Volume (Litres)	Max Power (W)	Holding Power (W)	Thermo-couple Type
BWF11/13	1100	115	1000	200x200x325	13	3	1200	K
BWF12/13	1200	130	1100	200x200x325	13	3100	1500	R

The holding power is measured at continuous operating temperature meaning that if the furnace is comparatively heated by 2KW power as in microwave, shorter heat-up time will be obtained not 115 minutes as in the table. This will take about 69 minutes to heat up the empty chamber to 1000˚C. If it is further assumed that heat-up rate is constant in time, a linear ramp will take about 41 minutes to heat empty furnace chamber to 600˚C from ambient condition of 15˚C. It then means that additional energy is needed in time to heat up the DPF if placed in the furnace. This can be estimated from the properties of DPF in Table 8.7 using a suitable simulation

program that considers proper geometry of the DPF and flow model in porous media (Yamamoto, K., and Nakamura, M., 2011) but not presently pursued.

Table 8.7 The properties of DPF

	Material	Mass of DPF (kg)	Specific heat capacity (j/kg K)
Catalysed DPF	SiC+ catalyst (unknown)	2.39	750
Non-catalysed DPF	SiC	1.83	750

Comparatively, the DPF bearing PM mass of 17.9g was regenerated in the microwave cavity, wrapped as previously described; air flow rate was indirectly estimated using its flow speed in a pipe of 56mm internal diameter (measured with a hand held anemometer) and approximate air density of 1.2 kg/m³ at ambient condition as in Table 8.8.

Table 8.8 Estimates of air flow rates as measured by extractor fan speed
[Tube diameter: 56mm; Tube Area: 0.246dm²; Flow = m/s x 0.246 x 10 = Flow (l/s)]

Drive Hz	Flow m/s	Flow l/s	Flow (l/hr)	Flow rate (Kg/hr)
10	1.5	3.7	13320	15.984
20	5	12.3	44280	53.136
30	7.6	18.7	67320	80.784
40	10	24.6	88560	106.272
50	13.5	33.2	119520	143.424
60	16	39.4	141840	170.208
66	19	46.7	168120	201.744

In line with the preliminary effort, 2 kW microwave energy was launched into the cavity and air flow rate of 10Hz (which implies ~16kg/hr) was flown for 30minutes before microwave was switched off. Quick surface measurement with temperature probe gave 410°C and DPF was allowed to cool and was re-weighed. It was found that 18.04% of the PM was reduced as in Table 8.10. Then the cavity was reheated for 35 minutes without air and microwave momentarily switched off for quick

surface probe-temperature measurement which gave 511°C. Then microwave was re-switched, and cavity heated, spots of mild orange-coloured glow on the DPF insulator wrap could be seen from the cavity window (by the 40th minute) and air was introduced at the speed of 20 Hz representing ~ 53.14kg/hr. The increase in air flow was purposeful in order to ensure better air draft through the DPF channels as it was placed in a cross-flow position inside the cavity as explained; and this continued for 10 minutes before the microwave was shut off and the DPF allowed to cool and was re-weighed. Final weight showed that only 0.3g of PM was left in the DPF which could qualify as ash content. This means that 98% of the PM was burnt off within this process and time. Although a platform of equal energy supply to the two regeneration schemes was not established, a reasonable (at least qualitative) comparison could be deducted. This is presented in the discussions.

Table 8.9 Mass of PM burnt off

Time (minutes)	Mass 'MC' (g)	% Reduction in PM 'MC'
0	17.9	100
30	14.67	18.04
40	0.3	98.32

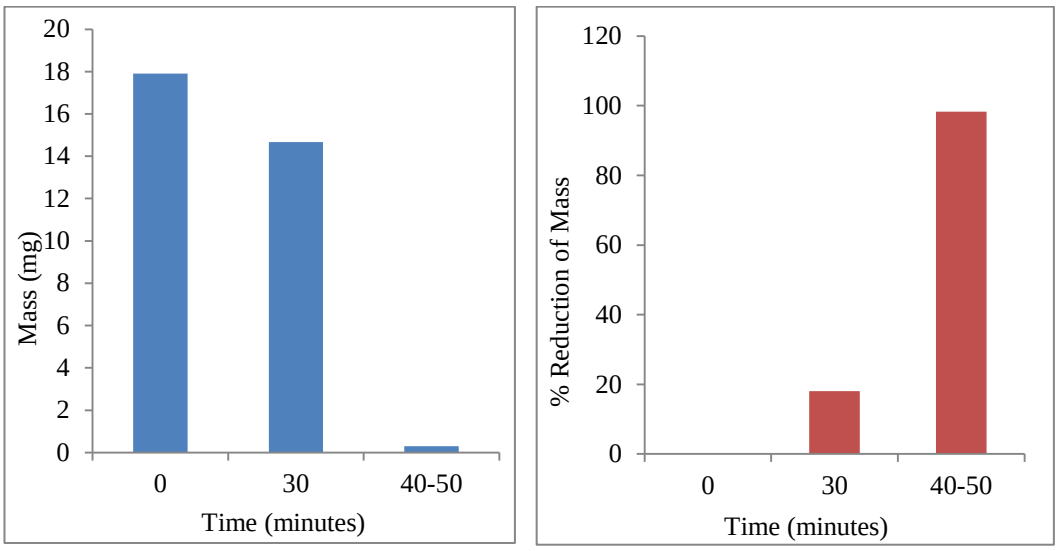

Figure 8.13 Percent of PM burn-off in the microwave cavity

8.4.2.3 Regeneration of Catalysed DPF

As highlighted in section 8.4.0, current after-treatment technology for mitigation of diesel exhaust emissions employs catalysed DPF in the train. The sole aim is to lower the temperature needed for PM regeneration. The peculiarity of mitigating diesel exhaust emissions requires appreciation of the diametrically opposed conditions for removing NOx and Particulate Matter (PM). Somehow, oxidation catalysts made a come-back in the diesel sector upon realisation that NO_2 is itself an oxidiser for PM combustion which in the presence of some precious metals (catalysts) enables PM oxidation to occur at lower temperatures (Eastwood P. , 2001; Eastwood P. , 2008; Majewski, W. A.; Khair, M. K., 2006; Murtagh, M. J., and Johnson T. V., 2014). In principle, when considering PM mitigation, there is no concurrent interest for NOx reduction; and for NOx mitigation, no consideration is made for PM. This demands that another technique is needed for mitigation of NOx after handling PM. With this separate approach, it becomes convenient to employ oxidation catalyst ahead of DPF where NO is converted to NO_2, which then becomes an oxygen carrier for particulate oxidation, and leaves the DPF again as NO. Conversion of NO depends on the space velocity over the catalyst (Eastwood P. , 2001). At low space velocity, the formation proceeds via:

$$NO + \frac{1}{2}O_2 \rightarrow NO_2 \quad \text{.....8.1}$$

And at high space velocity via:

$$2NO \rightarrow NO_2 + \frac{1}{2}N_2 \quad \text{.....8.2}$$

Then particulate (elemental carbon or soot) combustion proceeds via:

$$NO_2 + C \rightarrow NO + CO \quad \text{.....8.3}$$

The above studies demonstrated that:

(i) Soot oxidation virtually ceases when NO is not available in the feed-gas, even if oxygen was present.

(ii) Soot oxidation can continue just as effectively if NO_2 is substituted for NO.

(iii) Platinum catalysts are known to be active for conversion of NO to NO_2 in the temperature regimes of interest.

As currently applied, catalysed DPF runs on continuous regeneration and the factor for this continuous operation is merely the attainment of the catalyst light-off temperature.

8.4.2.4 Bench Test regeneration of catalysed DPF with application of MW

With the above hindsight, a small diesel generator set (2 kW), which can produce NO concentration up to 440 ppm and NO_2 concentration of about 90ppm at exhaust flow rate of 15 l/s when operated at medium load, was used to supply exhaust gas containing the NOx to regenerate catalysed DPF. The setup is shown in Figure 8.14. In addition to the temperature measurement, gas concentration of NOx was measured using Testo 350 potable gas analyser. Figure 8.15 shows the NOx concentration of the exhaust gas from the generator set piped into the regeneration cavity. One of the catalysed DPF filled with soot from Cambustion DPG was placed inside the quartz tube 'in-line' with the exhaust flow from the 2 kW generator-set. Initially the MW cavity with DPF alone was heated using 2 kW power (without the exhaust from the small gen-set) to enhance rapid heating until the temperature of the DPF (surface temperature from the top as done before) reached ~300 °C. Then the gen-set and extractor fan were switched 'on' and the exhaust gas was passed through the DPF for another 20 minutes to investigate the soot burn-out with expected NO_2 converted from NO as oxidiser in the presence of the DPF catalyst. The temperature profile of the DPF during the test is shown in Figure 8.16A. The DPF temperature reached ~ 300 °C in 15 minutes and when the exhaust from the gen-set was introduced, temperature dropped for few minutes before it rose back to about 300 °C in another 15 minutes. The reason for drop in temperature was due to lower temperature of the exhaust gas (~145 °C) compared to DPF.

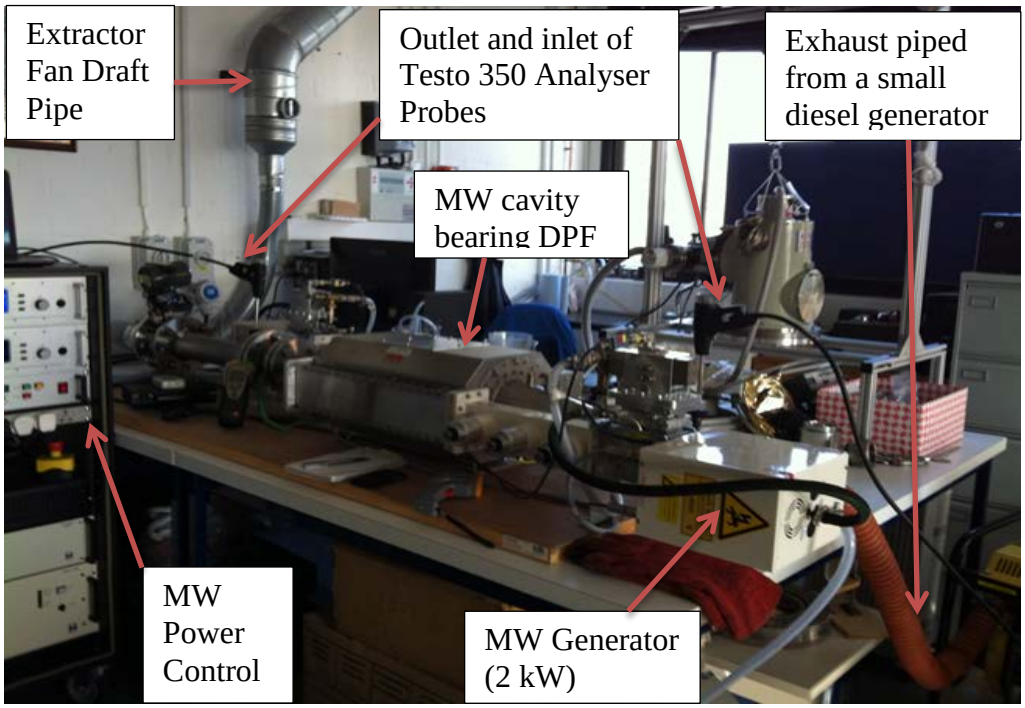

Figure 8.14 Layout of the set-up for MW regeneration of catalysed DPF.

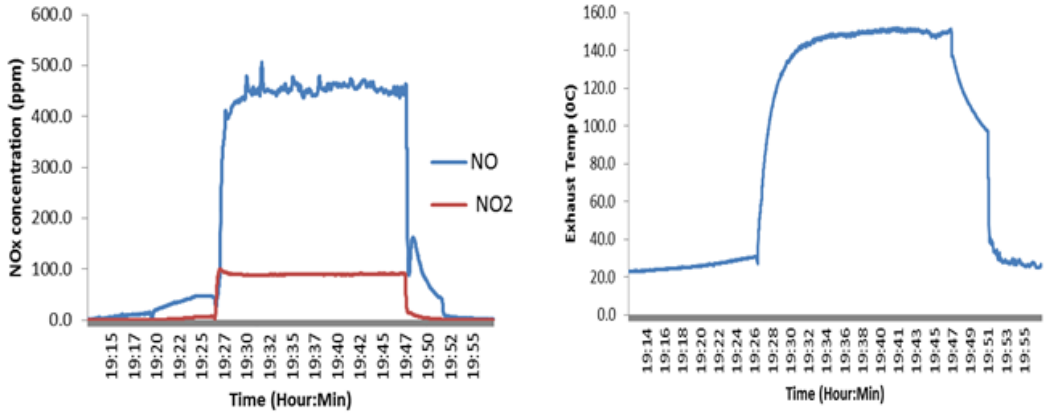

(a) NOx concentration (b) Temperature

Figure 8.15 Exhaust gas condition.

Within five minutes of regeneration (from time 30-35 mins) 10 g of soot was removed, which is approximately 44% of PM trapped in the DPF. At this point regeneration was stopped due the blockage of exhaust gas flow downstream of the DPF along the pipe ducting to extractor fan. The safety mesh was clogged with fluffy debris arising from the insulation material and blocked the flow. The mesh was cleaned and flow through the duct was restored. The experiment was repeated and similar result was achieved with removal of 11.75 g or 55.92% of total PM trapped.

Thus complete regeneration was achieved and the temperature and time profile is shown in Figure 8.16B. At this point the objective of low temperature regeneration of the catalysed DPF was achieved with the set-up which utilised the whole exhaust output from the small gen-set. It was then decided to also test the continuous regeneration mode on engine bed presented in the next section before discussions.

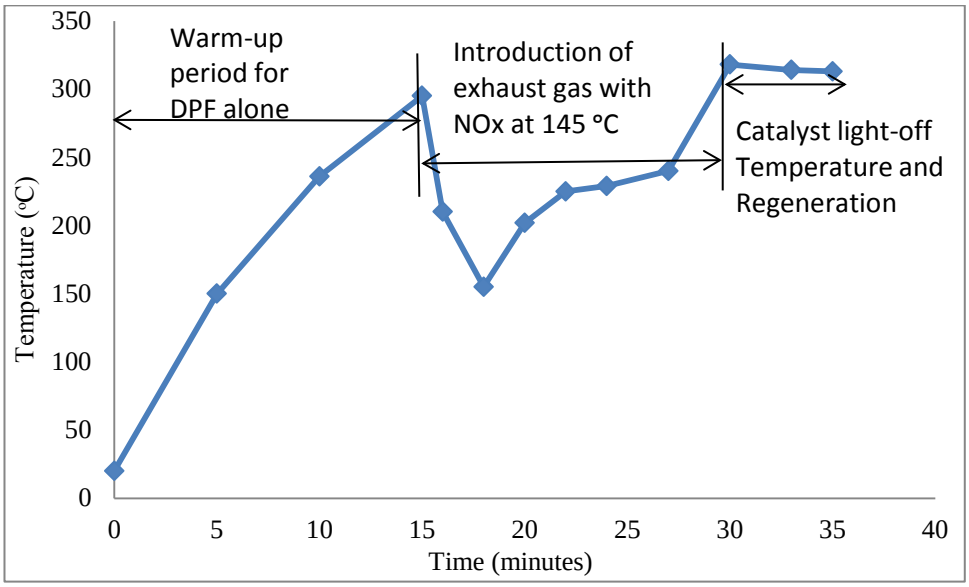

Figure 8.16A first Temperature vs time profile during regeneration of catalysed DPF using diesel exhaust containing NOx

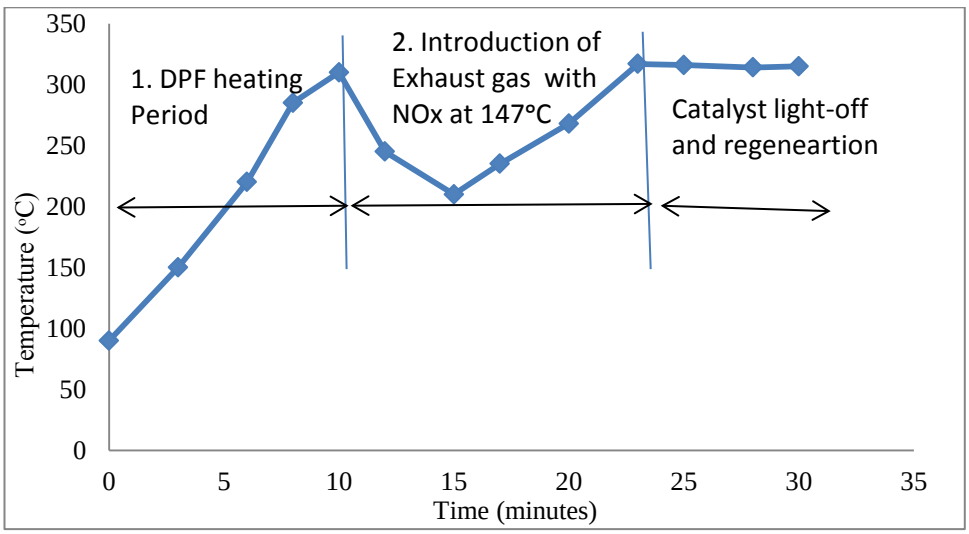

Figure 8.16B second Temperature vs Time profile during regeneration of catalysed DPF using diesel exhaust containing NOx

8.4.2.5 Continuous regeneration test of the catalysed DPF on the engine

The pressure drop across the DPF was used as the characterising parameter to test catalysed DPF on continuous regeneration mode. The pressure rise during the transient period and rate of pressure rise at the upstream was observed to be faster initially than in the non-catalysed filter at high speed as shown in Table 8.10 and Figure 8.17. This was attributed to narrower channels due to the catalyst impregnation (Lee et al 2011). Similarly, it was viewed that the high speed contributed to sharp pressure rise and therefore engine speed was reduced to 1800 RPM, and the operation repeated. The results on this condition are shown in Figure 8.18 and Table 8.11. This speed permitted PM loading of the DPF with moderate upstream pressure rise. It could be observed that the light-off temperature of the DPF is about 400°C because at this exhaust temperature, the DPF operated on continuous regeneration mode and upstream pressure became fairly constant at stable engine load. A repeat test was conducted on the same catalysed DPF. The transient period was now operated at the chosen speed of 1800 RPM and stabilised using the baseline condition of 9^{o} BTDC injection timing.

Table 8.10 Preliminary Experimental conditions in the use of catalysed DPF

Engine operating conditions (Nm/RPM)	Time (hr:min)	DPF Upstream pressure P1 (milibar)	DPF Downstream pressure P2 (milibar)	Pressure drop(ΔP) (milibar)	Exhaust Temp. (^{o}C)
Start, idle at /2000	14.42	-	-	-	-
	14.44	260	110	150	
	14.45	270	110	160	
	14.46	270	120	150	
10/2000	14.47	320	130	190	
20/2000	14.49	330	140	190	
30/2000	14.51	360	150	210	
40/2000	14.54	400	160	240	
50/2000	14.57	430	170	260	271
60/2000	15.01	470	170	300	311
70/2000	15.04	500	180	320	375
80/2000	15.07 – 15.09	520 - 540	190	350	

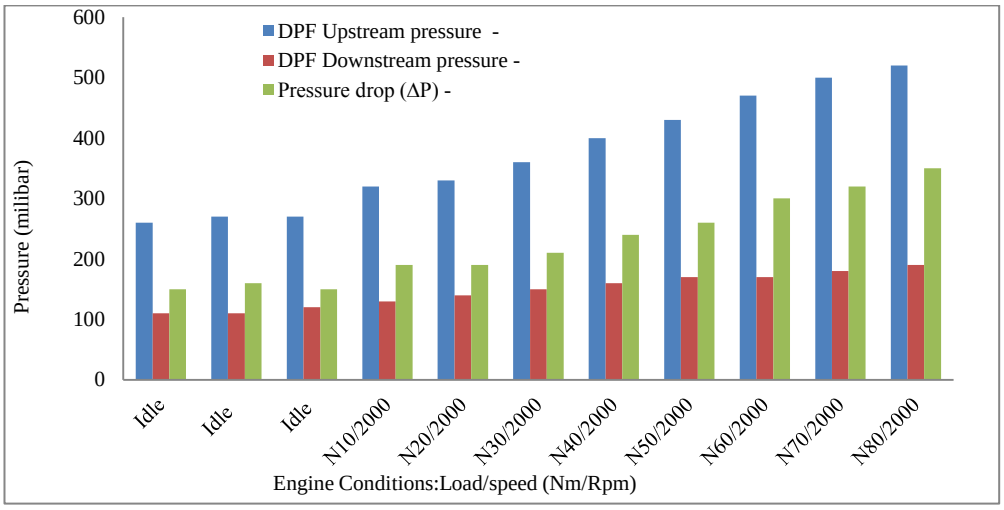

Figure 8.17 Preliminary tests on catalysed DPF

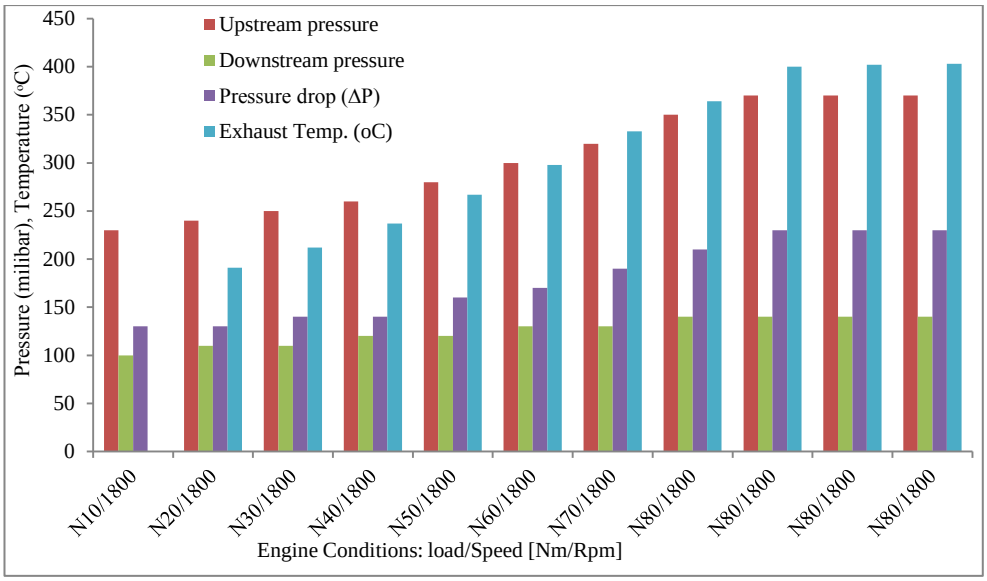

Figure 8.18 Engine back pressure versus load

Table 8.11 Experimental conditions (A)

Engine operating conditions (Nm/Rpm)	Time (min)	DPF Upstream pressure P1 (milibar)	DPF Downstream pressure P2 (milibar)	Pressure drop (ΔP) (milibar)	Exhaust Temp. (°C)
Idle/1800	15.11	-	-	-	-
10/1800	15.13	340	120		
20/1800	15.16	350	120		
30/1800	15.17	360	120		

40/1800	15.18	370	120		
50/1800	15.20	380	130	250	301
60/1800	15.24	410	130	280	321
70/1800	15.27	420	140	280	353
80/1800	15.29	440-460 (Stable)	140	320	384
80/1800	15.35	470-480	150	330	400
80/1800	15.40	450	150	300	404
	15.50	430	150	280	404
	16.00	410	150	260	404
	16.10	390	150	240	407
	16.20	380	150	230	408
	16.30	370	140	220	407

As seen in Table 8.12, the upstream pressure rise gradually peaked at 370 milibar. As exhaust gas temperature reached 400°C, the DPF exhibited continuous regeneration as inferred from the stable upstream pressure; confirming that as the catalyst light off temperature.

Table 8.12 Experimental conditions (B)

Engine operating conditions (Nm/RPM)	Time (min)	DPF Upstream pressure P1 (milibar)	DPF Downstream pressure P2 (milibar)	Pressure drop (ΔP) (milibar)	Exhaust Temp. (°C)
10/1800	10.00	240	-		
20/1800	10.18	240	110	130	191
30/1800	10.28	250	110	140	212
40/1800	10.40	260	120	140	237
50/1800	10.50	280	120	160	267
60/1800	11.00	300	130	170	298
70/1800	11.08	320	130	190	333
80/1800	11.17	350	140	210	364
80/1800	11.28	370	140	230	400
80/1800	11.34	370	140	230	402
80/1800	11.38	370	140	230	403
Investigating effect of Injection Timing on the same condition					
80/1800 @15 ^{o} BTDC	11.43	340	140	200	413
80/1800 @12^{o} BTDC	11.51	360	140	220	406

80/1800 @9^{o} BTDC	12.01	380	140	240	411
80/1800 @6^{o} BTDC	12.17	380	140	240	419
80/1800 @ 3^{o} BTDC	12.29	370	140	230	422
80/1800 @TDC	12.44	360	140	230	432
80/1800 @3^{o} ATDC	12.51	360	140	220	464
Operate Back at Base line condition					
80/1800 @9^{o} BTDC	13.00	370	140	230	411
80/1800 @9^{o} BTDC	14.06	370	140	230	410

Similarly, investigation was carried out to check if injection timing was of significant effect in to the pressure drop as PM was loaded. It was observed that advanced and retarded injection timing conditions slightly reduced upstream pressures, compared to baseline injection time of 9^{o} BTDC shown in Figure 8.19.

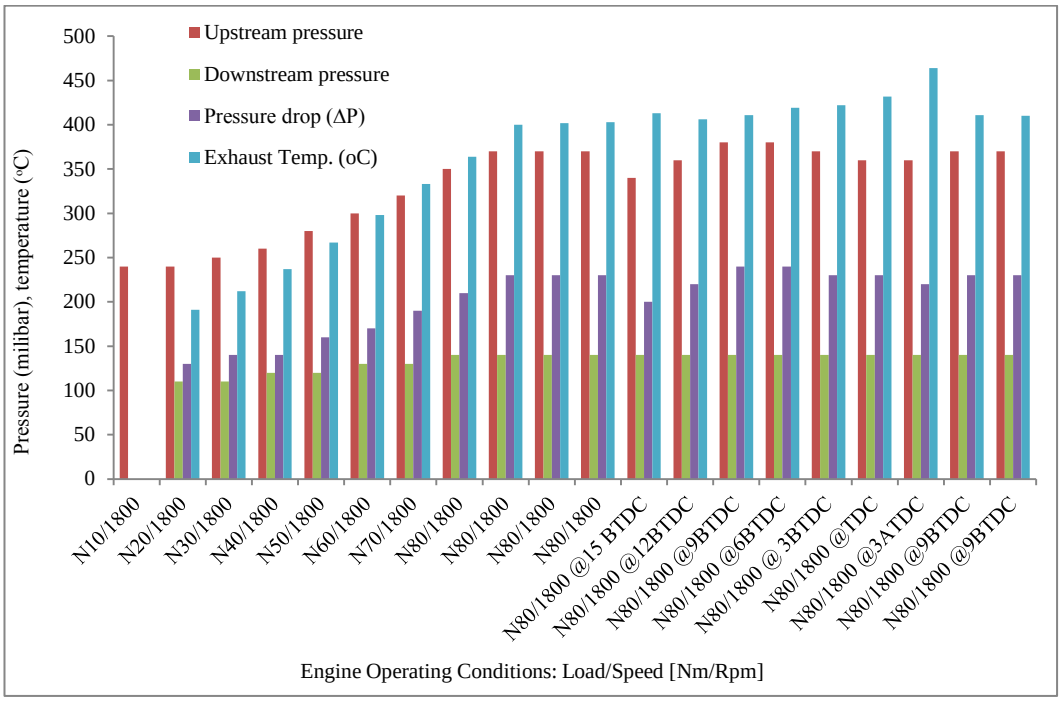

Figure 8.19 Engine operating conditions

The result correlates well to engine physics as explained in chapter 5. Advance of injection timing enables more time for soot burn-out in typical diesel engine (Majewski, W. A. and Khair, M. K., 2006). The retarded injection timing condition provided for high temperature which enabled the catalyst to operate comfortably on a

continuous regeneration mode. Conventionally from earlier sweeps in chapter 5, engine was optimised for maximum sooting condition at 9BTDC without any boosting or exhausts gas recirculation (EGR).

Discussions

The feasibility tests have been pursued to achieve regeneration using existing microwave cavity, based on what is known about DPF application to diesel engine. The aim of this level of the project is to gain enough insights toward design and fabrication of purposeful experimental rig as well as to design experiments to optimise the use of this technique to regenerate DPF in a 200 KW marine diesel engine. The observations from the tests gave good information that supports the viability of microwave application to DPF regeneration. These are as follows:

1. ***Tests with Non Catalysed DPF***
   The non-catalysed DPF was allowed to regenerate with introduction of air at estimated temperature of 550°C after 30 minutes of DPF heating in the cavity and air flow rate of 53kg/hr for 10 minutes. This gave 98% PM burn out with air draft (although not directly through the axis of the DPF), despite the peculiarity of cavity as presented, yet regeneration was almost complete. Estimated time in the electrical heating for only the chamber without DPF at the same 2kW power supply, will take about 40 minutes to warm-up without flow of oxidising air and by implication, no thermal loss in a perfectly insulated chamber. Obviously, this shows that microwave heating process is faster compared to the resistive heating process.
2. ***Catalysed DPF***
   In the case, the catalyst light-off temperature during regeneration in the microwave cavity was approximately 305°C with total NOx of about 450ppm in the exhaust gas that provided for catalytic oxidation of soot. In the engine test bed, total NOx was about 1270ppm and catalyst light temperature was exhibited at about 400°C, implying hotter exhaust air. This shows about 100°C reduction in temperature with the use of microwave energy.

These observations are cogent to the benefit of microwave assisted regeneration. As in similar studies, one common problem with this technique is the issue of

temperature measurement where the use of metallic thermocouple is not feasible and the option of available infra-red probe is limited to surface temperature. Pyrometers that are based on optical fibre will be most appropriate (Matthews, Undated). Some studies that adopted miniature laboratory set-ups used small quantity of soot in TGA oxidation experiments (An, H., Kilroy, C., McGinn,P. J., 2005; Palma et al 2010; Palma et al 2007), have pointed out that central to the efficacy of microwave regeneration of DPF is the selective heat absorption characteristic. It was established that the microwave absorption capacity of diesel generated PM is at least 10^5 times greater than that of ceramic material used in DPF (Babu, V. S., Farinash, L., and Seehra, M. S., 1995). This is the most plausible reason for faster soot combustion by the use of microwave compared to other forms of heating. A study of permittivity of materials and microwave heating effect reported by (Ma et al 1997) shows that the dielectric property of a material is characterised by real and imaginary parts, and expressed as:

$$\varepsilon = \varepsilon' - \varepsilon'', \qquad \text{.....} \quad 8.4$$

The term (ε') stands for the real part; it represents the dielectric constant which is indicates the energy in a material stored in form of electric field. The term (ε'') is the imaginary part representing the dielectric loss factor; it is a measure of heat energy that a material is capable of dissipating. The power P, absorbed by a material when microwave energy is applied depends on three parameters: the complex permittivity of the material ε', the intensity of the electric field E and the frequency of the microwave irradiation f and is expressed as:

$$P = 55.63 f E^2 \varepsilon' tan\delta \qquad \text{.....} \quad 8.5$$

Where $tan\delta = \varepsilon''/\varepsilon'$

And the terms are the following units: P (W m^{-3}), E (kV m^{-1}) and f (MHz). Therefore the ability of a material to absorb microwave energy and convert it to heat energy depends on its permittivity complex. By implication, if a material has high dielectric constant with concurrent high loss factor, then it can effectively be utilised in microwave heating. Selection of suitable filter material and formulation of catalysts that can further enhance reduction in temperature during soot regeneration using microwave energy have been the trust of many investigations (Palma et al 2010;

Palma et al 2007; Palma et al 2011; Palma et al 2013; Palma et al 2015). The dielectric properties of various materials show that silicon carbide has superior dielectric constant and dielectric loss factor that makes it suitable for microwave application – Table 8.13.

Table 8.13 Dielectric properties of various materials (Palma et al 2015)

Material	**Dielectric constant ε'**	**Dielectric loss factor ε''**
Diesel soot	10.70	3.600
Quartz	3.80	0.001
Cordierite	2.90	0.140
Alumina ceramic Al_2O_3	8.90	0.009
Silicon Carbide SiC	30.00	11.000

From our results and in comparison with information, some conclusive remarks are tenable as follows:

(i) Diesel generated soot is a good absorber of microwave energy due to the characteristic high values of the dielectric constant and loss factor.

(ii) The choice of silicon carbide DPF is complementary as it also susceptible to microwave irradiation with high absorption capacity and loss factor.

(iii) Catalysis in the presence of microwave is enhanced. Commercial catalyst are proprietary, the catalysed DPF was sourced from Johnson Matthey without knowledge of the catalyst constitution. However, the activity at continuously regenerating mode under microwave irradiation compared to its activity on the engine has 100˚C temperature reduction. This is will definitely translate to huge energy and time savings when proper accounts of energy transfers are made. From small laboratory scale silicon carbide foam to full engine capacity substrates (Palma et al 2007; Palmac et al 2015), filters dosed with catalyst of different genre (example: Iron (Fe), Vanadium (V), Potassium (K), and Copper (u)) base and/or their combinations have demonstrated good reduction in power requirements during regeneration translating to lower temperature and time for the process.

(iv) Essentially, successful deployment of microwave energy to DPF regeneration will reduce pressure drop across the filter and enhance better engine operation.

8.5 Design of microwave cavity for investigation of Thermal energy requirements for DPF regeneration

As a prelude to the substantive sets of experiments ear-marked for optimal design of microwave regeneration technique, a model design has been made with the use of COMSOL multiphysics software. In the scheme, finite element models (FEM) based in COMSOL multiphysics have been used to simulate regeneration of diesel particulate filter following the layout we have in the existing microwave cavity as in Figure 8.2A. The study utilized the physics packages in the software to model the electric field distribution and thermal profiles which parallels the heat energy generated during DPF regeneration within the cavity. The software was used to establish dimensions for cavity and the commercial DPF with dimensions 143mm in diameter, and 183mm in length. It was possible to integrate the thermal properties of the silicon carbide used in the DPF substrate and the electric field to study the profiles of thermal energy for the established dimensions. It will be recalled that in the experiments, microwave power was generated by a 2.45GHz magnetron into the existing microwave cavity to regenerate DPF. The thermal profiles from the simulations were compared with experimental observations during DPF regeneration and it showed close agreements. The scheme was therefore utilized to improve cavity design for better utilization of the microwave energy for efficient DPF regeneration.

8.5.1 Steps to model microwave heating of the cavity and DPF using COMSOL multiphysics

The COMSOL multi-physics modelling make use of in-built Finite Element Method (FEM) to solve computational problems in relation to the physics selected. The approach to modelling involved following steps: setting up the geometry, specification of the material properties, definition of the physics involved, creation of the mesh, running the simulation and post-processing the results. These are core functional capabilities built into the software.

Setting up geometry

The setting up of the model geometry is to create the physical object in the software system. The purpose is to create the functional geometry of the object as accurate as possible. It starts with selection of space dimension for the model which can be in 3D, 2D axisymmetric, 2D, 1Daxisymmetric or 0D. Appropriate simplifications were made where it helped to ease computational time without sacrificing accuracy. Therefore with regards to our typical cavity, Figure 8.20 (A and B) show the scheme used to detail the geometry according to engine-determined criteria for DPF size specification. The exact number of DPF channels was a selection default set by the manufacturers as chosen by engine capacity. The geometry was developed in a computer aided design (CAD) environment and imported to COMSOL. However as later discovered, the number of domains for study was beyond the computer capacity, rather requiring computational space only available to supper computers. Therefore modelling effort was tailored to find the best locations in the cavity where the DPF will be exposed to high intensities of the electric field.

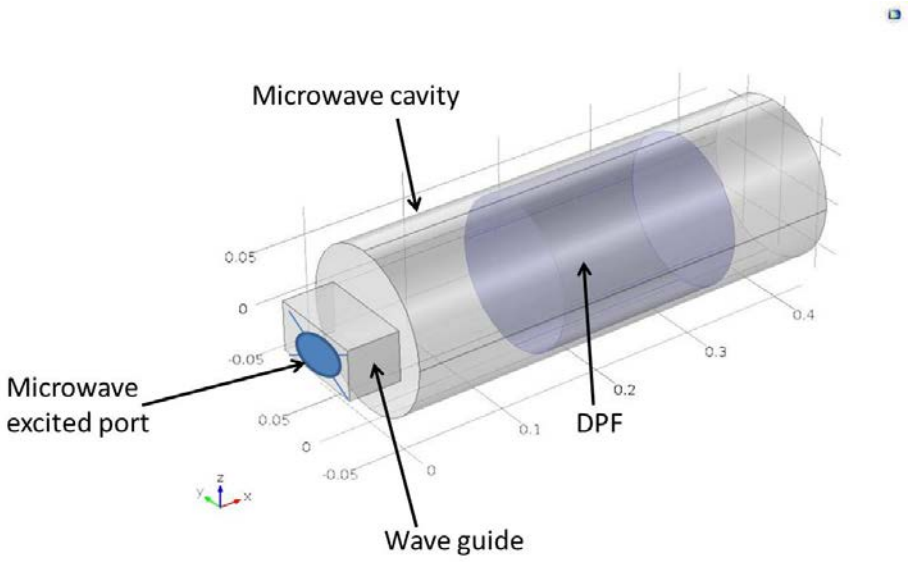

Figure 8.20A Microwave injection and cavity

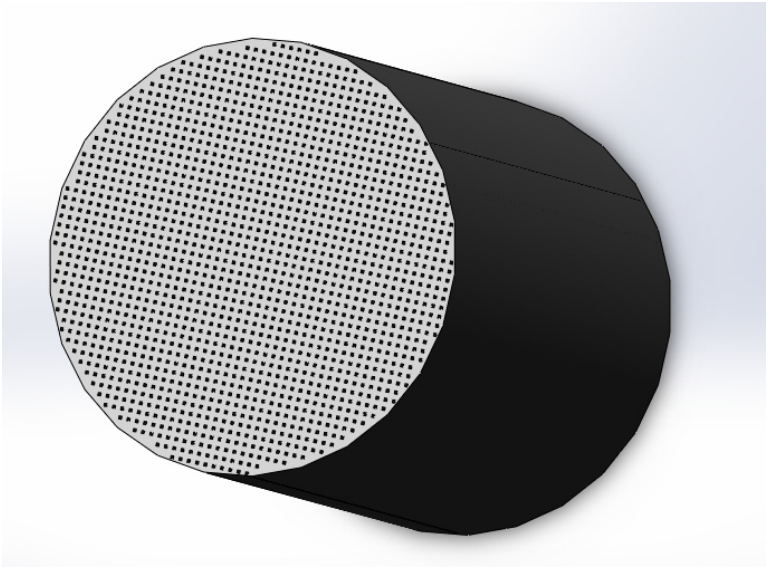

Figure 8.20B DPF Geometry

The intensity of the electric field translates to the thermal energy generated within the DPF. The dielectric properties of soot and material used in making DPF has been given in Table 8.14. As explained in with equation 8.4 and 8.5, the dielectric constant (ε') of a material is its capacity to store microwave energy and dielectric loss factor (ε'') is the material's ability to convert the stored microwave energy to heat. The ratio between ε'' and ε' measures energy coupling is known as dissipation factor or (*tan* δ). The dielectric heating equation used in modelling was a modification taken from (Gautam et al 1999), and similar to equation 8.4:

$$\boldsymbol{P = 2\pi f \varepsilon_o \varepsilon'' E_i^2} \qquad (8.6)$$

Where,

P - Power dissipated in the medium [W/m^3]

f - Microwave frequency [Hz]

ε_o - Electric permittivity in vacuum [8.854x10^{-12} F/m]

E_i - Electric field intensity in the medium

ε'' - Dielectric loss factor of the medium

Material Selection

COMSOL library enables one to select materials and even add new ones. The properties of the materials chosen are specified for the geometry already described. On can also amend or assign new properties to the materials. The materials involved in the modelling are stainless steel used for the cavity body, silicon carbide used as the DPF substrate and air that filled the chamber. However, the silicon carbide was modified to fit the specification of which COMSOL user friendly capability comes in handy. The properties of the materials as specified in the simulation are as seen from the screen shots below as ticked.

Property	Name	Value	Unit	Property group
✓ Relative permeability	mur	1	1	Basic
✓ Relative permittivity	epsilonr	1	1	Basic
✓ Electrical conductivity	sigma	0[S/m]	S/m	Basic
✓ Heat capacity at constant pressure	Cp	Cp(T[1/K])[J/(kg*K)]	J/(kg·K)	Basic
✓ Density	rho	rho(pA[1/Pa],T[1/K])[kg/m^3]	kg/m³	Basic
✓ Thermal conductivity	k	k(T[1/K])[W/(m*K)]	W/(m·K)	Basic
Dynamic viscosity	mu	eta(T[1/K])[Pa*s]	Pa·s	Basic
Ratio of specific heats	gamma	1.4	1	Basic
Speed of sound	c	cs(T[1/K])[m/s]	m/s	Basic
Refractive index	n	1	1	Refractive index
Refractive index, imaginary part	ki	0	1	Refractive index

(i) Air

Property	Name	Value	Unit	Property group
✓ Relative permittivity	epsilonr	30-11*j	1	Basic
✓ Relative permeability	mur	1	1	Basic
✓ Electrical conductivity	sigma	0.001	S/m	Basic
✓ Thermal conductivity	k	120	W/(m·K)	Basic
✓ Density	rho	3000	kg/m³	Basic
✓ Heat capacity at constant pressure	Cp	750	J/(kg·K)	Basic

(ii) Silicon carbide

Property	Name	Value	Unit	Property group
✓ Relative permeability	mur	1	1	Basic
✓ Electrical conductivity	sigma	4.032e6[S/m]	S/m	Basic
✓ Relative permittivity	epsilonr	1	1	Basic
Heat capacity at constant pressure	Cp	475[J/(kg*K)]	J/(kg·K)	Basic
Thermal conductivity	k	44.5[W/(m*K)]	W/(m·K)	Basic
Coefficient of thermal expansion	alpha	12.3e-6[1/K]	1/K	Basic
Density	rho	7850[kg/m^3]	kg/m³	Basic
Young's modulus	E	200e9[Pa]	Pa	Young's modulus and Poisson's ratio
Poisson's ratio	nu	0.33	1	Young's modulus and Poisson's ratio
Murnaghan third-order elastic moduli	l	-3.0e11[Pa]	N/m²	Murnaghan
Murnaghan third-order elastic moduli	m	-6.2e11[Pa]	N/m²	Murnaghan
Murnaghan third-order elastic moduli	n	-7.2e11[Pa]	N/m²	Murnaghan
Lamé parameter λ	lambLame	1.5e11[Pa]	N/m²	Lamé parameters
Lamé parameter μ	muLame	7.5e10[Pa]	N/m²	Lamé parameters

(iii) Stainless steel

Figure 8.21 Properties of the materials as specified in the simulation program

Physics

Definition of the physics simply involves assignment of appropriate physics from the COMSOL suite. For the model under consideration; electromagnetic wave theory, microwave heating, air flow and heat transfer were the appropriate physics modules. These were built into the model with requisite definitions. The ability to couple these modules in COMSOL depends on the computing capacity. Computer with high RAM size and fast processor is needed to accommodate the number of physics interfaced for evaluation in the meshed nodes.

The electric field that dictates the thermal profile in the cavity was defined by the electromagnetic wave equation and was used to evaluate the electric field. Equation 8.7 was solved in frequency domain by COMSOL to determine the electric field distribution in the waveguide and cavity:

$$\nabla \times \mu_r^{-1}(\nabla \times E) - K_0^2\left(\epsilon_r - \frac{j\sigma}{\omega\epsilon_0}\right)E = 0 \qquad (8.7)$$

Where

μ_r - permeability of the medium

ε_o - permittivity of medium

E - electric field vector

σ - density of medium

K_0 – wave number

The cavity walls and the wave guide were modelled as perfect conductors and therefore the boundary condition was adopted as in equation 8.8.

$$\boldsymbol{n} \times E = 0 \qquad (8.8)$$

Where $\boldsymbol{n}$ – is normal vector to the walls.

In line with the method adopted in wrapping the DPF with an insulating material, the outer cylindrical surface was considered as not having any heat loss, therefore equation used to model the thermal insulation is equation 8.9.

$$-\boldsymbol{n}.(-k\nabla T) = 0 \quad (8.9)$$

Where

T – Temperature of the material

k - Thermal conductivity of the material

Similarly, equation 8.10 was used to solve the heat transfer within the DPF. As said, the DPF was only modelled as a composite material without consideration for the channels since the objective was reduced to simple identification of locations in the cavity with best exposure to high intensities of electric field and the associated thermal profile.

$$\rho C_p.\nabla T = \nabla.(k\nabla T) + Q \quad (8.10)$$

Where

ρ - Density of the material

C_p - Specific heat capacitance at constant pressure (1 atmosphere)

Q - Heat source

Heat source (Q) in our case is microwave heating of DPF and defined by the set of equations below labelled as equation 8.11.

$$\begin{aligned} Q &= Q_{rh} + Q_{ml} \\ Q_{rh} &= \frac{1}{2}Re(\boldsymbol{J}.\boldsymbol{E}^*) \\ Q_{ml} &= \frac{1}{2}Re(\boldsymbol{B}.\boldsymbol{H}^*) \end{aligned} \quad (8.11)$$

Meshing

The next step in the modelling process is to generate the mesh. Meshing simply defines how many spots that the calculation will be performed over the geometry that has been created. It can be prescribed at different levels of fineness or coarseness

which depends on the intricacies of the geometry and relevant physics. As implied, modelling of DPF as porous media with channels alternately closed at the ends was avoided due to the complicated meshing implications, as the number of which is beyond the computer computational capacity. COMSOL multiphysics have interactive meshing environment the enables individual faces or domains to be meshed. Each meshing activity adds to the meshing sequence and the final mesh is built from all the individual meshing operations in the sequence.

Simulation

After completion of the meshing operations, simulation of the model was performed. This is also called 'study' and the software performs the calculations in each element. The parameters for the simulation were set as follows: the microwave frequency was set at 2.45 GHz, and the power at 1000 Watts. The study was carried out in a systematic manner in order to achieve some targets which include: determination of the correct waveguide dimensions; determination of the right size of the microwave cavity for regeneration; and good understanding of the temperature profiles over the DPF for better utilisation of microwave energy heating across it. It was actually during the study that it was discovered that ideal simulation of the DPF for all the 32000 cells as shown in Figure 8.21B was not feasible due to the incredible number of domains for simulation that were more than the computational capacity of an ordinary scientific Personal Computer.

Results

When the simulation is finished, results can be viewed, and further processed to any reporting format of choice. COMSOL multiphysics capabilities enable results to be presented in 1D, 2D and 3D options. The results obtained from the simulations are shown in Figures 8.22, 8.23, 8.24 and 8.25. Waveguides of two different cross-sections were used in the model, the first waveguide (WG1) is 78mm by 18mm and the second one (WG2) is 96mm by 48mm. The bigger one is the unit already built into the facility and the smaller wave guide is a mere comparative curiosity. In Figures 8.22A and 8.23A, the electric field distributions across the front faces of the DPF are shown; 8.22B and 8.23B show the electric field distributions along z

direction and the middle of the DPF looking from the front; 8.22C and 8.23C show the electric field distribution along x direction and through the middle of the DPF also showing the field's exponentially decay.

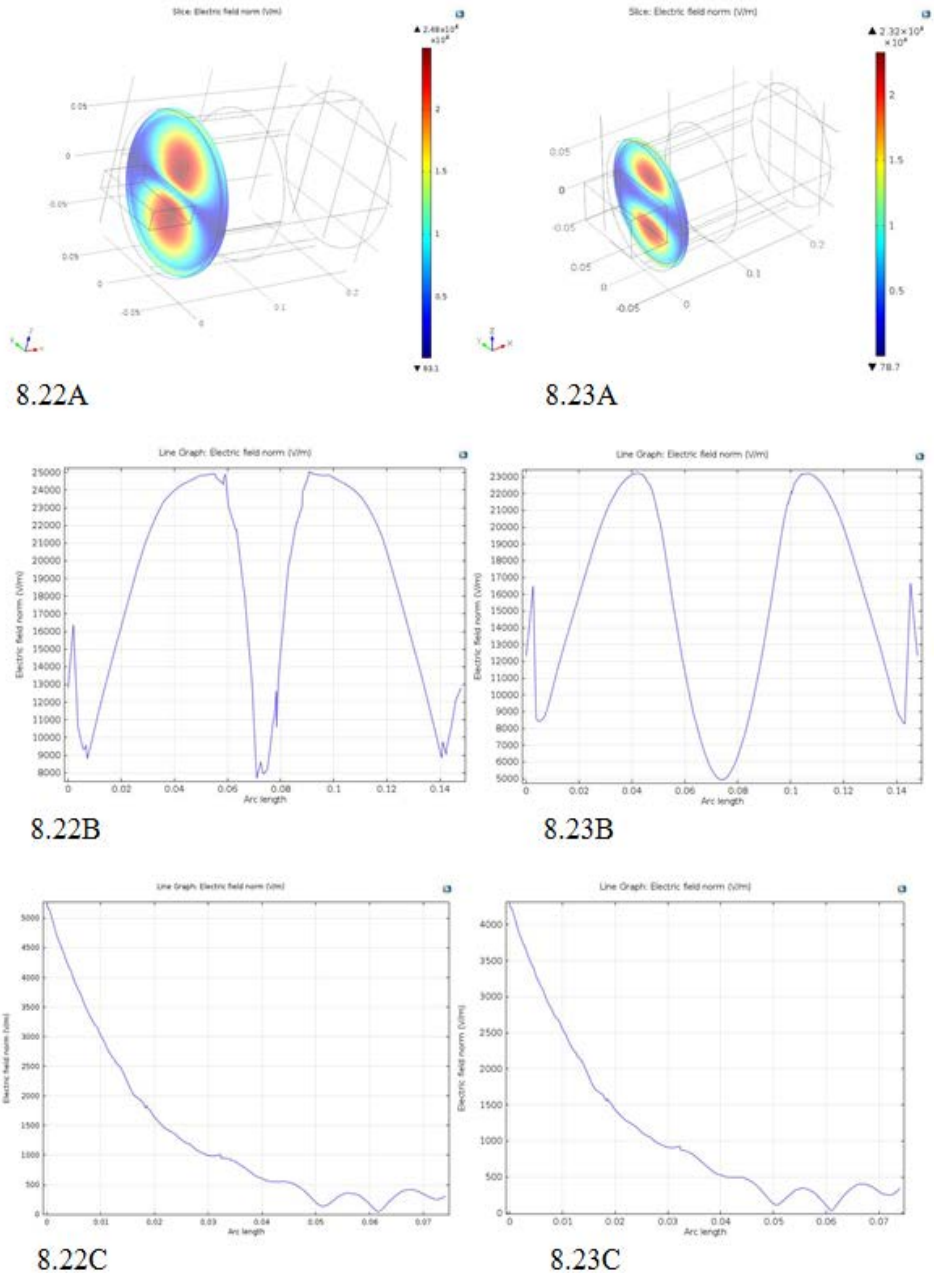

Figure 8.22 and 8.23 (A-C) The electric field distributions across the DPF

The electric field distributions are seen to be similar in two sets of dimensions producing two resonant peaks at the front face. However, the smaller waveguide (WG1) produced slightly better average electric field distribution within the DPF

than that of with WG2. Average electric field with WG1 is 825 V/m and with WG2 is 777 V/m. The results of the simulation for the thermal profile of the DPF are presented in Figure 8.24 and 8.25 (A – C) for microwave energy fed through wave guides 1 and 2 respectively. Figures 8.24A and 8.25A show the temperature profiles across the face of the DPF from the front and Figures 8.24B and 8.25B show the temperature in the z-direction while the Figures 8.24C and 8.25C show the temperature in the x-direction. The temperature is seen to be high at the centre and reduces gradually in the radial direction. Thus the DPF is proportionally heated by microwave according to the equation 8.6 and heat conduction across the DPF is governed by the equation 8.10. The difference between maximum temperature and minimum temperature across the front face of DPF is 8 ^{o}C and 4.5 ^{o}C by using WG1 and WG2 respectively, which is only a fraction of the average temperature across the front face of the DPF. WG1 produced slightly higher temperature than that WG2 which corresponds to the electric field distribution. The DPF temperature drops along the x-direction as shown in the third row according to electric field pattern, exponentially along the x-direction. However, the temperature difference between maximum and minimum is only 20 ^{o}C and 16 ^{o}C for WG1 and WG2 respectively. Simulations were performed with the bigger waveguide (96mm x 48mm), which is the size available in microwave facility used in the DPF experimental regeneration. These simulations were aimed at finding the right location for DPF within the microwave cavity.

Similarly, the length of the cylindrical cavity is varied to understand the behaviour of the electric filed pattern which depends on the resonance frequency of the microwave cavity. Four lengths are used in the simulations (333 mm, 433 mm, 483 mm and 533 mm) and the results are shown in Figure 8.26 shows the. The presence of DPF was purposefully not included in these simulations in order to speed up the simulations. In Figure 8.26, cavities with lengths 433 mm and 533 mm show areas of high electric field in the middle of the cavity, where DPF can be placed.

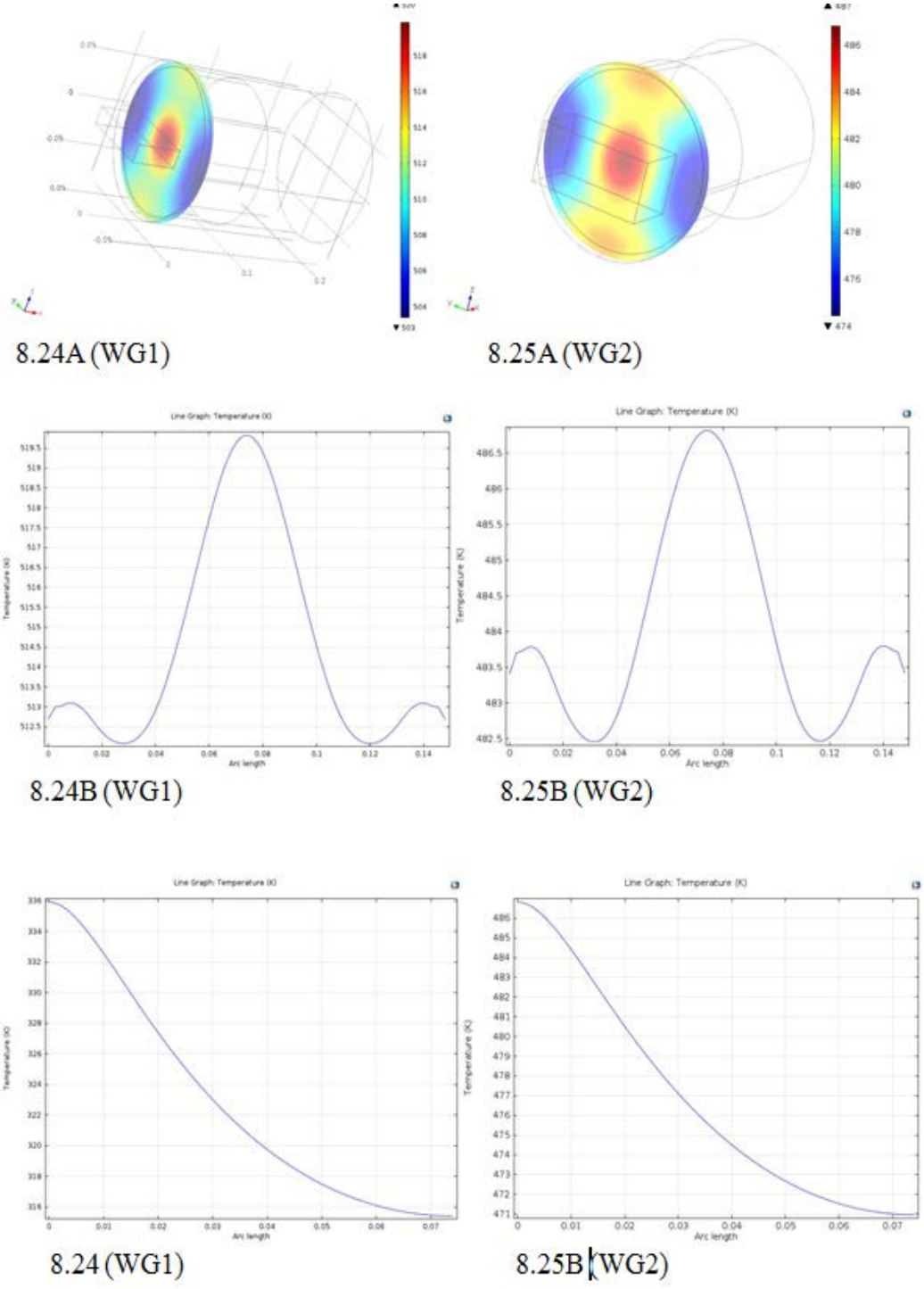

Figure 8.24 and 8.25 (A-C), Temperature profile within DPF for two waveguides [WG1 = (78mm x 18mm); WG2 = (96mm x 48mm)]

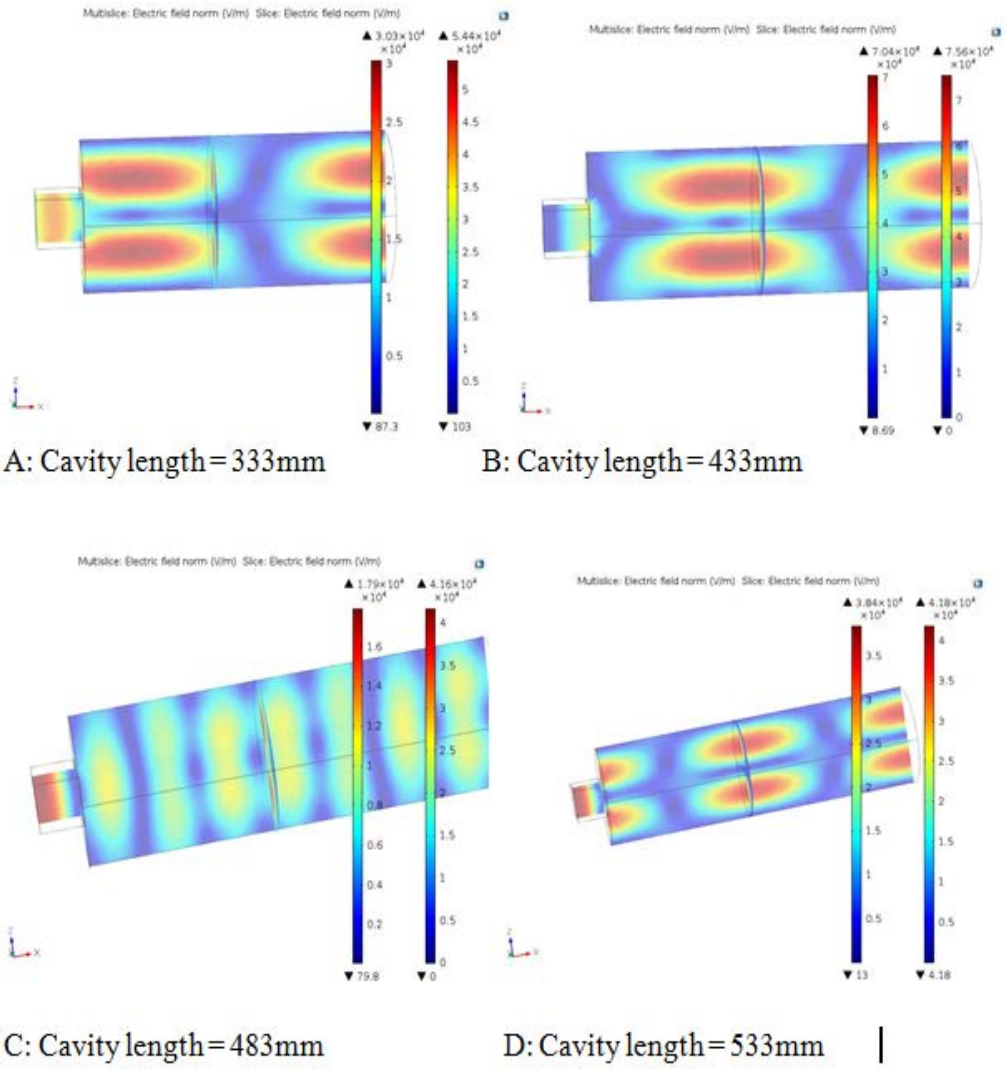

Figure 8.26 Electric field pattern in ZX plane (y = 0) cylindrical microwave cavity with various lengths.

Summary

In this chapter, the feasible use of MW energy as an efficient source regenerating both catalysed and non-catalysed DPFs has been demonstrated.

1. The continuous regeneration temperature for the catalysed DPF using MW energy was shown to occur about 305℃ compared to engine test bed continuous regeneration which occurred at about 400-404℃. This shows a remarkable decrease in energy consumption when utilising MW energy. Similarly regeneration of non-catalysed DPF was possible about 550˚C within a very short time upon reaching this temperature. This also is an improvement over resistive heating approach known for longer time at 600℃.
2. Although accurate temperature and flow measurements were challenging, the techniques adopted lend the results to meaningful deductions according to conventional trends in literatures.
3. Essentially, successful deployment of microwave energy to DPF regeneration will reduce pressure drop across the filter and enhance better engine operation.
4. The use of COMSOL multiphysics has enabled model design of uni-mode cavity with determination of optimal DPF location in the cavity for maximum exposure to electric field intensity and heat energy.
5. In the next level of experiments, experienced gained from these initial result will be used to optimise regeneration efficiency. These will include issues like:

- Appropriate technique for DPF Temperature measurement
- Better real time pressure measurement across DPF with respect to datum
- Better measurement of exhaust flow rate
- Better exposure of the DPF to the electric field in the cavity that will give it homogenous heat distribution according to insights gained from the simulation results.

CHAPTER 9

CONCLUSIONS AND RECOMMENDATIONS FOR FURTHER WORK

9.1 Thesis Summary.

In this study, experimental measurements of particulate matter generated from a high speed diesel engine using low and medium load conditions have been carried out. These were used to investigate the influence of dilution conditions on PM number and size distributions; this was extended to compare the influence of using different dilution gases. Next was to study the influence of biodiesel on PM emissions and their oxidations relevant to regeneration; and finally was the investigation on the use of microwave power on DPF regeneration. The objectives are based on the fact that dilution is central to correct PM emissions measurement and its oxidation is fundamental to proper DPF design and regeneration. The use of biodiesel is gaining attention as an avenue for reducing soot emissions in diesel engine. These issues involved in PM measurement, trapping and burn-out are central to the use of after treatment techniques in mitigating its emission into the atmosphere. Much ingenuity has been put in designing and carrying out the experiments as explained in methodologies adopted; and good measure of success was achieved. The major findings which conclude this work follow the objectives outlined in chapter 1.

9.2 Conclusions

1. The literature reviews in chapters 2 and 3 show that issues involved in the study of PM are many and varied. The complexity stems from the very nature of diesel fuel and engine combustion whereby, the nature of fuel changes through the mechanism of its admittance, spray, mixing and combustion. Complex thermo-physio-chemical and flow conditions that depend on the engine duty are involved even as combustion is partly kinetic and partly diffusional. These define the state of the exhaust gas at blow down. Then the aerosol begins another complex transformation due to expansion and decrease in temperature; and whether in the laboratory or in the atmosphere, dilution effect due to mixing with air adds to the complexity. Therefore the study of particulates is

complicated with regards to issues like their nature, types, size, shape, transport, transformation and deposition in the course of formation inside the engine, flow through the length of exhaust line and ultimately to the atmosphere.

2. The preliminary tests done in chapter 5 to obtain baseline engine operating conditions gave emission results consistent with diesel engine combustion and emission characteristics. The sweeps of engine load and speed conditions were used to obtain stable operation that generated emissions rich in volatile particulate matter on low load (2.7 bar BMEP) and maximum sooting condition at medium load (5.0 bar BMEP). Then, injection parameters were also manipulated to understand the soot emissions characteristics as injection pressure was varied in steps of 100 bar from 800 bar to 1200 bar and injection timing from 15degrees *BTDC* to 3degres *ATDC* in steps of 3 degrees of crank angle. It was established that increase in injection pressure led to decrease in soot emissions and therefore 800bar was chosen and similarly, 9degrees *BTDC* gave the highest soot emission. These were all as deduced on the basis of filter smoke number (FSN). Filter smoke number is an index of blackness of the exhaust gas due to the presence of dry soot particles. Therefore, without the use of any EGR, engine operations were optimised for the two load conditions at 800bar and 9BTDC for PM measurements used in the study. The low load condition represents about 20% of the maximum power usually adopted for stationary driving cycle when testing automotive diesel engines while the medium load load is about 37 - 40% for 1500 and 2000 Rpm as used.

3. In chapter 6, the effects of dilution on PM generated at low and medium loads were studied. In PM measurement, the major concern is about the solid carbonaceous particles and this necessitates vaporisation of adsorbed volatile particles using hot dilution before measurement. Therefore correct interpretation of results depends on how well the relevant physics in the dilution process is explained. PM generated at low load, containing high volatile particles was better in studying these effects. The dilution phenomenon has been investigated and interpreted in terms of mixing and cooling the aerosol samples and investigating the effects on the particle number and size distributions. This was used to establish that the dynamics

of phase transformation is rooted in the saturation characteristics of the volatile components. Key results from this chapter are:

(i) Saturation determines how the interplay of mixing temperature and concentration of species influence nucleation of particles from volatile species. By implication, nucleation of particles was highest at the lowest temperature which was only limited by species concentrations.

(ii) Measured particle number concentrations were well correlated to mass estimates by exploring the underlying physics involved in dilution.

(iii) Dilution phenomenon was further evaluated using parameters of particle number concentration reduction factor (PCRF) and volatile removal efficiency (VRE) to extend its meaning. This showed that rigorous use of dilution ratio to interpret dilution effect is limited in a sense.

(iv) The use of PCRF and VRE parameters were used to evaluate comparative effects of using nitrogen, air and filtered exhaust as dilution gases. This study showed that air is a superior carrier gas when volatile reduction is needed (especially at low dilution ratios) which suggests a further oxidation reaction; and on the other hand, nitrogen is better where it is necessary to freeze further oxidation reaction.

(v) This technique was further used to study two-stage hot dilution technique similar to the PMP protocols. The two-stage dilution scheme gave better PCRF and VRE; ultimately it was further deduced that these parameters could be used to better express dilution effect and possibly reveal artefact in measurements.

(vi) By extension, the two stage dilution technique was used to measure PM from different biodiesels. Baseline concentrations without applying dilutions showed that PM samples from biodiesel have marginally higher concentrations at sub 30nm diameter range; but are generally lower than petrodiesel beyond 30nm. Similarly, although there were some slight variations between the target and measured

DRs, in both primary and secondary dilutions the true effects of dilutions were captured when the PCRFs were evaluated. Generally the PM from biodiesels gave higher particle number reduction factors which are regarded as indices of nucleation activity.

4. In chapter 7, the influence of blending petrodiesel with biodiesel at 20% and 40% proportions on PM oxidation was investigated. This aim was to further investigate the benefits of using biodiesel to reduce engine emissions. The PM from petrodiesel was first subjected to isothermal oxidation to evaluate some kinetic parameters for comparison with published data and as a basis for comparing results from non-isothermal oxidations. The kinetic parameters like reaction order and activation energy from oxidation of volatile organic fractions and soot components are consistent with published data. Non-isothermal protocol was adopted to investigate oxidation of PM samples generated with biodiesel blends. Comparatively, there was not much difference in the oxidation characteristics between B20 and B40 samples, although increases are encountered with increased blending. The samples were collected above 100 ˚C to avoid water-bound condensates and therefore volatile particles were viewed to be generically organics and were less in samples with biodiesels compared to petrodiesel and also lesser with increased blending. The differences in oxidation characteristics are viewed to be inherent in the fuel physical properties and the evaluated characteristic temperatures did not give much difference between the blends and pure petrodiesel PM. However results with UCOME blends gave very high oxidation rates that needed re-validation. The kinetic parameters based on the Arrhenius plots showed reduced activation energies for the three biodiesel blends compared to petrodiesel PM. Key conclusions made from this investigation include:
   (i) The degree of devolatilization before oxidation affects the combustion characteristics and stability of diesel PM.
   (ii) The PM oxidised by non-isothermal process has lower values of activation energy; this is attributed to energy contribution from oxidation of volatile organic fractions.

(iii) PM generated from biodiesel blends oxidises faster compared to that from pure petrodiesel. When related to observations existing in literature, two key reasons that lead to these observations are the influence of fuel oxygen carried by biodiesels and the disordered soot microstructure of biodiesel generated soot which provides favourable sites for oxidations.

5. In chapter 8, effort was successfully made to use an existing multimode microwave cavity to regenerate catalysed and non-catalysed diesel particulate filters. This involved two innovative inputs: modification of existing engine exhaust line to incorporate a DPF canister with metering and instrumentation ports; and modification of and existing multimode microwave cavity to achieve regeneration the filled DPFs. The non-catalysed DPF was filled on the engine whereby the pressure drop across the filter is the parameter for measuring limit for soot loading while the catalysed DPF was filled at the DPG facility of CAMBUSTION with simulated engine soot. Key results are as follows:
   (i) It was established that the microwave energy regenerated non-catalyse DPF around 550-600^{o}C within a time considered shorter than it would have taken with the use of electrical resistant heating method.
   (ii) This reduction in energy requirement is due to selective heating nature of microwave energy. Good dielectric materials like silicon carbide used in making the DPF substrate is susceptible to microwave irradiation with higher absorption capacity and high loss factor. Similarly, the engine-out soot itself has characteristic high values of the dielectric constant and loss factor and therefore is selectively heated within the MW field.
   (iii) When the catalysed DPF was regenerated in the MW cavity, catalyst light-off temperature was approximately 305 °C with total NOx of about 450ppm in the exhaust gas that provided for catalytic oxidation of soot. In the engine test bed, total NOx was about 1270 ppm and catalyst light temperature was exhibited at about 400 °C, implying 100 °C reductions in temperature with the use of microwave energy.

(iv) The reductions in regeneration temperatures translate to huge energy and time savings when proper accounts of energy transfers are made. Essentially, successful deployment of microwave energy to DPF regeneration will reduce pressure drop across the filter and enhance better engine operation.

It is therefore conclusive that microwave energy can further enhance DPF regeneration if properly harnessed. As a feasibility study, rigorous and intuitive knowledge of diesel generated PM and DPF regeneration have been adopted. It therefore provides enough insight that will enable better design of experiments than can be used to optimise commercial adaptation of MW energy for DPF regeneration with proper and better energy accounts.

9.3 Assessing the achievement of the core project objectives

The project objectives as stated in section 1.2 were formulated around the following questions: What is diesel Particulate Matter, how is it formed, how is it measured and to what regulatory standard, how is it controlled and are there alternative methods? As said, the aim is to develop core competence in measurement designs, understanding and use of appropriate techniques and devices; and to carry out investigations on control measures.

(i) Understanding the nature of PM

The literature review was purposefully separated into chapters 2 and 3 in which the properties of diesel fuel and factors of engine combustion in relation to in-cylinder formations of the species found in diesel engine combustion were first highlighted in chapter 2. It was in this context that PM was introduced and in chapter 3, it was properly dissected to explain its constituents according to existing literature. The insight gathered from reviews were tested in the first series of experiments that characterised the engine operating conditions by examining the relative volumes of fuel consumption and the air/fuel mixing ratios. By using the opaqueness of soot emissions calibrated as filter smoke numbers (FSN), the degree of combustion achieved in the engine at various loads and speeds as well as injection conditions were examined through the measured FSN and

exhaust temperatures. This paved the way for setting measurement baselines for the PM and for comparing results obtained with alternative fuel (biodiesel) based on known fuel properties.

(ii) Measurement of PM

The objective of characterising engine-out PM through measurements is centred on accurate determination of solid carbon particles after stripping off the volatile condensates that adsorb on it. This study has been pursued with available facilities; the methodologies adopted and results obtained have demonstrated the expertise achieved in PM conditioning, measurement and pursuit of PMP standards. In the scheme, evaluations of results were extended to show the real implications for dilution in terms of particle number concentration reduction factor (PCRF) and volatile removal efficiency (VRE). This provided platform to further evaluate the influence of three dilution gases that could be used in conditioning PM sample; and to ascertain reliability of the technique, measurement was extended with the use of different biodiesels.

(iii) Control of PM emissions

The after treatment technologies currently in use for control of tailpipe emissions of PM are through further oxidation of the volatile matter with oxidation catalysts (DOC), reduction of NOx and trapping of soot with a diesel particulate filter (DPF). The use of DPF imposes further challenge of pressure drop across the filter which affects normal exhaust gas flow and therefore requires periodic burn off. The process of burning off accumulated PM in the DPF (as in this study where DOC was not involved) requires additional energy to initiate and sustain combustion and the ways in which this energy penalty is minimised is an issue of current research interest. It is with these views that two studies reported in chapters 7 and 8 were designed. Biodiesel blending of petrodiesel has been an option to reduce PM generation and this study extended investigation on its effect on PM oxidation. The results of oxidation parameters show that reaction in PM with biodiesel blending is faster than petrodiesel. Although image study done for only raw PM samples showed

slight difference in microstructure, some similar published studies with devolatilized samples at elevated temperatures show that soot from biodiesels tends to have more disordered microstructure which is responsible for faster oxidation compared to soot generated from petrodiesel.

To burn-off of trapped soot in a real time engine system, the temperature and device to initiate combustion are factors for consideration in design and operation. For automotive application, catalyst enhances burn-off at lower temperature and ensures the so called passive and continuous regeneration at catalyst light-off temperature using the exhaust gas temperature; but this imposes restriction of locating the DPF near the engine to take advantage of high temperature. Some published studies with small quantities of soot using ceramic foams and TGA suggest that microwave energy can be used to burn off soot at a lower temperature and enhance catalytic regeneration even at a much lower temperature. The feasibility of this possibility on real time engine-generated PM means that it will be possible to locate the DPF at any convenient position along the exhaust line with incorporation of a magnetron to intermittently supply and focus microwave energy on the DPF face bearing the soot to initiate combustion to auto-accelerating temperature and burn off the soot. This is the focus of study in chapter 8 and it was successful. Microwave regeneration of non-catalysed DPF was estimated to have occurred between 550-600^{o}C at a time frame considered shorter than it will take electrical resistive heating approach to regenerate the DPF. Similarly it was established that under microwave irradiation, the catalyst light-off temperature is 100^{o}C lower than without microwave irradiation. These prove the technique hold a potential for future regeneration energy savings in engine PM control.

9.4 Challenges and suggestions for further work

Some challenges encountered during the study were surmounted before results were achieved. However there is room for improvements and further work.

(i) The measurement device used (the electrical mobility spectrometer) gave difficulties in its dilution calibration. This led to the use of external dilution (the porous tube diluter coupled to evaporation tube) in diluting exhaust samples in experiments for determination of PCRF and VRE. However, much as it gave useful information it left concern for accuracy of data. The dilution technique need better refinement with incorporation of appropriate instrumentations to improve the accuracy of results.

(ii) The PM from light duty vehicles has drastically reduced in current legislations and is measured in particle number concentrations; however measurements in mass concentrations especially for heavy duty engines are still relevant. Part of the validation for examining the accuracy of the study was in evaluating the measured number concentrations to mass concentrations from mere first principles and simplified assumptions. Accurate determination of mass numbers could be improved through model refinements and striping of most assumptions and then revalidated with experiments.

(iii) On the PM oxidation characterisation study, investigations using isothermal protocol require generation of many samples and also their oxidation needs to be carried out of at three temperature regimes which are time consuming. Therefore only baseline test was done using isothermal protocol and tests on other samples obtained from blends of biodiesel were on non-isothermal protocol. Although adequate considerations were given in the experimental methodology to eliminate factors that could affect accuracy of results obtained, it would have been better if all samples were subjected to isothermal investigations.

(iv) In the study of PM mitigation using particulate trap, structural difficulties in terms of space constraints in the engine test cell made installation of the DPF substrate to the canister and mounting it to the engine as well as its retrieval quite demanding. In the set up used, many bends were involved unlike the real automotive scenario where DPF orientation is axial to the flow of exhaust gas stream and at the same datum. This could have affected the way pressure drop was encountered in the study.

(v) Similarly, in the regeneration of DPF using the available multimode microwave cavity, some measure of ingenuity was exercised. The

orientation of the slots in the wave guide for deployment of microwave power is across the axis of air flow in the cavity. This necessitated the re-orientation of the DPF across the axis of the air flow as preference was given to exposure of microwave irradiation. Also, real time temperature measurements as would have been preferred through embedding of thermocouples into the DPF substrate was not possible since the presence of metallic material will distort the microwave field intensity. Better utilisation of microwave power and accuracy of result is possible by improving the cavity design so that power is deployed along the same axis of air flow. In addition, the use of pyrometers based on optical fibre to measure temperature will improve the quality of data and information derived from such.

APPENDIX

HRTEM IMAGES

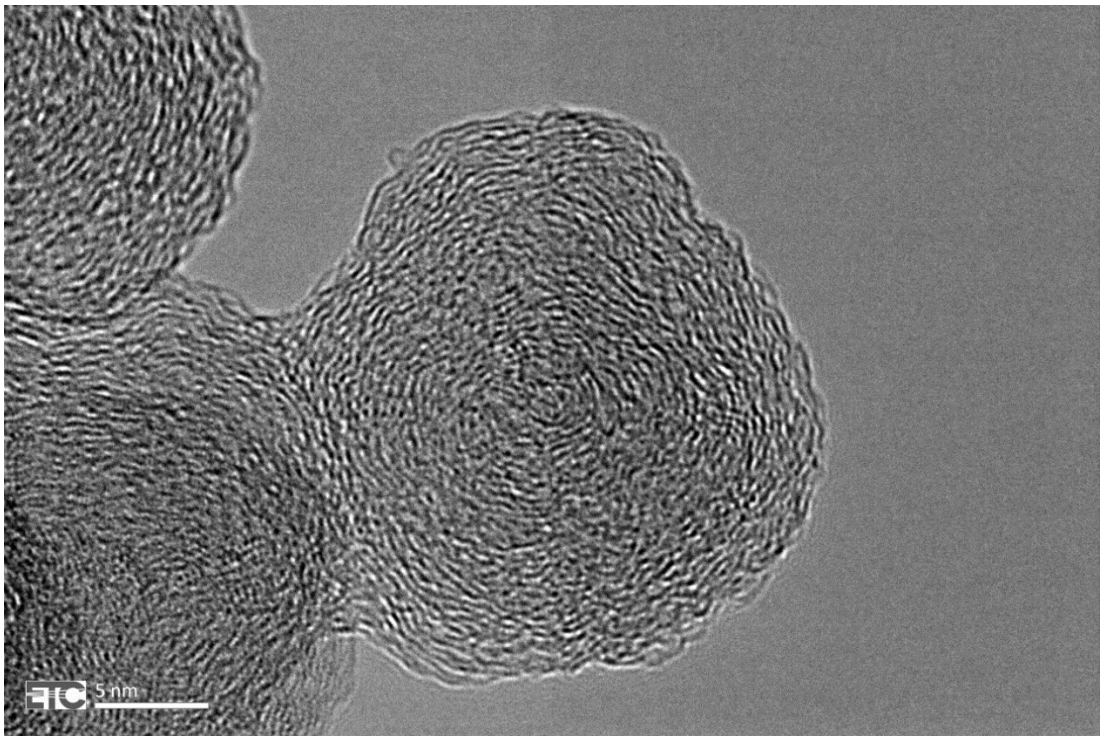

(i)

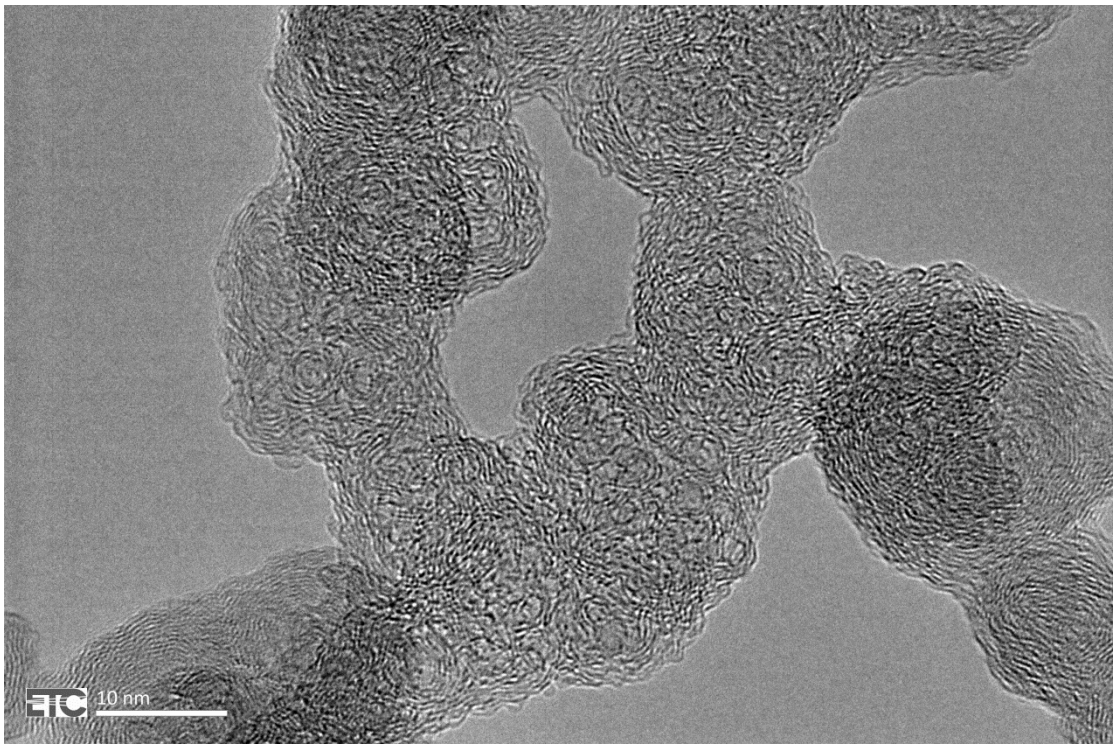

(ii)

A: Petrodiesel

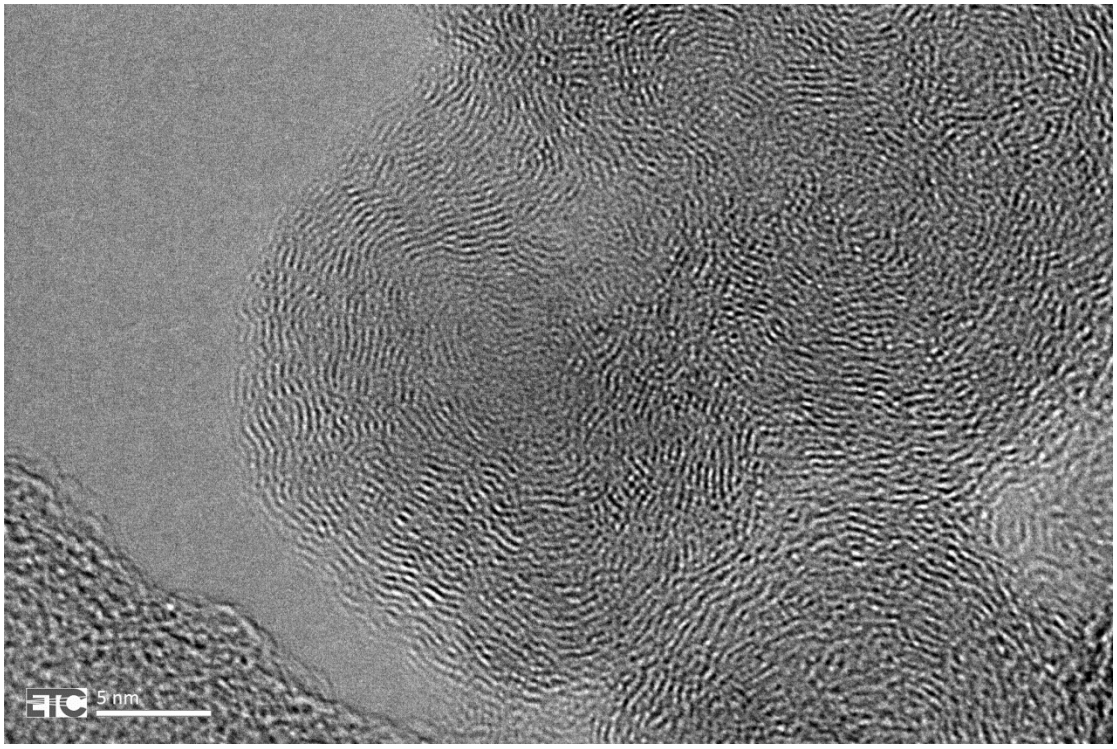

(i)

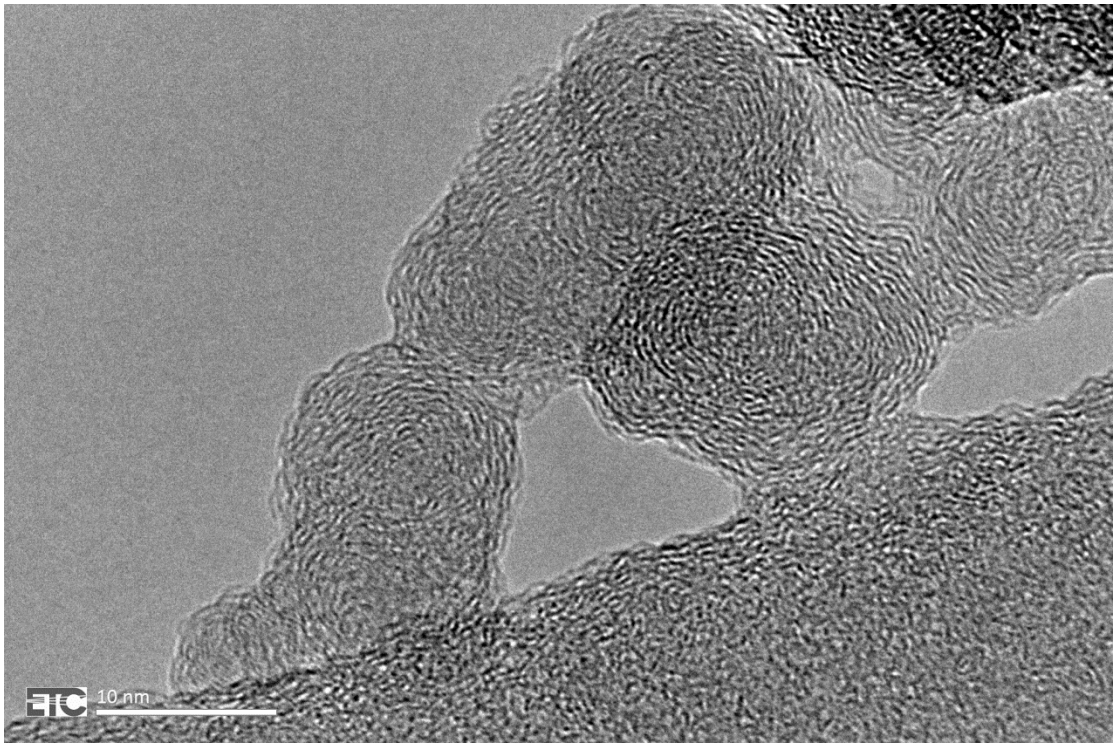

(ii)

B: B20 RME

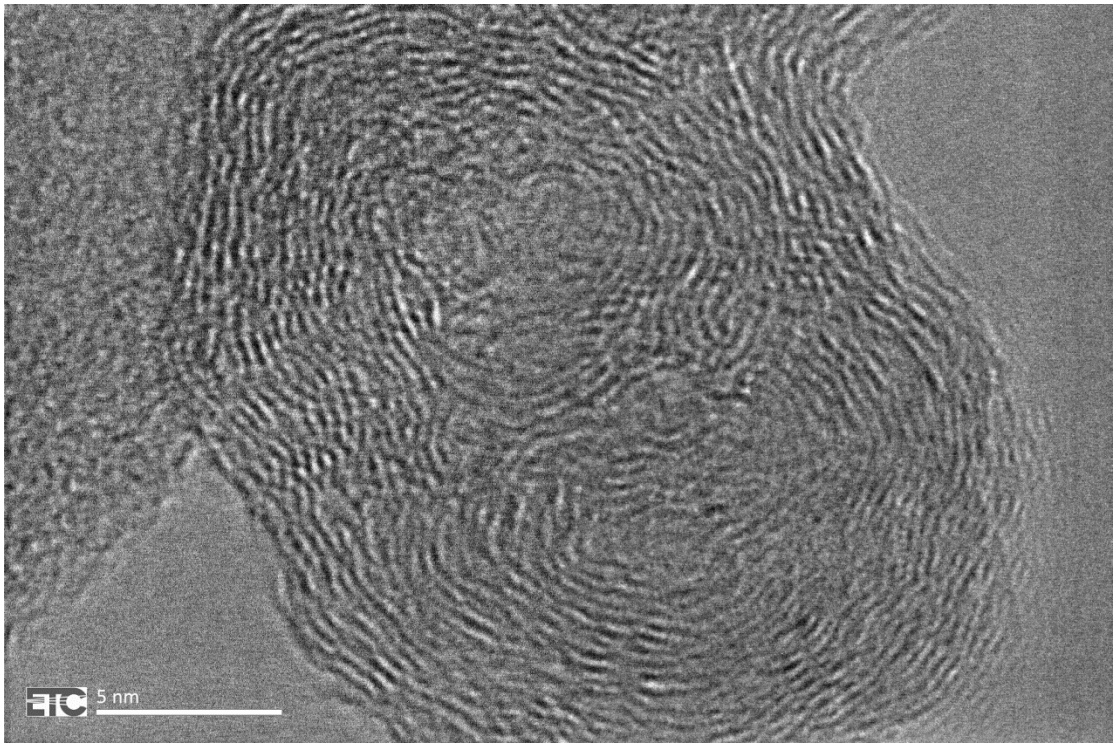

(i)

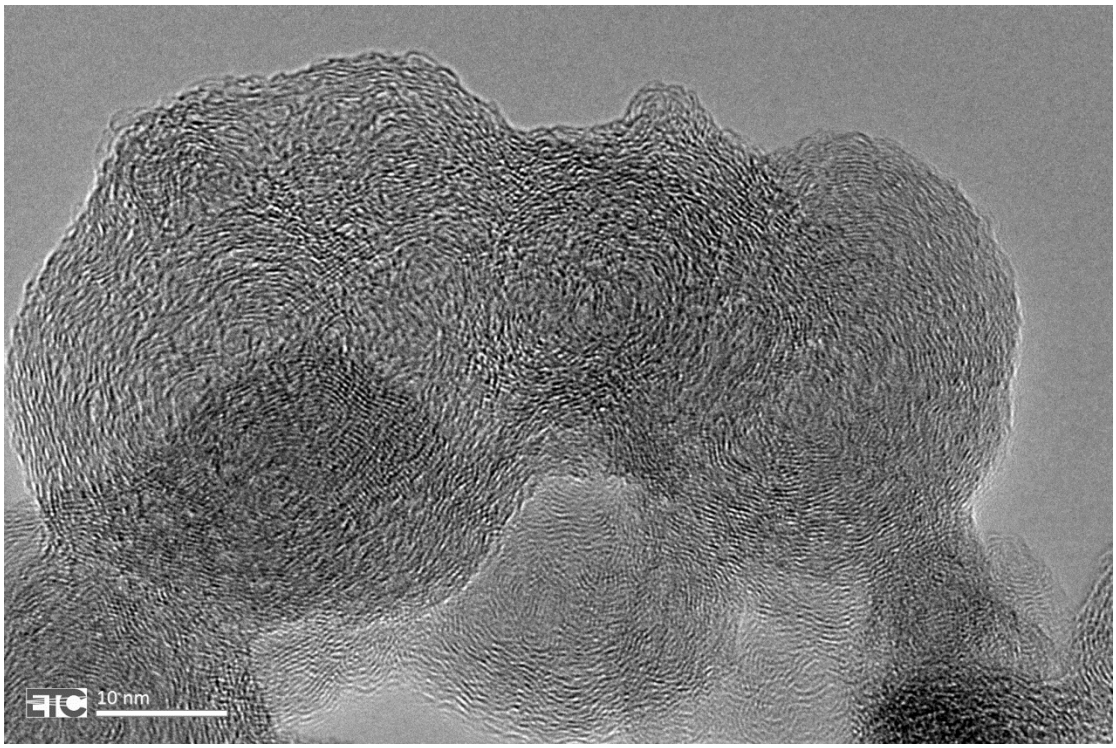

(ii)

C: B20 SME

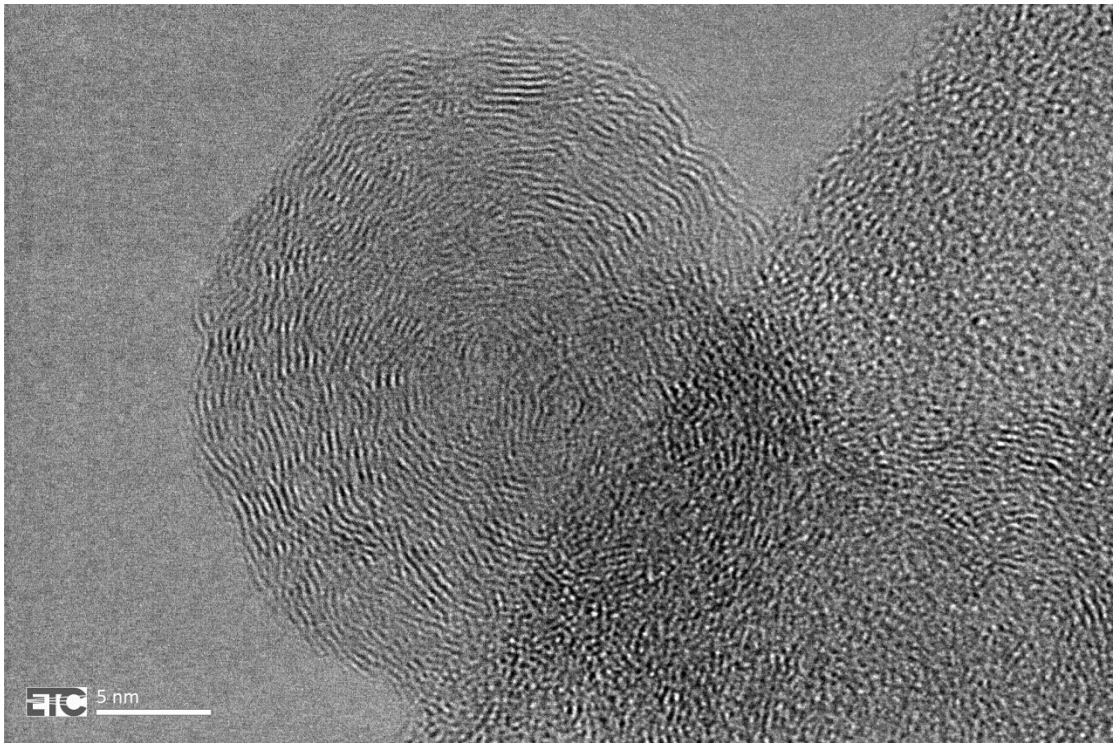

(i)

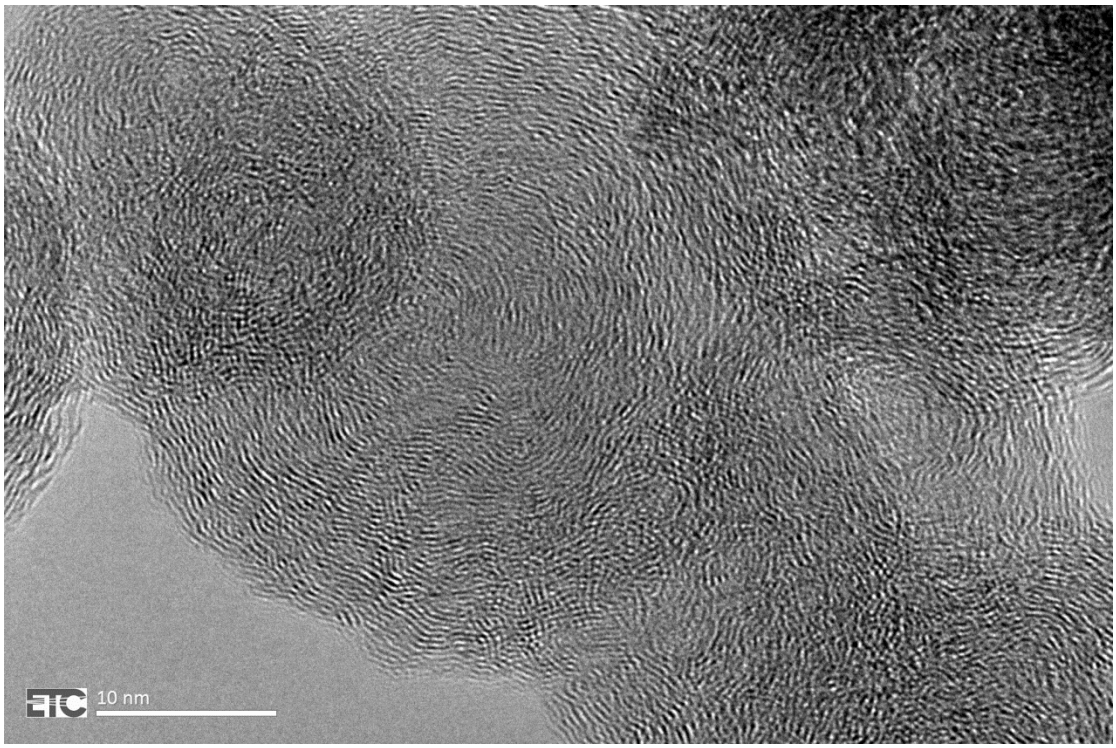

(ii)

D: B20 UCOME

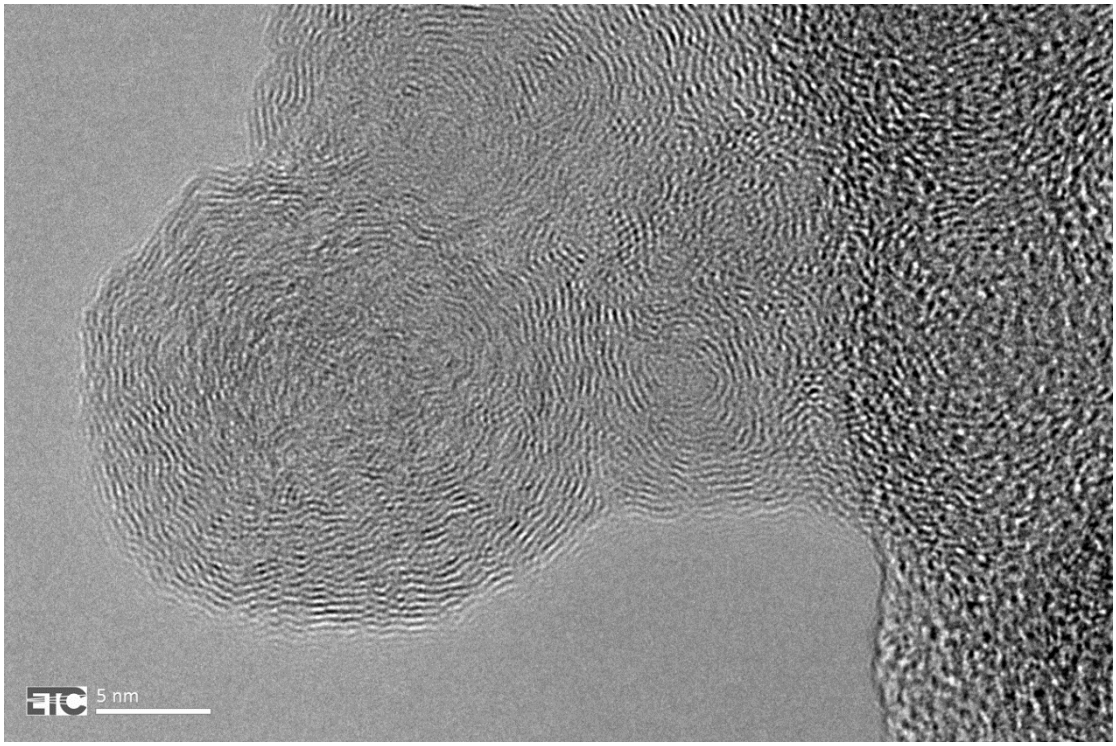

(i)

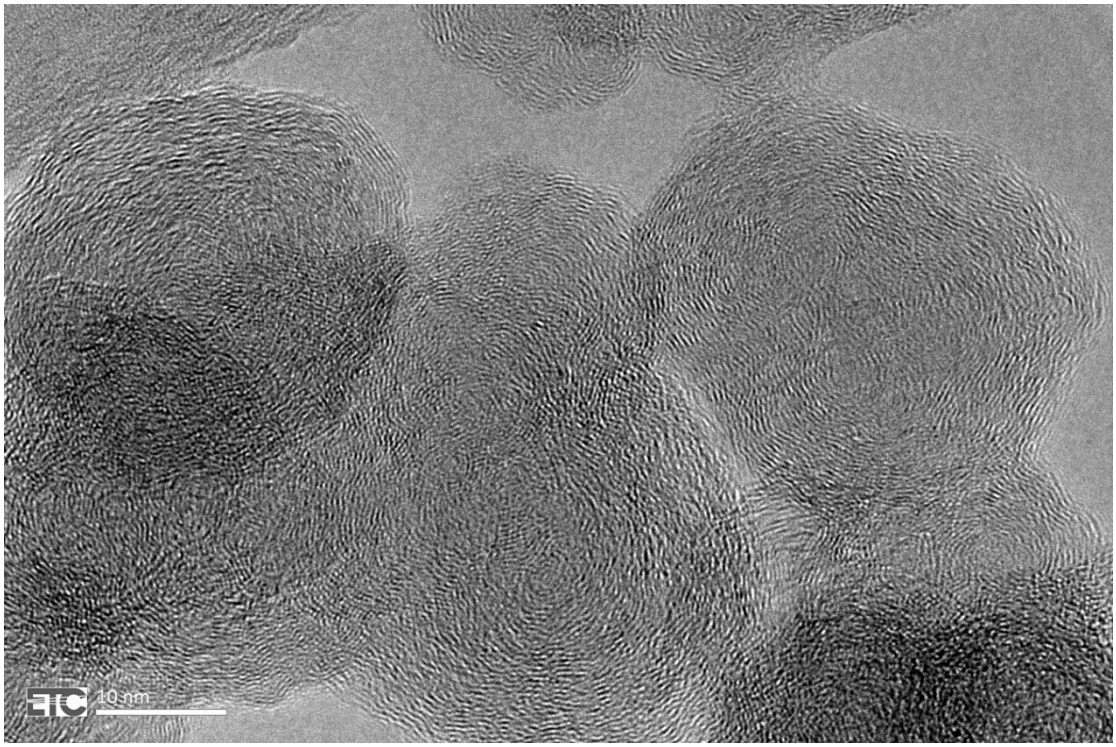

(ii)

E: B40 RME

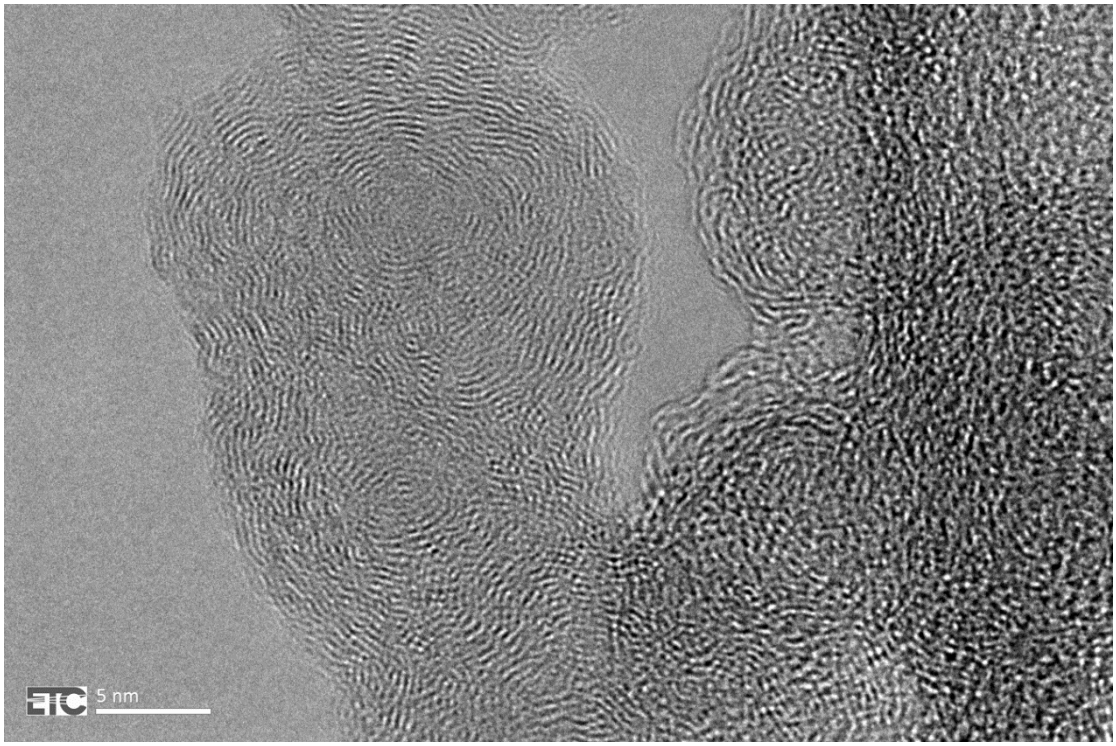

(i)

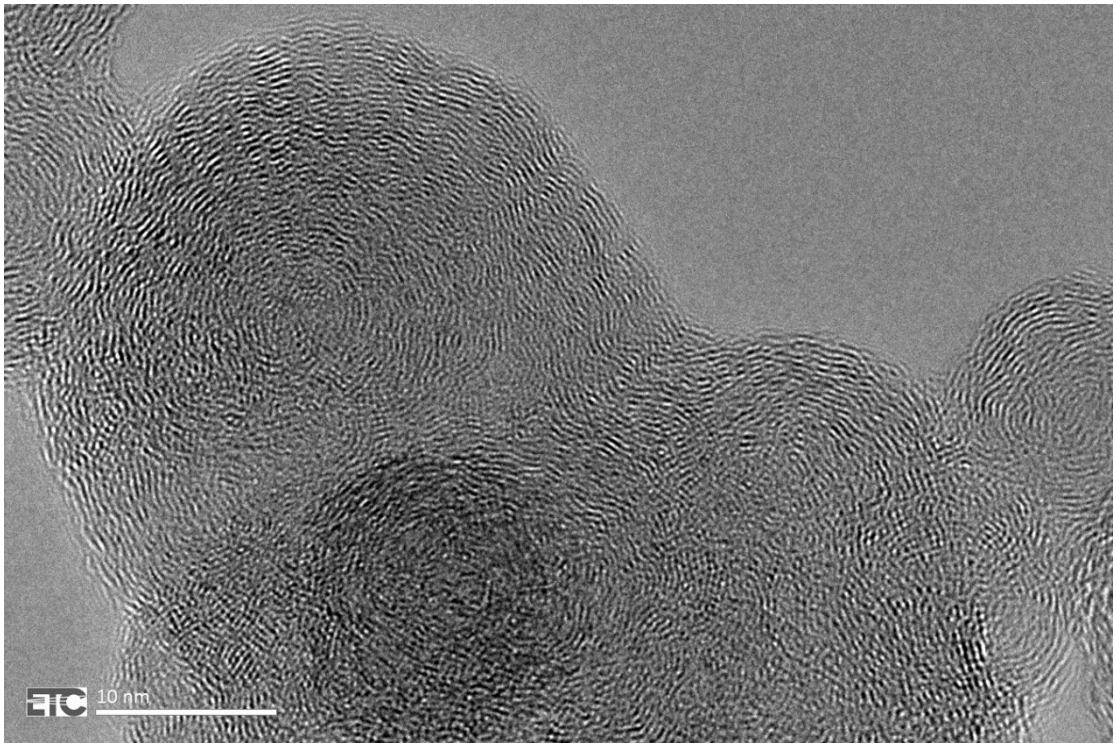

(ii)

F: B40 SME

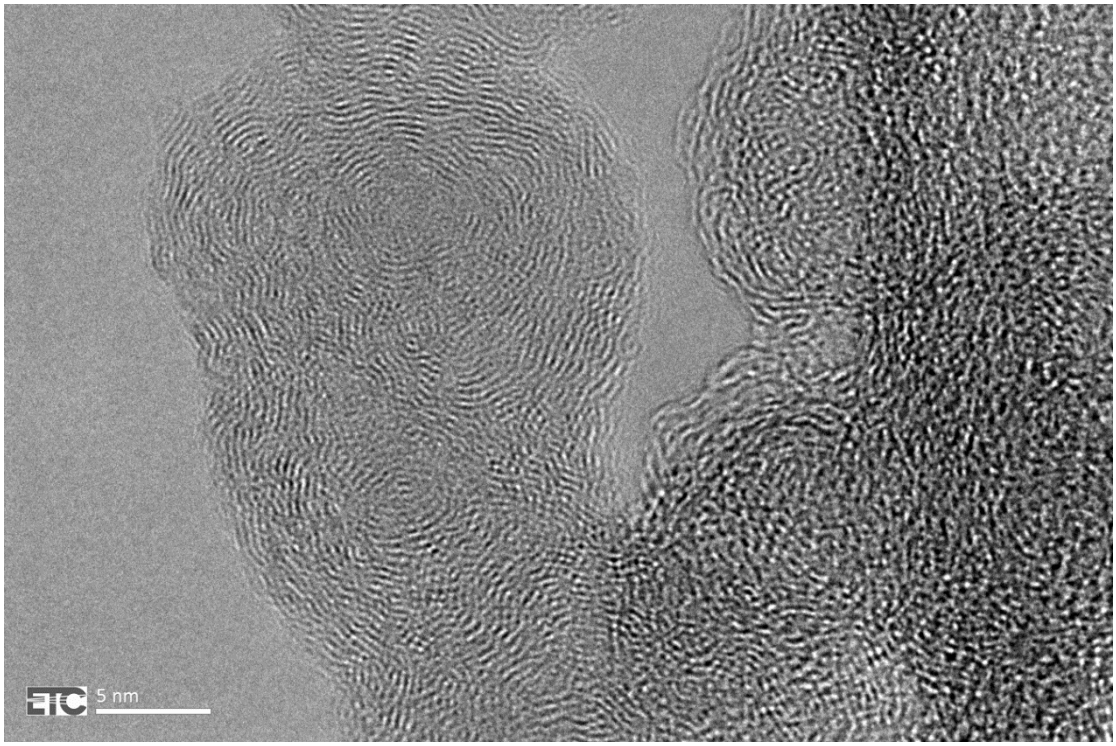

(i)

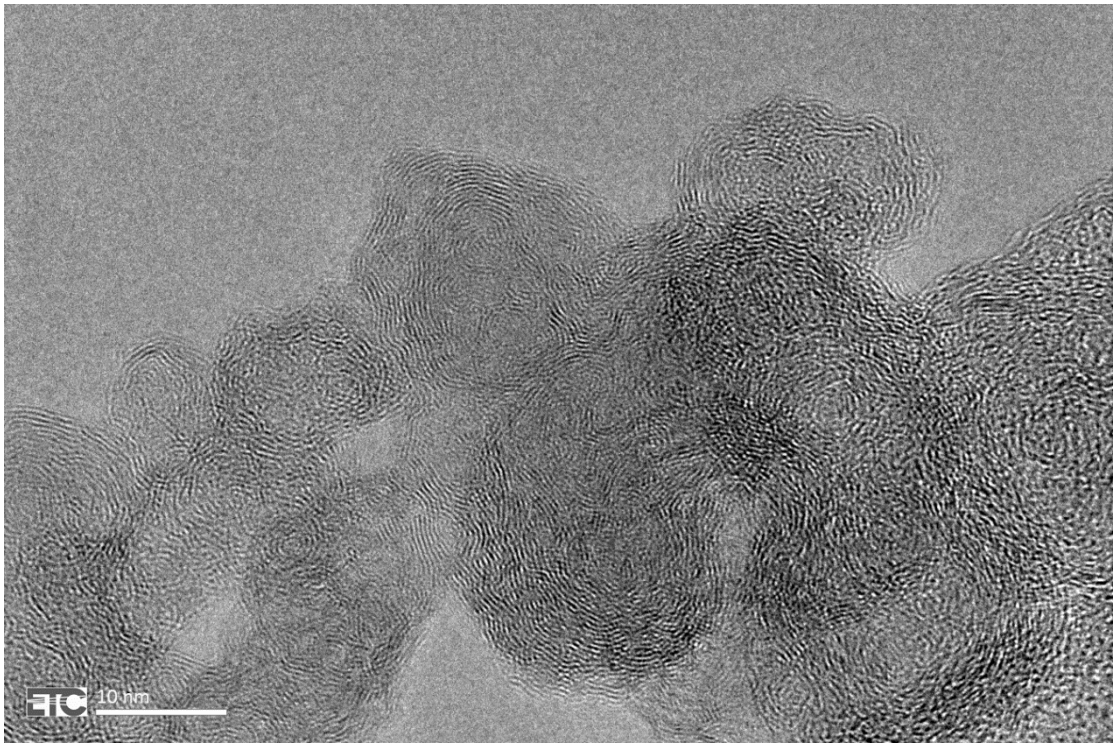

(ii)

G: B40 UCOME

HRTEM images of PM samples from various fuel blends at (i) 5nm and (ii) 10 nm resolutions taken at ambient temperatures. A: Petrodiesel, B: B20 RME, C: B20 SME, D: B20 UCOME, E: B40 RME, F: B40 SME and G: B40 UCOME

Publications

(i) D M Peirce, **N S Alozie**, D W Hatherill, and L C Ganippa, "Premixed Burn Fraction; Its Relation to the Variation in Nox Emissions between Petro and Biodiesel" Published in *Energy & Fuels* 27, 2013

(ii) **N S Alozie**, D M Peirce, A Lindner, W Winklmayr and L C Ganippa, "Influence of Dilution conditions on diesel Exhaust Particle Measurement Using Mixing Tube Diluter" *SAE Paper No 2014-01-1568*, Presented at *Society of Automotive Engineers* World Congress, Detroit 2014.

(iii) **N S Alozie**, D M Peirce and L C Ganippa, "Comparative Influences of Air and Nitrogen as Dilution Gases in Measurement of Diesel Engine Particle Number Concentrations" *SAE Paper No. 2014-01-1576*, Presented at *Society of Automotive Engineers* World Congress, Detroit 2014.

(iv) N Manivannan, **N S Alozie**, D Brennan, M Abbod, W Balachandran and L C Ganippa, "DPF Regeneration Using Microwave (MW) Energy" Presented at COMSOL Multiphysics Conference in Pune, India 2015.

(v) W Balachandran, N Manivannan, R Beleca, M Abbod, D Brennen, **N S Alozie** and L C Ganippa "Non Thermal Plasma System for Marine Diesel Engine Emissions Control" *IEEE Transactions on Industry Applications* - Manuscript ID 2015-EPC-0681.R1 – ACCEPTED

(vi) **N S Alozie**, D M Peirce, G Fern and L. C Ganippa "Influence of Biodiesel Blending on Particulate Matter (PM) Oxidation Characteristics" Under preparation for submission to *Journal of FUEL*

(vii) **N S Alozie**, L C Ganippa, N Manivannan, D Brennan, M Abbod, and W Balachandran "Diesel Particulate Filter Regeneration using Microwave Energy" Under preparation for submission to *Journal of Applied Energy*

REFERENCES

Abdul-Khalek, I. S., and Kittelson, D. (1995). Real Time Measurement of Volatile and Solid Exhaust Particles using a Catalytic converter. *SAE Technical Paper 950236* (pp. 1-17). Detroit: SAE International.

Abdul-Khalek, I., Kittelson, D. B., and Bear, F.,. (1999). Influence of Dilution conditions on diesel exhaust particle size distribution measurements. *SAE Technical Paper 1999-01-1142, doi: 10.4271/1999-01-1142*. Detroit: SAE International.

Adachi, M. a. (2014). *Engine Emissions Measurement Handbook.* Warrendale, PA 15096-0001 USA: SAE International (For Horiba Automotive Test Systems).

Adolph, D. R. (2009,). Gas Exchange Optimization and the Impact on Emission Reduction for HSDI Diesel Engines. *SAE Technical Paper* (pp. SAE Technical Paper 2009-01-0653, 2009, doi:10.4271/2009-01-0653.). Detroit: SAE International.

Alozie, N. S., Peirce, D and Ganippa, L. (2014B). Comparative Influenves of Air and Nitrogen as Dilution Gasesin Measurement of Diesel Engine Particle Number Concentrations. *Society of Automotive Engineers Technical Paper 2014-01-1576.* Detroit: SAE International.

Alozie, N. S., Peirce, D., Lindner, A., Winklmayr, W., and Ganippa, L. (2014A). Influence of Dilution Condition on Diesel Exhaust Particle Measurement using a Mixing Tube Diluter. *SAE Technical Paper 2014-01-1568, doi:10.427/2014-01-1568.* Detroit: SAE International.

Amann, C. A., Stivender, D. L., Plee, S. L., and MacDonald, J. S. (1980). Some rudiments of Diesel particulate emissions. *Society of Automotive Engineers 800251*. Detriot: SAE International.

An, H., Kilroy, C., McGinn,P. J. (2005). An Examination of microwave heating to enhance diesel soot combustion. *Thermochimica acta 435*, 57-63.

Andersson, J., Giechaskiel, B., Munoz-Bueno, R., Sandbach, E., and Dilara, P. (2007). *Particle Measurement Programme(PMP) Light-duty Inter-laboratory Correlation Exercise(ILCE_LD) Final Report, EUR 22775 EN.* Luxembourg: European Commission Joint Research Centre; Institute for Environmental Sustainability.

Andersson, J., Mamakos, A., Giechaskiel, B., Carriero, M., and Martini, G. (2010). *Particle measurement Programme (PMP) Heavy-duty Inter-laboratory Correlation Exercise (ILCE_HD) Final Report (EU24561 EN).* Luxembourg: European Commission Joint Research Centre.

Andersson, Jon. (2011). *Summary Report of Module 1- Biofuel Effects on Diesel Performance, Emissions and Economy in Conventional and Advanced Technologies.* West Surssex: Ricardo UK Lt

Andrews, G. E., Clarke, A. G.,Rojas, N. Y., Sale, T., and Gregory, D.,. (2001). Diesel Particle Size Distribution: The Conversion of Particle Number Size to Mass Distribution. *Society of Automotive Engineering Conference Paper 2001-01-1946.* Detroit: SAE International.

AVL. (2012). *Euro 5&6 Regulations EU Passenger Cars, Light Duty Vehicles, Medium Duty Vehicles* . AVL List GmbH 1996-2011 .

Babu, V. S., Farinash, L., and Seehra, M. S. (1995). Carbon in diesel particulate matter: structure, microwave adsorption, and oxidation. *Journal of materials Research*, 1075 -1078.

Banus, E. D. (2013). *cdn.intechopen.com/pdfs-wm/44436.pdf.* Retrieved December 14th, 2015, from (http://creativecommons.org/licenses/by/3.0.

Bartok, W. and Sarofim, A. F. (1991). *Fossil fuel combustion: A source book.* New York: Wiley.

Baumgard, K. J., and Johnson , J. H.,. (1996). The EFfect of Fuel and Engine Design on Particle Size Distributions. *Society of Automotive Engineers Conference Paper 960131.* Detroit: SAE International.

Bermudez, V., Serrano, J.R., Piqueras, P. andGarcía-Afonso, O. (2012). Influence of DPF Soot Loading on Engine Performance with a Pre-Turbo Aftertreatment Exhaust Line. *Society of Automotive Engineers Paper 2012-01-0362.* Detroit: SAE International.

Bhardwaj, O. P., Luers, B., Kolbeck, A. F., Koerfer, T., Kremer, F., Pischinger, S., Berg, A. V., and Roth, G. (2013A). Tailor Made Biofuels: Effect of Fuel properties on the soot microstructure and consequences on particle filter regeneration. *Proceedings of the ASME on Internal Combustion Engine Division , Fall Technical Conference* (pp. 1-14). Dearborn Michigan: ASME, ICEF2013-19165.

Bhardwaj, O.P., Kolbeck, A. F., Kkoerfer, T., and Honkanen, M. (2013B). Potential of Hydrogenated Vegetable Oil (HVO) in Future High Efficiency Combustion System. *2013-01-1677.* Detroit: SAE International.

Birch, M. E. and Cary, R. A. . (1996). Elemental Carbon-Based Method for Monitoring Occupational Exposures to Particulate Diesel Exhaust. *Aerosol Science and Technology, 25:3,* 221-241.

Bobba, M., Musculus, M.,and Neel, W. (2010). Effect of Post Injections on In-Cylinder and Exhaust Soot for Low -Temperature Combustion in a Heavy Diesel Engine. *SAE Internattional Journal of Engines,* 496-516.

Boehman, A. (2013). Fuel and Combustion Strategy Impacts on Soot Nanostructure and Reactivity. *ERC Symposium.* Michigan.

Boehman, A. L., Song, J., and Alam, M. (2005). Impact of Biodiesel Blending on Diesel Soot and the Regeneration of Diesel Particulate ilters. *Energy and Fuels 19,* 1857-1864.

Boggavarapu, P. and Singh, S. (2011). Computational study of Injection rate shaping for emissions control in diesel engines. *Society of Automotive Engineers* (pp. 1-13). Detroit: SAE International.

Bowman, C. T. (1992). Control of combustion-generated nitrogen oxide emissions: Technology driven by regulation. *Twenty-Fourth Symposium (International) on Combustion/The Combustion Institute, Invited Lecture* (pp. Vol. 24, No. 1, pp 859-878). Elsevier.

Brockmann, J. E. (2011). Aerosol Transport in Sampling Lines and Inlets. In P. B. Kulkarni, *Aerosol Measurement: Principles, Techniques and Applications* (pp. 69 - 106). New Jersey: John Wiley and Sons.

BS. (2013). *Automotive Fuels - diesel (Requirements and Testing).* The BSI Statandards Limited.

Burtscher, H. (2005). Physical characterization of particulate emissions from diesel engines: a review. *Aerosol Science 36* , 896–932.

Burtscher, H., Baltensperger, U., Bukowiecki, N., Cohn, P., Huglin, C., Mohr, M., Matter, U., Nyeki, S., Schmaltloch,V., Streit, N., and Weingnartner, E.,. (2001). Separation of Volatile and Non-Volatile Aerosol Fractions by Thermodesorption: Instrumentation Development and Applications. *Journal of Aerosol Science 32:*, 427-442.

Cambustion. (n.d.). Soot load vs DP characteristic measurement on the DPG. *Application Note DPG001v02*. Cambridge, UK: Cambustion.

Cantrell, B. K., and Watts, W. F. (1977). Diesel Exhaust Aerosol: Review of Occupational Exposure. *Applied Occupational Environmental Hygiene,* 10109-1027.

CARBOLITE, L. H. (n.d.). Ovens and Furnaces. *Ovens and Furnaces*. Sheffield, Hope Valley S33 6RB: Carbolite, Part of VERDER Scientific.

Choi, M. Y., Hamins, A., Mulholland, W., and Kashiwagi. (1994). Simulataneous Optical Measurement of Soot Volume Fraction and Temperature in Premixed Flames. *Combustion and Flame, 99,* 174-186.

Chong, H. S., Aggarwal, S. K., Lee, K. O., Yang, S. Y., Seong, H. (2013). Experimental investigation on the Oxidation Characteristicsof Diesel Particulates relevant to DPF Regeneration. *Combuation Science and Technology (DOI:10.1080/00102202.2012.709563)*, 95-121.

Christian, R., Knopf, F., Jaschek, A., and Schindler, W. (1993). A new Method For measuring the Filter Smoke Number Measurement with Improved Sensitivity. *AVL Particulate Measurement Tecnology, Translated from MTZ Motortechnische Zeitschrift 54*, 1-8.

Dantes, J., Arregle, J., Lopez, J., and Gracia, A.,. (2007). A Comprehensive Study of Diesel Combustion and Emissions with Post-injections. *Society of Automotive Engineers.* Detroit: SAE International.

David Kittelson, D. B., Watts, F. W ., and Arnold, M. (1998). *Review of Diesel PM Sampling Methods (Supplemental Report Number 2) Aerosol Dynamics, Laboratory and On - Road Studies.* Minneapolis, MN: University of Minnesota Center for Diesel Research.

DCEN. (2014). *Curbing Diesel Pollution in Our Nation's Capital City* . Washington, DC : DC Environmental Network < http://www.dcen.net/current-campaigns/dc-diesel-clean-up-campaign/#sthash.8Q4gkk4i.dpuf>.

Dec, J. E. (1992). *SAE 9202115, Technical Transactions,* (pp. Soot Distribution in a Diesel Engine using 2-D Imaging of Laser-Induced Incandenscence, Elastic scattering, and flame luminosityVol. 101 Sec. 4, pp101-112,). Detroit: SAE International.

Dec, J. E. (1997). A Conceptual Model of DI diesel combustion based on laser-sheet imaging. *Society of Automotive Engineers SAE 970873.* Detroit: SAE International.

Dec, J. E. (2009). Advanced Compression Ignition Engines: Uderstanding In-Cylinder Process. *Proceedings of the Combustion Institute, 32,,* (pp. 2727-2742).

Dec, J. E. and Espey, C. (1995). Ignition and Early Soot Formation in a D. I. Diesel Engine Using Multiple 2-D Imaging Diagonistics. *SAE 950456 Technical Transactions* (pp. 853-875). Detroit: SAE International.

Dec, J. E., zur Loye, A. O., and Siebers, D. L. (1991). Soot Distribution in a D I Diesel Engine Using 2-D Laser-Incandenscence Imaging. *Society of Automotive Engineers* (pp. 277-288). Detroit: SAE International.

Dec, J.E. and Coy, E. B. (1996). OH Radical Imaging in a D I Diesel Engine and the Structure of Early Diffussion Flame. *SAE Paper 960831.* Detroit: SAE International.

DeCarlo, P. F., Slowik, J. G., Woorsnop, D. R., Davidovits, P., and Jimenez, J. L. (2004). Particle Morphology and Density Characterisation by Combined Mobility and Aerodynamic Diameter Measurement, Part 1: Theory. *Journal of Aerosol Science and Technology, 38,* 1185-1205.

Dekati. (2015). Dekarti FPS 4000. *Dekarti FPS 4000*. Dekati Ltd. .

Desantes, J. M., Bermúdez, V., Molina, S., and Linares, W. G. (2011). Methodology for Measuring Exhaust Aerosol Size Distributions using Engine Test under Transient Operating Conditions. *Measurement Science and Technology, Vol.22: DOI:10.1088/0957-0233/22/11/115101,* 115101.

Dhaniyala, S., Fierz, M., Keskinnen, J., and Marjamaki, M. (2011). Instruments Based on electrical Detection of aerosols. In P. B. Kulkarni, *Aerosol Measurement: Principles, Techniques and applications* (pp. 393-416). New Jersey: John Wiley ansd Sons.

Dieselnet. (2014). *Cars and Light DutyTrucks Tiers 1, 2 ands 3.* https://www.diselnet.com/standards/us/li_t1; /ld_t2; /ld_t3.

DieselNet. (2015, December). *Emissions Standards China.* Retrieved January 05, 2016, from https://www.dieselnet.com/standards/cn/: http//www.brunel.ac.uk

DiselNet. (2015, December). *Emissions Standard India.* Retrieved January 05, 2016, from https://dieselnet.com/standards/in/: http://www.brunel.ac.uk

Dockery, D. W., Luttmann-Gibson, H., Rich, D. Q., Link, M. S., Mittleman, M. A., Gold, D. R., ... & Verrier, R. L. (2005). Association of air pollution with increased incidence of ventricular tachyarrhythmias recorded by implanted cardioverter defibrillators. *Environmental health perspectives*, 670-674.

Eastwood, P. (2001). *Critical Topics in Exhaust Gas Aftertreatment.* Baldock Hertfordshire, England: Research Studies Press.

Eastwood, P. (2008). *Particulate Emissions from Vehicles* . West Sussex, England: John Wiley and Sons Limited.

EC, E. (2008). *Directive 2008/50/EC of the European Parliament and of the Council on ambient air quality and cleaner air for Europe.* Strasbourg: Official Journal of the European Union.

EC, E. C. (2001). *Directive 2001/81/EC of the European Parliament and of theCouncil on national emission ceilings for certain atmospheric pollutants.* Luxembourg: Official Journal of the European Communities.

ECE, G. R. (2012). *Global Technical Regulations on Worldwide harmonized LIght Vehicle Transporrt Test Procedures.* Geneva: ECE/ Trans /180/ADD/1.5/Appendix 1 (Global Registry).

EMEP/EEA. (2012). *EMEP/EEA emission inventory guidebook* . EMEP/EEA.

EPA. (2002). *Health Assessment Document for Diesel Engine.* Washington: National Center for Environmental Assessment.

EPA, F. R. (2013). *National Ambient Air Quality Standards for Particulate Matter; Final Rule.* Washington DC: Environmental Protection Agency.

Epsey, C., Dec, J. E., Litzinger, T. A., and Santavicca, D. A. (1994). Quantitative 2-D Fuel Vapor Concentration Images in a Firing D. I. Diesel Engine Using Planar Laser-Induced Rayleigh Scattering. *SAE 940682 Technical Transactions* (pp. 1145-1160). Detriot: SAE International.

Espey, C. and Dec, J. E. (1993). Diesel Engine Combustion Studies in a newly Designed Optical-Access Engine Using High Speed Visualisation and 2-D Laser Imaging. *Society of automotive Engineers Transactions* (pp. 703-723). Detroit: SAE International.

Espey, C. and Dec, J. E. (1995). The Effect of TDC Temperature and Density on the Liquid-Phase Fuel Penetration in a D. I. Engine. *SAE Technical Paper 952456* (pp. 1400 - 1414). Detroit: SAE International.

Esworthy, R. (2013). *Air Quality: EPA's 2013 Changes to the Particulate Matter (PM) Standard.* Washington DC: Congressional Research Service .

Exodus. (22:6). *Holy Bible.*

Fernandez, S. (2012). *Diesel Particulates:Importance of standardizing diesel particulate sampling.* Wangara: GASTECH Australia.

Fierz, M., and Burtscher, H. (2003). *Separation of Solid and Volatile fraction by Thermodesorption and Hot Dilution.* Windich, Switzerland: Institute for Sensor and Signals, University of Applied Sciences 5210 .

Flagnan, R. (2011). Electrical Mobility Methods for Submicrometer Particle Characterisation. In P. B. Kulkarni, *Aerosol Measurement: Principles, techniques and Applications.* (pp. 339-364). Hoboken, New Jersey: Wieley and Sons Inc.

Friedrich, R. and Reis, S. (2004). *Emissions of Air Pollutants.* New York: Springer.

Gautam, M., Popuri, S., Rankin, B., and Seehra, M. (1999). Development of A Microwave Assisted Regeneration System for A Ceramic Diesel Particulate System. *Society of Automotive Enginees (SAE 1999-01-3565)* (pp. 1-16). Detroit: SAE International.

Giakoumis, E. G. (2014). Particulate Matter Emissions during Transient DieselEngine Operation with various Diesels/Biofuel Blends (Biodiesel, Ethanol and N-Butanol). In P. Pesridis, *Automotive Exhaust Emissions and Energy Recovery* (pp. 91-130). New York: NOVA Publishers

Giechaskiel, B., Arndt, M., Schindler, W., Bergmann, A., Silvis, W. and Drossinos, Y. (2012A). Sample Non-Volatile Vehicle Exhaust Particles: A simplified Guide. *SAE Journal doi:10.4271/2012-01-0443*, 379 - 399.

Giechaskiel, B., Carriero, M., Martini, G., Krasenbrink, A., Scheder, D. (2000). Calibration and Validation of Various Commercial Particle Number Measurement Systems. *Society of Automotive Engineers, Technical paper 2009-01-115.* Detroit: SAE International.

Giechaskiel, B., Carriero, M., Martini, G., Krasenbrink, A., Scheder, D. (2009). Calibration and Validation of Various Commercial Particle Number Measurement Systems. *Society of Automotive Engineers Technical paper 2009-01-115.* SAE International.

Giechaskiel, B., Cresnoverh, M., Jörgl, H., Bergmann, A. (2010). Calibration and Accuracy of a Particle Number Measurement System. *Measurement Science and Technology. Doi:10.1088/0957-0233/21/4/045102.*, 045102.

Giechaskiel, B., Dilara, P., and Anderson, J. (2008B). Particle Measurement Programme (PMP) Light-Duty Inter-laboratory Correlation Exercise: Repeatability and Reproducibility of Particle Number Method. *Journal of Aerosol Science and Technology, 42, DOI: 10.1080/02786820802220241*, 528- 543,.

Giechaskiel, B., Dilara, P., Sandbach, E., and Anderson, J. (2008). Particle Measurement Programme (PMP) Light-Duty Inter-laboratory Correlation Exercise: Comparison of different Particle Number Measurement Systems. *Measurement Science and Technology vol.19:095401*.

Giechaskiel, B., Mamakos, A., Anderson, J., Dilara, P., Martini, G., Schindler, W., and Bergmann, A. (2012). Measurement of Automotive Non-volatile Particle Number Emissions within the European Legislative Framework: A Review. *Journal of Aerosol Science and Technology*, 719-749.

Giechaskiel, B., Schindler, W., Jörgl, H., Vescoli, V., and Bergmann, A. (2007). Accuracy of Particle Number Measurements from Partial Flow Dilution Systems. *SAE Technical Paper 2011-24-0207. DOI: 10.4271/2011-24-0207.* Detroit: SAE International.

Giechaskiel, B., Schindler, W., Jörgl, H., Vescoli, V., and Bergmann, A. (2011). Accuracy of Particle Number Measurements from Partial Flow Dilution Systems. *SAE Technical Paper 2011-24-0207. DOI: 10.4271/2011-24-0207.* Detroit: SAE Interntional.

Gilot, P., Brillard, A., and Stanmore, B. R. (1995). Geometric effects ofn mass transfer during thermogravimetric analysis:application to the reactivity of of diesel soot. *Combustion Flame*, 102: 471-480.

Glassman, I. (1988). SOOT FORMATION IN COMBUSTION PROCESSES. *Twenty-Second Symposium (International) on Combustion.* (pp. 295-311). The Combustion Institute

Gulijk, C.V., Marijnissen, J.C.M., Makkee, M., Moulijn, J. A., and Schmidt, A. (2004). Measuring Diesel Soot with a Scanning Mobility Particle Size and an Electrical Low-Pressure Impactor: Performance Assessment with a Model for Fractal-like Agglomerates. *Journal of Aerosol Science, 35*, 633-655.

Hansen, K. F. (1997). Chemical and biological characteristics of exhaust emissions from a DI diesel engine fuelled with rapeseed oil methyl ester (RME). *Society of Automotive Engineers 971689.* Detroit: SAE International.

Harvard, M. S. (2012). *Lung Cancer Overview.* Massachusetts: Community Connect to Research (On line resource).

Hawley, B., L'Orange, C., Olsen, D. B., Marchese, A. J. and Volckens, J. (2014). Oxidative Stress and Aromatic Hydrocarbon Response of Human Bronchial Epithelial Cells Exposed to Petro or Biodiesel Exhaust Treated with a Diesel Particulate Filter. *Oxford Journal of Toxicological Sciences, 141(2),* 505–514.

Heejung, J., Kittelson, D. B. and Zachariah, M. R. (2003 .). The influence of engine lubricating oil on diesel nanoparticle emissions and kinetics of oxidation. *SAE Technical Paper, No. 2003-01-3179.* Detroit: SAE international.

HEI. (2010). *Traffic Related Air Pollution: A critical review of literature on emissions, exposure and health effects.* Boston, Massachusetts: Health Effects Institute.

HEI, D. L. (n.d.). Dekati ejector diluter in exhaust measurements v2.1. *Dekati Ltd Technical Note*. FIN-33700 Tampere, Finland: DekartiLtd.

Henein, N. A. (1976). Analysis of pollutant and control and fuel economy in diesel engines. *Progress in Energy an combustion Science*, 165-207, vol.1.

Hering, S. V., Stolzenburg, M. R.,. (2005). A method for particle size amplification by water condensation in a laminar thermally diffusive flow. *Aerosol Science and Technology (39)*, 428 - 436.

Heywood, J. B. (1988). *Internal Combustion Engine Fundamentals.* New York: McGraw-Hill.

Higgins, B., Siebers, D. and Aradi, A. (2000). Diesel-spray ignition and pre-mixed burn behaviour. *Society of Automotive Engineers* (pp. SAE Technical Paper 2000-01-0940). Detroit: SAE International.

Hinds, T., Twigg, M., and Gallinger, M. (2010). A New Instrument for Diesel Particulate Filter functional Tests in Development and Quality Control Applications. *Society of Automotive Engineers (SAE 2010-01-0809).* Detroit: SAE International.

Hinds, W. C. (1999). Aerosol Technology - Properties, Behavior, and Measurements of Airborne Particles.New York: Wiley - Interscience; 2nd edition.

Hinds, W. C. (2011). Physical and Chemical Processes in Aerosol Systems. In P. B. Kulkarni, *Aerosol Measurement: Principles, Techniques and Applications* (pp. 36-39). New Jersey: Wiley and Sons.

Hofeldt, D. and Chen, G.,. (1996). Transient Particulate Emissions from Diesel Buses During the Central Business District Cycle. *SAE Technical Paper 960251, doi:10.4271/960251.* SAE International.

Hong, S., Margaret S. Wooldridge,M. S., Im, H. G., Assanis, D. N., and Pitsch, H. (2005). Development and application of a comprehensive soot model for 3D CFD reacting flow studies in a diesel engine. *Combustion and Flame 143,* 11–26.

Huang, Y. T., Li, Z., Carter, J. D., Soukup, J., Schwartz, D. A. and Yang, I. V. (2009). Fine Ambient Particles Induce Oxidative Stress and Metal Binding Genes in Human Alveolar Macrophages. *American Journal Respiratory Cell & Molecular Biology Vol 41.*, 544–552.

IARC. (2012). *IARC: DIESEL ENGINE EXHAUST CARCINOGENIC.* Lyon: World Health Organisation.

Jääskeläinen, H. (2007). *https://www.dieselnet.com/tech/diesel_exh_pres.php*. Retrieved October 15th, 2015, from www.DieselNet.com (Copyright Ecopoint Inc. Revision 2007.03a): http:/www.brunel.ac.uk

Jaussi, F. (2008, November 12, 13, 14). Critical effects of filters on engines and on filters by engines. *CARB/AQMD Course on Ultrafine Diesel Particles and retrofit technologies for Diesel Engines*. CH -1752 Villars-sur-Glâne, Fribourg, Switzerland: CARB/AQMD .

Jung H., Kittleson, D. B., and Zachariah, M. R. (2006). Characteristics of SME Biodidiesl-Fuelled Diesel Particle Emissions and Kinetics of Oxidation. *Environmental Science and Technology (40)*, 4949-4955.

Kandylas, I. P. and Stamatelos, A. M. (1999). Modeling catalytic regeneration of of diesel particulate filters, taking into account adsorbed hydrocarbon oxidation. *Ind. Eng. Chem. Res., 38 (5)*, pp 1866–1876.

Karabektas, M. (2009). The effects of turbocharger on the performance and exhaust emissions of a diesel engine fuelled with biodiesel. *Renewable Energy, vol.34*, 989–993, .

Kasper, M. (2004). The Number Concentration of Non-Volatile Particles : Designstudy for an Instrument according to the PMP recommendations. *Saociety of Automotive Engineers: SAE2004-01-0960, doi: 10.4271/2004-01-0960* . Detroit: SAE International.

Kawai, T., Goto, Y., and Odaka, M.,. (2004). Influence of Dilution Process on Engine Exhaust Nano Particles. *SAE Technical Paper 2004-01-0963.* Detroit: SAE International.

Khair, M. K. (1998). *Turbocharging systems for internal combustion engines.* Washington, DC: U.S. Patent No. 5,771,868. .

Khalek, I. A. (2007). Sampling for Solid and Volatile Exhaust Particle Size, Number and Mass Emissions. *SAE Technical Paper 2007-01-0307.* Detroit: SAE International.

Khalek, I. A. (2007b). *Final Report: Diesel Particulate Measurement Research.* San Athonio, Texas: Southwest Research Institute.

Khalek, I. A., Kittelson, D.B., and Bear, F. (2000). Nanoparticles growth during dilution and cooling of diesel exhaist : Experimental investigationand theoretical assessment . *Society of Automotive Engineers.* Detroit: SAE International.

Khalek, I.A., and Bougher, T. (2011). Development of a Solid particle Measurement System Using a catalitic Stripper Technology. *SAE Technical Paper 2011-01-0635.* Detroit: SAE International.

Khan, M. I. (1969). Formation and Combustion of Carbon in a Diesel Engine. *Proceedings of the Institute of Mechanical Engineers, Vol.184, Part 35*, 36-43.

Kitamura, T. I. (2002). Mechanism of smokeless diesel combustion with oxygenated fuels based on the dependence of the equivalence ratio and temperature on soot particle formation. *International Journal of Engine Research 3.4*, 223-248.

Kittelson, D .B., Arnold, M., Watts, W. F. (1999). *Review of Diesel Particulate Matter Sampling Methods: Final Report.* Minneapolis: Department of Mechanical Engineering, Univesity of Minnesota.

Kittelson, D. (2003). Sampling and Dilution Issues. *ACES Worksop.* Denever.

Kittelson, D. B. (1998.). Engines and Nanoparticles: A Review. *Jornal of Aerosol science. 29,No 5/6*, 575-588.

Kittelson, D. B., Arnold, M. and Watts,W. F. (Jr). (1999). *Review of Diesel Particulate matter samplingmethods - Final Report.* Minneapolis, MN: University of Minnesota, Center for Diesel Research.

Kittelson, D. B.,Watts, W. F., and Arnold, M. (1998). *Review of Diesel Particulate Matter Sampling Methods: Supplemental Report No.1, Diesel Exhaust Particle Measurement Instruments.* Minneapolis, MN: University of Minnesota Center for Diesel Research.

Kittelson, D., Ambs, J., and Hadjkacem, H.,. (1990). Particulate Emissions from Diesel Engines:Influence of In-Cylinder Surface. *SAE Technical Paper 900645, doi:10.4271/900645.* Detroit: SAE International.

Kittelson, D., Watts, W., Wei, Q., Drayton, M., Paulsen, D. and Bukowiecki, N. (2000). Diesel Aerosol Sampling in the Atmosphere. *SAE Technical Transactions Paper 2000-01-2212.* Detroit: SAE International.

Knothe, G. S. (2006, 20). Exhaust emissions from biodiesel, petro diesel, neat methyl esters, and alkanes in new technology engine. *Energy Fuels* , 3-8.

Kolmanovsky, I. e. (1999). *Issues in modelling and control of intake flow in variable geometry turbocharged engines.".* Chapman and Hall CRC research notes in mathematics.

Kook, S., Bae, C., Miles, P. C., Choi, D., Bergin, M., and Reitz, R. D. (2006). The Effect of Swirl Ratio and Fuel Injection Parameters on CO Emission and Fuel Conversion Efficiency for High-Dilution, Low-Temperature Combustion in an Automotive Diesel Engine. *Society of Automotive Engineers* (pp. SAE 2006-01-0197). Detroit: SAE International.

Kosaka, H., Aizawa, T., and Kamimoto, T. (2005). Two-dimensional imaging of ignition and soot formation processes in a diesel flame. *International Journal of Engine Research*, 21-42, vol. 6 no. 1, doi: 10.1243/146808705X7347.

Kumar, P. R. (2010). A Review of the Characteristics of Nanoparticles in the Urban Atmosphere and the particles for Developing Regulatory Controls . *Atmospheric Environment 44*, 5035-5052.

Labecki, L., Cairns, A., Xia, J., Zhao, H. and Ganippa, L. C. (2012). Combustion and Emission of Rapeseed Oil Blends in Diesel Engine. *Applied Energy, 95*, 139-146.

Lapuerta, M., Armas, O., and Rodrıguez-Fernandez, J. (2008). Effect of biodiesel fuels on diesel engine emissions. *Progress in Energy and Combustion Science 34*, 198–223.

Lapuerta, M.,Martos, F. J., and Herreros, J. M. (2007). Effect of engine operating conditions on the size of primary particles composing diesel soot agglomerates. *Aerosol Science 38*, 455 – 466.

Lee, K. O. and Zhu, J. (2005). Effects of Exhaust system components on particulate morphology in a light duty diesel engine. *SAE Paper 2005-01- 0184.* Detroit: SAE International.

Lee, K. O., Cole, R., Sekar, R., Choi, M. Y.,Zhu, J., Kang, J.,and Bae, C. (2001). Detailed characterization of morphology and dimensions of diesel particulates via thermopheric sampling. *SAE Paper 2001-01-3572.* Detroit: SAE International.

Lee, K. O., Cole, R., Sekar, R., Choi, M.Y., Kang,J.S., Bae, C. S.and Shin, H. D. (2002). Morphological investigation of the microstructuredimensions, and fractal geometry of diesel particulates. *Proceedings of the Combustion Institute, Volume 29.*, (pp. 647–653).

Lee, K., Yang, S., Seong, H., Howden, K., and Singh, G. (2011). *Development of Advanced Diesel Particulate Filtration (DPF) Systems.* Chicago: Argonne National Laboratory.

Lemon, D. (2014). Emissions Mitigation and Control Systems. In A. Pesiridis, *Automotive Exhaust Emissions and Energy Recovery* (pp. 1-28). New York: Nova Science Publishers, Inc.

Liang, B., Ge, Y., Tan, J., Han, X., Gao, L., Hao, L., Ye, W. and Dai, P. (2013). Comparison of PM Emissions from a Gasoline Direct Injected (GDI) Vehicle and a Port Fuel Injected (PFI) Vehicle Measured by Electrical Low Pressure Impactor (ELPI) with Two Fuels: Gasoline and M15 methanol Gasoline. *Journal of Aerosol Science, 57*, 22-31.

Lighty, J. S., Veranth, J. M., and Sarofirm, A. F. (2000). Combustion Aerosols: Factors Governing their Size and Comoposition and Implications to Human Health. *Journal of the Air and Waste Management Association DOI: 1080/10473289.2000.10464197*, 1565-1618.

Lin, Y. C., and Cheng, M. T. (2007). Evaluation of formation rates of NO_2 to gaseous and particulate nitrate in the urban atmosphere. *Atmospheric Environment 41*, 1903–1910.

Lin, Y. C., Cheng, M. T., Ting, W. Y. and Yeh, C. R. (2006). Characteristics of gaseous HNO_2, HNO_3, NH_3 and particulate ammonium nitrate in an urban city of Central Taiwan. *Atmospheric Environment 40*, 4725–4733.

Lopez-Fonseca, R., Landa, I., Elizundia, U., Gutierrez-Ortiz, M. A.,and Gonzalez-Velasco, J. R. (2006). Thermokinetic modeling of the combustion of carboneceous particulate matter. *Combustion and Flame (144)*, 398-406.

Loye, Z., Siebers, A. O., and Dec, J. E. (1990). 2-D Soot imaging in a direct injection diesel engine using laser-induced incandedescence imaging. *Symposium on Diagnostics and Modelling of Combustion in Internal Combustion Engine COMODIA90*, (pp. 523-528).

Lu, T., Cheung, C.S., Huang, Z. (2013). Influence of Waste Cooking Oil Biodiesel on the Particulate Emissions and Particle Volatility of a DI Diesel Engine. *Aerosol and Air Quality Research 13*, 243–254.

Lupuerta, M., Ballesteros, R., and Rodriguez-Fernandea, J. (2007). Thermogravimetric analysis of diesel particulate matter. *Measurement Science and Tecnology (18)*, 650-658.

Lyyränen J., Jokiniemi J., Kauppinen E. I., Backman U., and Vesala H. (2004). Comparison of Different Dilution Methods for Measuring Diesel Particle Emissions. *Aerosol science and Technology 38:1, DOI:10: 1080/02786820490247579*, pp12-23.

Ma, J., Fang, M., Li, P., Zhu, B., Lu, X., and Lau, N. T. (1997). Microwave-assisted catalytic combustion of diesel soot. *Applied Catalysis A: General 159*, 211l-228.

Majewski, W. A. and Khair, M. K. (2006). *Diesel Emissions and Controls.* Warrendale: SAE International.ää

Majewski, W. A. (n.d.). *DieselNet.* Retrieved December 24, 2014, from Google: http://www.DieselNet.com

Manivannan, N. A. (2015B). Modelling of DPF Regeneration using Microwave Energy. *COMSOL CONFERENCE.* Pune, India: COMSOL.

Manivannan, N. B. (2015A). Microwave PlasmaSystem Design and Modelling for Marine Diesel Exhaust Gas Abatment of NOx and SOx. *International Journal of Environmental Science and Development, 6*, 151.

Mansurov, Z. A. (2005). Soot Formation in combustion process (Review). *Combustion, Explosion, and Shock Waves*, 727-744, vol41.

Maricq, M. M. (2007). Chemical characterization of particulate emissions from diesel engines: A review. *Journal of Aerosol Science 38* , 1079 – 1118.

Maricq, M. M. (2007b). Coagulation Dynamics of Fractal-Like Soot Aggregates. *Journal of Aerosol Science, 38*, 141-156.

Maricq, M. M., and Xu, N.,. (2004). The Effective Density and Fractal Dimension of Soot Particles from Premixexd Flames and Motor Exhaust. *Journal of Aerosol Science, 35*, 1251-1274.

Maricq, M. M., Xu, N., Chase, R. E. (2006). Measuring Particulate mass Emissions with the Electrical Low Pressur Impactor. *Journal of aerosol science and Technology, 40*, 68-79.

Mariq, M. M. (2007 B). Coagulation Dynamics of Fractal-Like Soot Aggregates . *Journal of Aerosol Science, 38*, 141-156.

Marjamäki, M. and Keskinen, J. (2005). *Vehicle exhaust particulates characterisation, properties, instrumentation and sampling requirements.* European Commission – DG TrEn, 5th Framework Programme Competitive and Sustainable Growth Sustainable Mobility and Intermodality.

Marple, V. A., and Olson, B. A. (2011). Sampling and Measurement using inertial, gravitational, centrifugal, and thermal techniques. In P. B. Kulkarni, *Aerosol Measurement: Principles, Techniquesand Applications* (pp. 129-151). Hoboken, New Jersey: John aand Sons Inc.

Marquard, A. (2007). Uni[polar field and diffusion charging in the transition regime - Part 1: a 2-D limiting-sphere model. *Journal of Aerosol Science Technology 41*, 597-610.

Martyn, V. T. and Phillips, P. R. (2009). Control of diesel particulate emissions from passenger cars. *Pantinium Metals Rev. 53 (1)*, 27-34.

Martyr, A. J., and Plint, M. A. (2007). *Engine Testing.* Oxford: Butterworth-Heinemann.

Mathis, U., Ristimaki, J., Mohr, M., Keskinen, J., Ntziachristos, L., Samaras, Z., and Mikkanen, P.,. (2004). Sampling Conditions for the Measurement of Nucleation Mode Particles in the Exhaust of a Diesel Vehicle. *Journal of Aerosol Science and Technology, 38*, 1149-1160.

Matthews, E. K. (Undated). Industrial Applications of a Fiber Optic Emissivity Measuring Infrared Thermometer. Boston (SPIE - The Internatinal Societyfor Optical Engineering), Massachusetts , United States of America.

Matthey, J. (2007). Catalyst Handbook: The right chemistry for Tier 4. *Catalyst Handbook: The right chemistry for Tier 4*. Johnson Matthey.

McEnally, C. S. and Pfefferle L. D. (2004b). Fuel decomposition and hydrocarbon growt processes for practical fuel components in non-premixed flames: MTBE and related alkyl esters. *International Journal of Chemical Kinetics; 36*, 345-358.

McEnally, C. S. and Pfefferle, L. D. (2004a). Experimental study of fuel decomposition and hydrocarbon processes for cyclo-hexane and related compounds in non-premixed flames. *Combustion and Flames; 136*, 155-167.

McEnally, C. S. and Pfefferle, L.D. (2005). Decomposition and hydrocarbon growth processes for hexenes in nonpremixed flames. *Combustion and flames; 143,* 246-263.

McEnally, C. S., Pfefferle, L. D., Atakan, B., and Kohse-Ho¨inghaus, K. (2006). Studies of aromatic hydrocarbon formation mechanisms in flames Progress towards closing the fuel gap. *Progress in Energy and Combustion Science, 32*, 247–294.

MedicalPrimer. (2010). *Lung Cancer.* Center for patient partnership: Online resource Centre Philippines.

Mehta, P. S., and Tamma, B. (1998). Effect of Swirl and Fuel Injection Characteristics on Premixed Phase of Diesel Combustion. *SAE Technical Paper SAE 980534.* Detroit: SAE International.

Miller, J. A. and Bowman, C. T. (1989). Mechanisms and Modeling of Nitrogen Chemistry in Combustion. *Progress in Energy and Combustion Science,* 287-338.

Miller, J. A., Michael J. Pillingb, M. J. and Troec, J. (2005). Unravelling combustion mechanisms througha quantitative understanding of elementary reactions. *Proceedings of the Combustion Institute 30,* 43–88.

Moffat, R. J. (1988). Describing the Uncertainties in Experimental Results. *Experimental Thermal and Fluid Science, 1*, 3-17.

Monyem, A., Van-Gerpen, J. H., and Canakci, M. (2001). The effect of timing and oxidation on emissions from biodiesel-fueled engines. *Trans ASAE 44(1)* (pp. 35–42.). American Society of Agricultural Engineers.

Müller, J. O., D.S. Su, D .S., Jentoft, R.E., Kröhnert, J., Jentoft, F.C., and Schlögl, R. (2005). Morphology-controlled reactivity of carbonaceous materials towards oxidation. *Catal. Today 102-103,* 259-265.

Murtagh, M. J., and Johnson T. V. (2014). Diesel Particulate Filter Overview: material, Geometry and Application. In A. Pesiridis, *Automotive Exhaust Emissions and Energy Recovery* (pp. 173-201). New York: Nova Sciences Publishers Inc.

Musculus, M. P. B., Miles, P. C., and Pickett, L. M. (2013). Conceptual models for partially premixed low-temperature diesel combustion. *Progress in Energy and Combustion Science,* 246-283, vol.39.

Naber, J. and Reitz, R.,. (1988). Modeling Engine Spray/Wall Impingement. *Society of Automotive Engineers* (pp. SAE Technical Paper 880107, doi:10.4271/880107.). Detroit: SAE International.

Naber, J. D. and Siebers, D. L. (1996). Effects of gas Density and Vaporisation on Penetration and Dispersion of Diesel Sprays. *SAE Technical Paper 960034.* Detroit: SAE International.

Nauss, K. (1995). *Diesel Exhaust: A Critical Analysis of Emissions, Exposure, and Health Effects.* Massachussets: Health Effects Institute .

Neeft, J. P. A., Nijihuis, X., Smakman, E., Makkee, M., and Moulijn, J. A. (1997). Kinetics of the oxidation of diesel soot. *Fuel 76 (12),* 1129-1136.

Neer, A., and Koylu, U. O. (2006). Effect of operating conditions on the size, morphology, and concentration of submicrometer particulates emitted from a diesel engine. *Combustion and Flame 146*, 142–154.

Ntziachristos, L., Giechaskiel, B., Pistikopoulos, P., Samaras, Z., Mathis, U., Mohr, M., Ristimäki, J., Keskinen, J., Mikkanen, P., Casati, R., Scheer, V., Vogt, R. (2004). Performance Evaluation of a Novel Sampling and Measurement System for Exhaust Particle Characterization. *SAE Technology Paper 2004-01-1439, 2004 SAE World Congress.* Detroit, USA: SAE International.

Numbers. (35:33-34). *Holy Bible.*

Nwafor, O.M. I., Rice, G., and Ogbonna, A. I. (2000). Effect of advanced injection timing on the performance of rapeseed oil in diesel engines. *Renewable Energy*, 433-444, Vol. 21.

O'Connor, J. and Musculus M. (2013). Post Injections for Soot Reduction in Diesel Engines: a Review of Current Understanding. *SAE International* (pp. 400-421). Detriot: SAE International.

O'Connor, J. and Musculus, M. (2014). In-Cylinder Mechanisms of Soot Reduction by Close-Coupled Post-Injections as Revealed by Imaging of soot Luminosity and Planar Laser-Induced Soot Incandescence in a Heavy-Duty Diesel Engine. *SAE Journal of Engines*, 673-693, SAE:2014-01-1255. doi:10.4271/2014-01-1255.

Okamoto, W. K.,Gorse, R. A. and Pierson, W. R. (1983). Nitric Acid in Diesel Exhaust. *Journal of the Air Pollution Cotrol Association, 33:11 DOI: 10.1080/00022470.1983.10465703*, 1098-1100.

Owen, K., and Coley, T. (1995). *Automotive Fuels Reference Book.* Warrendale: Society of Automotive Engineers, Inc.

Palma, V., Ciambelli, P., & Meloni, E. (2011). Influence of operative parameters on microwave regeneration of catalytic soot wff for diesel engines. *Chemical Engineering Transactions 25*, (pp. 1001-1006.).

Palma, V., Ciambelli, P., Meloni, E., and Sin, A. (2013). Study of the catast load for a microwavesusceptible catalytic DPF. *Catalysis Today 216,* 185-193.

Palma, V., Ciambelli, P., Meloni, E., and Sin, A. (2015). Catalytic DPF microwave assisted active regeneration. *Fuel 140*, 50-61.

Palma, V., D'Amore, M., Russo, P., D'Arco, A., and Ciambelli, P. (2010). Regeneration of a soot-trap ceramic foarm by a single-mode microwave

cavity. *Cumbustion Science and Technology 174*, 295-308 DOI: 10.1080/713712957.

Palma, V., Russo, P., Matarazzo, G., and Ciambelli, P. (2007). Microwave improvement of catalyst performance in soot oxidation without additives. *Applied Catalysis B: Environmental 70*, 254–260.

Peirce, D. (2015). *Biodiesels and Oxides of Nitrogen: Inestigation into their relationship.* London: PhD Thesis Submitted to Brunel University London.

Peirce, D. M., Alozie, N. S. I., Hatherill, D. W. and Ganippa, L. C. (2013). Premixed Burn Fraction: Its Relation to the Variation in NOx Emissions between Petro- and Biodiesel. *Energy and Fuels, 2013, 27 (7),* pp 3838–3852.

Pesiridis, A. (2014). *Automotive Exhaust Emissions andEnergy Recovery.* New York: NOVA.

Pickett, L. M. and Lopez, J. J. (2005). Jet-wall interaction effects on diesel combustion and soot formation. *Society of Automotive Engineers* (pp. SAE 2005-01-0921). Detroit: SAE International.

Pickett, L. M. and Siebers, D. L. (2004). Soot in diesel fuel jets: effects of ambient temperature,ambient density, and injection pressure. *Combustion and Flame*, 114-135.

Pickett, L. M., Manin, J., Genzale, C. L., Siebers, D. L., Musculus, M. P. B. and Idicheria, C.A. (2011). Relationship between Diesel Fuel Jet Vapor penetration/dispersion and local fuel mixture-fraction. *SAE Technical Paper 2011-01-0686* (pp. 764-799). Detroit: SAE International.

Pierpont, D. A. and Reitz, R. D. (1995). Effects of Injection Prssure and Nozzle Geometry on D. I Diesel Emissions and Performance. *Society of Automotive Engineers* (pp. 15-24). Detriot: SAE Inc.

Pirjola, L., Parviainen, H., Hussein, T., Valli, A., Ha¨ meri,K., Aaalto, P., Virtanen, A., Keskinen, J., Pakkanen,T.A., Ma¨ kela¨, T., and Hillamo, R.E. (2004). ‘‘Sniffer’’—a novel tool for chasingvehicles and measuring traffic pollutants. *Atmospheric Environment 38*, 3625–3635.

Pope, C. A., Burnett, R. T., Thun, M. J., Calle, E. E., Krewski, D.l., Ito, K., Thurston,G. D. (2002). Lung Cancer, Cardiopulmonary Mortality, and Long-term Exposure to Fine Particulate Air Pollution. *The Journal of the American Medical Association:)doi:10.1001/jama.287.9.1132*, 1132-1141.

Prassad, R. and Bella V. R. (2010). A Review on Diesel Soot Emission, its Effect and Control. *Bulletin of Chemical Reaction Engineering & Catalysis, 5 (2),*, 69 - 86

Price, P., Stone, R.,Collier, T., and Davies, M.,. (2006). Particulate Matter and Hydrocarbon Emissions Measurements: Comparing First and Second Generation DISI with PFI in Single Optical Engines. *Society of Automotive Engineers conference Paper 2006-01-1263.* Detroit: SAE International.

Pronk, A., Coble, J., and Stewart, P. A. (2009, 19). Occupational exposure to diesel engine exhaust : A Literature Review. *Jorunal of Exposure Science and Environmental Epidemology*, 443-457.

Pundir, B. P. (2002). *IC Engines: Combustion and Emissions.* New Delhi: Narosa.

Rayne, S. (2015). Low sulphur fuel benefits: Vehicle Fuel economyand emissions. *National Association of Automobile Manufacturers of South Africa/ford Motor Company.*

Reischl, G. P. (1991 A). Measurement of of Ambient aerosols by Differential Mobility Analyser Method: Concewptsand Realisation for the size range between 2 and 500nm. *Aerosol Science and Technology 14*, 5-24.

Reischl, G. P. (1991 B). The relation ship of input and output Aerosol Characteristics for an ideal Deferential Mobility Analyser Particle Standard. *Journal; of Aerosol Science 22, No 3*, 297-312.

Reischl, G. P. (2006). Characterisation of Particulate Motor Vehicle Emissions by Electrostatic Measurement Techniques . *International Colloquin on the Measurement of and Characterisation of Diesel Soot and other Particulate Matter.* Kyoto, Japan: Institute of Experimental Physics, University of Vienna, Austria.

Reitz, R. D,. and Patterson, M. A. (1998). Modeling the Effects of Fuel Spray Characteristics on Diesel Engine Combustion and Emission. *Society of Automotuive Engineers* (pp. SAE Technical Paper 980131, 1998, doi:10.4271/980131.). Detroit: SAE International.

Richter, H. and Howard, J.B. (2000). Formation of polycyclic aromatic hydrocarbons and their growth to soot—a review of chemical reaction pathways. *Progress in Energy and Combustion Science 26*, 565–608.

Robert Bosch . (1993). *Bosch Automotive Handbook*, . Stuttgart, Germany: SAE.

Rodriguez-Fernandez, J., Oliva, F., Vazquez, R. A. (2011). Characteriztion of Diesel Soost Oxidation Process through an Optimized Thermogrvimetric Anlysis. *Energy and Fuels*, 2039-2048.

Roy, M. M. (2006). Effect of Engine Operating Parameters, Fuel Propertiy and Exhaust gas Treatment on Odour in Direct Injection Diesel Engines. *Proceedings of the Institution of Mechanical Engineers, Part D: Journal of Automobile Engineering*, 595-609.

Sawyer, R. F. and Johnson, J. J. (1995). *Diesel emissions and control technology. In: Diesel Exhaust: A Critical Analysis.* Massachussets: Health Effects Institute.

Schneider, J., Hock, N., Weimer, S., Bormann, S., Kirchner, U., Vogt, R., and Scheer, V. (2005). Nucleation Particles in Diesel Exhaust: Composition Inferred from In-Situ Mass Spectromeric Analysis. *Environmental Science and Technology 39*, 6153-6161.

Schutz, T. s. (2015). *schutz-hamburg.de/application_cn_info.* Retrieved November 24, 2015, from http://schutz-hamburg.de/application_cn_info.asp?id=184: http://www.brunel.ac.uk

Shapiro, M., Vainshtein, P., Dutcher, D., Emery, M., Stolzenburg, M., Kittelson, D. B., and McMurry P.H. (2012). Characterization of Agglomerates by Simultaneous Measurement of Mobility, Vacuum Aerodynamic Diameter and Mass. *Journal of Aerosol Science, 44*, 24-45.

Sharma, H. N., Pahalagedara, L, Joshi, A., Suib, S. L. and Mhadeswar, A. B. (2012). Experimental Study of Carbon Black and Diesel Engine Soot Oxidation Kinetics Using Thermogravimetric Analysis. *Energy and Fuels*, 5613-5625.

Siebers, D. (1999). Scaling liquid-phase fuel penetration in diesel sprays based on mixing-limited vaporization . *SAE 1999-01-0528 Technical Transaction* (p. 703 728). Detroit: SAE International.

Siebers, D. L. (1998). Liquid-phase fuel penetrationin diesel sprays. *Society of Automotive Engineers* (p. SAE Technical). Detroit: SAE International.

Siebers, D. L.and Higgins, B. S. (2001). Flame lift-off on direct injection diesel sprays under quiescent conditions. *SAE Technical paper 2001-01-0530* (pp. 400-421). Detroit: SEA international.

Simmie, J. M. (2003). Detailed chemical kinetic models for the combustion of hydrocarbon fuels. *Progress in Energy and Combustion Science 29*, 599–634.

Slowik, J. G., Stainken, Davidovits, P., Williams, L. R., Jayne, J. T., Kolb, C. E., Worsnop, D. R., Rudich, Y., DeCarlo, P. F., and Jimenez, J. l. (2004). Particle Porphology and Density Characterisationby Combined Mobilityand Aerodynamic DiameterMeasurements, Part 2. application to Combustion Generated Soot Aerosols as a Function of Fuel Equivalence Ratio. *Journal of Aerosol Science and Technology, 38*, 1206-1222.

Song, J., Alam, M., Boehman, A. L., and Kim, U. (2006). Examination of the Biodiesel Oxidation Behavior of Biodiesel Soot. *Combustion anfd Flame*, 589-604.

Stanmore, B. R. (2001). The Oxidation of Soot: a review of experiments, mechanisms and models. *Carbon*, 29: 2247-2268.

Stanmore, B. R., and Gilot, P. (1995). The influence of sample containment on the thermogravimetric measurement of of carbon black reactivity. *Thermochin Acta*, 261:151-164.

Stanmore, B., Brilhac, J. F., and Gilot, P. (1999). The Ignition and Combustion of Cerium Doped Diesel Soot. *Society of Automoyve Engineers* (pp. SAE Paper 1999-01-0115). Detroit: SAE International.

Stobart, R., and Wijewardane, A. (2011). Exhaust System heat exchanger design for thermal energy recovery in passenger vehicle applications. *Vehicle Thermal*

Management Systems Conference and Exhibitions (pp. 609-622). Gaydon, Warwickshire, Uk: Institution of Mechanical Engineers.

Stone, R. (1999). *Introduction to Internal Combustion Engines.* London: Macmillan Press Ltd.

Stratakis, G. A. and Stematelos, A. M. (2003b). Thermogravimetric analysis of soot emitted by a modern diesel engine run on catalyst-doped fuel. *Combustion and Flame (132)*, 157-169.

Stratakis, G. A., Konstantas, G. S., and Stamatelos, A. M,. (2003). Experimental investigation of the role of soot volatile organic fraction in the regeneration of diesel filters. *Proceedings of the Institution of Mechanical Engineers, Part D: Journal of Automobile Engineering vol. 217 no. 4*, 307-317.

Swanson, J., and Kittelson, D.,. (2010). Evaluation of Thermal Denuder and Catalytic Stripper Methods for Solid Particle Measurements. *Journal of Aerosol Science 41*, 1113-1122.

Tao, F., Golovitchev, V. I.and Chomiak, J. (2004). A phenomenological model for the prediction of soot formation in diesel spray combustion. *Combustion and flame 136*, 270-282.

Tree, D. R., and Svensson, K. I. (2007). Soot Processes in Compression Ignition Engines. *Progress in Energy and Combustion Science, Volume 33, Issue 3.*, 272-309.

TSI, I. (n.d.). Sampling, diluting and conditioning for characterizing particle emissions. *Model 379020A Rotatinng Disk Brochure*. TSI Incorporated .

Turns, S. R. (2012). *An introduction to Combustion, Concepts and Applications.* New Delhi: Tata - McGraw Hill.

Twigg, M. V., and Phillips, P. R. (2015). Cleaning the Air We Breathe – Controlling Diesel Particulate Emissions from Passenger Cars. *JOHNSON MATTHEY TECHNOLOGY REVIEW Original publication: Platinum Metals Rev., 2009, 53, (1), 27 DOI: 10.1595/147106709X390977*, 27-34.

UNECE. (2007). *Global technical regulation No. 4 ECE/TRANS/180/Add.4.* Geneva: UN global registry.

UNECE, G.-6. (2013). *Pollutant Emissions in the Transport Sector.* Transmitted by the Secretariat: UNECE Informal document NO. 09-Rev.1

Ushakov, S. (2012). *Particulate matter emission characteristics from diesel engines operating on conventional and alternative marine fuels - Doctoral thesis* . NTU-Trondheim: Norwagian University of Science and Technology.

Vander Wal, R. L. and Mueller, C.J. (2006). Initial Investigation of Effects of Fuel Oxygenation onNanostructure of Soot from a Direct-Injection Diesel Engine. *Energy & Fuels, 20*, 2364-2369.

Vander Wal, R. L., Aaron, T., and Tomasek, A. J. (2003). Soot Oxidation : dependence upon initial nanostructure. *Combustion and Flame, 134, 1-2*, 1-9.

Vincenzo Palma, V. R. (n.d.).

Wakisaka, Y. and Azetsu, A. (2002). Effects of Fuel injection rate shaping on combustion and emission formation in intermittent spray. *Society of Automotive Engineers.* Detroit: SAE Inc.

Warner, J. R., Huynh, C., Janakiraman, G., Johnson, J., Bagley, S. T. (2002). Oxidation Catalyic Converter and Emulsified Fuel Effects on Heavy Duty Diesel Engine Particulate Matter Emissions. *Society of Automotive Engineers Conference Technical Paper 2002-01-1278.* Detroit: SAE International.

Way.org.UK, W. (n.d.). *http://ww.workthisway.org.uk/programmes/waste-oil-recycling-in-prisons.* Retrieved September 27th, 2015, from http:workthisway.org.uk

Wei, Q., Kittelson, D. B., and Watts, W.F. (2001). Single-Stage dilution tunnel design. *Society of Automotive Engineers 2001-01-0207.* Detroit: SAE International.

Weijers, E. K. (2004). Variability of particulate matter concentrations along roads and motorways determined by a moving measurement unit. *Atmospheric Environment 38* , 2993–3002.

Williams, A. M. (2006). *Biodiesel Effects on Diesel Particle Performance.* Colorado: National Renewable Energy Laboratory.

Williams, A., Black, S., McCormick, R. L. (2010). Biodiesel Fuel Property Effects on Particulate Matter Reactivity. *6th International Exhaust Gas and Particulate Matter Emissions Forum* (pp. 1-9). Ludwigsburg, Germany: National Renewable Energy laboratory NREL/CP-540-47286.

Winklmayr, W. R. (1991). A new electriical mobility spectrometer for the measurement of Aerosol of Size Distributions ranging from 1 to 1000nm. *Journal Aerosol Science 22, No 3*, 289-296.

Yamamoto, K., and Nakamura, M. (2011). Simulation on Flow and Heat Transfer in Diesel Particulate Filter. *Journal of Heat Transfer (DOI:10.1115/1.4003448)*, 1-6.

Yang, S., Lee, K., and Chong, H. (2010). Characterisation of Oxidation Behaviors and Chemical-Kinetics parameters of Diesel Particulates Relevant to DPF Regeneration. *Society of Automotive Engineers* (pp. SAE 2010-01-2166). Detroit: SAE International.

Yehliu, K., Vaner Wal, R. L., Armas, O., and Boehman, A.L. (2012). Impact of fuel formulation on the nanostructure and reactivity of diesel soot. *Combustion and Flame, 159*, 3597-3606.

Yung-Sung, C. (2011). Condensation Particle Counters. In P. B. Kulkarni, *Aerosol Measurement; Principles, Techniques and Applications.* (pp. 381-392). Hoboken, New Jersey: Wiley and Sons Inc.

Zhao, H. (2007). *HCCI and CAI Engines forthe Automotive Industry.* Cambridge: Woodhead Publishing Limited, Abington Cambridge.

Zhu, Y., Zhao, H., and Ladommatos, N. (2003). Computational Study of the Effects of Injection Timing, EGR and Swirl Ratio on a HSDI Multi-Injection Diesel Engine Emission and Performance. *Society of Automotive Engineers* (pp. 2003-01-0346). Detroit: SAE International.

Zouaoui, N., Brilhac, J. F., Mechati, F., Jeguirim, M., Djellouli, B., and Gilot, P. (2010). Study of Experimental and Theoretical procedures when using thermogravimetric analysis to determine kinetic parametersof carbon black oxidation. *Journal of Thermal Analysis and Calorimetry*, 102: 837-849.